Doctor of Philosophy

Optimal Design of Nonlinear Multiple Tuned Mass Dampers with Frictional Mechanism

마찰도입 비선형 다중동조질량감쇠기의 최적설계

by

Sung-Yong Kim

August 2017

서울대학교 대학원
건축학과
김 성 용

Doctor of Philosophy

Optimal Design of Nonlinear Multiple Tuned Mass Dampers with Frictional Mechanism

마찰도입 비선형 다중동조질량감쇠기의 최적설계

by

Sung-Yong Kim

August 2017

서울대학교 대학원
건축학과
김 성 용

Abstract

Modern development of design techniques and material science in architectural engineering contributes to increase in demand for buildings with longer span and light weight structure. In spite of its advantageous aspects, such advances in technologies often leads to problems with undesired discomfort caused by excessive vibration. In order to help dampen the unwanted excessive vibration, a variety of relevant techniques have been investigated, among which tuned mass damper (TMD) is one of the most widely used techniques so as to control the problematic vibration.

This study first investigates the optimal solution of linear multiple tuned mass dampers (linear MTMDs, LMTMDs) of various configurations. The configurations considered in this study include the cases where the frequency ratios are linearly distributed, the damping coefficients are uniformly distributed, the mass distributions are linearly distributed, or these constraints are combined in some ways. Two different optimization techniques are employed: Nominal Performance Optimization (NPO) and Robust Performance Optimization (RPO). The NPO searches a solution that minimizes the objective function deterministically, while the RPO minimizes the mean value of the objective function, assuming that the associated structural parameters are probabilistic rather than deterministic. Further, this study provides contour maps for the root-mean-square (RMS) displacement of main structure and the largest RMS displacement of LMTMDs, which can be useful in the design process.

Next, this study seeks the optimal solution of frictional multiple tuned mass dampers (FMTMDs) in which the Coulomb-type frictional force is incorporated in either purposefully or unintentionally. In this study, four of the feasible FMTMD configurations are formulated and comparably analyzed. The investigated configurations

involve: 1) no constraint on either the frequency ratios or the coefficient of friction (COF) is imposed; 2) the frequency ratios are linearly distributed and equally spaced; 3) the COFs are identically distributed; 4) the frequency ratios are equally spaced and the COFs are identical. In order to cope with the difficulties inherent in nonlinearity of the problem, this study adopts a statistical linearization technique, which enables the complicated nonlinear force terms to be linearized in a statistical sense. Some miscellaneous considerations such as stroke limitations and design procedure are also aptly included.

This study mainly addresses RMS responses and extreme value distributions for the frictional multiple tuned mass dampers (FMTMDs). In designing of optimal FMTMD, the original nonlinear system arising from the frictional elements is replaced with an equivalent linear system by means of statistical linearization. In order to improve the accuracy for the estimation of peak distribution of MTMDs, this study exploits a statistical nonlinearization technique which replaces the nonlinear system at hand with a class of other nonlinear systems whose exact solution has been already explicitly derived. A correction factor that defines the ratio of RMS displacement between nonlinear and linear system is derived based on the results of statistical nonlinearization technique. This study also provides an explicit formula for evaluating a peak factor for frictional TMDs. The correction factor and the peak factor proposed are validated with Monte Carlo Simulation.

Several application examples of MTMDs are included in this thesis. of multiple tuned mass dampers (MTMDs). In the first section, a mechanism-based frictional pendulum tuned mass damper (FPTMD) is proposed, which contributes to overcome some shortcomings of conventional translational TMDs with viscous damping. In the second section, a numerical study is carried out to provide a design procedure of MTMDs, which covered modal analysis based on finite element method, optimal design of tuned mass dampers, and evaluating their control performance and robustness under

the frequency-perturbed states. The final section presents a project in an attempt to mitigate an excessive vibration of a problematic structure. The overall process of the project includes the vibration performance evaluation, modal analysis based on finite element method and optimal design and manufacturing of tuned mass dampers.

Keywords: Tuned mass damper, Multiple tuned mass damper, Friction mechanism, Vibration control, Statistical linearization, Statistical nonlinearization

Student Number: 2011-30173

Contents

List of Figures

List of Tables

Chapter 1

Introduction

1.1 Background

In recent years, there have been many important developments in constuction fields, including numerical techniques, material science, and associated design techniques. These developments enables building industries to satisfy the recent trend towards great heights, longer span, and lightweight floor system. In spite of its positive aspects, such a tendency to reduce the weight and cost of structures sometimes brought a problematic vibration which yields undesired discomfort for building occupants. In order for bulidings to satisfy the necessary vibration performance, various design techniques and control schemes have been discussed up to now.

Tuned mass damper (TMD) is a passive control device which help dampen the dynamic response of the structure efficiently. The basic concept of employing a TMD is to attract vibration energy of the main structure by resonance into itself, and to dissipate the transferred energy through built-in energy dissipation devices. Owing to their simple mechansim and novel functionality, enormous applications for TMDs

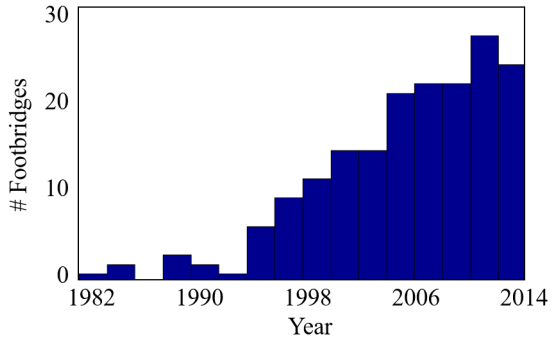

Figure 1.1: The number of footbridges with TMDs installed by GERB Engineering and Maurer Söhne, taken from Van Nimmen et al. (2016).

has been made over the past few decades. For instance, one of the statistics reported by Van Nimmen et al. (2016) indicates that the total use of TMDs in footbridges was consistently increasing from 30 years ago to the present (see Figure 1.1). Considering the increases of current demands for lightweight and highrise bulidings, the demand for TMDs is expected to increase continuously in the future.

One of the simplest and most widely concerned configurations is the single linear TMD which consists of unit moving mass, a viscous dashpot and a spring. Many researchers have been investigated the optimal values of relevant parameters such as optimal frequency ratio and optimal damping ratio of the single linear TMDs. For instances, Den Hartog (1956) and Warburton (1982) proposed the optimal parameters, which are still widely used in the academic area as well as in the application fields. Various applications have been consistently reported, confirming that the single linear TMDs are quite efficient in mitigating excessive vibrations.

Although their efficiency, however, the single linear TMDs have also some drawbacks. One of crucial drawbacks may be so-called detuning effect. When a main structure is subjected to floor mass variations from sources other than human presence, the natural frequency of the structure would be deviated from the predicted

level, resulting in the performance degradation of the TMD. Not only a fluctuation in the natural frequency of the structure, but also the liquid leakage of the viscous dampers may also be a drawback causing performance degradation of TMDs. With repetitive operations during a long lifetime, the dashpot employed in TMDs can be degraded due to aging and they also have a risk of leakage.

Multiple tuned mass damper (MTMD) is a system consists of multiple units of TMDs, often referred to as the case where each of TMDs has different dynamic characteristics. In the early stage of research, MTMD configurations with simplified and limited conditions were discussed so as to reduce the number of associated design variables. For instance, the MTMD of large numbers of units with equally spaced natural frequencies and each of which having equal damping constant was studied by Xu and Igusa (1992) based on an asymptotic analysis, and it was shown that such a MTMD is effective in reducing the response of the main structure. For a finite number of MTMDs with similar constraints, Joshi and Jangid (1997) and Jangid (1999) found the optimal parameters of the MTMD for undamped and damped primary structure, respectively. MTMDs with equal damping ratios and equally spaced natural frequencies were also investigated by various researchers including Yamaguchi and Harnpornchai (1993), Abé and Fujino (1994), and Kareem and Kline (1995).

Until recently, various studies have been conducted for the MTMDs with relaxed constraints, for example, Igusa and Xu (1994), Li (2002), Hoang, Fujino, and Warnitchai (2008), Zuo and Nayfeh (2005), Li and Ni (2007), and Yang, Sedaghati, and Esmailzadeh (2015a). The main differences in these studies involve 1) considered excitation, such as harmonic forcing function and the ground acceleration, 2) the objective function, such as the RMS response of the primary structure or the maximum of the frequency response and 3) employed optimization strategies.

Existing studies, however, only conducted a comparison with other configurations in a limited way. Li and Ni (2007), for instance, only compared the performance

between their non-uniformly distributed MTMD and the one with equal frequency spacing and damping ratio on the basis of frequency response function. Li (2002), one of the comparative studies on various configurations, provided the optimal parameters only for the case where the natural frequencies are equally spaced. Hoang, Fujino, and Warnitchai (2008) also conducted a similar study. Li and Liu (2002) also conducted.

Meanwhile, incorporating dry fiction mechanism can be another viable solution to eliminate the detrimental effects of employing viscoud dashpots. Some researchers tried to incorporate the Coulomb-type force into the TMD as an energy dissipative mechanism. Inaudi and Kelly (1995) proposed a nonlinear TMD that uses friction dampers acting transversely to the direction of the motion of the mass damper as a means for energy dissipation. Based on the statistical linearization procedure that can effectively simplify for computing the RMS response of the system, they showed that, when appropriately designed, the nonlinear system achieves the same level of performance that an ideally linear TMD would provide.

1.2 Scope and Objectives

The main objective of this thesis is principally to provide a framework for the design of MTMDs. Firstly, this thesis revisited the design of linear MTMDs (LMTMDs), of which optimal conditions are well-established by various researchers. For six of practial configurations of LMTMDs, the characteristics of optimal solutions and control performances are discussed in detailed. Specifically for one of the considered configurations that composed of identical stiffnesses and viscous damper, and linearly distributed frequency ratios, a set of approximate design formula are provided.

Based on the conclusions for the optimal solutions of LMTMDs, the sequel chapter proposed the concept of frictional MTMDs (FMTMDs), in which the viscous dashpots are replaced with nonlinear elements with the Coulomb-type frictional force. Such a

nonlinearity, however, provokes difficulties in solving the governing equations compared to their linear counterparts. In order to circumvent the difficulties, this study exploited a statistical linearization technique, which replaces the original nonlinear forces with statistically equivalent linear ones.

The statistical properties of the response of FMTMDs and associated peak factor are then discussed. The discrepancy of RMS response of FMTMDs between the original nonlinear system and the statistically equivalent system is significant. In order to correct the discrepancy, this study exploited the statistical nonlinearization, which replaces the original nonlinear forces with statistically equivalent nonlinear ones where the probability of their response is mathematically well-established. Followed by deriving a correction factor that corrects the RMS displacement of FMTMDs, the peak factor that allows to predict the peak displacement is also provided.

The applicability of the proposed MTMDs are examined with both numerical and experimental ways. Based on the design procedure proposed by the previous chapters, this study provides detailed steps, which includes field measurements, finite element analyses and field applications. This study also covers vibration performance evaluation and corresponding modeling procedure of the structure, as well as design of MTMDs in order to attenuate the problematic level of footfall-induced vibration.

1.3 Outline of Dissertation

This thesis is categorized into three parts. The first part of this thesis is intended to provide a literature review of recent results in both theoretical development and application of TMDs. The literalture review covers a wide range of relevant research areas including existing optimization criteria and techniques, design schemes, the characteristics of multiple tuned mass dampers (MTMDs), nonlinear TMDs and various applications. Some miscellanies associated with designing of TMDs are also discussed,

which include the issue on the stroke limitations and reliability based optimization schemes.

The second and main part of this thesis provides a framework for the design of LMTMDs and FMTMDs. Chapter 3 presents optimal design and analysis of linear multiple tuned mass dampers with various configurations. Two different optimization techniques are employed: Nominal performance optimization (NPO) and Robust performance optimization (RPO). The NPO minimizes the objective function that is deterministic, whereas the RPO minimizes the mean value of the objective function, assuming that the associated structural parameters are probabilistic. Six of feasible configurations are formulated and comparably analyzed, each of which is constrained in a way of linearly distributed frequency ratios, uniformly distributed damping coefficients, linearly distributed mass ratios, and/or combinations thereof. An approximate design formula is developed for $\text{LMTMD}_{\gamma\zeta}$ configuration, which is as efficient as the best optimal configuration. Further, this study provides contour maps that enables designer to consider the maximum stroke of LMTMDs, which may be of importance in its housing design.

Chapter 4 investigates optimal design and analysis of frictional multiple tuned mass dampers, in which the Coulomb-type frictional force is incorporated in either purposefully or unintentionally. Four of the feasible FMTMD configurations are formulated and comparably analyzed, each of which is constrained in a way of linearly distributed frequency ratios, uniformly distributed coefficients of friction (COFs), and/or combinations thereof. An approximate design formula is developed for $\text{FMTMD}_{\gamma\tau}$ configuration utilized under the constraint of frequency ratios and COFs. In order to cope with the difficulties inherent in nonlinearity of the system, this study adopted a statistical linearization technique, which enables the complicated nonlinear force terms to be linearized in a statistical sense.

Chapter 5 addresses RMS responses and extreme value distributions for the fric-

tional multiple tuned mass dampers (FMTMDs). In designing of optimal FMTMD, the nonlinear system arising from the frictional elements were replaced into an equivalent linear system by means of statistical linearization. However, a discrepancy of RMS response between those two systems arises in nature. In order to improve an accuracy for the estimation of peak distribution of MTMDs, this study exploits a statistical nonlinearization technique, which replaces nonlinear systems with a class of other nonlinear systems of which exact solution has been explicitly derived. A correction factor that defines the ratio of RMS displacement between nonlinear and linear system was derived, based on the result of statistical nonlinearization technique. This study further derived an explicit formula for evaluating a peak factor for the frictional TMD. Those correction factor and formula for the peak factor are examined with Monte Carlo Simulation.

The third and final part of this thesis deals with the applicability of the MTMDs. Section 1 shows development of frictional pendulum tuned mass damper. Section 2 develops TMD to suppress human-induced vibration on an indoor footbridge. The hallway at the 5th floor of Building 39 of Seoul National University was selected as the example floor. This study covers vibration performance evaluation and corresponding modeling procedure of the structure, as well as design of MTMDs in order to attenuate the problematic level of footfall-induced vibration.

Chapter 2

Literature Review

This chapter is concerned with a literature review of recent results in the theoretical development and applications of tuned mass dampers (TMDs). In Section 2.1, existing optimization criteria and techniques are reviewed, which are widely accepted optimization schemes in the design of TMDs. Section 2.2 discusses design schemes and the characteristics of multiple tuned mass dampers (MTMDs). Section 2.3 deals with nonlinear TMDs, particularly the theoretical investigation and applications. Section 2.4 provides various applications of TMDs including mitigation of wind excitation, reduction of seismic risks, and floor vibration attenuation. Robustness issue is discussed in details. Some miscellanies associated with TMDs are discussed in Section 2.5, which include the issue on the stroke limitations and reliability based optimization schemes. Diverse optimization criteria and techniques have been proposed until now, and three typical optimization techniques are of importance in the historical manner.

2.1 Optimization Criteria and Techniques

In this section, some of representative optimization criteria and relevant techniques are briefly reviewed: H_2, H_∞ optimization, and stability maximization. H_∞ optimization aims to minimize the maximum of the frequency responses under harmonic excitations. H_2 optimization seeks to minimize the H_2 norm defined as a quantity evaluated by integrating the frequency response over the whole frequency domain, thus it also has physical interpretation as the root mean square (RMS) value of the output in response to white noise excitation. Stability maximization tries to identify the optimal conditions such that all poles of the transfer function of the system are far from the imaginary axis in the left-half system, by which the transient vibration of the system can be attenuated as soon as possible.

2.1.1 H_∞ optimization

H_∞ optimization is the first strategy appeared in the history of the designing of TMD, which seeks to find the relevant parameters within all admissible frequency range such that the maximum of the amplitude of the frequency responses (called H_∞ norm) is minimized. One classical solution that is yet widely used in the field was proposed by Den Hartog (1956) for viscously damped TMDs under harmonic loading, which is now called the fixed-point theory.

The fixed-point theory seeks to find the optimal parameters by controlling the intersection point of the frequency response curves of the main structure, A and B, which are independent of the damping value of TMDs (see Figure 2.1). If these points can be appropriately located, and since the purpose of adding a TMD is to reduce the resonant peak of the main system to its lowest possible, the most favorable response curve is the one which passes through the higher of the two fixed points with a horizontal tangent.

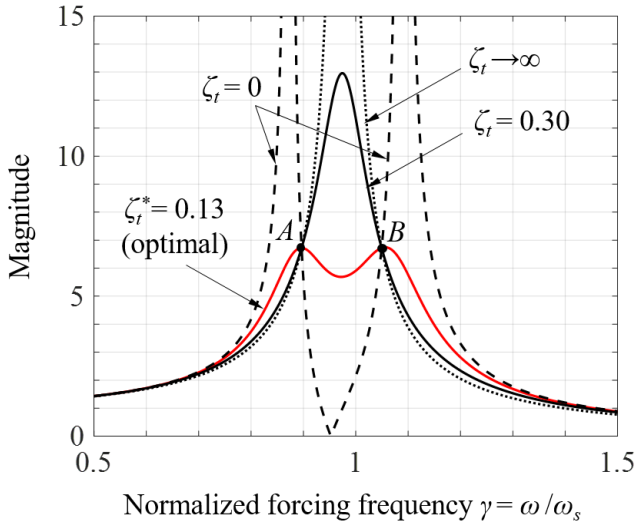

Figure 2.1: Two fixed intersection points (A and B) of all response curved in the fixed-point theory proposed by Den Hartog ($\mu = 5\%$ and $\gamma_t = 0.95$)

Den Hartog's optimal solution for the optimal frequency ratio γ_t^* and optimal damping ratio ζ_t^* are given as a function of the ratio μ of the mass of the TMD and the relevant modal mass of the main structure as follows:

$$\gamma_t^* = \frac{1}{1+\mu} \tag{2.1a}$$

$$\zeta_t^* = \sqrt{\frac{3\mu}{8(1+\mu)}} \tag{2.1b}$$

Warburton (1982) extended this approach to obtain optimum parameters of TMDs under various combinations of a force applied to the main mass or an acceleration imposed on the frame for excitation parameter with an optimized response quantity including structural displacement, velocity and acceleration. Optimal TMDs for damped SDOF system were also investigated by various researchers (Halsted III and

Taylor, 1981; Nishihara and Asami, 2002; Soom and Lee, 1983; Thompson, 1981; Tsai and Lin, 1993). The main differences in these studies involve 1) considered excitation, such as harmonic forcing function versus the white-noise random excitations, and 2) employed numerical searching procedure to identify the optimal conditions.

2.1.2 H_2 optimization

H_2 optimization considers the H_2 norm that is defined in the frequency domain as integrating the magnitude of the transfer function over frequency. The H_2 norm can also be given another interpretation as a measure of the expected RMS value of the output in response to white noise excitation (Skogestad and Postlethwaite, 2007). Because of its nice mathematical and numerical properties, the H_2 optimization is accepted as the optimization criteria in the design of TMDs.

One of the first researches that applied the H_2 optimization in TMD was conducted by Crandall and Mark (1963). They studied a two-degree-of-freedom system under white noise excitation, and showed that the mean square acceleration of the primary structure can be decreased as the uncoupled natural frequency of TMD is appropriately tuned to that of the main body. With a parametric study, McNamara (1977) found TMD design parameters for reducing wind-induced structural response of buildings, and presented the efficiency of TMD from wind tunnel test results. Luft (1979) provide a simple closed form expressions for the maximum damping of the equivalent single-degree-of-freedom system. Warburton (1982) derived the optimal tuning parameters which minimize a various value of the output response such as displacement, velocity and acceleration of a main structure subjected to harmonic and white noise random excitations. For a dampened system, an exact closed-form solution was proposed by Asami et al. (2002).

For white noise excitation of spectral density S_0 the variance of a response quantity x_s, σ_s^2, is given by

$$\sigma_s^2 = \int_{-\infty}^{\infty} S_0 |H(\omega)| \, \mathrm{d}\omega \tag{2.2}$$

as the variance equals the mean square value for a random quantity with zero mean, where $H(\omega)$ is the complex transfer function of the main structure. The optimizing conditions can be determined by following first order necessary condition for optimal:

$$\frac{\partial(\sigma_s^2)}{\partial \gamma_t} = 0 \tag{2.3a}$$

$$\frac{\partial(\sigma_s^2)}{\partial \zeta_t} = 0 \tag{2.3b}$$

Applying these conditions, simple expressions for γ_t^* and ζ_t^*.

Warburton's optimal solution for the optimal frequency ratio γ_t^* and optimal damping ratio ζ_t^* are given as a function of the ratio μ of the mass of the TMD and the relevant modal mass of the main structure as follows:

$$\gamma_t^* = \frac{(1 + \mu/2)^{1/2}}{1 + \mu} \tag{2.4a}$$

$$\zeta_t^* = \sqrt{\frac{\mu(1 + 3\mu/4)}{4(1 + \mu)(1 + \mu/2)}} \tag{2.4b}$$

2.1.3 Stability maximization

Stability maximization tries to find the optimal conditions such that all poles of the transfer function of the system are far from the imaginary axis in the left-half system, by which the transient vibration of the system can be attenuate as soon as possible.

Villaverde (1985) found the favorable conditions of TMD parameters with the help of complex modal analysis, from which the author found damping ratio and natural frequency of TMD that can balance the complex natural frequencies and

damping ratios of two modes of the resulting structure-attachment system. Sadek et al. (1997) showed that the TMDs according to the authors' optimal parameters can effectively reduce the displacement and acceleration response of the structure subjected to seismic excitations. Recently, Krenk (2005) proposed the scheme that the motion of the structural mass and the relative motion of the damper mass at the frequency corresponding to free vibrations of the combined mass with the damper locked. The proposed criterion led to an applied optimal damping ratio that is 15% larger than the classical solution by Den Hartog (1956).

Yamaguchi's optimal solution for the optimal frequency ratio γ_t^* and optimal damping ratio ζ_t^* are given as a function of the ratio μ of the mass of the TMD and the relevant modal mass of the main structure as follows:

$$\gamma_t^* = \frac{1}{1+\mu} \tag{2.5a}$$

$$\zeta_t^* = \sqrt{\frac{\mu}{(1+\mu)}} \tag{2.5b}$$

Figure 2.2 shows various design curves and frequency response functions of the main structure with TMDs. Note that the solutions by Den Hartog (1956), Warburton (1982) and Sadek et al. (1997) are obtained according to the H_2, H_∞, and stability maximization, respectively.

2.2 Multiple Tuned Mass Dampers

Multiple tuned mass damper (MTMD) is a system consisting of multiple units of TMDs, often referred to as the case where each of TMDs has different dynamic characteristics. MTMDs exhibits several advantages over a single TMD. Design of multiple units is usually much complex than that of a single unit of TMD. In particular, the number of design parameters which must be specified in the MTMD design

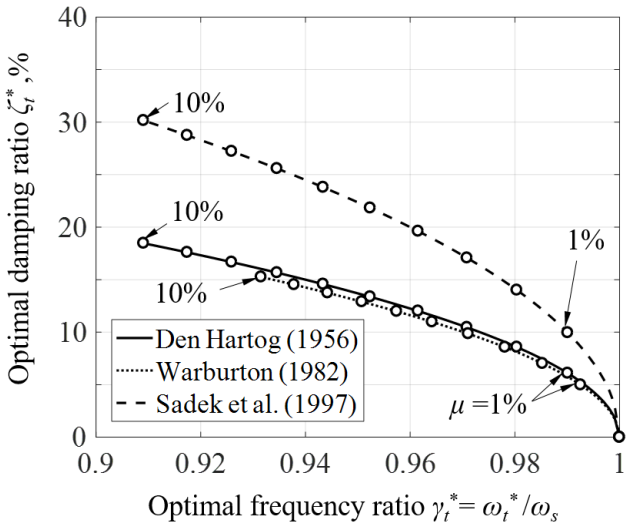

(a) Design curves

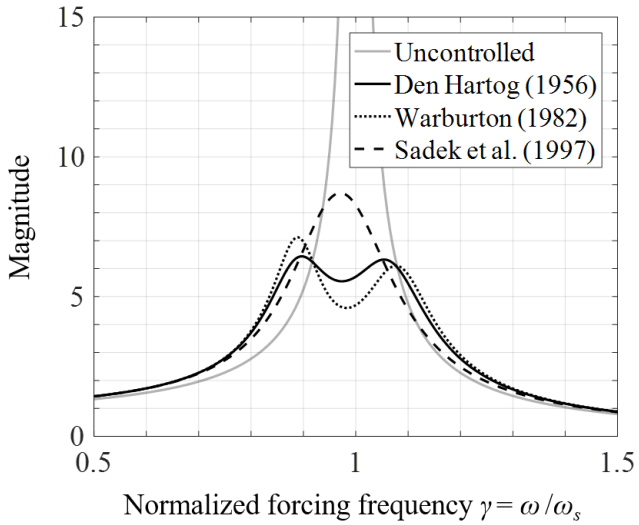

(b) Frequency responses with various optimal solutions ($\mu = 5\%$)

Figure 2.2: Design curves and frequency response functions with those optimal designs

is typically much higher than that for single TMD. In order to reduce the relevant design parameters, some researchers have imposed several design restraints as will be discussed in the following section.

In the early stage of research, MTMD configurations with simplified and limited conditions were discussed so as to reduce the number of associated design variables. For instance, the MTMD of large numbers of units with equally spaced natural frequencies and each of which having equal damping constant was studied by Xu and Igusa (1992) based on an asymptotic analysis, and it was shown that such a MTMD is effective in reducing the response of the main structure. For a finite number of MTMDs with similar constraints, Joshi and Jangid (1997) and Jangid (1999) found the optimal parameters of the MTMD for undamped and damped primary structure, respectively. MTMDs with equal damping ratios and equally spaced natural frequencies were also investigated by various researchers including Yamaguchi and Harnpornchai (1993), Abé and Fujino (1994), Kareem and Kline (1995).

Jangid (1999) proposed explicit expressions as follows:

$$\zeta_T^* = \frac{3\mu_T}{8(1+\mu_T)(1-\mu_T/2)} + \sqrt{\mu_T} h_1(\mu_T) h_2(N) \tag{2.6a}$$

$$\beta_\gamma^* = \sqrt{\mu_T} h_1(\mu_T) \frac{h_3(N)}{\sqrt{N}} \tag{2.6b}$$

$$\gamma_T^* = \frac{\sqrt{1-\mu_T/2}}{1+\mu_T} + \frac{h_1(\mu_T)}{\sqrt{\mu_T}} \frac{h_3(N)}{\sqrt{N}} \tag{2.6c}$$

Table 2.1: Regression coefficients for Eq. (2.7) (Jangid, 1999)

Coefficient	Corresponding value		
	ζ_T^*	β_γ^*	γ^*
a_1	0.5474	0.42113	-0.00241
a_2	0.1038	0.04479	0.72152
a_3	-0.4522	-0.38909	-0.43970
a_4	0.7604	-0.73518	-0.66385
a_5	0.3916	0.11866	-0.01138
a_6	0.0403	4.86139	0.99522

where

$$h_1(\mu_T) = a_1 + a_2\sqrt{\mu_T} + a_3\mu_T \tag{2.7a}$$

$$h_2(N) = a_4\left(\frac{1}{\sqrt{N}} - 1\right) + a_5\left(\frac{1}{N} - 1\right) + a_6(\sqrt{N} - 1) \tag{2.7b}$$

$$h_3(N) = a_4\left(\frac{1}{\sqrt{N}} - 1\right) + a_5(N - 1) + a_6(\sqrt{N} - 1) \tag{2.7c}$$

The values of coefficients in Eq. (2.7) are given in Table 2.1.

Jangid and Datta (1997) investigated the dynamic response behavior of a simple torsionally coupled system controlled by MTMDs with equally spaced natural frequencies and identical damping ratios. They found that, if MTMDs are designed for asymmetric buildings by ignoring their torsional coupling, then the effectiveness of MTMDs becomes worse than expected. However, for torsionally very stiff asymmetric buildings such that the torsional frequency is twice larger than the translational frequency, the design of MTMDs by ignoring the torsional mode is effective. It was also

shown that MTMDs are more effective than single TMD even for torsionally coupled system, but the advantage becomes decreasing with increase in the eccentricity ratio.

Until recently, various studies have been connected for the MTMDs with relaxed constraints, such as Igusa and Xu (1994), Li (2002), Hoang, Fujino, and Warnitchai (2008), Li and Ni (2007), Fu and Johnson (2010), and Yang, Sedaghati, and Esmailzadeh (2015a). The main differences in these papers involve 1) considered excitation, such as harmonic forcing function and the ground acceleration, 2) the objective function, such as the RMS response of the primary structure or the maximum of the frequency response and 3) employed optimization strategies.

Existing research, however, has performed a comparison with other configurations in a limited way. Li and Ni (2007), for instance, only compared the performance between their non-uniformly distributed MTMD and the one with equal frequency spacing and damping ratio on the basis of frequency response function. Li (2002), one of the comparative studies on various configurations, provided the optimal parameters only for the case where the natural frequencies are equally spaced. Hoang, Fujino, and Warnitchai (2008) also conducted a similar study. Li and Liu (2002) also conducted.

Clark (1988) discussed the performance distinction between SDOF and MDOF TMD systems. Considering a hypothetical eight story building with single TMD and four TMDs that are respectively implemented at the 3rd, 5th, 6th, and 8th floor though such two systems were designed according to the same mass ratio (total weight of TMDs were designed to be 5% of the first modal mass) and followed by Den Hartog's design equation, he showed that MTMD can provide motion reductions between 40% to 60 % whereas the reduction level was only 11% by STMD.

Zuo and Nayfeh (2004) configured minimax optimization in order to find the optimal parameters of MDOF TMDs including series connected TMD. In formulating their optimization scheme, they chose the maximum of the modal damping ratios as the objective function, and applied decentralized optimization techniques.

Lin et al. (2005) applied the MTMD in order to control the train-induced vibration of high-speed railway bridge. In comprising the MTMD, they used a configuration in which each of TMDs has the same mass ratio and damping ratio. And they found the optimal parameters by which minimizes the H_∞ norm. They concluded that the proposed MTMD is more effective and reliable than a single TMD in reducing dynamic responses during resonant speeds.

Zuo (2009) proposed MTMD in which the multiple absorber masses are connected to the primary structure in series comprising chain-like system. Based on the numerical H_2 optimization, it was shown that such a series MTMD outperforms compared to single TMD and parallel MTMD in terms of its performance and robustness. Particularly in the case of two DOF series MTMD, it was found to be optimal when the damping of the absorber which is directly attached to the primary structure is zero.

Li et al. (2010) investigates the use of MTMD so as to minimize the crowd-induced random vibration of footbridge. An optimization procedure based on the minimization of maximum RMS acceleration, or H_2 optimization, of footbridge was conducted. Numerical analysis shows that the proposed MTMD can reduce the vibration response significantly.

Many researchers have proposed MTMDs with closely distributed natural frequencies including Xu and Igusa (1992), Yamaguchi and Harnpornchai (1993), Abé and Igusa (1995), Jangid and Datta (1997). Xu and Igusa (1992) considered a specific class of MTMDs each of which natural frequencies of the natural frequencies are equally spaced. With an asymptotic approach, they found that the equivalent damping induced by the MTMD is proportional to the masses of MTMD, inversely proportional to the spanning of natural frequencies, and independent of damping. One of the remarkable comments is concerned with the damping: they showed that the MTMDs can be facilitated significantly under low damping values.

For the configuration of MTMDs with equal damping ratios and equally-spaced

natural frequencies, Yamaguchi and Harnpornchai (1993) found the optimal parameters numerically, and concluded that the optimum MTMD can be more effective solution than the optimum single TMD. Discussing on the robustness issue, they found a notable conclusion that the most effective MTMD is not very robust but that is possible to design a MTMD which has almost the same effectiveness as the optimum single TMD but is much more robust.

In determining the optimal damping ratio, they discussed the effect on the damping ratio of TMDs, particularly the existence of the optimal parameters in terms of minimizing the maximum of the frequency function, or H_2 norm. For given mass ratio, frequency bandwidth, and the number of TMDs, they showed that there is an optimum below which the performance decreases due to the excessive motion of the TMDs, and above which the performance in turn also decreases due to the sticky motion of the TMDs.

For a structure-MTMD system which consists of identical mass and damping, and uniformly distributed natural frequencies, Abé and Fujino (1994) analytically derived modal properties, and found a favorable condition of the MTMD using a perturbation technique which allows robust performance by providing the tuning frequency bandwidth of TMD exceeds a certain value. They also noted that the damping of the MTMD is to be smaller than that of the STMD for the efficiency as noted by Xu and Igusa (1992), though they additionally commented that such a condition may be a drawback in certain cases of application of the TMD that enables TMD exhibits large stroke in controlling.

Joshi and Jangid (1997) found the optimum parameters of MTMD with equally-distributed natural frequencies and identical damping coefficient based on H_2 optimization under base-excited damped system. Jangid (1999) also found the optimal parameters of MTMD for undamped primary structure.

Li (2002) conducted a study to find the optimal parameter of MTMDs for differ-

ent combinations of the mass, damping coefficient and stiffness, all of which natural frequencies are uniformly distributed. Based on the selective criteria such as the displacement dynamic magnification factor and the acceleration dynamic magnification factor, Li found the optimal parameters of MTMDs and demonstrated their efficacy and robustness.

In implementing a two-objective optimization strategy that consists of effectiveness and robustness performance criteria, Dehghan-Niri et al. (2010) considered two different MTMD configurations: uniform MTMDs that composed of uniformly distributed natural frequencies and equal damping ratios for all TMDs; and irregular MTMDs that only independent design parameters are to be determined. They concluded that beside the performance advantage of irregular MTMD design, the practical drawback of increased complexity in manufacturing and implementation should be considered.

It should be also precisely noted that the standard solution for this problem is to use higher damping values than the optimal value, which makes TMDs less sensitive to off-tuning (Fujino and Abe, 1993).This approach sacrifices some of the performance of the TMDs to promote their robustness.

Zuo and Nayfeh (2005) proposed an optimization technique to find the individual stiffness and damping parameters of MTMD. The proposed technique treats the MTMD system as a decentralized H_2 controller, of which the control gain matrix is composed of the spring stiffnesses and damping coefficients. The authors found that the optimal conditions obtained by their optimization technique provide a better performance compared to the case of uniform frequency spacing and damping.

Hoang and Warnitchai (2005) and Li and Ni (2007) investigated the optimal parameters of MTMDs of unconstrained design variables by using gradient-based methods. The key differences of those researchers are in the objective functions: Hoang and Warnitchai (2005) investigated the optimal solution that minimize RMS responses of

the structure; Li and Ni (2007) minimized the maximum of structural displacement. Both researches found that the most efficient configuration of MTMDs is achieved when the natural frequencies and damping ratios are non-uniformly-distributed, and the configuration with uniform frequency and equal damping ratios can also be a viable solution for practical design purposes. Moreover, by employing robustness performance optimization that may be categorized into "average method", Hoang and Warnitchai (2005) provided more robust solution that have higher damping ratios and narrower frequency range compared to the nominal solution.

Fu and Johnson (2010) developed a new type of synergistic system between structural and environmental controls through integrating shading fins and mass dampers. An example of the synergistic system proposed by the authors is depicted in Figure 2.3. In the proposed system, the rotatable shading fins act as TMDs that resonant and dissipate energy during structural motions. By using a pattern search method, the proposed system is optimized. It was shown that a near-optimal condition of proposed system outperforms a single TMD system.

By summarizing those researches on MTMDs, the following conclusions can be drawn:

1. For the same mass ratio, the optimum designed MTMD is found to be more effective than the optimum single TMD system.

2. The optimal damping ratio for the MTMD is found to be low as compared to that of a single TMD. The optimum damping ratio increases with an increase in the mass ratio, being more pronounced for a single TMD system as compared to the MTMD system.

3. The optimum frequency bandwidth of the MTMD increases with increasing of the mass ratio.

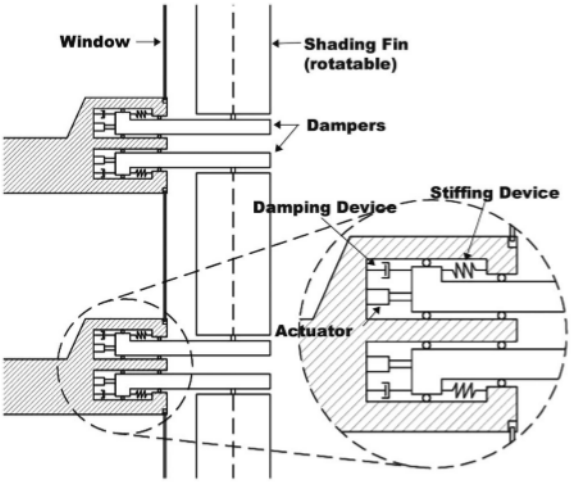

Figure 2.3: Example shading fin mass damper detail, excerpted from Fu and Johnson (2010)

2.3 TMDs on Nonlinear Structures

Extreme excitation such as earthquake may deteriorate the structural performance of the structure, and such deterioration may cause undesired off-tuning effect that affect performance degradation of TMDs. To avoid the significant performance degradation, several researchers conducted studies on TMD design on the nonlinear primary structure.

Zhang and Balendra (2013) investigated the feasibility of using STMD in controlling of bilinear hysteretic structures under narrow band seismic motions. The authors adopted "averaging method" that can linearize given nonlinear system in a statistical sense in order to modeling the bilinear structure, and find the optimal TMD that minimizes the maximum of the frequency response within a band of concerned frequencies.

2.4 Nonlinear Tuned Mass Dampers

Although theoretically well-established and show satisfactory performance in many applications, Linear TMDs (LTMDs) are ineffective due to the following reasons. First, LTMDs usually require a frictionless guide which enables the moving mass facilitates the smooth movement. In general, such a guide requires high cost for not only fabrication but also maintaining the frictionless movement. The maintenance problem of LTMDs also should be addressed as an important issue, because such viscous damping elements mounted in LTMDs can be degraded due to aging and they also have a risk of liquid leakage. Moreover, LTMDs, tuned to the fundamental frequency of the structure, could suppress little or even amplify the dynamic response of higher modes and therefore may fail to reduce the total response under these conditions.

In order to regard the problems, nonlinear TMDs (NTMDs) in which nonlinear elements are incorporated into the TMDs were developed in a various ways. Regarding the first and second problems, friction force was incorporated. As a solution for the third problem, a power-type damping force is provided.

One of the alternative ways is to employ frictional devices or mechanism instead of linearly viscous element. Incorporating frictional mechanism has its advantage because it is insensitive to varying temperature and not prone to be degraded under aging and liquid leakage. Moreover if one can characterize the friction coefficient precisely rather than implementing the frictionless guide, the cost in implementing such a frictionless guide can be saved effectively providing economic advantages.

Several researches have been carried out on the efficacy of TMDs with frictional devices on the vibration response of linear structures. Inaudi and Kelly (1995) proposed and studied a nonlinear TMD which uses friction damper. Statistical linearization method was employed with aim to evaluate the structural response of the system.

The study confirmed that the efficacy of their TMD is comparable to that of a linear TMD for a wide range of excitation intensity. It is interesting to note the remarks of them that the statistically linearized parameters, in this case, are independent of the intensity of the excitation process and only dependent on the its frequency content.

Nonlinear TMDs that dissipates the input energy by hysteresis behavior, which includes the frictional mechanism, were developed and investigated by some researchers (Carpineto et al., 2014; Wang, 2011). As a way of suppressing vibration and chatter in machining operations, Wang (2011) proposed nonlinear TMD, in which Coulomb-type frictional dissipating mechanism is accommodated, and examined its feasibility through numerical simulations. Based on the evaluation of FRF with the harmonic balancing method, the optimal design parameters of the nonlinear TMD are obtained by minimizing the magnitude of the real part of the real FRF. The author concluded that the nonlinear TMD proposed by the author can outperform a common linear TMD in machining stability improvement. However, there still are some disadvantages, among which the main disadvantage is that the friction force applied on the friction interfaces has to be adjusted to match the amplitude of the dynamic cutting force according to the optimal force. Because the cutting force amplitude varies under different cutting condition, the optimal value of the normal force needs to be either estimated according to the machining conditions or directly obtained by cutting experiments.

Carpineto et al. (2014) examined the applicability of nonlinear TMDs consisted of steel wire ropes, of which hysteretic behaviors are able to be described in terms of Bouc-Wen constitutive law. From their theoretical investigation, it was found that the optimal tuning condition corresponds to reaching equally controlled response amplitudes at the resonances of the in-phase and out-of-phase modes of the modified structure. HYS1 type of softening hysteresis exhibited a higher stiffness at a higher frequency below the target excitation and a lower stiffness at a lower frequency above

the target, arising a detuning in the frequency ratio. Based on the comparative study with linear TMDs, it was found that detuning effect observed in the considered TMDs can be found to exhibit a variation of the frequency of the order of 10 percent, which seems to be tolerable from an engineering point of view.

Abé (1996) proposed a design method of TMDs with bilinear hysteresis that enable the main structures with bilinearity to be efficiently controlled in a wide range of excitation levels. The bilinearity of either main structure or TMDs, which is given in Figure 2.4, is approximated in a linear form by means of stochastic averaging method. The linearized stiffness and damping coefficients for the bilinear model are expressed in terms of R as

$$k^{\mathrm{eq}} = A(R)/R \tag{2.8a}$$

$$c^{\mathrm{eq}} = c_o - B(R)/(\omega R) \tag{2.8b}$$

where ω is the excitation frequency, R is the amplitude of the response and

$$A(R) = \begin{cases} \dfrac{k_o R}{\pi}\left[\eta\theta + (1-\eta)\pi - \dfrac{\eta}{2}\sin(2\theta)\right] & \text{if } R > x_0 \\ R & \text{if } R \le x_0 \end{cases} \tag{2.9a}$$

$$B(R) = \begin{cases} -\dfrac{k_o R}{\pi}\sin^2\theta & \text{if } R > x_0 \\ 0 & \text{if } R \le x_0 \end{cases} \tag{2.9b}$$

$$\theta = \cos^{-1}\left(1 - \frac{x_0}{2R}\right), \tag{2.9c}$$

$$\eta = 1 - \frac{k_1}{k_0}. \tag{2.9d}$$

By applying this linearization, the steady-state response subjected to harmonic excitations is calculated by a frequency domain. The TMDs are designed to be always

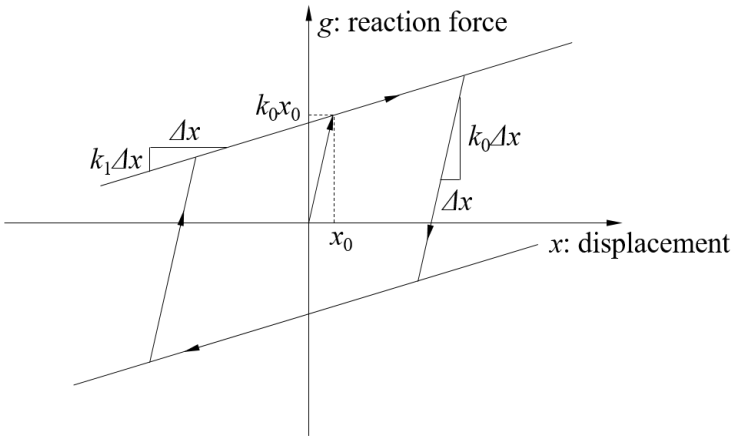

Figure 2.4: Force-displacement diagram of bilinear model

tuned to the changed dynamic properties of main structure. The author concluded that the appropriately designed bilinear TMDs outperform linear optimal TMDs even when the equivalent natural frequency and damping ratio of the main structure shift by bilinearity at the higher excitation levels.

Ricciardelli and Vickery (1999) considered a TMD with linear stiffness and dry friction damping and derived closed-form expressions for the optimum tuning and for the optimum friction force as well as for the steady-state amplitudes of vibration of main system. The authors also showed that the friction damper tends to be more effective as the amplitude of the excitation becomes large.

Poovarodom et al. (2003) investigated nonlinear MTMD, in which damping force induced by induced force of the immerse section is modeled as quadratic form. The results from the numerical study found that their effectiveness and robustness were similar to those of the linear MTMDs. The relevant test results were in good agreement with the results from the numerical study.

Rüdinger (2007) investigated the effect of TMD with nonlinear viscous damping elements. In calculating the RMS displacement of the main structure, the author

employed statistical linearization method, which is able to provide very accurate results. It was shown from the study that the optimal damping parameter values for the nonlinear TMD depend on the displacement magnitude and excitation intensity, in constrast to the case of a linear TMD. However, the response magnitude is relatively insensitive to the exact value of the damping parameters of the mass damper, and it is therefore not important to know the magnitude of the vibration too accurately.

Alexander and Schilder (2009) explored the performance of a nonlinear TMD, which is modeled as a two DOF system with a cubic nonlinearity. The numerical results conducted by the authors were negative since the TMD with a cubic nonlinearity and constant damping ratio does not provide an improvement over an optimal linear TMD. From an engnieering perspective the cubic hardening nonlinearity reduces only the amplitude of the higher-frequency response.

Gewei and Basu (2010) investigated the effectiveness of the nonlinear tuned mass dampers in which dry friction force is employed. In the analysis, they adopted harmonic solution and statistical linearization to calculate the vibrational response and then found the optimal friction coefficient of friction TMDs. It was found from the research that the optimal friction coefficient depends on the response of the TMD, which is almost proportional to the intensity of the excitation.

Love and Tait (2015) employed statistical non-linearization to represent the nonlinear damping as amplitude-dependent viscous dapming and predicted the RMS response of the structure-TMD system. They obtained probability density function for the TMD dispacement and estimated the peak response distribution.

2.5 Applications and Structural Implementations

2.5.1 Wind-induced vibration attenuation

In recent years, buildings have become more taller, lighter and flexible, and the wind effect on the dynamic response of buildings has become important. With an aim of attenuating the wind-induced response of a tall building, TMDs were widely implemented as an energy dissipation devices to the building systems. Examples of TMD applications for attenuation of wind-induced vibration are well documented in Kareem, Kijewski, and Tamura (1999).

Tanaka and Mak (1983) conducted wind tunnel model tests with a small scale of 1:1000, and showed that the TMD system was highly effective in suppressing the dynamic response of the building. The reduction of response was significant, in the range of 30 to 60%.

Kwok and Macdonald (1990) presented the wind-induced acceleration responses at the top of the Sydney Tower in Australia, and compared the responses before and after TMD installation. The results showed that both the peak along-wind and peak cross-wind acceleration responses were attenuated significantly after the installation of TMD.

Kawaguchi et al. (1992) simulated a time history wind force to predict the response of a building with a TMD, and investigated the suppressing effect of a TMD. Based on the numerical simulations, it was found that TMDs can mitigate the response of the primary mode of a building to around 60% when the mass ratio to the primary modal mass is 0.5%, and to around 45% with its mass ratio of 2%.

Liu et al. (2008) developed a mathematical model for predicting wind-induced vibrations of a high-rise building with a TMD when the soil-structure interation is involved. They found that TMDs are beneficial in reducing wind-induced vibrations of tall buildings, particularly being more effective for the higher soil stiffness.

Ghorbani-Tanha et al. (2009) examined the effective of TMD on the suppression of wind-induced motion of Milad Tower with a numerical analysis. In their analyses, the fluctuating wind speed is assumed to be a stochastic process identified by an appropriate power spectral density function. It was shown that a TMD of 400 ton at the sky dome connected with a spring tuned to the first natural frequency of the tower and with a viscous damper with a 7% damping ratio reduces the dynamic responses of the tower to around 60% of the uncontrolled case.

2.5.2 Seismic response mitigation

In seismic applications, TMDs can be utilized as an efficient apparatus that diminishes the internal loads in the structural members by attenuating the displacement of the building relative to the ground. Gupta and Chandrasekaran (1969) studied the seismic response of linear singled degree of freedom systems controlled by the TMD systems which provide elasto-plastic restoring force and viscous type of damping, and claimed that the TMDs are not effective for seismic excitations as compared to sinusoidal excitations.

Wirsching and Campbell (1973) determined the optimal parameters of STMD which minimize the response of a SDOF system under a stationary white noise base excitation, and showed that the absorber system is effective for both single- and multi-degree-of-freedom linear systems. In addition, they appointed the required additional studies which enables the device to be possibly implemented, including the effect of the absorber on higher modes of a structure, the behavior of the absorber under the nonlinear behavior of the primary structure, and the absorber with the various damping mechanism involving non-linear absorber damping. Wirsching and Yao (1973) demonstrated the adequacy of the TMD under a nonstationary stochastic process having statistical characteristics similar to actual earthquakes and showed that the absorber was found to be extremely effective in reducing the seismic response

thereby the probability of failure of a multistory structure.

Sladek and Klingner (1980) investigated the efficiency of TMDs designed by three different techniques according to Den Hartog, Wiesner, and Wirsching-Campbell under a strong ground motion. They considered the prototype building of 25-story with a mass ratio of 0.026% relative to the first-mode effective mass. It was found that all of the considered TMDs implemented are ineffective in reducing the maximum seismic response. They appointed such a inefficacy as the passiveness of the TMD, because if the maximum response occurs early in the record, the TMD may not have time to produce a significant effect.

Villaverde (1985) showed that the attachment of a small heavily-damped system in resonance can increase the damping of a guilding and reduce thus its response to earthquake excitation.

Clark (1988) compared the peak acceleration response of a main system without and with the 5% mass TMD design in single and multiple configuration, where the TMDs used in the study are designed according to Den Hartog's procedure as well. It was shown that single TMD is not effective in reducing response of multiple degree of freedom main structure, but multiple TMD systems can yield reduction between 40% and 60% for a 5% increase in the mass of the building.

Several researchers more positively reported the efficiency of TMDs under seismic excitations. Wirsching and Campbell (1973) and Wirsching and Yao (1973) showed that the absorber system is effective in reducing the mean response of the primary structure. Additionally, they noted that the effectiveness of the absorber may diminish when the primary structure exhibits high intensity seismic excitation because the natural frequency of the structure becomes smaller than the absorber frequency due to the elasto-plastic behavior.

Tsai (1995) applied the TMD into the base-isolated structures. It was shown that the response on base-isolated structures equipped with the TMD is quite dependent

on the input seismic motion. It was further discussed that combining TMD with base-isolation system can reconcile the drawbacks inherent in TMD-primary structure that TMDs are inefficient for the short period structure, which isolated structure lengthen the period.

Based on the optimal parameters obtained by using numerical searching procedure in equating equal damping ratio followed by the optimal values of the frequency ratio and the damping ratio of TMD, Sadek et al. (1997) showed that the TMDs according to the authors' optimal parameters can effectively reduce the displacement and acceleration response. Additionally, they showed that it is less effective in reducing the response when the TMDs are implemented in short period structure. They also emphasized that TMDs with a large mass ratio must be used for structures with higher damping ratios, implying that structures which exhibit highly nonlinear behavior should be equipped with TMDs with a higher mass ratio.

Soto-Brito and Ruiz (1999) conducted a suite of analyses involving SDOF systems and 22-story frame building, and concluded that the maximum roof displacements are more significantly reduced when the frames are subjected to moderate motions, rather than to high-intensity ones, in which the structural behavior are associated with linear behavior.

Wong and Chee (2004) discussed the efficacy in the energy perspective, and showed that TMDs are effective in limited condition with a moderate to long period of vibration than those for short period structures. In the similar to the discussion provided by Sadek et al. (1997), the authors also noticed that TMD is not effective in reducing the energy of the primary structures with the short natural period vibration of less than 1.3 sec, but became effectively if the period of the structure is longer than 2.0 sec.

A case study conducted by Pinkaew et al. (2003) again showed that although TMD is not effective in reducing the peak displacement of the controlled structure

after yielding, it can significantly reduce cumulative damage to the structure. They also emphasized that the inclusion of cumulative damage measure due to low cycle fatigue is important in order to properly evaluate TMD effectiveness under severe seismic excitation.

Li and Zhu (2006) tried to find the optimal parameters of the double TMDs, consisting of one larger mass block and one smaller mass block attached to the larger one, and showed that the proposed TMDs can exhibit their controllability with maintaining its robustness and effectiveness.

Li and Qu (2006) configured multiple TMDs with identical stiffness and damping coefficient but different mass for suppressing both translational and torsional responses. Taking into account the varying ratio of the torsional and translational modal frequencies, they showed that optimally designed MTMDs according to their optimization scheme can mitigate responses of both modes providing enough effectiveness and robustness of the control device. In similar, Lin et al. (2000) dealt with optimum installation location in plan and in elevation and moving direction with the consideration of torsional mode as well as translational modes. They noted that the floor corresponding to the tip of controlled mode shape is the optimum installed floor of TMD.

Chen and Wu (2001) proposed the strategies for determining the optimal location of TMDs for effectively reducing the floor acceleration of multistory building structures under earthquake loads. With a sequential procedure proposed by the authors, it was shown that MTMDs are not advantageous over a conventional TMD for displacement control.

Hoang et al. (2008) applied a TMD with purpose of retrofitting of the first longitudinal mode of Minato Bridge employing a floor deck isolation system that can be treated as the optimally designed TMD. They showed that the characteristic ground frequency is highly relevant to the optimal tuning frequency rather than the optimal

damping ratio of TMD. Based on the response spectrum analyses, they showed that the optimum TMD designed according to their scheme performs suitable for ground motion time histories of similar frequency content.

Leung et al. (2008) optimized the key parameters of TMDs for non-stationary random excitation applied to a linearly damped primary structure. It was shown from their numerical simulation on the equivalent SDOF system, the performance was satisfied.

Wong (2008) exhibits the effectiveness of emplying TMDs in terms of various forms of energy involving kinetic, damping and input energy, and concluded that the use of TMD can enhance the energy dissipation of the structure by accumulating a large amount of energy when the structure is at a point near yielding, and can help in transferring this storage energy to the structure at the less critical state. The same approach was adopted for the usage of multiple TMD in the successive research in Wong and Johnson (2009). It should be noted about their discussion that the inelastic structural performance is rather insensitive to the locations of TMD placements, and therefore either multiple TMDs placed at various levels or one TMD placed at the roof exhibits of no different performance. They also emphasized that TMDs may be ineffective if the earthquake ground motion is believed to cause significant inelastic demand in the upper structures, and one way to enhance the robustness of the TMD is to increase the member sized in the upper stories such that energy can be dissipated more efficiently. Wong and Harris (2012) studied the fragility analysis on the primary-TMD system, and concluded that while a TMD is ineffective in protecting a structure at earthquake levels associated with life safety (LS), it can enhance performance of the structure at low seismic levels where frame response can be predominantly elastic.

Recently, Sgobba and Marano (2010) carried out the optimal design of linear STMDs for structures with nonlinear behavior which is described by the Bouc-Wen hysteresis model. Taking into account both various mechanical situations such as the

strength reduction factor and the hardening ratio and soil conditions including soft and stiff soil, they investigated the optimal parameters of TMDs which minimizing mean displacement ratio, damage induced in inelastic region, mixed criterion. They concluded that the efficacy of STMD decreases as the strength ratio, which is the inverse of the strength reduction factor, or the post-yielding stiffness ratio increases because of detuning effect that occurs in the plastic region. Relevant to the observations, the use of TMD seems more effective in the case when the structure is in a moderate to long period of vibration compared to for short period structures.

2.5.3 Floor vibration control

In recent years, many vibration problems have been reported after they occurred in existing floors in buildings and footbridges. When the problematic situations occurred, the vibration performance of the floor should be improved through various available remedial measures, including reduction of vibration effects, relocation of vibration sources, reducing mass, damping increases, and stiffening the structure.

Among the available measures, installing TMDs can be efficient and economical for attenuating the floor vibration. One of the advantages of using TMDs is that TMDs are versatile because of its applicability without interrupting operational or human activities in the building. Moreover TMDs are versatile such that they can be designed in various shapes and sizes as needed, and as required to accommodate space limitations.

Webster and Vaicaitis (1992) implemented TMDs and demonstrated their efficiency in attenuating the vibration of an existing composite floor system. With the implemented TMDs, the floor vibrations were reduced by at least 60 percent. Moreover, the cost of the installation of TMDs was reduced to less than 15 percent of the estimated cost for structural stiffening with constructing new columns.

Setareh and Hanson (1992) applied five pairs of TMDs to control two distinct

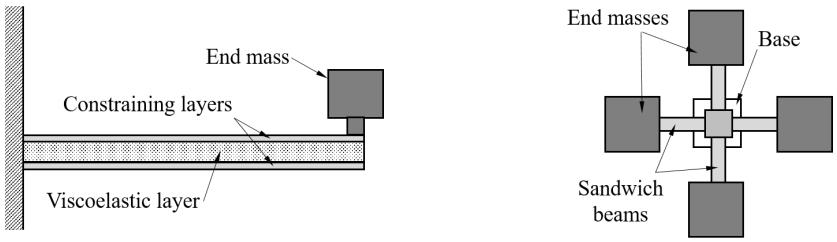

(a) Single sandwich beam TMD

(b) MTMD configuration

Figure 2.5: Schematic of a viscoelastic sandwich beam-type TMD and its MTMD configuration

modes of an existing balcony, two of which were targeted to the first mode with their mass ratio of about 3%, and the others were for the second mode with their mass ratio of about 1%. Results of the tests after implementation showed that the TMDs can effectively suppress the resonant vibration response, increasing the floor damping from the original value of 1.6% to about 8%.

Setareh et al. (2006) presented a pendulum TMD, of which mass is distributed along the pendulum arm, viscous dampers are attached to the end of the pendulum, and springs are designed as movable so that the natural frequency of the TMD can be fine-tuned. Based on analytical and experimental studies, it was shown that proposed PTMDs were effective in reducing excessive vibrations of floors due to human activities. It was also noted that TMDs may lose their efficacy due to off-tuning caused by floor occupancy.

Casado et al. (2010) implemented TMD with a mass ratio around 1% of the 51 meters span modal mass to fulfill the vibration serviceability requirements of an in-service lively footbridge. The field test results showed that the TMD of 1% mass ratio was enough to improve the efficient damping of the bridge providing considerable reduction in its acceleration response, and enabled the bridge to fulfill the comfort criteria recommended in most codes and guidelines.

Saidi et al. (2011) developed a cantilever-type TMD that consists of a sandwich beam incorporated with a constrained rubber layer, of which configuration is depicted in Figure 2.5a. The optimal parameters of the device including end mass, length of the beam and thickness of the rubber layer were determined according to the classical solution proposed by Den Hartog (1956). With experimental studies, it was shown that the proposed control device can mitigate the excessive floor vibration substantially. Nguyen et al. (2012) further developed the cantilever-type TMD in the form of MTMDs, each of which dynamic properties such as the natural frequency and damping ratio are identical (see Figure 2.5b). The developed TMD system is implemented in an existing office floor, and successfully reduced the floor vibrations by at least 40% to a level that was well within the acceptable limit for human comfort.

Through laboratory tests, Varela and Battista (2011) evaluated the performance of the TMDs in reducing the problematic vibrations induced by people walking on large span composite slabs. In this study, each of TMD incorporates with its mass of only 0.5% of the modal mass of the targeted mode and its value of the damping ratios fell in the range of 1 to 1.5%. The results showed that, for any of considered walking scenarios, the TMD provides significant reductions in excessive vibrations.

Kashani et al. (2012) presented the application of TMDs for attenuating excessive vibration of three large balcones at a performing arts center. Based on numerical and experimental studies of the balconies, it was shown that the TMDs effectively attracted oscillatory energy of the structure and dissipated it successfully.

A variety of numerical investigation on the efficiency of TMDs in floor vibration control were also conducted. Li et al. (2010) presented the application of MTMDs in mitigating crowd-induced vibration of footbridge. Based on the single footfall force model and followed by the crowd-footbridge random vibration model, the vibration prone to occur resonance can be substantially reduced. Recently, Van Nimmen et al. (2016) applied TMDs in reducing the excessive vibration of footbridge, and showed

its efficacy via numerical and experiments. Lievens et al. (2016) also proposed a design methodology by which the optimal parameters for quantifying its robustness and efficacy can be considered. Yang et al. (2015b) designed and implemented two-DOF TMD in mitigating of milling vibration, and Wang et al. (2003) evaluated the applicability of TMDs to suppress train-induced vibration on bridges.

2.6 Other Issues

2.6.1 Stroke limitations

Considering the stroke limitations of TMDs is of importance when the structure is expected to be exposed under a severe conditions such as earthquake excitation. In order to configure the optimal TMDs within the stroke limitation constraints, some researchers tackled the problem in the perspective of multi-objective optimization.

Wang et al. (2009) proposed a two-stage optimization, in which the structural response is to be minimized as usual strategies at the first stage, and the RMS response of the TMD with weighting an unknown factor is then incorporated as a part of the objective function that is to be minimized. Later, Lin et al. (2010) extended the optimization scheme into the case of MTMDs optimization, and verified their design algorithm with shaking table tests of a three-story building. The test results showed that the MTMD designed according to their approach is both effective in reducing the structural response and successful in suppressing their stroke.

The second and final stage of the optimization procedure is of worth to discuss more in detailed ways. In their procedure, the objective function is set as a linear combination of two quadratic functions – RMS response of the primary structure and of the TMD – and a factor which accounts for determining the weighting to whether the optimization procedure would be weighting. Such an optimization procedure is a kind of Pareto optimization, so that there can be a compromising solution.

Also it should be stressed that the weighing factor which determines the weighting ratio between the structural vibration response of the primary structure and the response of the MTMDs is chosen as arbitrary rather than quantified in a deducing way. Hence it is of importance to provide the way of determining such a weighting factor a priori.

2.6.2 Reliability-based optimization

There are many potential reasons that detuning could occur such as change in structural properties over time, liquid leakage of damping device or inaccurate estimation of dynamic properties. In order to overcome the risks associated with detrimental effect of detuning, researchers investigated the optimal design techniques that are able to take account for uncertainty.

Chakraborty and Roy (2011) presented optimal TMDs that minimizes the probability of failure of the primary structure under stochastic earthquake, modeling the associated system parameters as uncertain but bounded type parameters. First, the authors formulated an optimization problem that involves the reliability of a mechanical system with a TMD. The objective function of the optimization problem is the conditional failure probability $p_f(X)$ in a given period $[0, T]$ for the performance quantity y_s under the structural and the excitation model specified by X as follows:

$$\begin{aligned} p_f(X) &= 1 - \exp[-\nu_\beta(X)T] \\ &= 1 - \exp\left[-\frac{\sigma_{\dot{y}_s}(X)}{\pi\sigma_{y_s}(X)}\exp\left(-\frac{\beta^2}{2\sigma^2_{y_s}(X)}\right)\right] \end{aligned} \tag{2.10}$$

where σ_{y_s} and $\sigma_{\dot{y}_s}$ are the RMS response of the considered quantity y_s and its derivative $\dot{y}_s$, respectively, and β is a given threshold value in a given life time period T.

Then the sensitivity of probability of failure is explicitly obtained by differentiating the quantity with respect to the i-th uncertain parameter x_i. Thereby, the interval

region of the probability of failure function is separated out to the upper and lower bound p_f^u and p_f^l as follows:

$$p_f^u = \bar{p}_f + \sum_{i=1}^{m} \left| \frac{\partial p_f}{\partial x_i} \right| \Delta x_i \tag{2.11a}$$

$$p_f^l = \bar{p}_f - \sum_{i=1}^{m} \left| \frac{\partial p_f}{\partial x_i} \right| \Delta x_i \tag{2.11b}$$

where $\bar{p}_f$ is the probability of failure under the nominally determined X, and Δx_i represents the maximum deviation of x_i from its nominal value.

Marano, Greco, and Sgobba (2010) conducted a comparative study on different optimization criteria: conventional deterministic optimization criterion, robust single-objective criterion and robust multi-objective criterion. As the deterministic criterion concerns the objective function under a nominal condition, the other two robust criteria consider the first two statistical moments of a predefined objective function, which includes the first two statistical moments of the objective function. The authors investigated the optimal design of TMD with a direct perturbation method that accounts for the uncertainty for structural parameters and soil parameters. The authors found that under the small variation the optimal design via conventional way does not differ from the robustness considered scheme. As the uncertainty increases, however, the conventional solution of TMD cannot guarantee the optimum of the mean response and, further, the variance of the response would be even increases resulting the lack of robustness. Lucchini, Greco, Marano, and Monti (2013) investigated the optimal TMDs, considering the robust multi-objective criterion as Marano, Greco, and Sgobba (2010) conducted but a physical interpretation is additionally considered.

Yu et al. (2013) proposed a framework for a reliability based robust optimization and applied it into the optimal TMD design. The framework seeks to optimize the structural RMS displacement with constraints on a prescribed threshold of the

probability of failure of the primary structure. To improve computational efficiency, the authors proposed a sequential strategy that decouple reliability analysis from the optimization procedure, and succeeded in finding optimal solutions while reducing the number of complicated reliability analysis.

Mrabet et al. (2015) presented a technique for optimization of TMD in the presence of uncertain bound structural parameters. The technique involves two stage, in which the first stage is basically based on the stochastic response such as RMS response or the failure probability under the stationary process, and the second stage tries to evaluate the extreme value of the indices.

The statistics of the response indices were estimated by using direct perturbation method, which consists in approximating the response as a polynomial of the uncertain parameters (Lutes and Sarkani, 2004). However, such a way is not convenient and contains an error when one tries to consider the asymmetric probability density. One of the lacks is that it is not available to deal with Gumbel distribution, which is one of the widely used distribution for extreme events.

Rathi and Chakraborty (2016) conducted a similar way to the Marano et al. (2010) approach, except for the response surface method, one of the estimating techniques, was adapted. Further, owing to the way of response surface method, they can find the optimal conditions with regarding to the Gumbel distribution of the ground input intensity.

$$\begin{aligned} &\underset{x}{\text{minimize}} && J(x, y^*) \\ &\text{subject to} && J_{th} - (\mu_J + \beta\sigma_J) \leq 0 \\ &&& x \in \Omega_x \, y \in \Omega_y \end{aligned} \tag{2.12}$$

Chapter 3

Linear Multiple Tuned Mass Dampers

This study presents optimal design and analysis of linear multiple tuned mass dampers with various configurations. Two different optimization techniques are employed: Nominal Performance Optimization (NPO) and Robust Performance Optimization (RPO). The NPO minimizes the objective function that is deterministic, whereas the RPO minimizes the mean value of the objective function, assuming that the associated structural parameters are probabilistic. Six of practical configurations are formulated and comparatively analyzed, and each of the configurations is constrained in a way of linearly distributed frequency ratios, uniformly distributed damping coefficients, linearly distributed mass ratios, and/or combinations thereof. An approximate design formula is developed for $\text{LMTMD}_{\gamma\zeta}$ configuration, which is as efficient as the best optimal configuration. Further, this study provides contour maps that enable designers to accommodate the moving mass within maximum stroke limitation.

3.1 Introduction

Tuned mass damper (TMD) is one of the fascinating vibration control devices which dissipates the vibration energy of a main structure through an internal damping element. Since Frahm (1911) proposed its concept through his patent, numerous studies have been conducted on the optimal solution of TMDs in order to determine the parameters such as optimal frequency and optimal damping ratio. The solution proposed by Den Hartog (1956) is still widely used in the academic area as well as in the application fields. The optimal conditions of Warburton (1982), which accounts for various loading conditions and objective functions, is also popular nowadays.

Multiple tuned mass damper (MTMD) is a system consists of multiple units of TMDs, often referred to as the case where each of TMDs has different dynamic characteristics. In the early stage of research, MTMD configurations with simplified and limited conditions were discussed so as to reduce the number of associated design variables. For instance, the MTMD of large numbers of units with equally spaced natural frequencies and each of which having equal damping constant was studied by Xu and Igusa (1992) based on an asymptotic analysis, and it was shown that such a MTMD is effective in reducing the response of the main structure. For a finite number of MTMDs with similar constraints, Joshi and Jangid (1997) and Jangid (1999) found the optimal parameters of the MTMD for undamped and damped primary structure, respectively. MTMDs with equal damping ratios and equally spaced natural frequencies were also investigated by various researchers including Yamaguchi and Harnpornchai (1993), Abé and Fujino (1994), and Kareem and Kline (1995).

Until recently, various studies have been conducted for the MTMDs with relaxed constraints, for example, Igusa and Xu (1994), Li (2002), Hoang, Fujino, and Warnitchai (2008), Zuo and Nayfeh (2005), Li and Ni (2007), and Yang, Sedaghati, and Esmailzadeh (2015a). The main differences in these studies involve 1) considered exci-

tation, such as harmonic forcing function and the ground acceleration, 2) the objective function, such as the RMS response of the primary structure or the maximum of the frequency response and 3) employed optimization strategies.

Existing studies, however, only conducted a comparison with other configurations in a limited way. Li and Ni (2007), for instance, only compared the performance between their non-uniformly distributed MTMD and the one with equal frequency spacing and damping ratio on the basis of frequency response function. Li (2002), one of the comparative studies on various configurations, provided the optimal parameters only for the case where the natural frequencies are equally spaced. Hoang, Fujino, and Warnitchai (2008) also conducted a similar study. Li and Liu (2002) also conducted.

Meanwhile, in designing the optimal TMD, it is crucial to consider the performance deterioration caused by so-called detuning effect, in which the natural frequency of the TMD is deviated from that of the main structure, thus its control performance cannot be fully attained. Several researchers proposed the methods for the robust design of MTMDs including Lucchini, Greco, Marano, and Monti (2013), Hoang and Warnitchai (2005), De, Wojtkiewicz, and Johnson (2017). However, the study on the design of MTMDs considering robustness is still very limited, requiring researches on that subject.

The primary purpose of this study is to develop a framework for design of LMTMDs, which can provide guidance about all aspects of the LMTMDs including the MTMD configurations, issue on the robustness, and the stroke limitation issue. First, this study investigates the optimal parameters of various LMTMD configurations, of which constraints are such as the frequency ratios, damping ratios, mass distributions and combinations thereof. Second, two different optimization schemes are employed: Nominal performance optimization (NPO) and Robust performance optimization (RPO). NPO searches a solution the minimizes the objective function itself, while RPO minimizes the statistically estimated objective function, assuming that

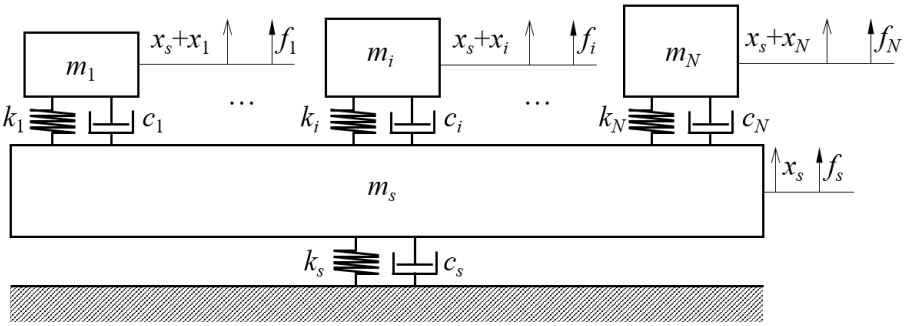

Figure 3.1: Structure-LMTMD system

the associated parameters are probabilistic rather than deterministic. For the RPO problem, this study adopted Point estimation method (PEM), which is one of the simple and reasonable methods for evaluating the statistical property of a complicated function. Third, in order to allow the designer to consider the performance evaluation and the stroke limitations simultaneously, this study provides contour maps for the RMS displacement of the main structure and the largest RMS displacement of the LMTMDs that can be useful in the design process.

3.2 Model Formulation

3.2.1 Governing equations of motion

Consider a system comprised of a primary structure and N units of linear TMD (see Figure 3.1). The equations of motion of the structure-MTMD system can be written as

$$(m_s + m_T)\ddot{x}_s + \sum_{i=1}^{N} m_i\ddot{x}_i + c_s\dot{x} + k_s x = f_s \tag{3.1a}$$

$$m_i(\ddot{x}_s + \ddot{x}_i) + c_i\dot{x}_i + k_i x_i = f_i \qquad i = 1, \cdots, N \tag{3.1b}$$

where m_s, c_s and k_s are the mass, damping coefficient and spring constant of the primary structure; m_i, c_i and k_i are the mass, damping coefficient and spring constant of the i-th TMD; N is the number of TMDs; m_T is the total mass of TMDs defined by $\sum_{i=1}^{N} m_i$; x_s is the displacement of the primary structure, and x_i is the relative displacement between the i-th TMD and the primary structure; A dot notation signifies a derivative with respect to time t; The external force exerted on the primary structure and on the i-th unit of the MTMD are denoted as f_s, and f_i, respectively. When the whole system is subjected to a zero-mean white-noise base acceleration, each force term f_i is zero and the force term exerted on the primary structure is $-(m_s+m_T)\ddot{u}_g$, where $\ddot{u}_g$ is the ground acceleration with a constant spectral intensity $S_{\ddot{u}_g}$ given by

$$E[\ddot{u}_g(t)\ddot{u}_g(t+\Delta t)] = 2\pi S_{\ddot{u}_g}\delta(\Delta t) \tag{3.2}$$

where $E[\cdot]$ is an expectation operator and $\delta(\cdot)$ is the Dirac-delta function.

In order to standardize the subsequent treatment, we introduce the following terms:

$$\mu_i = \frac{m_i}{m_s}, \tag{3.3a}$$

$$\gamma_i = \frac{\omega_i}{\omega_s} = \sqrt{\frac{k_i}{m_i}}\sqrt{\frac{m_s}{k_s}} = \sqrt{\frac{k_i}{k_s}}\mu_i^{-1/2}, \tag{3.3b}$$

$$\zeta_i = \frac{c_i}{2\gamma_i m_i \omega_s}, \tag{3.3c}$$

and let μ_T be the total mass ratio defined by $\sum_{i=1}^{N} \mu_i$. With these terms, the equations of motion becomes

$$(1+\mu_T)\ddot{x}_s + \sum_{i=1}^{N} \mu_i \ddot{x}_i + 2\zeta_s\omega_s\dot{x} + \omega_s^2 x = -(1+\mu_T)\ddot{u}_g \tag{3.4a}$$

$$\ddot{x}_s + \ddot{x}_i + 2\zeta_i\gamma_i\omega_s\dot{x}_i + \gamma_i^2\omega_s^2 x_i = 0 \qquad i = 1, \cdots, N. \tag{3.4b}$$

A suitable substituting of non-dimensional variables enables us simplify and parameterize the equations of motion. First, x_s and x_i can be non-dimensionalized by normalizing them to the RMS displacement of the uncontrolled structure x_{ref}. With the help of the theoretical results for the stochastic response of a single-degree-of-freedom (SDOF) system excited by a white-noise stationary process (Lutes and Sarkani, 2004), the RMS displacement of the uncontrolled system can be calculated by

$$x_{\text{ref}} = \sqrt{\frac{\pi S_{\ddot{u}_g}}{2\zeta_s\omega_s^3}}. \tag{3.5}$$

Further, introducing non-dimensional displacements $y_s = x_s/x_{\text{ref}}$ and $y_i = x_i/x_{\text{ref}}$, and a time scale $t_o = \omega_s t$, the equations of motion can be non-dimensionalized as follows:

$$(1+\mu_T)y_s'' + \sum_{i=1}^{N}\mu_i y_i' + 2\zeta_s y_s' + y_s = -(1+\mu_T)w_g'' \tag{3.6a}$$

$$y_s'' + y_i'' + 2\gamma_i\zeta_i y_i' + \gamma_i^2 y_i = 0 \qquad i = 1, \cdots, N \tag{3.6b}$$

where a prime notation denotes the derivation with respect to the non-dimensional time t_o, and w_g'' is the non-dimensionalized ground acceleration exerted on the primary structure with its spectral intensity $S_{w_g''}$ given by

$$S_{w_g''} = \frac{S_{\ddot{u}_g}}{x_{\text{ref}}^2\omega_s^3} = \frac{2\zeta_s}{\pi}. \tag{3.7}$$

Rearranging Eq. (3.6) into the matrix form yields the following expression:

$$My'' + Cy' + Ky = fw_g'' \tag{3.8}$$

where $y = [y_s, y_1, \cdots, y_N]^{\mathrm{T}}$, $f = [-(1+\mu_T), 0, \cdots, 0]^{\mathrm{T}}$ and the corresponding matrices are given by

$$M = \begin{bmatrix} 1+\mu_T & \mu_1 & \cdots & \mu_N \\ 1 & 1 & \cdots & 0 \\ \vdots & \vdots & \ddots & \vdots \\ 1 & 0 & \cdots & 1 \end{bmatrix}, \tag{3.9a}$$

$$C = \begin{bmatrix} 2\zeta_s & 0 & \cdots & 0 \\ 0 & 2\gamma_1\zeta_1 & \cdots & 0 \\ \vdots & \vdots & \ddots & \vdots \\ 0 & 0 & \cdots & 2\gamma_N\zeta_N \end{bmatrix}, \tag{3.9b}$$

$$K = \begin{bmatrix} 1 & 0 & \cdots & 0 \\ 0 & \gamma_1^2 & \cdots & 0 \\ \vdots & \vdots & \ddots & \vdots \\ 0 & 0 & \cdots & \gamma_N^2 \end{bmatrix}. \tag{3.9c}$$

With introducing a non-dimensional state vector $z = [y^{\mathrm{T}}, y'^{\mathrm{T}}]^{\mathrm{T}}$, a first-order state-space model can be formulated as follows:

$$z' = Az + Bw_g'' \tag{3.10}$$

where the corresponding matrices A and B are given by

$$A = \begin{bmatrix} O & I \\ -M^{-1}K & -M^{-1}C \end{bmatrix}, \tag{3.11a}$$

$$B = \begin{bmatrix} O \\ -f \end{bmatrix}. \tag{3.11b}$$

If the external loading w_g'' is a steady-state stationary white noise with its spectral strength $S_{w_g''}$ as assumed previously, the covariance matrix $Q = E[zz^{\mathrm{T}}]$ can be obtained by solving the following Lyapunov equation (Lutes and Sarkani, 2004):

$$AQ + QA^{\mathrm{T}} + 2\pi S_{w_g''} BB^{\mathrm{T}} = O. \tag{3.12}$$

3.2.2 LMTMD configurations

This study considers six of practical LMTMD configurations: LMTMD_{o} is a configuration on which no constraint on the frequency ratios or the damping coefficients is imposed; LMTMD_{γ} is the case where the frequency ratios are linearly distributed; LMTMD_{ζ} is the case where the damping constants are uniformly distributed; $\text{LMTMD}_{\gamma\zeta}$ is the case in which the frequency ratios and the damping ratios are distributed linearly and uniformly, respectively; LMTMD_{μ} and $\text{LMTMD}_{\mu\zeta}$ are the ones that the masses are linearly distributed, but an additional restraint of equal damping constants is imposed upon $\text{LMTMD}_{\mu\zeta}$. For all of these configurations, the stiffness of each TMD is presumed to be identical. The constraints for the considered LMTMD configurations are summarized in Table 3.1.

Table 3.1: Constraints for considered LMTMD configurations

Configuration	Constraints			
	Masses	Damping coefficients	Spring constants	Frequency ratios
LMTMD_{o}	-	-	U†	-
LMTMD_{γ}	C†	-	U	L†
LMTMD_{ζ}	-	U	U	-
$\text{LMTMD}_{\gamma\zeta}$	C	U	U	L
LMTMD_{μ}	L	-	U	C
$\text{LMTMD}_{\mu\zeta}$	L	U	U	C

†: U = Uniformly distributed, C = Constrained and L = Linearly distributed.

Spring constants uniformly distributed

One of the practical configurations is to incorporate springs having identical stiffness. Given that the spring constants are uniformly distributed, the mass ratio of the i-th TMD, μ_i, is expressed in terms of the total mass ratio μ_T and the frequency ratios γ_i. Suppose that the spring constant of each TMD is identical to k_o. Then according to its definition Eq. (3.3b), the mass ratio becomes

$$\mu_i = \frac{k_o}{k_s}\gamma_i^{-2} \qquad i = 1, \cdots, N \tag{3.13}$$

where k_s is the stiffness of the primary structure. Then, adding up all the mass ratios of Eq. (3.13) gives the following expression:

$$\frac{k_o}{k_s} = \frac{\mu_T}{\sum_{i=1}^{N} \gamma_i^{-2}}. \tag{3.14}$$

Substituting Eq. (3.14) into Eq. (3.13) gives the expression of μ_i written in terms of the frequency ratios γ_i and a predetermined total mass ratio μ_T as follows:

$$\mu_i = \frac{\gamma_i^{-2}}{\sum_{i=1}^{N} \gamma_i^{-2}}\mu_T \qquad i = 1, \cdots, N. \tag{3.15}$$

Equation (3.15) implies that the mass ratios of TMDs can be completely replaced with the terms of frequency ratios. Accordingly, if no additional constraint is imposed upon just as $\mathrm{LMTMD_o}$, the associated design vector γ_d is given by

$$\gamma_d = [\gamma_1, \cdots, \gamma_N]^{\mathrm{T}}. \tag{3.16}$$

Frequency ratios linearly distributed

If the frequency ratios are linearly distributed (that is, those are equally spaced), only two of those determine the whole frequency ratios. Under the constraint, the frequency ratio of the i-th TMD is expressed as follows:

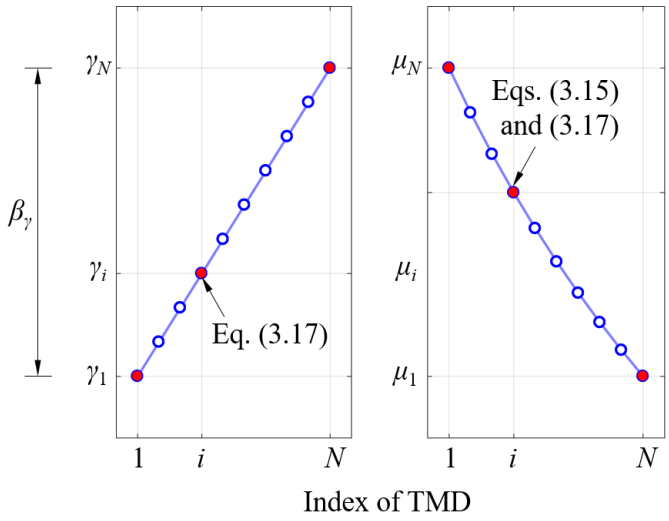

Figure 3.2: Spatial aspects of constraint for linearly distributed frequency ratios

$$\gamma_i = \gamma_1 + \frac{i-1}{N-1}\beta_\gamma \qquad i = 1, \cdots, N. \tag{3.17}$$

Note that the frequency ratios can be determined by the first frequency ratio, and the bandwidth determined as $\beta_\gamma = \gamma_N - \gamma_1$. Thus under the constraint for linearly-constrained frequency ratios, the associated design vector for frequency ratios γ_d is given by

$$\gamma_d = [\gamma_1, \beta_\gamma]^{\mathrm{T}}, \tag{3.18}$$

and the remained frequency ratios can be determined by Eq. (3.17).

Accoridng to this constraint, the distribution of masses is also determined directly. Figure 3.2 graphically represents the spatial aspects of the constraint for linearly-constrained frequency ratios. The masses of the TMDs are found to be densely distributed in a heavy side, and sparsely in a light side. Such a distributed pattern is

attributed to the relationship written in Eq. (3.15) that the mass ratio is inversely proportional to the square of the frequency ratio.

Damping coefficients uniformly distributed

Given that the viscous coefficients of MTMD are uniformly distributed (that is, those are identical), associated damping ratios yield to be proportional to the frequency ratios. Suppose that the viscous coefficient is identical to c_o. Then corresponding constraint is given by

$$c_1 = c_2 = \cdots = c_N = c_o. \tag{3.19}$$

Or equivalently, Eq. (3.15) can be rewritten in terms of normalized variables as follows:

$$2\mu_1\gamma_1\omega_s\zeta_1 = 2\mu_2\gamma_2\omega_s\zeta_2 = \cdots = 2\mu_N\gamma_N\omega_s\zeta_N = c_o/m_s. \tag{3.20}$$

Eliminating mass ratios μ_i by substituting Eq. (3.15) into Eq. (3.20), and manipulating yields the following relationship:

$$\gamma_1^{-1}\zeta_1 = \gamma_2^{-1}\zeta_2 = \cdots = \gamma_N^{-1}\zeta_N = \zeta_o \tag{3.21}$$

or,

$$\zeta_i = \gamma_i\zeta_o \qquad i = 1, \cdots, N \tag{3.22}$$

where ζ_o is a fictitious damping ratio given by

$$\zeta_o = \frac{\sum_{i=1}^{N}\gamma_i^{-2}c_o}{2\mu_T m_s\omega_s}. \tag{3.23}$$

It can be seen from Eq. (3.22) that the damping ratio is proportional to the frequency ratio, and the only independent design variable for the damping coefficient constraint is the fictitious damping ratio as

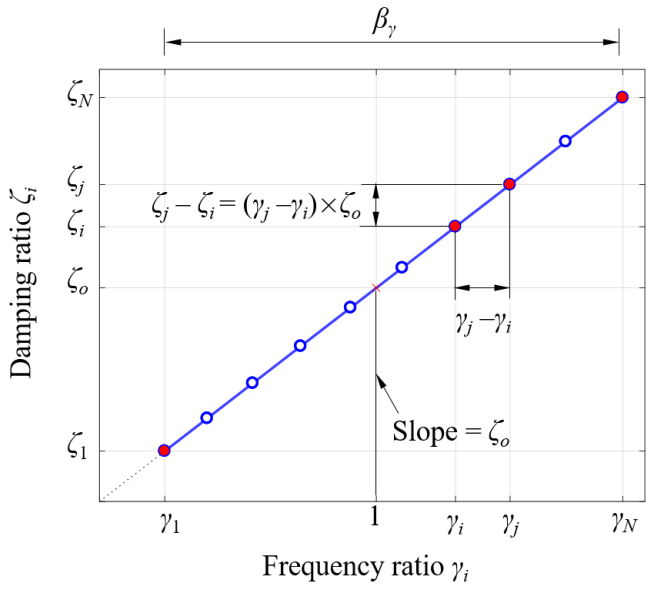

Figure 3.3: Spatial aspects of constraint for equal damping coefficients

$$\zeta_d = \zeta_o. \tag{3.24}$$

Figure 3.4 shows the spatial characteristics of the constraint for equal damping coefficients. In $(\gamma - \zeta)$ space, feasible points (γ_i^*, ζ_i^*) are restricted to be located on a straight line that passes through the origin of the space. In a geometrical sense, the fictitious quantity ζ_o can be read from the ζ^* that coincides with the unity frequency ratio, and can be interpreted as a slope of the straight line.

TMD masses linearly distributed

Figure 3.4 depicts the spatial distributions of the linearly-constrained masses. Under this constraint, the frequency ratios are relatively attracted to the lower side, because the mass ratios of the TMDs are distributed to be inversely proportional to the squared frequency ratio. The frequency ratio of the i-th TMD for the constraint is

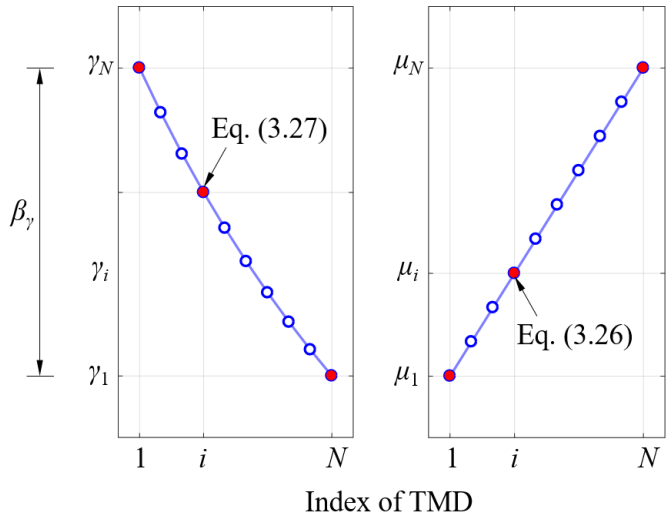

Figure 3.4: Spatial aspects of constraint for linearly distributed masses

expressed as follows:

$$\mu_i = \mu_1 + \frac{i-1}{N-1}(\mu_N - \mu_1) \qquad i = 1, \cdots, N. \tag{3.25}$$

Substituting Eq. (3.3b) into Eq. (3.25) gives

$$\mu_i = \frac{\mu_T}{\sum_{i=1}^{N} \gamma_i^{-2}} \left[\gamma_1^{-2} + \frac{i-1}{N-1}(\gamma_N^{-2} - \gamma_1^{-2}) \right] \qquad i = 1, \cdots, N. \tag{3.26}$$

Again substituting $\mu_T / \sum_{i=1}^{N} \gamma_i^{-2}$ with Eq. (3.26) and eliminating μ_i for both hand sides gives the following equation:

$$\gamma_i^{-2} = \gamma_1^{-2} + \frac{i-1}{N-1}(\gamma_N^{-2} - \gamma_1^{-2}) \qquad i = 1, \cdots, N. \tag{3.27}$$

The equation implies that the mass ratios of the TMDs can be completely replaced by the frequency ratios. Accordingly, if no additional constraint is imposed upon a configuration just as LMTMD_o, the associated design vectors γ_d is given as follows:

$$\gamma_d = [\gamma_1, \beta\gamma]^{\mathrm{T}} \tag{3.28}$$

where β_γ is the frequency ratio bandwidth defined by $\gamma_N - \gamma_1$. The remained frequency ratios can be determined by Eq. (3.27).

3.3 Optimization Strategies

This section introduces two different strategies to find the optimal solutions, which we call Nominal performance optimization and Robust performance optimization. Nominal performance optimization considers that the only source of randomness is in the loading that can be aptly modeled as a stochastic process, whereas all associated parameters are treated as deterministic. Robust performance optimization, on the other hand, considers not only the randomness of the loading but also the uncertainty involved in the structural parameters.

3.3.1 Nominal performance optimization

Nominal performance optimization (NPO) refers to an optimization technique that considers all associated parameters to be deterministic. In NPO, the external loading is modeled as a stochastic process, but the structural parameters such as the natural frequency of primary structure are treated to be deterministic values.

The response quantities of interest is the RMS displacement of the controlled main structure normalized to that of the uncontrolled one, σ_{y_s}. Due to its definition, the non-dimensional displacement of main structure σ_{y_s} would be in a range of zero to unity. Also it can be interpreted as a quantity for control efficiency such that σ_{y_s} is zero if the TMD completely suppress the vibration of main structure, and is unity when the TMD has no effect. The mathematical description of the response of quantity can be established as follows:

$$\sigma_{y_s}^2 = E[y_s^2] = E[(s^{\mathrm{T}}z)^{\mathrm{T}}s^{\mathrm{T}}z] = \mathrm{tr}[SQ] \tag{3.29}$$

where $\mathrm{tr}[\cdot]$ is a trace operator, $s = [1, 0, \cdots, 0]^{\mathrm{T}}$ is the weighting vector corresponding to sifting the structural displacement, and S is the weighting matrix which can be calculated by $S = ss^{\mathrm{T}}$.

The optimization problem is formulated as:

$$\begin{aligned} &\underset{\gamma_d,\,\zeta_d}{\text{minimize}} && J = \sigma_{y_s} \\ &\text{subject to} && \gamma_d \in \Omega_\gamma,\ \zeta_d \in \Omega_\zeta \end{aligned} \tag{3.30}$$

where γ_d and ζ_d are the design variable vectors defined in the previous section that corresponds to appropriate constraints, and Ω_γ and Ω_ζ are the feasible regions for γ_d and ζ_d, which are defined as positive orthants for the associated variables, respectively.

In the optimization process, a feasible starting point of the design variables affects the number of function evaluations to find the solution. One can provide the initial point by adapting the classical solutions for STMD, for example, those proposed by Warburton (1982):

$$\gamma^* = \frac{\sqrt{1+\mu_T/2}}{1+\mu_T}, \tag{3.31a}$$

$$\zeta^* = \sqrt{\frac{\mu_T(1+3\mu_T/4)}{4(1+\mu_T)(1+\mu_T/2)}}. \tag{3.31b}$$

where an asterisk in superscript (*) after a variable signifies that the variable is at its optimum.

The objective function is evaluated by solving Lyapunov equation, which can be efficiently solved by the well-established algorithm proposed by Bartels and Stewart (1972), which is implemented in a commercial program such as MATLAB®. In the optimization procedure, this study adapted an iterative method for solving a sequence of Quadratic Programming Sub-problems for its superior rate of convergence. At each iteration, to make an approximation of the Hessian matrix, Broyden-Fletcher-Goldfarb-Shanno algorithm was adopted for its effectiveness and good performance even for non-smooth optimization problems (Coleman et al., 1999).

3.3.2 Robust performance optimization

Robust performance optimization (RPO) is an extension of the NPO, concerning that the associated structural parameters are uncertain. The uncertainty may arise in various ways such as modeling error in identifying the structural properties, or random deterioration of material or structural properties over time. Modeling the associated as random variables gives the response quantity such as the RMS displacement also being a random variable. In order to accommodate random variables, the uncertain system should be distinguished from a nominal system.

Frequency-perturbed system

Here we define $\omega_{s,p}$ as the natural frequency of primary system, which is distinguished from the nominal one, ω_s. As done earlier, we normalize the equations of motion with respect to the displacement of the uncontrolled primary structure, but with the one of perturbed system. Again with the theoretical results for the stochastic response of a single-degree-of-freedom system excited by a white-noise stationary process, the RMS displacement, or the reference displacement, of the uncontrolled system is calculated by

$$x_{\text{ref}} = \sqrt{\frac{\pi S_{\ddot{u}_g}}{2\zeta_s \omega_{s,p}^3}} \tag{3.32}$$

Further, one can non-dimensionalize the above equations so as to simplify and standardize the problem. Introducing a nondimensionalized counterpart time scale $t_o = \omega_{s,p} t$ and nondimensional displacements $y_s = x_s / x_{\text{ref}}$ and $y_i = x_i / x_{\text{ref}}$, the equations of motion can be reformulated as follows:

$$(1+\mu_T) y_s'' + \sum_{i=1}^{N} \mu_i y_i' + 2\zeta_s \kappa y_s' + \kappa^2 y_s = -(1+\mu_T) w_g'' \tag{3.33a}$$

$$y_s'' + y_i'' + 2\gamma_i \zeta_i \kappa y_i' + \gamma_i^2 \kappa^2 y_i = 0 \qquad i = 1, \cdots, N \tag{3.33b}$$

where $\kappa = \omega_s/\omega_{s,p}$ is a factor that quantifies the extent of natural frequency perturbation, and w_g'' is the non-dimensionalized ground acceleration exerted on the primary structure with its spectral intensity of

$$S_{w_g''} = \frac{S_{\ddot{u}_g}}{x_o^2 \omega_{s,p}^3} = \frac{2\zeta_s}{\pi}. \tag{3.34}$$

In comparison Eq. (3.6), the perturbation factor in Eq. (3.33) allows for considering the uncertainty of the natural frequency of the primary structure. Hence the optimization problem defined by Eq. (3.30) can be modified in a statistical sense as follows:

$$\begin{aligned} &\underset{\gamma_d,\, \zeta_d}{\text{minimize}} && J = E[\sigma_{y_s}] \\ &\text{subject to} && \gamma_d \in \Omega_\gamma,\ \zeta_d \in \Omega_\zeta \end{aligned} \tag{3.35}$$

Compared to the NPO problem formulated, the RPO problem utilizes an expectation quantity to construct the objective function. Various techniques to evaluate the objective function can be adopted such as Monte Carlo Simulation (Yu, Gillot, and Ichchou, 2013), Direct Perturbation Method (Lucchini, Greco, Marano, and Monti, 2013; Marano, Greco, and Sgobba, 2010), and Response Surface Method (Rathi and Chakraborty, 2016). Among those possible techniques, this study employed point estimation method, which is one of the simple and efficient methods in the purpose.

Point Estimation Method

Point estimation method (PEM) is a class of numerical methods for evaluating the statistical moments of a given function that consists of random input variables. A typical work out of the method involves (1) determining specific points of input variables

and associated weighting factors, followed by (2) evaluating the statistical moments of the given function at the discrete points, and (3) combining all of evaluated statistical moments with associated weighting factors for the final calculation. The numerical answer can be treated as an approximate value of the statistical moments of the given function.

The PEM is effective and powerful compared to several relevant techniques such as direct integration method, Monte Carlo Simulation and Response Surface Method, especially when the associated random variables are in a large number. Some details on the determination of 'points' varies depending on the number of the specific points per an input variable.This study dealt with $2N + 1$ scheme which requires $2N + 1$ specific points per an input variable. The procedure for computing the moments of the output variables are summarized in Appendix A. More details on its theoretical aspects can be found in the literature Rosenblueth (1975) and Hong (1998), and those on its applications can also be found in Morales and Perez-Ruiz (2007) and Caramia et al. (2010).

Consider the objective function of the RPO problem defined by Eq. (3.35), and the perturbation variable of natural frequency. In this case, the perturbation factor κ is an uncertain variable with its standard derivation σ_κ. Followed by the procedure described in Appendix A, the two points and associated weighting factors are determined to be $\kappa_\mu = 1, \kappa_1 = 1 + \sqrt{3}\sigma_\kappa, \kappa_2 = 1 - \sqrt{3}\sigma_\kappa$; and $w_\mu = 2/3, w_1 = w_2 = 1/6$, respectively.

The mean of the objective function, hence, can be evaluated by following formula:

$$E[\sigma_{y_s}] = \sum_{k=1}^{2} w_k \sigma_{y_s}(\kappa_k) + w_\mu \sigma_{y_s}(\kappa_\mu) \tag{3.36}$$

where $\sigma_{y_s}(\kappa_k)$ denote the RMS displacement of main structure when the perturbation factor is κ_k.

Consequently with the help of the PEM, the expectation of the objective function can be calculated by a linear combination of the evaluated functions for deterministic points. Each of the functions for the deterministic points, hence, can be evaluated by adapting the procedure described in the NPO part. In the optimization procedure, the sequence of Quadratic Programming Sub-problems was used, which is the same as adopted in the NPO part.

3.4 Results and Discussion

This section discusses the optimal solutions obtained by means of Nominal performance optimization and Robust performance optimization. In the below, the main system is characterized by a damping ratio of 1%, and the total mass ratio of the MTMDs is predetermined to be in the range of 1% to 10% at intervals of 1%, though in some cases the parameter is held to be 5%. The number of TMD are increased from single unit to ten units.

3.4.1 LMTMDs designed by NPO

The nominal performance optimization provides a tool for obtaining the optimal parameters under the condition that all of associated structural parameters are deterministic. In the below, the control performance for considered configurations are compared, as well as the features of their optimal parameters and obtained frequency responses of the configurations are discussed. In an economical sense, total amount of damping coefficient was also compared.

Comparison of control performance

Figure 3.5 presents the non-dimensional RMS displacements of main structure (σ_{y_s}) with various LMTMDs, in which the range of possible values of σ_{y_s} is from zero to

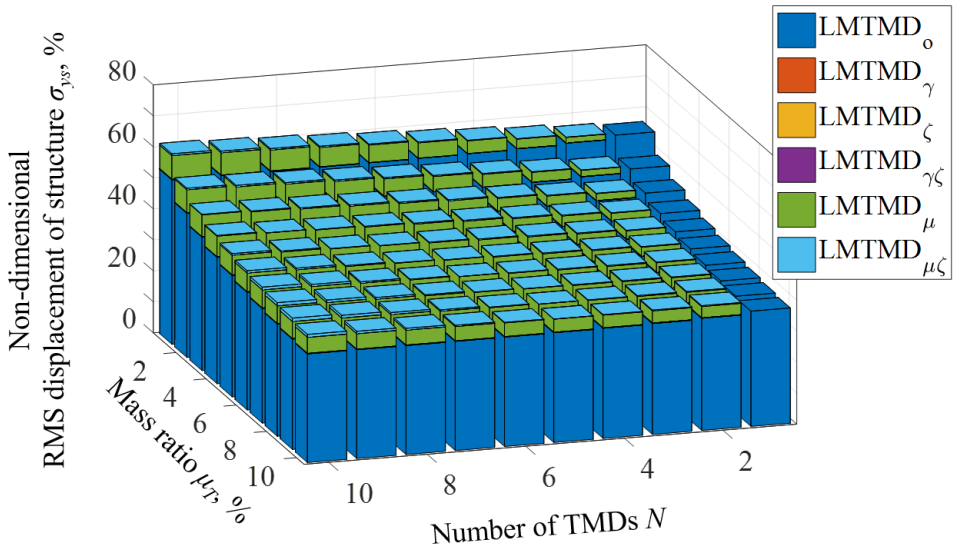

Figure 3.5: Non-dimensional RMS displacement of main structure σ_{y_s} for considered LMTMDs

unity, with σ_{y_s} tending to unity for an uncontrolled case. As for the rightmost columns of the figure, those for LMTMD$_o$ are only depicted since there is no difference for single TMD among considered configurations. It can be seen that, for all configurations, the control performance improves with increasing of the total mass ratio μ_T. Concerning the number of TMD, however, it does not affect the control efficiency significantly, and the control performance becomes even worse in the case of LMTMD$_\mu$ and LMTMD$_{\mu\zeta}$.

Although not clearly distinguished from Figure 3.5, it was also found that the control performance is better in the order of LMTMD$_o$, LMTMD$_\gamma$, LMTMD$_\zeta$, LMTMD$_{\gamma\zeta}$, LMTMD$_\mu$ and LMTMD$_{\mu\zeta}$, and those of the first four configurations was indistinguishably close. Hence in a comparative way of configurations, two main findings can be stated: 1) LMTMD$_o$ is the best optimal while the others can be regarded as sub-optimal; 2) LMTMDs with mass ratio constraints are ones those are inefficient.

In order to investigate further, the effective damping of the system is considered.

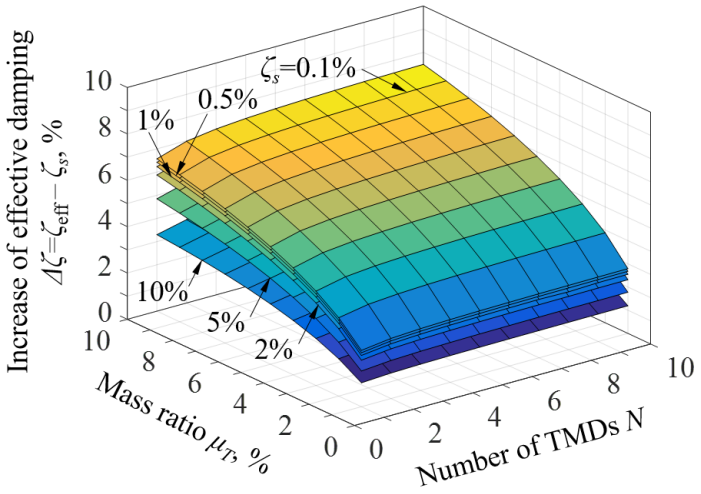

Figure 3.6: Effective damping increase

By analogy with a single-degree-of-freedom system the effective damping ratio is introduced as (Chang, 1999):

$$\zeta_s^{\text{eff}} = \frac{\pi S_{\ddot{u}_g}}{2\omega_s^3 \sigma_{x_s}^2} = \frac{\zeta_s}{\sigma_{y_s}^2}. \tag{3.37}$$

It can be seen from Figure 3.6 that the increase of effective damping $\Delta\zeta$ can be brought with the increasing of either the mass ratio or the number of TMDs, but its margin differs in a way that the number of TMDs is insensitive compared to the other.

Optimal parameters

It was found that the required damping ratios decrease exponentially with increasing the number of TMDs. Figure 3.7 shows the spatial distribution of the optimal frequency ratios γ_i^* and the optimal damping ratios ζ_i^* in $(\gamma - \zeta)$ space. In this figure the points for a single TMD coincide with the one obtained by the well-established

solution of Warburton (1982) ($\gamma_t^* = 0.97$ and $\zeta_t^* = 0.11$). From the optimal solution for the single TMD, the bandwidth of the frequency ratios becomes wider and the optimal damping ratios tend to decrease with increasing of the number of TMD units.

In the case of LMTMD_o on which no restrictive assumption on the frequency ratios or the damping ratios is imposed, the optimal tuning condition is achieved when the frequency ratios are non-linearly distributed, but are densely covered around the natural frequency of primary structure. Also it appears that TMDs located nearby the natural frequency of primary structure have lower damping ratios than other TMDs (see Figure 3.7a).

As for LMTMD_γ, it is observed that the optimal parameters are gradually deviated from those of LMTMD_o as the number of the TMDs increases. Due to the constraint that the frequency ratios are evenly spaced, some TMDs are compulsory located at the end of the frequency bandwidth (see Figure 3.7b). Under the condition, the TMDs located at the end of the bandwidth requires relatively large damping ratio compared to the unconstrained condition.

There is no considerable difference between LMTMD_γ and $\text{LMTMD}_{\gamma\zeta}$ except for the distribution of the frequency ratios. However, when comparing these two configurations to LMTMD_o, the optimal damping ratios are distributed in a way that form straight lines passing through the origin on the $(\gamma - \zeta)$ space. This pattern is predictable when reminding the restraint condition defined by Eqs. (3.22).

Compared to LMTMD_o, LMTMD_μ and $\text{LMTMD}_{\mu\zeta}$ show quite different patterns. Figure 3.7c shows the comparison between LMTMD_o and LMTMD_μ. Unlike the LMTMD_o, a large portion of the TMDs are located in low frequency range because of the aspect of the constraint referred in Eq. (3.27). An odd pattern is observed, in which the optimal damping ratios are significantly larger in the low region of the frequency bandwidth. In order to suppress the TMDs, those with low frequency ratios requires more damping to suppress in those region. Though the unduly patterns were

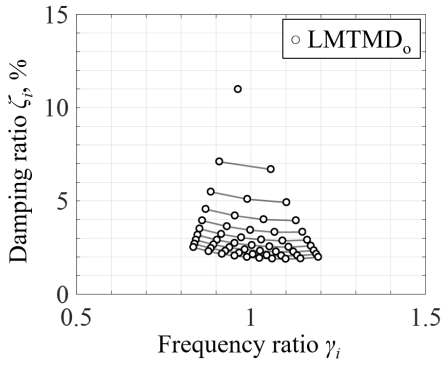

(a) LMTMD$_o$

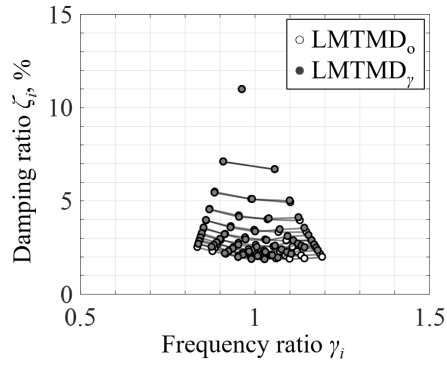

(b) LMTMD$_o$ and LMTMD$_\gamma$

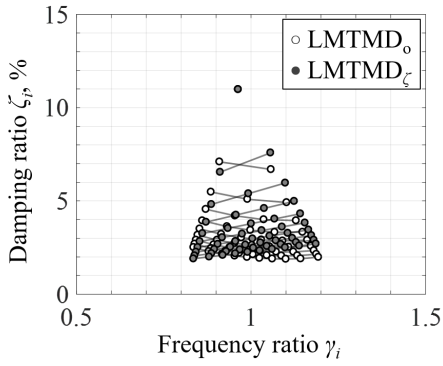

(c) LMTMD$_o$ and LMTMD$_\zeta$

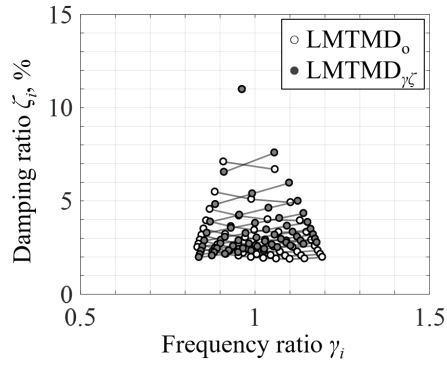

(d) LMTMD$_o$ and LMTMD$_{\gamma\zeta}$

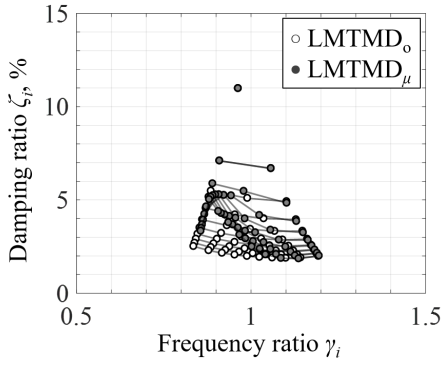

(e) LMTMD$_o$ and LMTMD$_\mu$

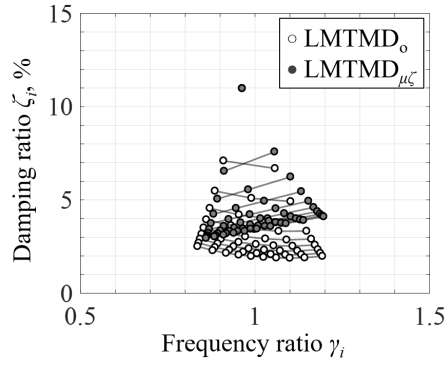

(f) LMTMD$_o$ and LMTMD$_{\mu\zeta}$

Figure 3.7: Spatial distributions of optimal variables of LMTMDs ($\mu_T = 5\%$)

not observed, the LMTMD$_{\mu\zeta}$ also shows clearly different pattern compared to the optimal LMTMD$_{\mathrm{o}}$, requiring much amount of damper. In addition to the ineffective frequency ratio patterns, the additional damping constraint results in the inefficient performance, hence the performance of this case is the worst of the considered configurations.

The optimal frequency ratios and damping ratios for various mass ratios in the range of 1 to 10 percent are depicted in Figures 3.8. The acute vortex represents STMD cases, showing those require much damping ratio than MTMDs as classical TMD solution indicates. In terms of mass ratio, it can be shown that irrespective of the MTMD configurations, the optimal frequency ratio becomes wider and the damping ratio becomes decreasing as the number of TMDs becomes larger. The decreasing margin for dampinf of TMD unit is larger when the mass ratio is larger. Moreover, it can be found that the marginal of the damping ratio becomes smaller, implying the existence of some convergence lines as the number of TMDs becomes larger. The patterns in the $\gamma - \zeta$ domain explained in the above are also observed in all the considered mass ratios for each of MTMD: while the LMTMD$_{\mathrm{o}}$ forms a widening funnel shape with circular sector, the LMTMD$_{\gamma}$ forms similar pattern with irregular circular sector, and the cases of constrained damping coefficients such as LMTMD$_{\zeta}$, LMTMD$_{\gamma\zeta}$ and LMTMD$_{\mu\zeta}$ form funnel shapes with triangular sector. LMTMD$_{\mu}$ shows irregular funnel due to the characteristic of the optimal condition shown in the previous section.

Total amount of damping constants

The total amount of damping coefficients ($c_T = \sum_{i=1}^{N} c_i$) is compared in Figure 3.9, which may provide economic and efficiency perspective. Figure 3.9a shows the required amount of damping for unit TMD mass divided by the natural frequency of the primary structure so as to non-dimensionalize. For any considered variables

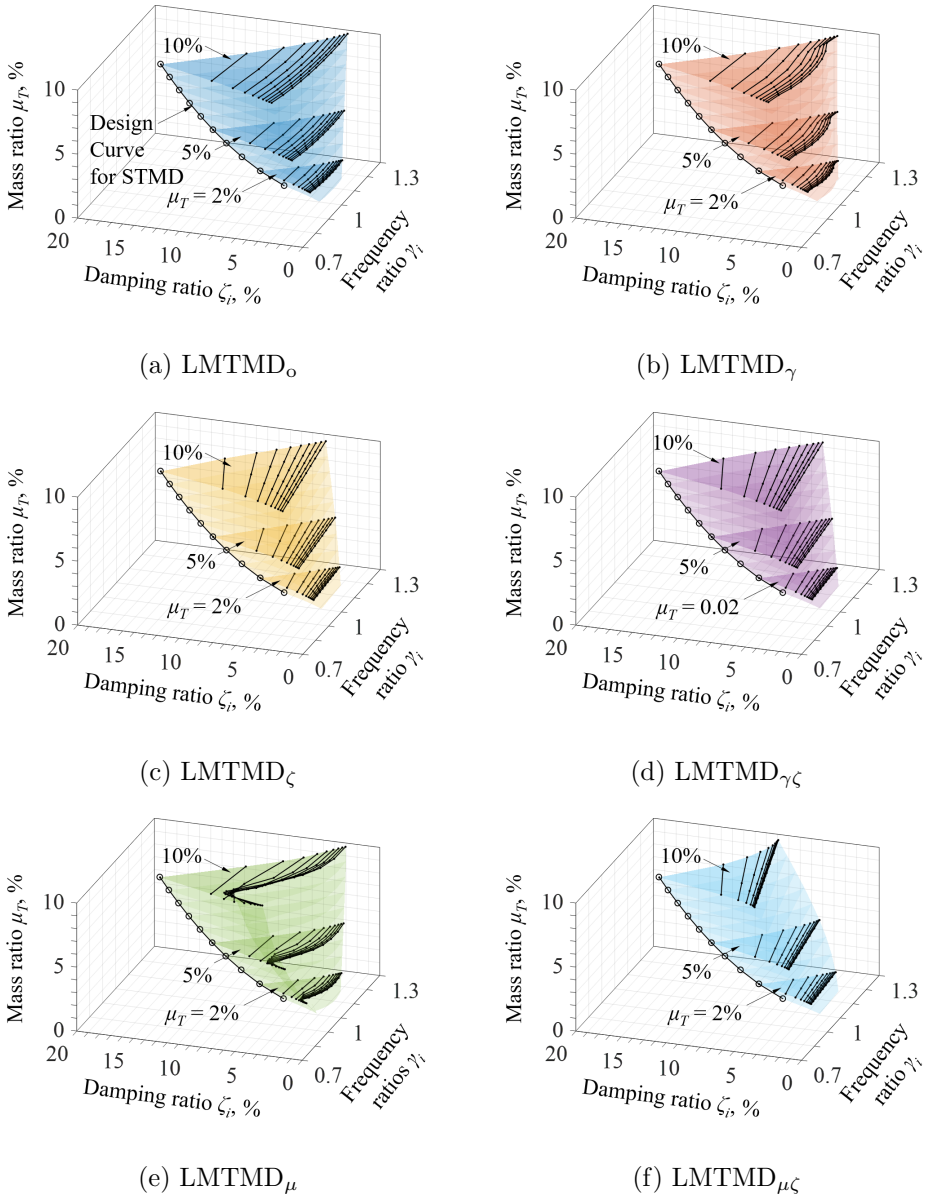

(a) LMTMD$_{\text{o}}$

(b) LMTMD$_{\gamma}$

(c) LMTMD$_{\zeta}$

(d) LMTMD$_{\gamma\zeta}$

(e) LMTMD$_{\mu}$

(f) LMTMD$_{\mu\zeta}$

Figure 3.8: Spatial representation for optimal frequency ratios and optimal damping ratios of LMTMDs

including the mass ratios and the number of TMDs, the required total damping coefficients increases in the order of LMTMD$_{\mathrm{o}}$, LMTMD$_{\gamma}$, LMTMD$_{\zeta}$, LMTMD$_{\gamma\zeta}$, LMTMD$_{\mu}$ and LMTMD$_{\mu\zeta}$. It can be seen that while it is not significantly different between first four configurations, the cases where the mass ratios are restricted show a considerable increase. Also it can be readily found that the required total damping coefficients increases as the mass ratio becomes higher, but decreases as the number of TMDs increases. The total amount of damping normalized to that of STMD is depicted in Figure 3.9b. Compared to STMD, the amount of damping decreases irrespective of mass ratio in the case of LMTMD$_{\mathrm{o}}$, but the degree of decreasing becomes slight larger under the sub-optimal conditions. And the economical advantage in the use of MTMD is not as efficient as LMTMD$_{\mathrm{o}}$ when using the LMTMDs that the mass ratios are constrained.

Comparison of transfer functions

To illustrate the efficiency of the considered MTMDs, we considered a primary structure with its damping ratio of 1% and MTMDs of 10 units with its total mass ratio of 5%. Figure 3.10 compares the frequency response functions (FRFs) for the displacement of primary structure with the response of the main mass alone. Although some minor differences in their shapes, all LMTMDs with considered configurations can reduce amplitudes effectively, of which frequency responses show $N + 1$ well-separated local modes.

Figure 3.10a compares the FRFs for LMTMD$_{\mathrm{o}}$ and LMTMD$_{\gamma}$, showing no significant differences among them. Also there is no considerable difference between LMTMD$_{\zeta}$ and LMTMD$_{\gamma\zeta}$ when comparing Figures 3.10b and 3.10c. Based on these comparisons, it can be concluded that there is no considerable effect in control performance when the constraint on the frequency ratios is taken into account.

Compared to LMTMD$_{\mathrm{o}}$, both LMTMD$_{\zeta}$ and LMTMD$_{\gamma\zeta}$ differ in a way that blunt

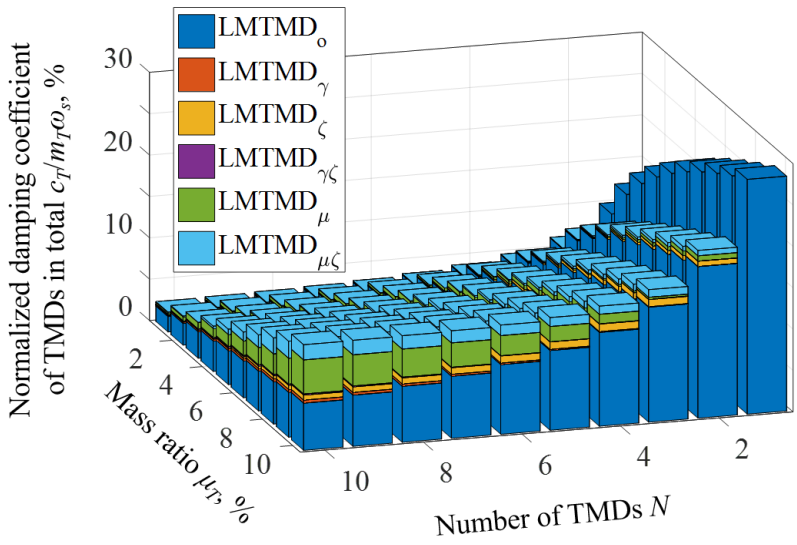

(a) Total damping coefficients per unit mass of MTMD

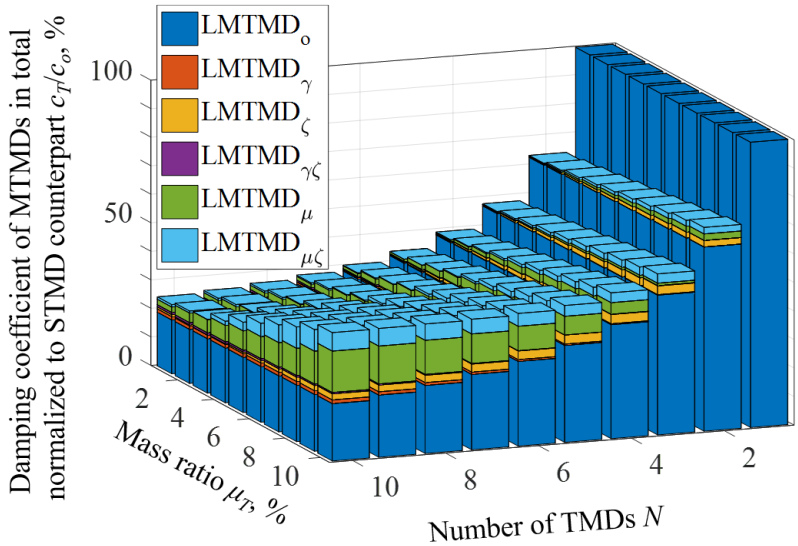

(b) Total damping coefficients normalized to that of STMD

Figure 3.9: Total damping amount of damping coefficients

peak appears at the low frequency range, and the following peaks gradually becomes sharper as the frequency increases (see Figure 3.10b and 3.10c). The characteristic shape is attributed to the constraint for identical damping constant, of which features were discussed in the preceding section on the damping coefficient restraint.

Figure 3.10d depicts the FRFs that mass ratios are constrained in a comparison with LMTMD_{o}. Unlikely the FRFs mentioned above, those for mass-constrained ones show irregular pattern and the maxima of the FRFs are considerably higher than the other ones. This trend states that, though well-optimized, the constraint for mass ratios are not effective in reducing the vibration responses. Comparing between LMTMD_{μ} and $\text{LMTMD}_{\mu\zeta}$, more higher peak was observed in the case where both the mass ratio and damping constraints are imposed on.

3.4.2 LMTMDs designed by RPO

Optimal parameters with RPO are discussed in detailed. Of possible consideration any uncertain parameters, this study dealt with the variation of the natural frequency of the primary structure. In the below, the features of their optimal parameters as well as the frequency responses of the configurations are discussed and compared with those by NPO solutions.

Optimal parameters

The optimal parameters obtained by RPO are depicted in Figures 3.11, where the optimal ones are obtained for the case of mass ratio are 2, 5 and 10 percent for the number of TMDs are 5 and 10, respectively. The blank circles are the optimal parameters by RPO and the filled circles are those by NPO. With different patterns, both LMTMDs have common trend that as the uncertainty of the involving parameters are dealt with, the frequency ratio becomes wider and the damping ratio becomes either larger. Such a trend was explained in a qualitative way by Hoang and Warnitchai

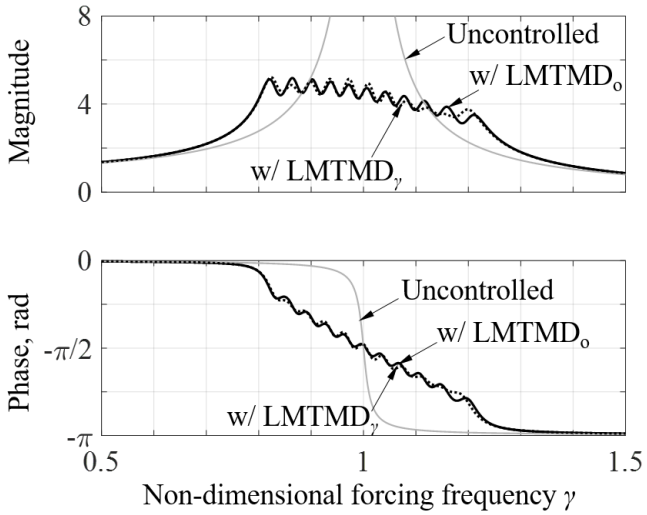

(a) LMTMD$_o$ and LMTMD$_\gamma$

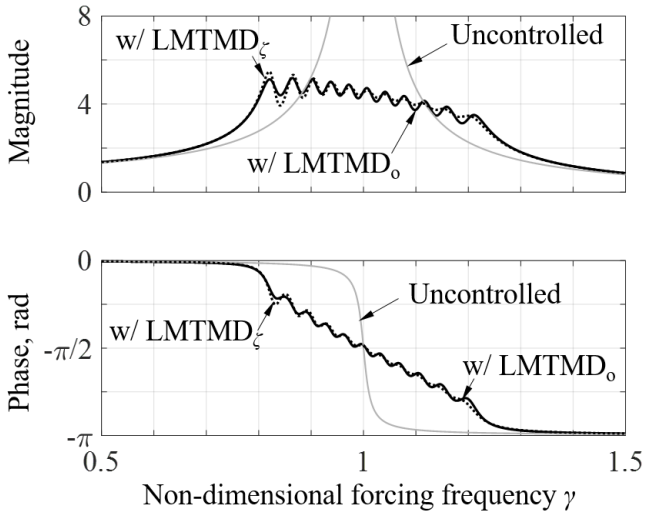

(b) LMTMD$_o$ and LMTMD$_\zeta$

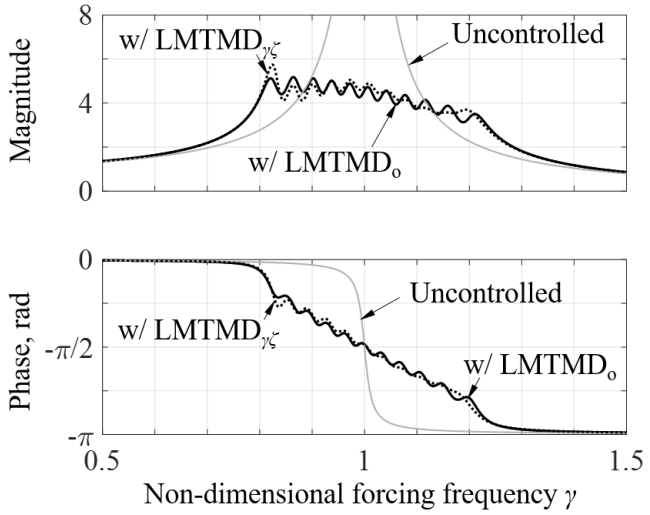

(c) LMTMD$_o$ and LMTMD$_{\gamma\zeta}$

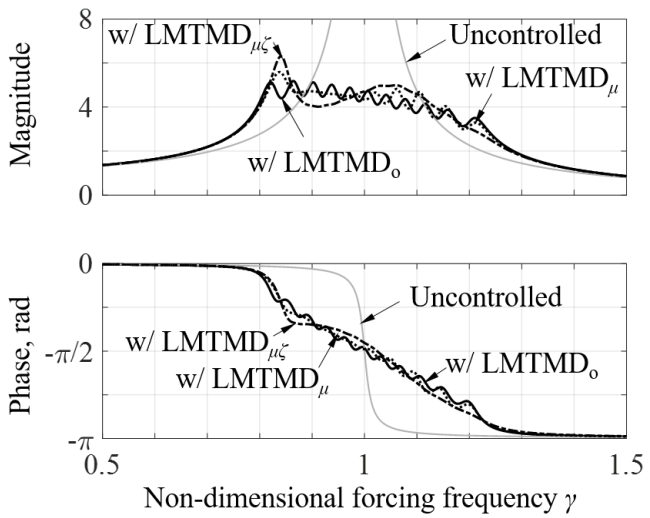

(d) LMTMD$_o$, LMTMD$_\mu$ and LMTMD$_\mu\gamma$

Figure 3.10: Comparison of FRFs for various LMTMD configurations ($\mu_T = 5\%$ and $N = 5$)

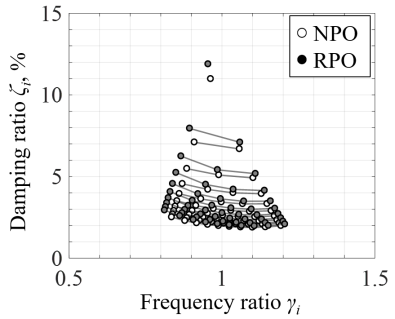

(a) LMTMD$_{\mathrm{o}}$

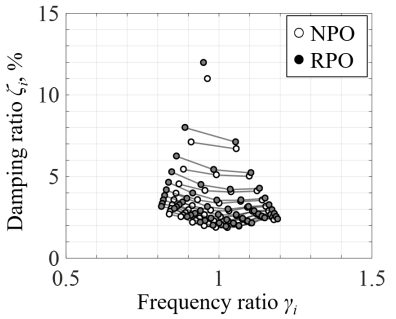

(b) LMTMD$_{\gamma}$

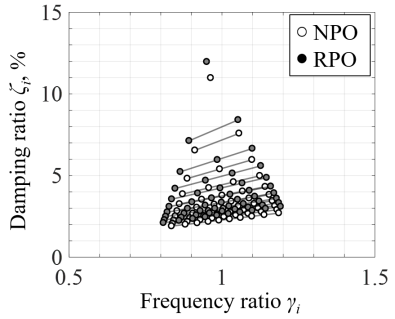

(c) LMTMD$_{\zeta}$

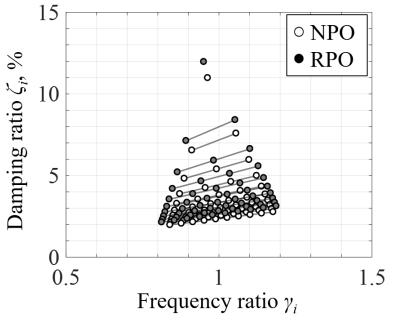

(d) LMTMD$_{\gamma\zeta}$

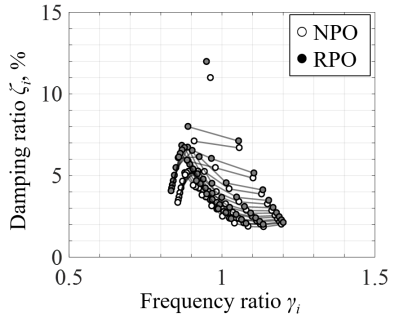

(e) LMTMD$_{\mu}$

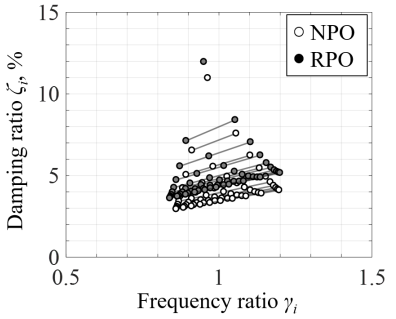

(f) LMTMD$_{\mu\zeta}$

Figure 3.11: Comparison of optimal parameters obtained by NPO and RPO ($\mu_T = 5\%$)

(2005) that the high damping ratio play a role of flattening the magnitude of FRF. Such a trend can be observed by looking into FRFs in detail, which are depicted in Figure 3.12. Because of its characteristics, LMTMDs have damper with less damping ratio, such that the excessive vibration can be occur when the natural frequency of the primary structure is detuned and resonant to itself. By looking at the blue lines which represents the well-tuned case, it is shown that the RPO solution tries to mingle the edge of the bandwidth by demanding larger damping ratio, and the opposite widening also occurs. Under the frequency-varied conditions, the edge of the bandwidth becomes more attenuated compared to the optimal system obtained by NPO.

One interesting thing is that the optimal line by RPO under a light mass ratio coincides with that by NPO under a heavier mass ratio (see Figure 3.12b). It can be interpreted that both the increasing of the mass ratio and securing the robustness have similar mechanism in suppressing the FRF. Or, in other words, if one tries to find an optimal parameters for pre-selected mass ratio with securing robustness, it can be a viable solution to apply the parameters for heavier parameters.

Comparison of transfer functions

To illustrate the efficiency of the LMTMDs obtained by RPO, we considered a primary structure with its damping ratio of 1%, and prescribed three different conditions of LMTMD_o configuration: 1) $\mu_T = 2\%$ and $N = 3$; 2) $\mu_T = 5\%$ and $N = 3$; and 3) $\mu_T = 5\%$, $N = 10$. Further to examine the robustness, we considered a perturbation of the natural frequency in the range of -10 to 10 percent with its offset of 2%. Figure 3.12 shows the FRFs for the displacement of primary structure equipped with prescribed MTMDs obtained by NPO and RPO respectively.

For both solutions, it can be shown that increasing the total mass ratio can provide more robust control performance. Compared to the case of $\mu_T = 2\%$ of three TMDs,

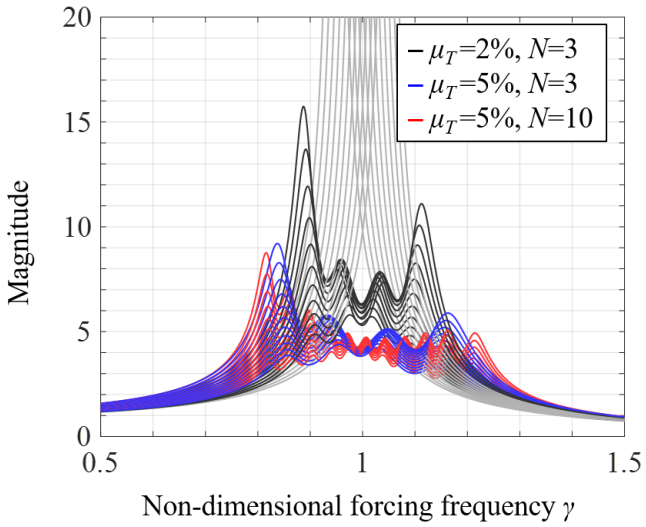

(a) With NPO solutions

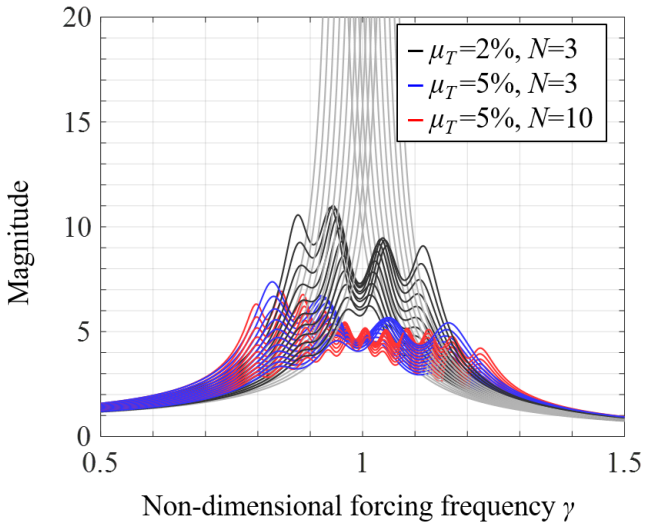

(b) With RPO solutions

Figure 3.12: FRFs under the perturbation of natural frequency

LMTMDs with same number but heavier one appears effective in suppressing the frequency response. Such a difference in control performance is already indicated in the preceding section. Although not as significant as the mass ratio, increasing the number of TMDs also affects its performance enhancement, especially when the extent of perturbation is large. The enhanced performance of the system with large number of TMDs can be explained as the many MTMDs permits more number of TMDs incorporate in dissipating the vibration energy.

Compared to the NPO solutions under same condition, the RPO solutions can suppress the frequency responses especially perturbed to large frequencies. The enhanced performance of the system with large number of TMDs can be explained as the many MTMDs permits more number of TMDs incorporate in dissipating the vibration energy.

3.4.3 Approximate solution for LMTMD$_{\gamma\zeta}$

So far in this study we have considered various LMTMD configurations, of which optimal solutions cannot be simply described for the numerous number of design variables. LMTMD$_{\gamma\zeta}$, however, can be determined its optimal condition with just three design variables such as two variables for frequency ratios γ_1 and β_γ, and a fictitious damping ratio ζ_o. It is fruitful to provide the approximate design equation, because LMTMD$_{\gamma\zeta}$ shows its control performance similar to the best optimal LMTMD$_{\mathrm{o}}$.

Figure 3.13 shows the parameters m_1, m_2 and ζ_o for various mass ratio and number of TMDs for optimal LMTMD$_{\gamma\zeta}$. As can be seen from the figure, the slopes m_1 and m_2 tend to decrease with increasing the number of TMDs and the mass ratio, and the fictitious damping ratio ζ_o decreases requiring exponentially decreased damping per unit TMD. In order to provide simple and useful ways, the regressive formula are established which provide sufficient agreement with the optimal solutions. The

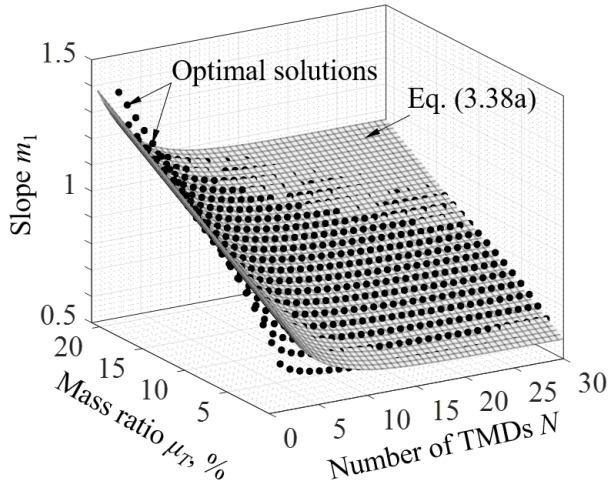

(a) Slope m_1

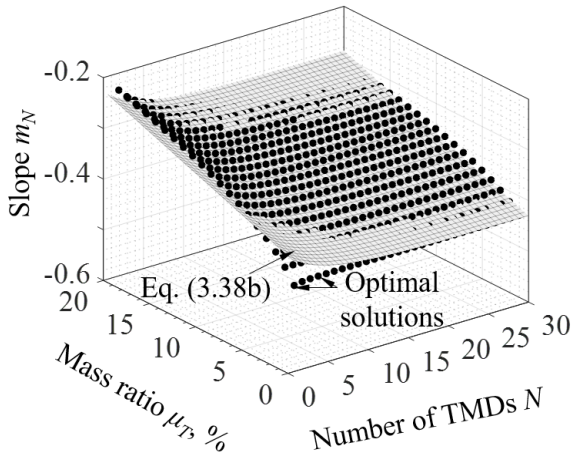

(b) Slope m_N

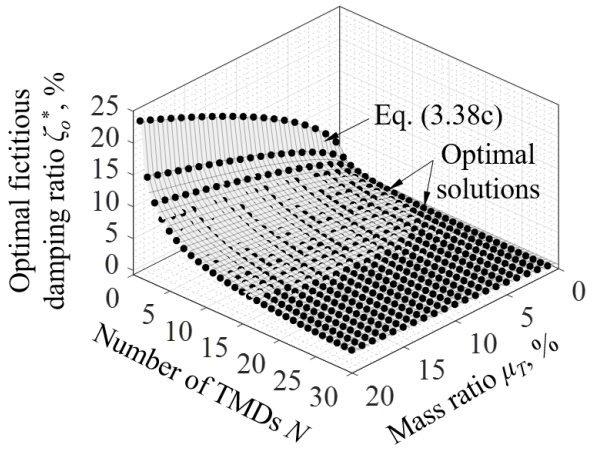

(c) Optimal fictitious damping ratio ζ_o^*

Figure 3.13: Shape parameters for optimal LMTMD$_{\gamma\zeta}$

formula are given by

$$m_1 \approx p_0 + p_1\mu_T + p_2\exp[-p_3(N-1)] \tag{3.38a}$$

$$m_2 \approx p_0 + p_1\mu_T + p_2\exp[-p_3(N-1)] \tag{3.38b}$$

$$\zeta_o \approx \frac{\sqrt{\mu_T(4+3\mu_T)(1+\mu_T)}}{2(2+\mu_T)} \exp\left[p_0\mu_T^{p_1}(N-1)^{p_2}\right] \tag{3.38c}$$

The optimal frequency ratios can be calculated by following formula [see Figure 3.14:

$$\gamma_1^* = \frac{\zeta_t^* - m_1\gamma_t^*}{\zeta_o - m_1} \tag{3.39a}$$

$$\gamma_N^* = \frac{\zeta_t^* - m_2\gamma_t^*}{\zeta_o - m_2} \tag{3.39b}$$

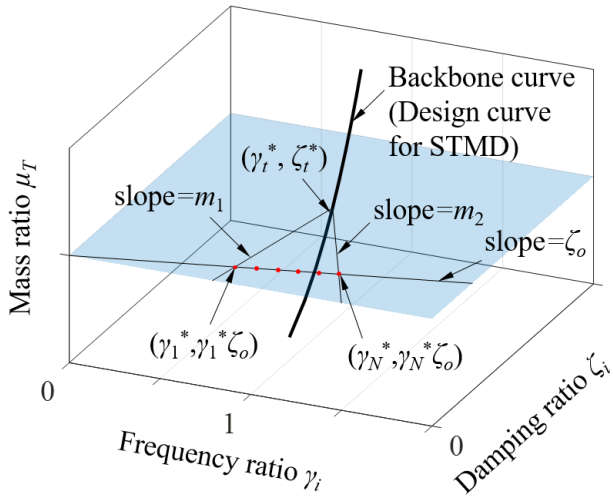

Figure 3.14: Graphical representation on spatial distribution of LMTMD$_{\gamma\zeta}$

Equations (3.38) and (3.39) can be useful in designing optimal LMTMD$_{\gamma\zeta}$. The other factors can be determined by some equations. The design parameters and regressive coefficients are summarized in Table 3.2.

Table 3.2: Design parameters and regression coefficients

Parameter	Coefficient				R^2
	p_0	p_1	p_2	p_3	
m_1 [Eq. (3.38a)]	0.5742	2.3400	0.2812	0.2806	0.9723
m_N [Eq. (3.38b)]	-0.4306	0.7147	0.0469	0.2153	0.9414
ζ_o^* [Eq. (3.38c)]	-0.4948	-0.0458	0.4395	-	0.9919

3.5 Stroke Consideration and Design Procedure

3.5.1 Stroke consideration

For design purposes it is desired to determine the maximum stroke of TMDs to encase the moving masses, especially when designing MTMD because the required damping exponentially decreases with increasing the number of TMDs that result in undesired stroke requiring more space in its housing. Lin et al. (2010) developed a two-stage design procedure, whereby considering both structural and TMD responses. In terms of H_∞ norm, it can be seen that limiting the maximum stroke of the MTMDs can helps not only the purpose itself, but also decreasing the peak point of the FRF within an appropriate weighting region. Such a trend was discussed in the study conducted by Yamaguchi and Harnpornchai (1993), in which the identical damping ratio of the MTMD have its optimum such that below the value, the maximum of the FRF is governed by excessive TMD stroke, and above the value, the structural response governs.

Figure 3.15a depicts the RMS displacement of main structure in its ordinate and maximum of the RMS displacements of TMDs in its abscissa, comparing LMTMD_o and $\text{LMTMD}_{\gamma\zeta}$. As stated in the part of the performance comparison, both the control performance and the maximum RMS displacement of the TMDs are similar. As for the TMD stroke, the maximum RMS displacement rapidly increases with increasing the number of TMDs, but the marginal increasing becomes decrease. Such a trend is predictable when recalling the dependency between the number of TMDs and the optimal damping ratios. In the design purpose, it is convenient to transform the information on Figure 3.15b into another $(N - \mu_T)$ space in a contour form. One can use Figure 3.15b as a design contour for evaluating the control efficiency and for limiting the maximum of TMD stroke.

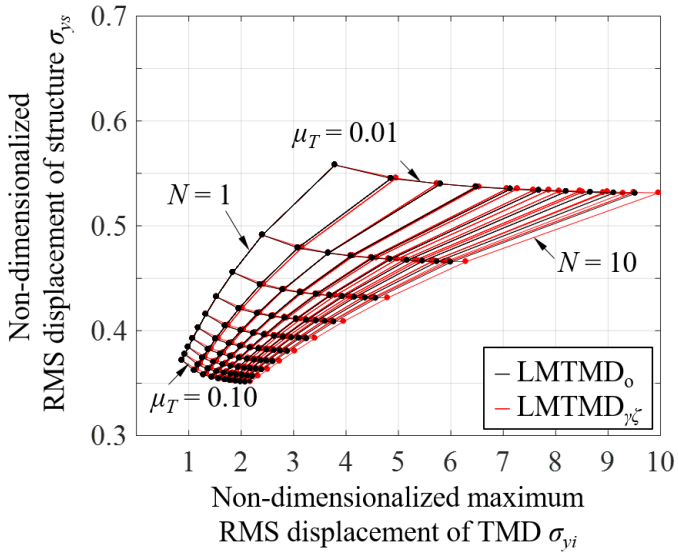

(a) Performance grid for LMTMD$_o$ and LMTMD$_{\gamma\zeta}$

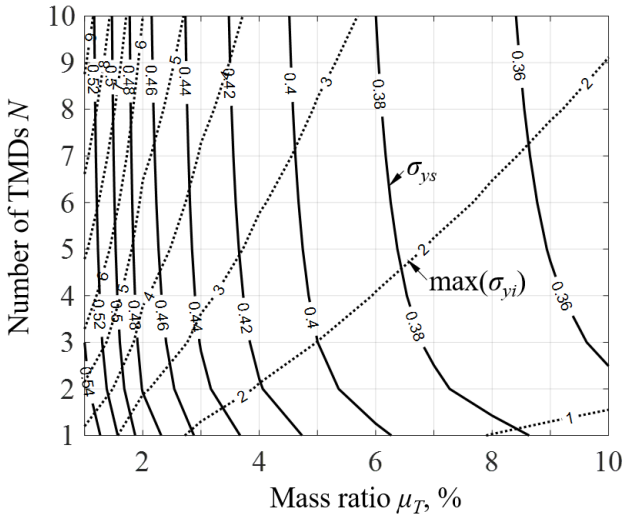

(b) Design contour for LMTMD$_o$

Figure 3.15: Performance and stroke grid for design

3.5.2 Design procedure

This section is dedicated to demonstrate the design procedure for the case of parallel type LMTMDs, each of which comprises a linear spring and a viscous damping element. The following design procedure covers not only the case of designing a new structure but also the case of mitigating the existing structures.

1. Determine the dynamic properties such as the structural mass m_s, structural damping coefficient c_s, and structural stiffness k_s. Those can be either assumed appropriately or estimated from field measurements.

2. Evaluate the anticipated structural response, for instance the structural displacement x_s, and determine the performance level to be attained.

3. Determine the total mass ratio of the LMTMDs $\mu_T = \sum_{i=1}^{N} \mu_i$, which directly yields the total mass of the LMTMDs, with the help of the relationship between the total mass ratio and the controlled structural RMS response normalized to the uncontrolled one.

4. Select the optimal frequency ratios and the optimal damping ratio for the configuration type and the number of TMDs what you prefers. Do not struggle with choosing the total number of TMDs in terms of performance, since it does not affect vibration mitigation level. However, keep in mind that increasing the number of TMDs yields decreasing the optimal damping ratios, demanding larger stroke limitations.

5. Check whether the stroke of LMTMDs chosen at the previous step exceeds the prescribed stroke limitations. If exceeds, two solution could be imposed: Reduce the number of TMDs, or make the chamber to absorb the excessive strokes.

3.6 Concluding Remarks

This study developed a framework for design of linear multiple tuned mass dampers (LMTMDs) in order to provide general guidance for their configuration, robustness, and stroke limitation issue. The optimal parameters for various LMTMD configurations were first investigated with considering the constraints on frequency ratios, damping ratios, mass distributions and combinations thereof. Next, two different optimization schemes were investigated for generality in design: Nominal Performance Optimization (NPO) and Robust Performance Optimization (RPO). In order to enable designers to consider the performance evaluation and the stroke limitations simultaneously during design, this study provided contour maps for the RMS displacement of the main structure and the largest RMS displacement of LMTMDs.

The key features can be drawn as follows:

1. It is demonstrated that LMTMD_{o} is found to be most efficient in terms of suppressing the structural vibration, but some configurations like LMTMD_{γ}, LMTMD_{ζ} and $\text{LMTMD}_{\gamma\zeta}$ can also exhibit their control performance similar to LMTMDo. Two other configurations LMTMD_{μ} and $\text{LMTMD}_{\mu\zeta}$, however, not only deteriorate their control efficiency but also require large amount of damping coefficient compared to other MTMDs, especially when the number of TMDs becomes larger.

2. The optimal parameters such frequency ratios and damping ratios of MTMDs are found under the condition that the main structure is excited by a ground motion of stationary zero-mean white-noise. From NPO solution, it was found that the optimal parameters of MTMDs extend that of the single TMD.

3. From the backbone curve predicted by the classical solution of Warburton (1982), the optimal frequency range tends to span further as the number of

TMDs increases, and as the damping ratio per an unit TMD becomes smaller.

4. The RPO solution was found, which helps take into account of the perturbation of the natural frequency of main structure. Compared to the NPO solution, the RPO solution provides more wider frequency spans and decreased damping ratio. Based on the comparative analysis in the frequency domain, the RPO based solution is shown to provide more robust solution.

5. Considering the analyzed result that the $\text{LMTMD}_{\gamma\zeta}$ exhibits the performance comparable to the optimal solution LMTMD_{o} with much reduced design variables, this study proposed an approximate solution for $\text{LMTMD}_{\gamma\zeta}$ was proposed.

Chapter 4

Frictional Multiple Tuned Mass Dampers

This study investigates optimal design and analysis of frictional multiple tuned mass dampers, in which the Coulomb-type frictional force is incorporated in either purposefully or unintentionally. Four of the feasible FMTMD configurations are formulated and comparatively analyzed, each of which is constrained in a way of linearly distributed frequency ratios, uniformly distributed coefficients of friction (COFs), and/or combinations thereof. An approximate design formula is developed for $\text{FMTMD}_{\gamma\tau}$ configuration formed under the constraint of frequency ratios and COFs. In order to cope with the difficulties inherent in nonlinearity of the system, this study adopted the statistical linearization technique, which enables the complicated nonlinear force terms to be linearized in statistical sense. Some miscellaneous but important considerations such as stroke limitations and design procedure were also aptly included.

4.1 Introduction

Tuned mass damper (TMD) is a passive control device, which help dampen the dynamic response of primary structures efficiently. In principle, TMD attracts vibration energy of the main structure by resonance, and dissipates the energy through built-in energy dissipation devices. Because of its novelty for controlling vibration, a various types of TMDs have been extensively studied and investigated among numerous researchers during the past several decades.

Multiple tuned mass damper (MTMD) is a system comprising multiple units of TMDs, often each TMDs having different dynamic characteristics. In the early stage of research, MTMDs with viscous dampers were studied due to its simplicity and clarity in a physical sense. For instance, linear MTMDs with equally spaced natural frequencies and each of which having equal viscous damping constant were studied by Xu and Igusa (1992) based on an asymptotic analysis, and it was shown that such a linear MTMD is effective in reducing the response of the main structure. Joshi and Jangid (1997) and Jangid (1999) found the optimal parameters of linear MTMDs for undamped and damped primary structure, respectively.

MTMDs with equal damping ratios and equally spaced natural frequencies were also investigated by various researchers including Yamaguchi and Harnpornchai (1993), Abé and Fujino (1994), Kareem and Kline (1995) and Jangid and Datta (1997). Until recently, various studies have been conducted for the linear MTMDs with relaxed constraints, such as Igusa and Xu (1994), Li (2002), Hoang, Fujino, and Warnitchai (2008), Zuo (2009), Li and Ni (2007), Fu and Johnson (2010), and Yang, Sedaghati, and Esmailzadeh (2015a). The main differences in these papers involve 1) considered excitation, such as harmonic forcing function and the ground acceleration, 2) the objective function, such as the RMS response of the primary structure or the maximum of the frequency response and 3) employed optimization strategies.

Despite its simplicity and effectiveness, linear TMDs have some drawbacks. One of the most significant drawbacks is that the incorporated dashpot is prone to lose its performance. With repetitive operations during a long lifetime, the dashpot would defeat its function caused by increasing of temperature of the damper fluid, and would lose its performance because of risk caused by liquid leakage.

To overcome these drawbacks, some researchers tried to incorporate the Coulomb-type force into the TMD as an energy dissipative mechanism. Inaudi and Kelly (1995) proposed a nonlinear TMD that uses friction dampers acting transversely to the direction of the motion of the mass damper as a means for energy dissipation. Based on the statistical linearization procedure that can effectively simplify for computing the RMS response of the system, they showed that, when appropriately designed, the nonlinear system achieves the same level of performance that an ideally linear TMD would provide.

Carpineto et al. (2014) and Wang (2011) developted Nonlinear TMDs that dissipates the input energy by frictional hysteretic mechanism. Wang (2011) proposed a nonlinear TMD, in which Coulomb-type frictional dissipating mechanism is accommodated, and examined its feasibility through numerical simulations. Based on the evaluation of frequency response function (FRF) with the harmonic balancing method, the optimal design parameters of the nonlinear TMD were obtained by minimizing the magnitude of the real part of the real FRF. Wang (2011) concluded that the nonlinear TMD proposed by the author can outperform a common linear TMD in machining stability improvement.

Rüdinger (2007) investigated the performance of TMDs with nonlinear viscous damping elements. In calculating the RMS displacement of the main structure, the author employed statistical linearization method. It was shown from this study that the optimal damping parameter values for the nonlinear TMD depend on the displacement magnitude and excitation intensity, in constrast to the case of a linear

TMD. However, the response magnitude is relatively insensitive to the value of the damping parameters of the mass damper.

Alexander and Schilder (2009) explored the performance of a nonlinear TMD, which is modeled as a two DOF system with a cubic nonlinearity. The numerical results obtained, however, were negative since the TMD with a cubic nonlinearity and constant damping ratio does not provide an improvement over an optimal linear TMD.

Gewei and Basu (2010) investigated the effectiveness of the nonlinear tuned mass dampers in which dry friction force is employed. They adopted harmonic solution and statistical linearization to calculate the vibrational response and found the optimal friction coefficient of friction (COF) of TMDs. It was found from this research that the optimal friction coefficient depends on the response of the TMD which is in turn almost proportional to the intensity of the excitation.

This study seeks to provide optimal solutions for the four practically feasible FMTMD configurations: 1) no constraint either on the frequency ratios or on the coefficient of friction (COF) imposed; 2) the frequency ratios are linearly distributed and equally spaced; 3) the COFs are uniformly distributed and identical; 4) the frequency ratios are equally spaced and the COFs are identical. To cope with the difficulties inherent in nonlinearity of the problem, this study adopted the statistical linearization technique, which enables the complicated nonlinear force terms to be linearized in a statistical sense. Some miscellaneous considerations such as stroke limitations and design procedure were aptly included.

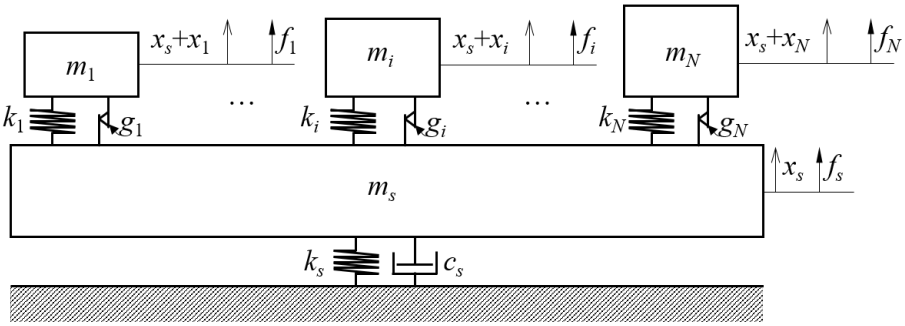

Figure 4.1: Structure-FMTMD system

4.2 Model Formulation

4.2.1 Governing equations of motion

Consider a system comprised of a primary structure and N units of auxiliary mass, each of which is connected with a linear spring and an energy dissipation element in parallel (see Figure 4.1). The structure-MTMD system can be represented as the following differential equations:

$$(m_s + m_T)\ddot{x}_s + \sum_{i=1}^{N} m_i\ddot{x}_i + c_s\dot{x} + k_s x = f_s \tag{4.1a}$$

$$m_i(\ddot{x}_s + \ddot{x}_i) + k_i x_i + g_i = f_i \qquad i = 1, \cdots, N \tag{4.1b}$$

where m_s, c_s and k_s are the mass, damping constant and spring constant of the primary structure; m_i and k_i are the mass and spring constant of the i-th TMD; N is the number of TMDs; g_i is a dissipation force arising from a relative motion of contacting surface between the primary structure and the i-th TMD; m_T is the total mass of TMDs calculated by $\sum_{i=1}^{N} m_i$; x_s is the displacement of the primary structure, and x_i is the relative displacement between the i-th TMD and the primary

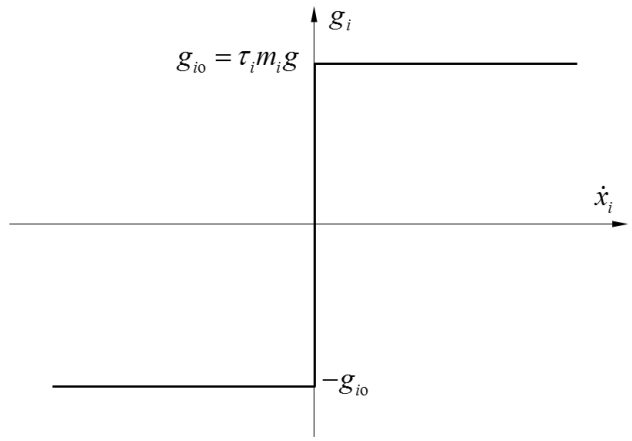

Figure 4.2: Idealized Coulomb-type frictional force

structure; A dot notation signifies a derivative with respect to time t; The external force exerted on the primary structure and on the i-th unit of TMD are denoted as f_s, and f_i, respectively.

If the whole system is excited by a zero white-noise base acceleration, each of the force terms associated the i-th unit of TMD, f_i, is zero and that on the primary structure, f_s, is defined as $-(m_s + m_T)\ddot{u}_g$, where $\ddot{u}_g$ is the ground acceleration with a constant spectral intensity $S_{\ddot{u}_g}$, i.e.,

$$E[\ddot{u}_g(t)\ddot{u}_g(t + \Delta t)] = 2\pi S_{\ddot{u}_g}\delta(\Delta t), \tag{4.2}$$

where $E[\cdot]$ is an expectation operator and $\delta(\cdot)$ is the Dirac-delta function.

The frictional force will be assumed as Coulomb-type, and the force term g_i can be modeled as shown in Figure 4.2. Thus

$$g_i = g_i(\dot{x}_i) = g_{io}\,\mathrm{sgn}(\dot{x}_i) = \tau_i m_i g\,\mathrm{sgn}(\dot{x}_i) \tag{4.3}$$

where g_{io} is the characteristic frictional force for the i-th TMD, τ_i is the coefficient of friction (COF), and $\mathrm{sgn}(\cdot)$ denotes a signum function.

Dividing Eqs. (4.1a) and (4.1b) by the mass of the primary structure m_s and that of the i-th TMD respectively yields the equations

$$(1+\mu_T)\ddot{x}_s + \sum_{i=1}^{N} \mu_i \ddot{x}_i + 2\zeta_s \omega_s \dot{x} + \omega_s^2 x = -(1+\mu_T)\ddot{u}_g \tag{4.4a}$$

$$\ddot{x}_s + \ddot{x}_i + g_i/m_i + \gamma_i^2 \omega_s^2 x_i = 0 \qquad i = 1, \cdots, N \tag{4.4b}$$

where the normalized terms μ_i and γ_i are the mass ratio of the i-th TMD (i.e. the ratio between the mass of the i-th TMD and that of the main structure), and the frequency ratio of the i-th TMD (i.e. the ratio between the frequency of the i-th TMD by itself and that of the main structure) given by

$$\mu_i = \frac{m_i}{m_s}, \tag{4.5a}$$

$$\gamma_i = \frac{\omega_i}{\omega_s} = \sqrt{\frac{k_i}{m_i}}\sqrt{\frac{m_s}{k_s}} = \sqrt{\frac{k_i}{k_s}}\mu_i^{-1/2} \tag{4.5b}$$

and μ_T is the ratio of the total mass given by $\sum_{i=1}^{N} \mu_i$.

A convenient reformulation of the equations of motion can be suitably made by replacing the associated terms with non-dimensional variables. First, x_s and x_i can be non-dimensionalized by normalizing them to the RMS displacement of the uncontrolled structure x_{ref}. With the help of the theoretical results for the stochastic response of a SDOF system excited by a white-noise stationary process (Lutes and Sarkani, 2004), the RMS displacement of the uncontrolled system can be calculated by

$$x_{\text{ref}} = \sqrt{\frac{\pi S_{\ddot{u}_g}}{2\zeta_s \omega_s^3}}. \tag{4.6}$$

Further, introducing non-dimensional displacements $y_s = x_s/x_{\text{ref}}$ and $y_i = x_i/x_{\text{ref}}$, and a time scale $t_o = \omega_s t$, the equations of motion can be non-dimensionalized as follows:

$$(1+\mu_T)y_s'' + \sum_{i=1}^{N} \mu_i y_i' + 2\zeta_s y_s' + y_s = -(1+\mu_T)w_g'' \tag{4.7a}$$

$$y_s'' + y_i'' + \psi_i + \gamma_i^2 y_i = 0 \qquad i = 1, \cdots, N \tag{4.7b}$$

where a prime notation denotes the derivation with respect to the non-dimensional time t_o, and w_g'' is the non-dimensionalized ground acceleration exerted on the primary structure with its spectral intensity of

$$S_{w_g''} = \frac{S_{\ddot{u}_g}}{x_{\text{ref}}^2 \omega_s^3} = \frac{2\zeta_s}{\pi}. \tag{4.8}$$

And the non-dimensionalized friction force term ψ_i is written as follows:

$$\psi_i = \psi_i(y_i') = \frac{g_i(\dot{x}_i)}{m_i \omega_s^2 x_{\text{ref}}} = \eta_i \,\text{sgn}(y_i') \tag{4.9}$$

where

$$\eta_i = \frac{g_{\text{io}}/\mu_i}{m_s \omega_s^2 x_{\text{ref}}} = \frac{1}{\omega_s^2 x_{\text{ref}}/g} \tau_i. \tag{4.10}$$

The matrix equation of motion for the combined system with $N+1$ degree-of-freedoms can be consequently derived as follows:

$$My'' + Cy' + Ky + \psi = fw_g'' \tag{4.11}$$

where $y = [y_s, y_1, \cdots, y_N]^{\mathrm{T}}$, $\psi = [0, \psi_1, \cdots, \psi_N]^{\mathrm{T}}$, $f = [-(1+\mu_T), 0, \cdots, 0]^{\mathrm{T}}$ and

$$M = \begin{bmatrix} 1+\Sigma\mu_i & \mu_1 & \cdots & \mu_N \\ 1 & 1 & \cdots & 0 \\ \vdots & \vdots & \ddots & \vdots \\ 1 & 0 & \cdots & 1 \end{bmatrix}, \tag{4.12a}$$

$$C = \begin{bmatrix} 2\zeta_s & 0 & \cdots & 0 \\ 0 & 0 & \cdots & 0 \\ \vdots & \vdots & \ddots & \vdots \\ 0 & 0 & \cdots & 0 \end{bmatrix}, \tag{4.12b}$$

$$K = \begin{bmatrix} 1 & 0 & \cdots & 0 \\ 0 & \gamma_1^2 & \cdots & 0 \\ \vdots & \vdots & \ddots & \vdots \\ 0 & 0 & \cdots & \gamma_N^2 \end{bmatrix}. \tag{4.12c}$$

4.2.2 FMTMD configurations

This study considers four of feasible MTMD configurations: $\mathrm{FMTMD_o}$ is a configuration on which no constraint for the frequency ratios or the COFs is imposed; FMTMD_γ is the case where the frequency ratios are linearly distributed; FMTMD_τ is the case where the COFs are uniformly distributed; $\mathrm{FMTMD}_{\gamma\tau}$ is the case in which the frequency ratios and the COFs are distributed linearly and uniformly, respectively. For all of these configurations, the stiffness of each TMD is presumed to be the same. These FMTMD configurations are summarized in Table 4.1.

Spring constraint uniformly distributed

Given that the spring constants of MTMD are uniformly distributed (that is, the stiffness of each TMD is identical), the mass ratio of the i-th TMD is written in terms of the total mass ratio μ_T and the frequency ratios γ_i.

If the spring constant of each TMD is identical to k_o, then Eq. (4.5b) becomes as follows:

$$\mu_i = \frac{k_o}{k_s}\gamma_i^{-2} = \frac{\gamma_i^{-2}}{\Sigma\gamma_i^{-2}}\mu_T \tag{4.13}$$

where k_s is the stiffness of the primary structure.

Then, adding up all the mass ratios of Eq. (4.13) gives the following expression:

$$k_o = \frac{\mu_T}{\Sigma\gamma_i^{-2}}k_s. \tag{4.14}$$

Substituting Eq. (4.14) into Eq. (4.13) gives the expression of μ_i written in terms of the frequency ratios γ_i and a predetermined total mass ratio μ_T as follows:

Table 4.1: Constraints for considered LMTMD configurations

Configuration	Constraints			
	Masses	Frictional coefficients	Spring constants	Frequency ratios
FMTMD_o	-	-	U†	-
FMTMD_γ	C†	-	U	L†
FMTMD_τ	-	U	U	-
$\text{FMTMD}_{\gamma\tau}$	C	U	U	L

†: U = Uniformly distributed, C = Constrained and L = Linearly distributed.

$$\mu_i = \frac{\gamma_i^{-2}}{\sum_{i=1}^{N} \gamma_i^{-2}} \mu_T \qquad i = 1, \cdots, N. \tag{4.15}$$

Eq. (4.15) implies that the mass ratios of the TMDs can be completely replaced by the frequency ratios. Accordingly, if no additional constraint is imposed upon a configuration just as $\mathrm{FMTMD_o}$, the associated design vector γ_d is given as $\gamma_d = [\gamma_1, \cdots, \gamma_N]^{\mathrm{T}}$.

Frequency ratios linearly distributed

In the case that the frequency ratios are linearly distributed (that is, those are equally spaced), the frequency ratio of the i-th TMD for the constraint is expressed as follows:

$$\gamma_j = \gamma_1 + \frac{j-1}{N-1}\beta_\gamma \quad \text{for } j = 2, \cdots, N \tag{4.16}$$

Note that the frequency ratios can be determined by the first frequency ratio, and the bandwidth determined as $\beta_\gamma = \gamma_N - \gamma_1$. Thus under the constraint for linearly-constrained frequency ratios, the associated design vector for frequency ratios γ_d is given by

$$\gamma_d = [\gamma_1, \beta_\gamma]^{\mathrm{T}} \tag{4.17}$$

and the remained frequency ratios are determined by Eq. (4.16).

Recalling the Figure 3.2 that graphically represents the aspects of the constraint for linearly-constrained frequency ratios, the masses of the TMDs are found to be densely distributed in the heavy side, as can be seen by inspecting Eq. (4.15) that the mass ratio is inversely proportional to the square of the frequency ratio.

Frictional coefficients uniformly distributed

Given that the nonlinear force only attributes the exertion force and the force is exerted by a friction arises from the TMD and the main structure with the extent of same COF, the non-dimensionalized frictional force can be determined by following expression:

$$\psi_i = \psi_i(y_i') = \frac{1}{\omega_s^2 x_{\text{ref}}/g}\tau \,\text{sgn}(y_i') \quad i = 1, \cdots, N \tag{4.18}$$

where τ are the identical COF.

Compared to the frictional force defined by Eq. (4.3), the non-dimensional force is independent on the TMD parameters including its mass.

4.2.3 Statistical linearization

One attractive method of solving stochastic nonlinear differential equations is a statistical linearization which can replace a set of the nonlinear equations by a set of linear ones that is equivalent in a statistical sense. Some theoretical aspects and applications of this technique are described in the literature (Roberts and Spanos, 2003; Socha, 2005a,b). For the equations of motion for structure-FMTMD system described as Eq. (B.23), the statistical linearization technique enables the nonlinear force term ψ to be replaced with an equivalent term that minimizes the mean square of the error $E[\varepsilon^2]$ (i.e. Euclidean norm) where the error ε is given by

$$\varepsilon = \psi - C^{\text{eq}} y' \tag{4.19}$$

where C^{eq} is a parametric matrix to be determined that minimizes the quantified error term.

Under the assumption of stationary Gaussian excitation, a procedure for minimizing the error based on the Euclidean norm falls into an explicit form of the

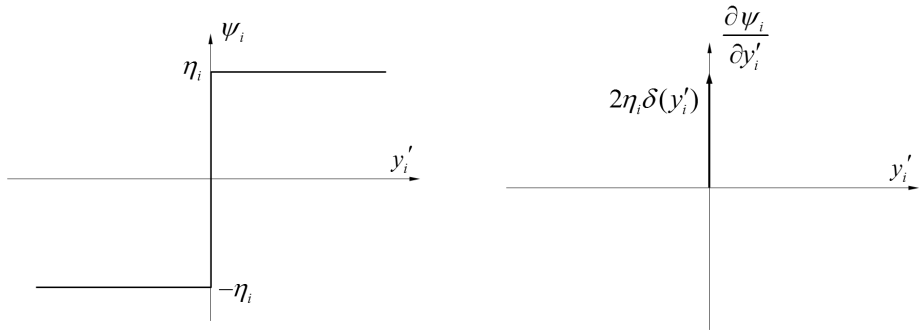

(a) ψ_i (b) $\partial_{y_i'}\psi_i$

Figure 4.3: Normalized frictional force ψ_i and its derivative $\partial_{y_i'}\psi_i$

parametric matrix C^{eq}. With applying the first order necessary condition for optimality, the parametric matrix can be expressed by the following simple expression (details are supplemented with Appendix B).

$$c_{i+1}^{\text{eq}} = E[\partial_{y_i'}\psi_i] = E\left[\frac{\partial \psi_i}{\partial y_i'}\right] \quad i = 1, \cdots, N \tag{4.20}$$

where ψ_i is the nonlinear force of the i-th TMD, and $\partial_{y_i'}\psi_i$ denotes its partial derivative with respect to the non-dimension velocity y_i'. The normalized Coulomb-type frictional force ψ_i and its derivative $\partial_{y_i'}\psi_i$ are idealistically depicted in Figure 4.3. It should be noted that $c_1^{\text{eq}} = 0$ as the first element of the nonlinear vector ψ is null [see its definition defined by Eq. (4.9)].

Further, under the assumption that the responses of the equivalent stationary system are stationary zero-mean Gaussian processes, the relative non-dimensional velocity of the i-th TMD, y_i', also becomes Gaussian with corresponding variance, say $\sigma_{y_i'}$. Substituting the partial derivative of the friction force and using the sifting property of the Dirac delta function, the equivalent damping element c_{i+1}^{eq} can be consequently evaluated. Connected with the equivalency of the equivalent damping coefficient and its normalized form, Eq. (4.20) can be rearranged into the following

form:

$$c_{i+1}^{\mathrm{eq}} = 2\gamma_i \zeta_i^{\mathrm{eq}} = \sqrt{\frac{2}{\pi}} \eta_i \frac{1}{\sigma_{y_i'}}. \tag{4.21}$$

Rearranging Eq. (4.21) in terms of the design variable, g_{io} or τ_i gives:

$$\eta_i = \frac{g_{io}/\mu_i}{m_s \omega_s^2 x_{\mathrm{ref}}} = \frac{\tau_i}{\omega_s^2 x_{\mathrm{ref}}/g} = \sqrt{2\pi}\gamma_i \zeta_i^{\mathrm{eq}} \sigma_{y_i'} \tag{4.22}$$

Hence we have a equivalent linear matrix C^{eq} comprised of the equivalent force term, so that the solution obtained from the linear MTMD part can be adapted.

The matrix equation Eq. (B.23) can be rewritten in terms of equivalent linearized system by substituting the statistically linearized term into the nonlinear vector as follows:

$$My'' + (C + C^{\mathrm{eq}})y' + Ky = fw_g'' \tag{4.23}$$

where the matrices M, C and K are previously defined as Eqs. (4.12) and the equivalent damping matrix C^{eq} is defined as the comprise of the equivalent terms defined by Eq. (4.21) as follows:

$$C^{\mathrm{eq}} = \begin{bmatrix} 0 & 0 & \cdots & 0 \\ 0 & c_2^{\mathrm{eq}} & \cdots & 0 \\ \vdots & \vdots & \ddots & \vdots \\ 0 & 0 & \cdots & c_{N+1}^{\mathrm{eq}} \end{bmatrix} \tag{4.24}$$

With introducing a non-dimensional state vector $z = [y^{\mathrm{T}}, y'^{\mathrm{T}}]^{\mathrm{T}}$, a first-order state-space model can be formulated as follows:

$$z' = Az + Bw_g'' \tag{4.25}$$

where the corresponding matrices A and B are given by

$$A = \begin{bmatrix} O & I \\ -M^{-1}K & -M^{-1}(C + C^{\mathrm{eq}}) \end{bmatrix}, \tag{4.26a}$$

$$B = \begin{bmatrix} O \\ -f \end{bmatrix}. \tag{4.26b}$$

Note that the equivalent damping matrix of the equivalent linear system consists of the non-dimensionalized relative velocities of TMDs [see Eq. (4.21)], and the relative velocities can be evaluated upon a determined system property [see Eq. (4.25)]. Hence, it is necessarily required to assume the initial system properties and to iterate the circumstances as the appropriate tolerance to be minimized.

If the external loading w_g'' is a steady-state stationary white noise with its spectral strength $S_{w_g''}$ as assumed previously, the covariance matrix $Q = E[zz^{\mathrm{T}}]$ can be obtained by solving the following Lyapunov equation (Lutes and Sarkani, 2004):

$$AQ + QA^{\mathrm{T}} + 2\pi S_{w_g''} BB^{\mathrm{T}} = O. \tag{4.27}$$

4.3 Optimization Strategies

The response quantities of interest is the RMS displacement of the controlled main structure normalized to that of the uncontrolled one, σ_{y_s}. Attributed to its definition, the non-dimensional displacement of main structure σ_{y_s} would be in a range of zero to unity. Also it can be interpreted as a quantity for control efficiency such that σ_{y_s} is zero if the TMD completely suppress the vibration of main structure, and is unity when the TMD has no effect.

The mathematical description of the response of quantity can be established as follows:

$$\sigma_{y_s}^2 = E[y_s^2] = E[(s^{\mathrm{T}}z)^{\mathrm{T}}s^{\mathrm{T}}z] = \mathrm{tr}[SQ] \tag{4.28}$$

where $\mathrm{tr}[\cdot]$ is a trace operator, $s = [1, 0, \cdots, 0]^{\mathrm{T}}$ is the weighting vector corresponding to sifting the structural displacement, and S is the weighting matrix which can be calculated by $S = ss^{\mathrm{T}}$.

Then the optimization problem is formulated as:

$$\begin{aligned} &\underset{\gamma_d,\, \zeta_d}{\text{minimize}} && J = \sigma_{y_s} \\ &\text{subject to} && \gamma_d \in \Omega_\gamma,\ \zeta_d \in \Omega_\zeta \end{aligned} \tag{4.29}$$

where γ_d and ζ_d are the design variable vectors defined in the previous section that corresponds to appropriate constraints, and Ω_γ and Ω_ζ are the feasible regions for γ_d and ζ_d, respectively. Here, the feasible regions Ω_γ and Ω_ζ were set in a way that the frequency ratios γ_i, the damping ratios ζ_i, the bandwidth of frequency ratio β_γ and the fictitious damping ratio ζ_o are required to be non-negative.

In the optimization process, an initial guess of the design variables affects the number of function evaluations to find the solution. One could provide an initial point by adapting the classical solutions for STMD, for example, those proposed by Warburton (1982):

$$\gamma_t^* = \frac{\sqrt{1 + \mu_T/2}}{1 + \mu_T}, \tag{4.30a}$$

$$\zeta_t^* = \sqrt{\frac{\mu_T(1 + 3\mu_T/4)}{4(1 + \mu_T)(1 + \mu_T/2)}}. \tag{4.30b}$$

where γ_t^* and ζ_t^* are the optimal frequency ratio and damping ratio of the STMD, in which an asterisk in superscript (*) after a variable signifies that the variable is at its optimum.

The above Lyapunov equation can be efficiently solved by the well-established algorithms, for instance the algorithm proposed by Bartels and Stewart (1972), which is implemented in a commecial program such as MATLAB®. In the optimization procedure, this study adapted an iterative method for solving a sequence of Quadratic Programming Sub-problems subjected to a linearized constraint functions for its superior rate of convergence. At each iteration, to make an approximation of the Hessian matrix, Broyden-Fletcher-Goldfarb-Shanno algorithm was adopted for its effectiveness and good performance even for non-smooth optimization problems (Coleman et al., 1999).

4.3.1 Set 1: FMTMD$_{\mathrm{o}}$ and FMTMD$_{\gamma}$

In the cases of FMTMD$_{\mathrm{o}}$ and FMTMD$_{\gamma}$, the optimal level of frictional force and associated COF can be determined from the optimal solution of equivalent linear system. Consider the first set of FMTMD$_{\mathrm{o}}$ and FMTMD$_{\gamma}$. The relationship between the nonlinear force to be optimized and relevant equivalent linear terms is given by Eq. (4.22), repeated here for convenience:

$$\eta_i = \sqrt{2\pi}\gamma_i \zeta_i^{\mathrm{eq}} \sigma_{y_i'}. \tag{4.22}$$

One can see from the relationship that the nonlinear force is determined explicitly in terms of the coefficients such as γ_i and ζ_i, and the normalized RMS velocity $\sigma_{y_i'}$ of the equivalent linear system. And the expression for the nonlinear term is explicit, since $\sigma_{y_i'}$ is not dependent on the nonlinear force η_i, but is determined by the parameters of the equivalent linear system, γ_i and ζ_i. Hence, seeking the optimal nonlinear parameter η_i falls into finding the optimal parameters of linearized system, that can be accomplished by the procedure used in LMTMD optimization.

The optimal friction force η_i^*, hence, can be determined by both optimal parameters γ_i^* and $\zeta_i^{\mathrm{eq}*}$, and associated RMS velocity $\sigma_{y_i'}$ of the equivalent system by following

expression:

$$\eta_i^* = \sqrt{2\pi}\gamma_i^*\zeta_i^{\mathrm{eq}*}\sigma_{y_i'}^* \tag{4.31}$$

where the optimal parameters γ_i^*, $\zeta_i^{\mathrm{eq}*}$ and $\sigma_{y_i'}^*$ can be obtained by the procedure used in LMTMD optimization.

4.3.2 Set 2: FMTMD$_\tau$ and FMTMD$_{\gamma\tau}$

It becomes tedious to find the optimal solution for the set of FMTMD$_\tau$ and FMTMD$_{\gamma\tau}$. In these cases, the optimal parameters are restricted in a way that all of the frictional coefficient are of equal, so that constrained optimization scheme should be adopted.

Consider the first set of FMTMD$_\tau$ and FMTMD$_{\gamma\tau}$. The relationship between the nonlinear force to be optimized and relevant equivalent linear terms is given by Eq. (4.22), repeated here again for convenience:

$$\frac{\tau_i}{\omega_s^2 x_{\mathrm{ref}}/g} = \sqrt{2\pi}\gamma_i\zeta_i^{\mathrm{eq}}\sigma_{y_i'} \tag{4.22}$$

As likely the previous set, the COF is determined explicitly in terms of the coefficients such as γ_i and ζ_i, and the normalized RMS velocity $\sigma_{y_i'}$ of the equivalent linear system. The optimal COF τ_i^*, hence, can be determined by both optimal parameters γ_i^* and $\zeta_i^{\mathrm{eq}*}$, and associated RMS velocity $\sigma_{y_i'}$ of the equivalent system.

In the case where the COFs are restrained to be identical, an additional constraint should be applied as follows:

$$\tau_1 = \tau_2 = \cdots = \tau_N. \tag{4.32}$$

Or equivalently, Eq. (4.32) can be rewritten in terms of normalized variables as follows:

$$\gamma_1\zeta_1^{\mathrm{eq}}\sigma_{y_1'} = \gamma_2\zeta_2^{\mathrm{eq}}\sigma_{y_2'} = \cdots = \gamma_N\zeta_N^{\mathrm{eq}}\sigma_{y_N'}. \tag{4.33}$$

It should be also taken into account that the optimal frictional coefficient depends on the optimal variables which can be found from the equivalent linear system. Hence, the previous chapter for linear MTMDs can be employed in obtaining such optimal variables. Since the optimal parameters are the ones under the linear assumption so that they do not depend on the excitation level or the vibration level of the primary structure, but the denumerator of the left hand side of the equation, x_{ref} depends on the excitation level. As a result, the optimum of the frictional coefficient of the TMDs also depends on the excitation level.

4.4 Results and Discussion

This section concerns numerical results including the features of the optimal parameters, the frequency responses of the system with optimized FMTMDs and input-sensitivity analysis result. Further, an approximate solution for designing FMTMD$_{\gamma\tau}$ is also considered. In the below, the main system is characterized by a damping ratio of 1%, and the total mass ratio of the MTMDs is predetermined to be in the range of 1% to 10% at intervals of 1%, though in some cases the parameter is held to be 5%. The number of TMD units are increased from one (i.e. single TMD) to ten.

4.4.1 Optimal parameters

Figure 4.4 depicts the optimal frequency ratios γ_i^* and the optimal equivalent damping ratios $\zeta_i^{\text{eq}*}$ in $(\gamma - \zeta)$ space, for a given total mass ratio of 5%. It follows that all cases have the same optimal condition for single TMD of $\gamma_1^* = 0.97$ and $\zeta_1^{\text{eq}*} = 0.11$, which corresponds to the well-established solution provided by Warburton (1982). From the optimal solution for single TMD, the bandwidth of the frequency ratios becomes wider and the optimal damping ratios tend to decrease with increasing of the number of TMD units.

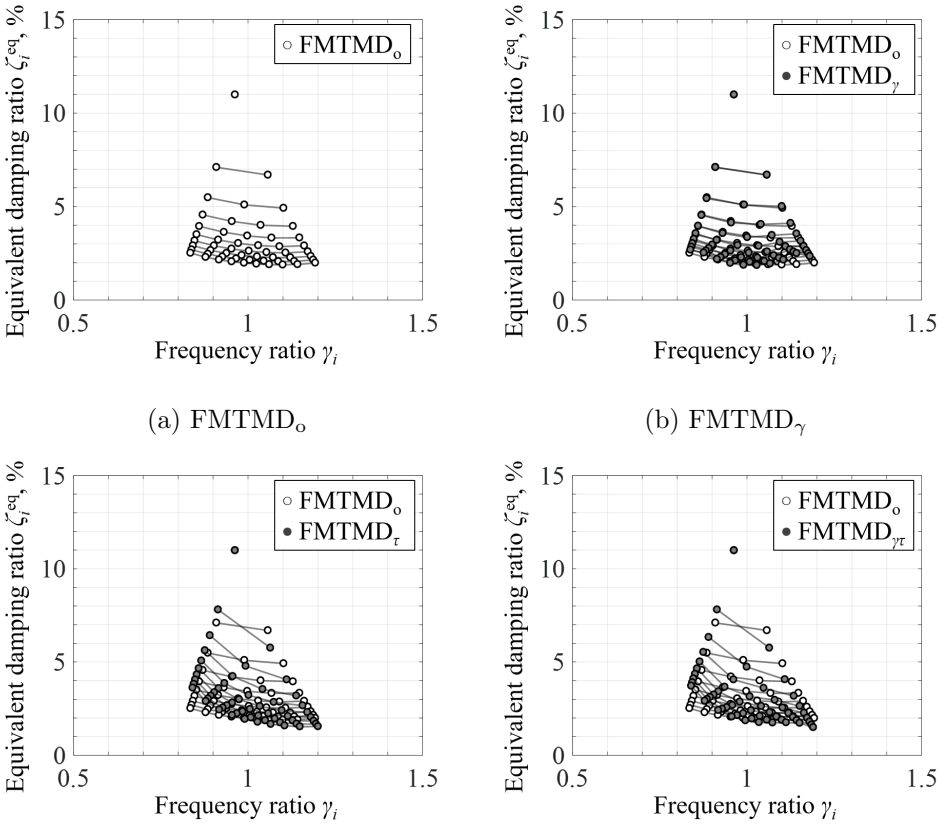

(a) FMTMD$_o$

(b) FMTMD$_\gamma$

(c) FMTMD$_\tau$

(d) FMTMD$_{\gamma\tau}$

Figure 4.4: Optimal frequency ratios and equivalent damping ratios for FMTMDs ($\mu_T = 5\%$)

In the case of FMTMD_o on which no restrictive assumption is imposed, the optimal tuning condition is achieved when the frequency ratios are not evenly spaced, but are densely covered around the natural frequency of primary structure. Also it appears that TMDs located nearby the natural frequency of primary structure tend to require lower damping ratios than other TMDs (see Figure 4.4a).

In FMTMD_γ, it is observed that the optimal parameters are gradually deviated from those of FMTMD_o with increasing of the the number of TMDs. Due to the constraint that the frequency ratios are evenly spaced, some TMDs are compulsory located at the end of the frequency bandwidth (see Figure 4.4b). Under the condition, the TMDs located at the end of the bandwidth requires relatively large damping compared to the unconstrained condition.

There is no considerable difference between FMTMD_τ and $\text{FMTMD}_{\gamma\tau}$ except for the distribution of the frequency ratios. However, when comparing these two configurations to FMTMD_o, the optimal equivalent damping ratios are distributed in a inconsistent way that the TMDs with high frequency ratio tends to dampen highly. This trend can be explained as follows: Under the constraint on the identical COF, multiplied value of the frequency ratio, equivalent damping ratio and its normalized RMS velocity of the i-th TMD is restrained to be a constant for all TMDs, as can be seen from Eq. (4.22). Of the components, though not explicitly, the TMD unit with lower equivalent damping ratio might experiences large velocity, constituting their multiplication to be almost constant. Hence, under the constraint, $\zeta_i^{\text{eq}*}\sigma_{y_i'}^*$ would be inversely proportional to the frequency ratio γ_i, and $\zeta_i^{\text{eq}*}$ also become inversely proportional to the one.

Figure 4.5 delineates the spatial distribution of optimal parameters such as frequency ratios and equivalent damping ratios under the predetermined total mass ratio μ_T in a range of 1 to 10% with an interval of 1%. In this figure, the solid line with circle marks on the very acute vortex represents a design curve for single TMD pro-

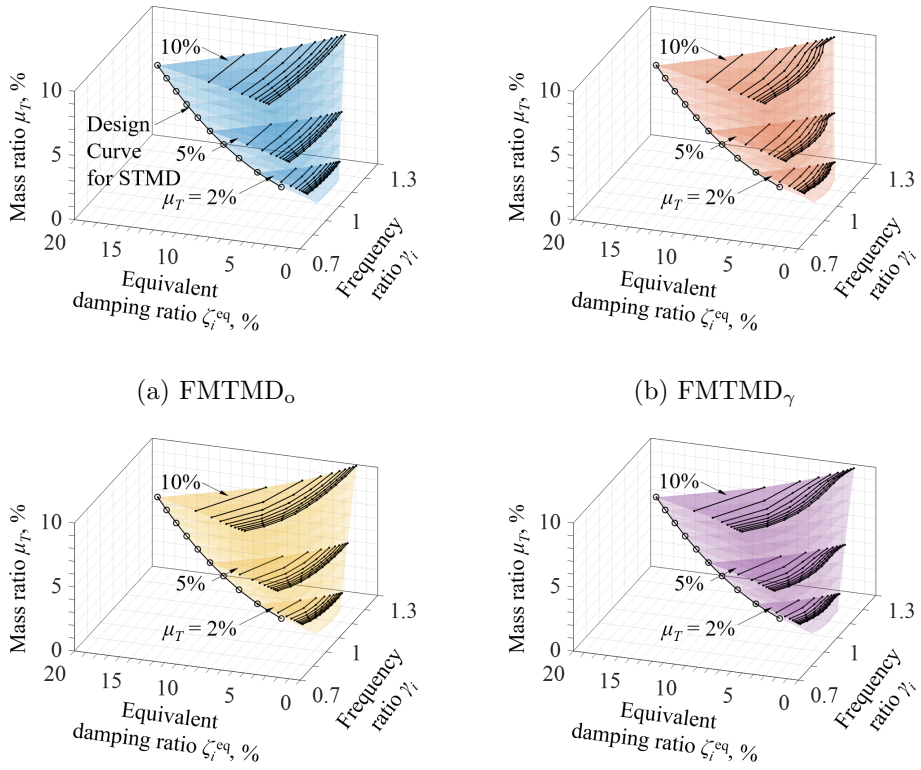

(a) FMTMD$_{\text{o}}$

(b) FMTMD$_{\gamma}$

(c) FMTMD$_{\tau}$

(d) FMTMD$_{\gamma\tau}$

Figure 4.5: Spatial representation for optimal frequency ratios optimal equivalent damping ratios of FMTMDs

posed by Warburton (1982). Each configuration exhibits a similar pattern showed by 4.5 within every layer of a predetermined mass ratio, involving the patterns that the optimal frequency ratio becomes wider and the damping ratio becomes decreasing as the number of TMDs becomes larger. With regard to the effect on the total mass ratio μ_T, the margin of decreasing the damping ratio becomes larger with increasing the mass ratio. Moreover, it can be found that the damping ratio becomes asymptotically smaller, implying the existence of some convergence lines as the number of TMDs under a sufficiently large number. The patterns in the $\gamma - \zeta$ domain explained in the above are also observed in all the considered mass ratios for each of MTMD: while the FMTMD_{o} forms a widening funnel shape with circular sector, the FMTMD_{γ} forms similar pattern with irregular circular sector, and the cases of constrained damping coefficients such as FMTMD_{τ} and $\text{FMTMD}_{\gamma\tau}$ form funnel shapes with triangular sector.

The optimal frequency ratios γ_i^* and optimal normalized friction forces η_i^* are depicted in Figures 4.6, in which the optimal friction force is transformed from Eq. (4.22). First of all, the backbone curve that is valid for the SFTMD can be determined by following procedure. The optimal frequency ratios and the optimal equivalent damping ratio for the STMD are proposed by Warburton (1982). Some characteristics are inherited from those of Figure 4.5, but the decreasing trend with increasing the number of TMDs becomes much steeper compared to those of optimal equivalent damping ratios. Such an aspect attributes to the feature of the relationship between the frictional force and the optimal linear properties expressed in Eq. (4.22), in which the optimal frictional force is not only proportional to the optimal equivalent damping ratio but also inversely proportional to the relative velocity of the TMD. As the relative velocity would be increase with decreasing the damping ratio for the increasing of the number of TMD, the optimal frictional force decreases rapidly caused by both the decreasing of damping ratios and the increasing of relative TMD velocity.

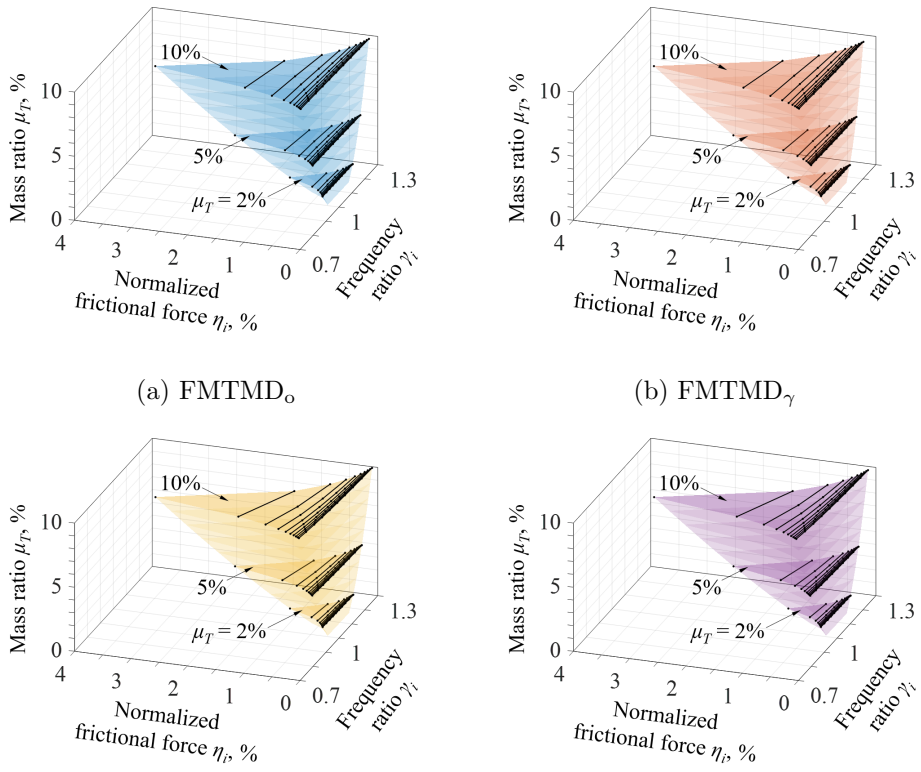

(a) FMTMD$_{\text{o}}$

(b) FMTMD$_{\gamma}$

(c) FMTMD$_{\tau}$

(d) FMTMD$_{\gamma\tau}$

Figure 4.6: Spatial representation for optimal frequency ratios optimal normalized frictional force of FMTMDs

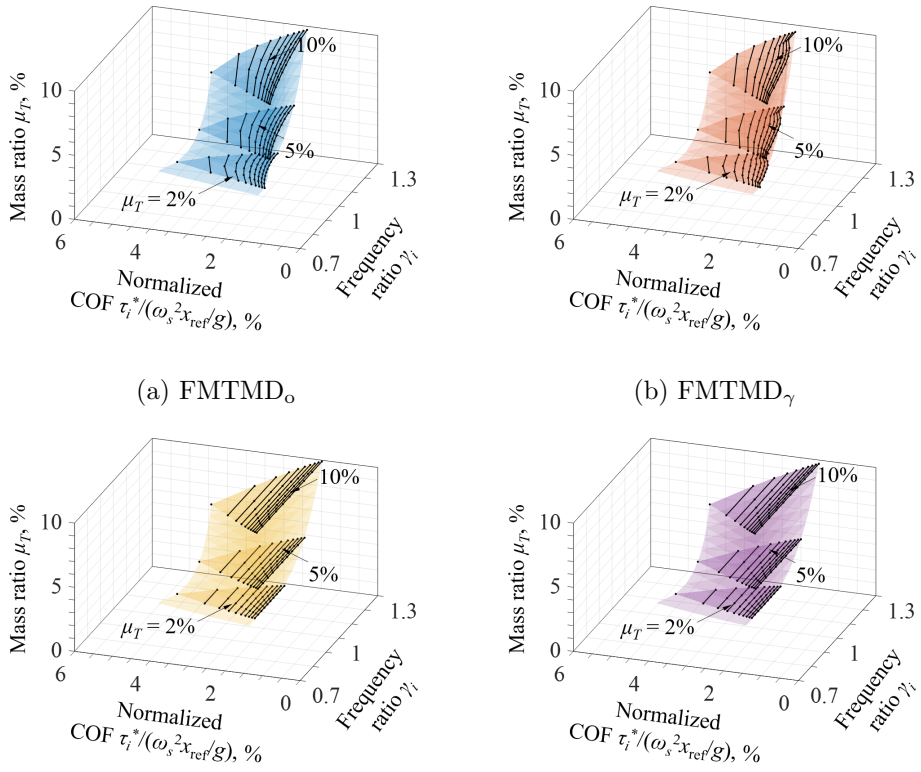

(a) FMTMD$_{\text{o}}$ (b) FMTMD$_{\gamma}$

(c) FMTMD$_{\tau}$ (d) FMTMD$_{\gamma\tau}$

Figure 4.7: Spatial representation for optimal frequency ratios optimal COFs of FMTMDs

The optimal frequency ratios and optimal COF are depicted in Figures 4.6, in which the optimal friction force is, further, transformed from Eq. (4.22). Again, the solid line with circle marks on the very acute vortex converted from the key equation and a design curve proposed by Warburton (1982). Key aspects of this figure can be found in Figures 4.7c and 4.7d that the spatial distribution of optimal parameters for given mass ratio lie on straight lines with uniform COF, for which the approximate solution would be provided in the following next section.

4.4.2 Frequency responses with optimal parameters

To illustrate the efficiency of the considered MTMDs, we considered a primary structure with its damping ratio of 1% and MTMDs of 10 units with its total mass ratio of 5%. Figure 4.8 compares the frequency response functions (FRFs) for the displacement of primary structure with the response of the main mass alone. Although some minor differences in their shapes, all LMTMDs with considered configurations can reduce amplitudes effectively, of which frequency responses show $N+1$ well-separated local modes.

Figure 4.8a compares the FRFs for FMTMD_{o} and FMTMD_{γ} and no significant difference was found. Also there is no considerable difference between FMTMD_{τ} and $\text{FMTMD}_{\gamma\tau}$ when comparing Figures 4.8b and 4.8c. Based on these comparisons, it can be concluded that there is no considerable effect in performance when the constraint on the frequency ratios is taken into account.

Compared to FMTMD_{o}, Both FMTMD_{τ} and $\text{FMTMD}_{\gamma\tau}$ differ in the way that sharp peak appears at the low frequency with the following peaks gradually becoming blunt as the frequency becomes higher (see Figures 4.8b and 4.8c). Such a feature is ascribed to the constraint for identical COF, which would provide larger damping force with heavier TMD with low frequency ratio. The difference between the FRFs of FMTMD_{τ} and $\text{FMTMD}_{\gamma\tau}$ is ascribed to the constraint for linearly distributed

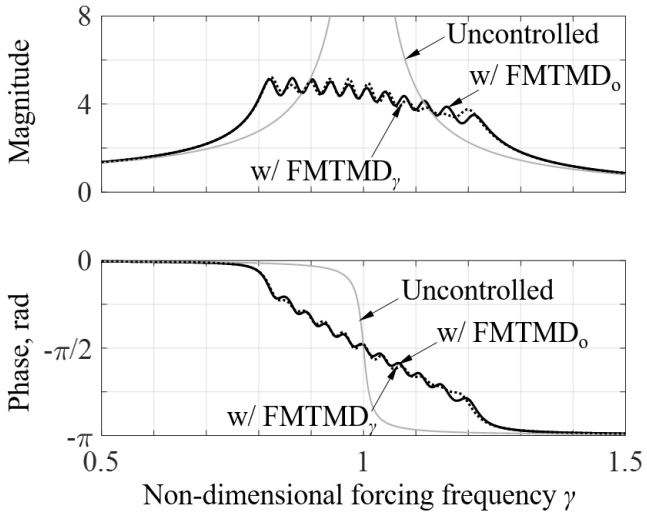

(a) FMTMD$_o$ and FMTMD$_\gamma$

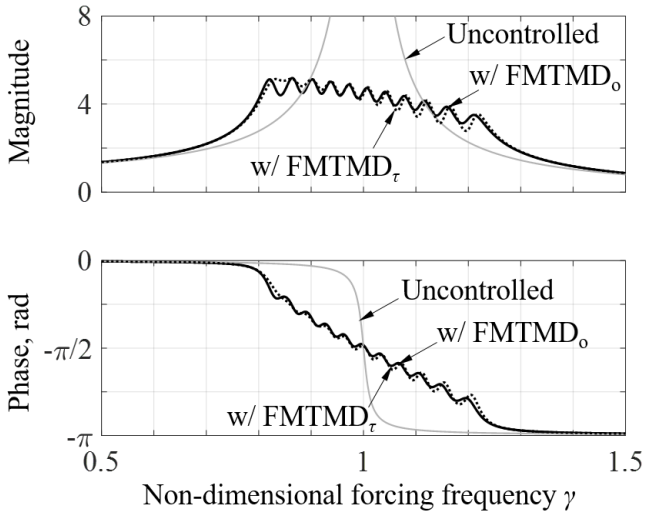

(b) FMTMD$_o$ and FMTMD$_\tau$

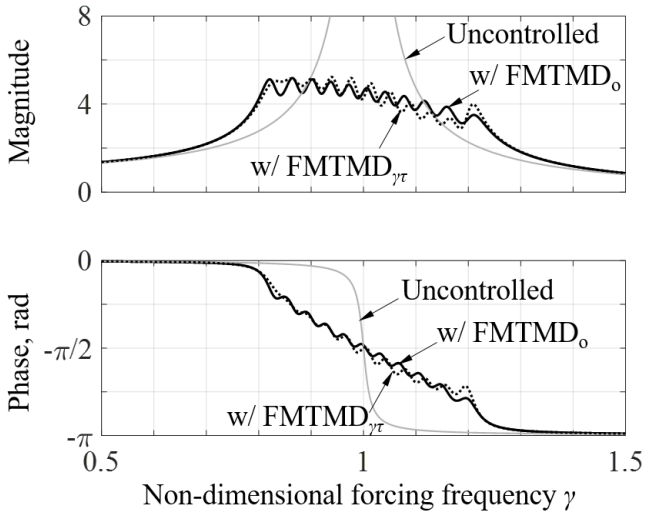

(c) FMTMD$_o$ and FMTMD$_{\gamma\tau}$

Figure 4.8: Comparison of FRFs for various FMTMD configurations under the targeted input level ($\mu_T = 5\%$ and $N = 10$)

frequency ratios.

4.4.3 Input-intensity sensitivity analysis

Since nonlinear systems involving the structure-FMTMD system do not described by an impulse response, the variation of the frequency responses caused by an input level should be strictly considered. The frequency responses described in the preceding subsection are valid only in a case that the external input strength is corresponding to the targeted or designed one. Although a specific condition is designed to meet a targeted performance level in a specific load level, the frequency responses for other level of excitation differ significantly, often yielding deteriorated performance.

In the below, an input-sensitivity analysis was extensively carried out. To illustrate the efficiency of the considered MTMDs, we considered a primary structure with its

damping ratio of 1% and MTMDs of 5 units with its total mass ratio of 5%. Two configurations FMTMD_{o} and FMTMD_{τ} are considered. Once the non-dimensionalized optimal parameters were determined under the input level of $S_{w_g''}$, the optimized structure are subjected to varying strength of input.

Figures 4.9 depict the FRFs of the considered FMTMDs under the input loadings are in a range from 0.5 to 1.5 with its interval of 0.1, and those for the cases of 0.5, 1.0 and 1.5 are highlighted with the colors of blue, purple and red, respectively. It can be seen from these figures that once the FRFs under a low level of input strength would blunt appearing the original structural mode becomes flatten with increasing the loading level to 0.5. Further increased loading to the originally-targeted loading enables the TMDs to facilitate in a active way until the targeted input strength. As the input level further increases beyond the targeted input level, the equivalent damping ratios decreases compared to those for targeted one, causing undesired and frivolous motions of TMDs resulting in their FRFs to be more increased peaks and deep valleys, which might be unhelpful in controlling the main structure. Comparing Figures 4.9a and 4.9b, FMTMD_{τ}, a configuration that the COF is comparably restricted to be identical, appears more detrimental compared to FMTMD_{o}. The reason for the trend is ascribed to the irregular pattern of the damping ratio as shown in the preceding section on the optimal parameters.

The input-dependent frequency responses would be problematic when the FRFs are concerned with loading input. Figures 4.10a and 4.10b depict the FRFs of considered FMTMDs_{o} under the various input loadings that is consistent with Figure 4.9, but the loading scale attributes. As in Figure 4.9, the figure plots the cases in a range from 0.5 to 1.5 with its interval of 0.1, and those for the cases of 0.5, 1.0 and 1.5 are highlighted with the colors of blue, purple and red, respectively. It can be seen that the aspects of the FRFs could be more problematic if the loading level exceeds the targeted level. As the input level further increases beyond the targeted

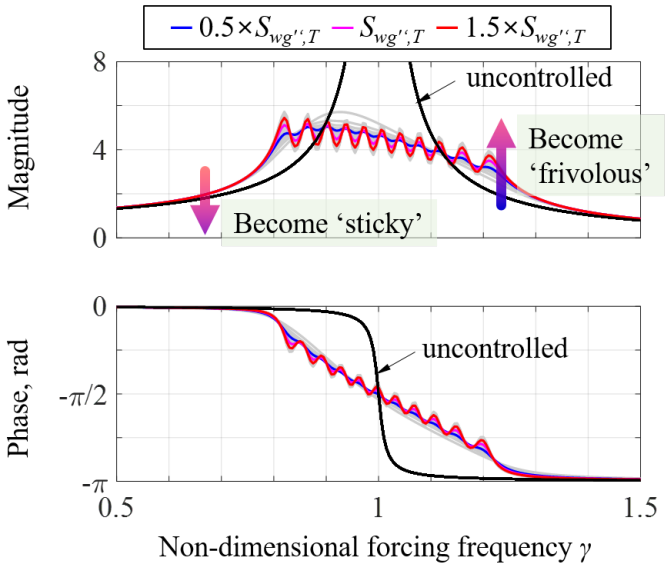

(a) FMTMD_{o}

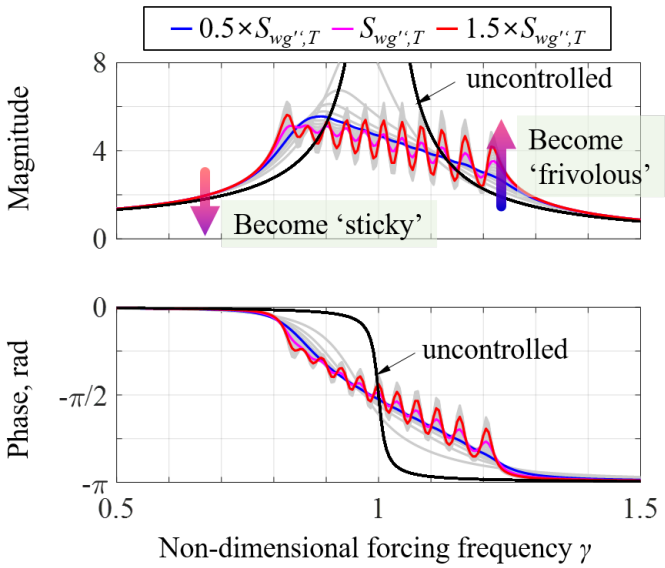

(b) FMTMD_{τ}

Figure 4.9: Sensitivity of normalized frequency response functions ($\mu_T = 5\%$ and $N = 5$)

input level, the equivalent damping ratios decreases compared to those for targeted one, causing undesired and frivolous motions of TMDs resulting in their FRFs to be more increased peaks and deep valleys, which might be unhelpful in controlling the main structure.

In order to concern the robustness issue with varying input strengths, we graphically plotted the relationship between the input level normalized to the targeted loading strength and the maximum of the FRFs. Figures 4.11a and 4.11b depict the input-sensitivity of the peak of maximum FRF of FMTMD_{o} and FMTMD_{τ}, respectively. In these plots, we can found an interesting feature such that under a slightly low level of the input strength, say in a range of 0.4 to 1.0 for two units of FMTMD_{o} configuration, helps suppressing the peak of the FRF.

4.4.4 Approximate solution for $\text{FMTMD}_{\gamma\tau}$

So far in this study we have considered various FMTMD configurations, of which optimal solutions cannot be simply described for the numerous number of design variables. $\text{FMTMD}_{\gamma\tau}$, however, can be determined its optimal condition with just three design variables such as two bound frequency ratios γ_1 and β_γ, and a COF τ.

Figure 4.12 shows the parameters m_1, m_2 and τ_i for various mass ratio and number of TMDs for optimal $\text{FMTMD}_{\gamma\tau}$. As discussed in preceding sections, parameters γ_1 decreases and increases β_γ with increasing the number of TMDs and the mass ratio, indicating the spread of frequency bandwidth, and the COF τ decreases requiring exponentially decreased damping per unit TMD. In order to provide simple and useful ways, the regressive formula are established, which provide sufficient agreement with the raw data. The formula are given by

$$m_1 \approx p_0 \exp(-p_2 * \mu_T^{p_3}) \tag{4.34a}$$

$$m_2 \approx p_0 \exp(-p_2 * \mu_T^{p_3}) \tag{4.34b}$$

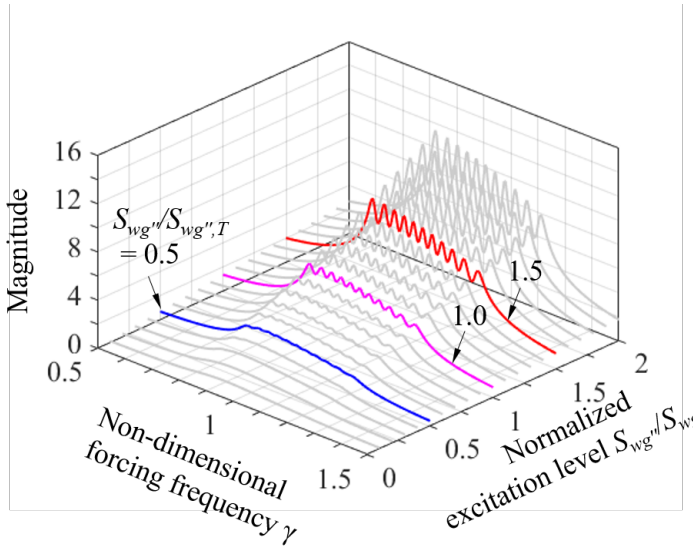

(a) FMTMD$_{\text{o}}$

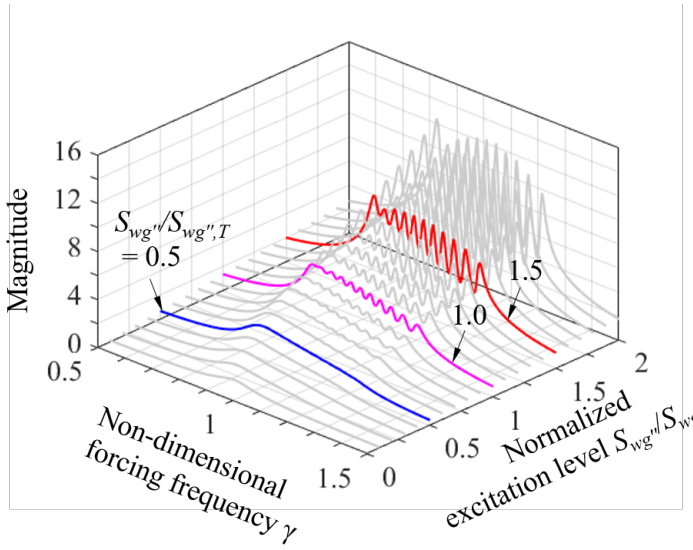

(b) FMTMD$_{\tau}$

Figure 4.10: Sensitivity of frequency response functions ($\mu_T = 5\%$ and $N = 5$)

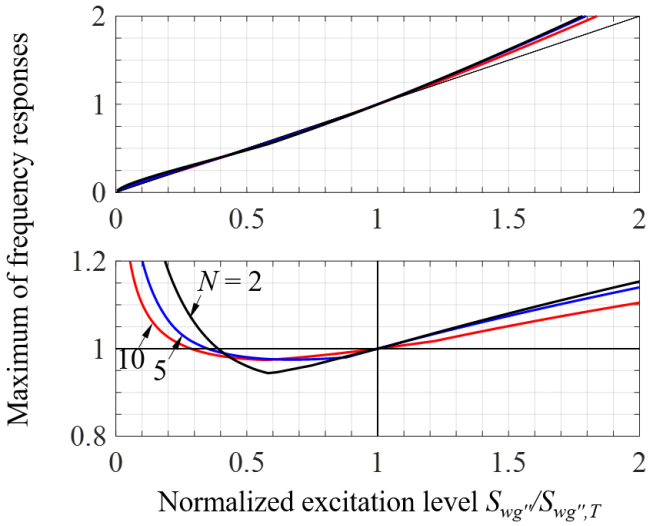

(a) FMTMD$_{\mathrm{o}}$

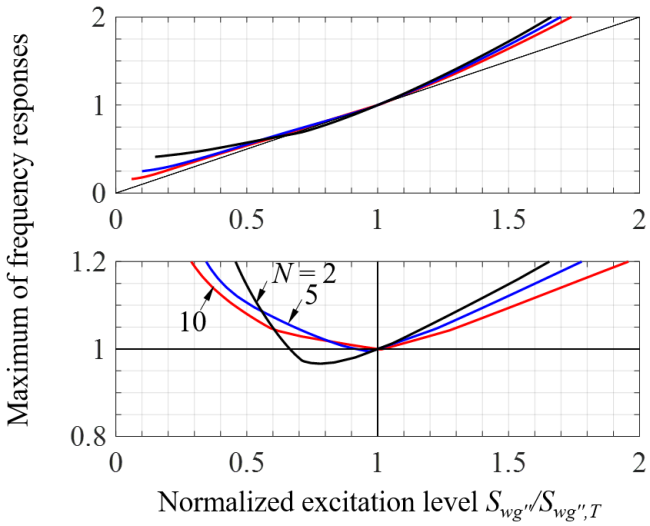

(b) FMTMD$_{\tau}$

Figure 4.11: Sensitivity of frequency response functions ($\mu_T = 5\%$ and $N = 5$)

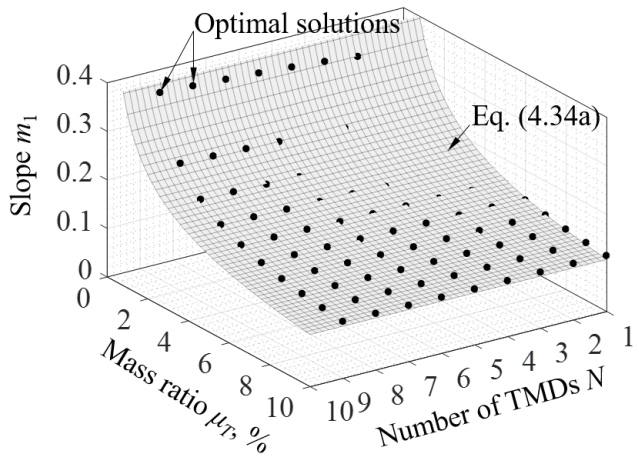

(a) Slope m_1

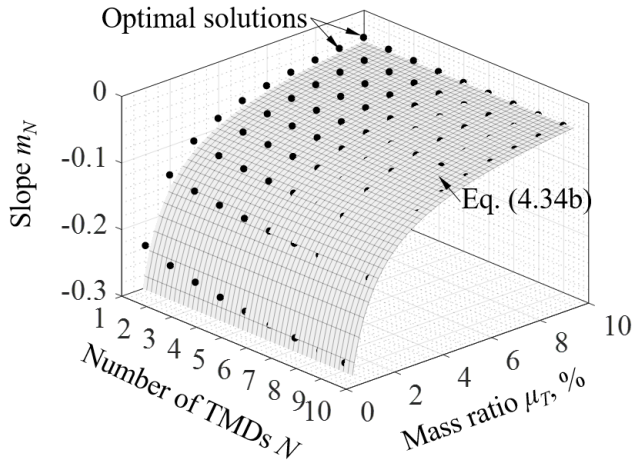

(b) Slope m_N

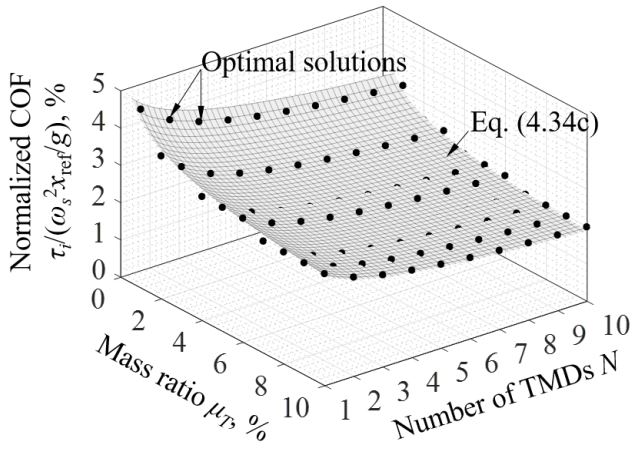

(c) Optimal normalized COF $\tau_i/(\omega_s^2 x_{\mathrm{ref}}/g)$

Figure 4.12: Shape parameters for optimal LMTMD$_{\gamma\zeta}$

$$\tau_i/(\omega_s^2 x_{\mathrm{ref}}/g) \approx p_0 \exp[p_1 N^{p_2} \mu_T^{p_3}] \tag{4.34c}$$

Equations. (4.34a) and (4.34b) can be useful in designing optimal FMTMD$_{\gamma\tau}$. The other factors can be determined by some equations. If more fitter equation is needed, one can use the following higher order equation. The design parameters and regressive coefficients are summarized in Table 4.2.

Table 4.2: Design parameters and regression coefficients

Parameter	Coefficient				R^2
	p_0	p_1	p_2	p_3	
m_1 [Eq. (4.34a)]	38.98	7.40	0.10	-	0.9872
m_N [Eq. (4.34b)]	-5547	13.78	0.07	-	0.9883
$\tau_i/(\omega_s^2 x_{\mathrm{ref}}/g)$ [Eq. (4.34c)]	1.423	-4.337	0.047	0.049	0.9631

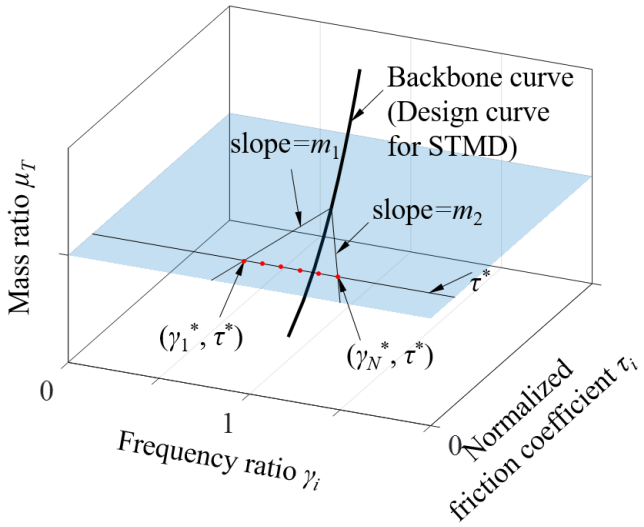

Figure 4.13: Graphical representation on spatial distribution of FMTMD$_{\gamma\tau}$

$$\gamma_1^* = \gamma_t^* + \frac{\tau_i^* - \tau_t^*}{m_1(\omega_s^2 x_{\text{ref}}/g)} \tag{4.35a}$$

$$\gamma_N^* = \gamma_t^* + \frac{\tau_i^* - \tau_t^*}{m_N(\omega_s^2 x_{\text{ref}}/g)} \tag{4.35b}$$

4.5 Design Procedure

This section is dedicated to demonstrate the design procedure for the case of parallel type MTMDs, each of which comprises a linear spring and a viscous damping element. The following design procedure covers not only the case of designing a new structure but also the case of mitigating the existing structures.

1. Determine the dynamic properties such as the structural mass m_s, structural damping coefficient c_s, and structural stiffness k_s. Those can be either assumed

appropriately or estimated from field measurements.

2. Evaluate the anticipated structural response, for instance the structural displacement x_s, and determine the performance level to be attained.

3. Determine the total mass ratio of the MTMDs $\mu_T = \sum_{i=1}^{N} \mu_i$, which directly yields the total mass of the MTMDs, with the help of the relationship between the total mass ratio and the controlled structural RMS response normalized to the uncontrolled one.

4. Select the optimal frequency ratios and the optimal damping ratio for the configuration type and the number of TMDs what you prefers. Do not struggle with choosing the total number of TMDs in terms of performance, since it does not affect vibration mitigation level. However, keep in mind that increasing the number of TMDs yields decreasing the optimal damping ratios, demanding larger stroke limitations.

5. Check whether the stroke of MTMDs chosen at the previous step exceeds the prescribed stroke limitations. If exceeds, two solution could be imposed: Reduce the number of TMDs, or make the chamber to absorb the excessive strokes.

4.6 Concluding Remarks

This study provided a framework for design of frictional multiple tuned mass dampers (FMTMDs), which can provide guidance about all aspects of the FMTMDs including the MTMD configurations, issue on the robustness for loading-sensitivity, and the stroke limitation issue. To this end, the optimal parameters of various FMTMD configurations are investigated, of which constraints are such as the frequency ratios and coefficient of friction.

The key features can be drawn as follows:

1. The optimal parameters like frequency ratios and equivalent damping ratios of MTMD, which are obtained from a statistical linearization technique, are found under the condition that the main structure is excited by a ground motion of stationary zero-mean white-noise.

2. From the backbone curve predicted by the classical solution of Warburton (1982), the optimal frequency range tends to span further as the number of TMDs increases, and the optimal equivalent damping ratio per an unit TMD becomes smaller. The rate of increasing the span and decreasing the damping ratio is drastic when the total mass ratio is larger, showing insignificant difference with a larger number of TMDs.

3. An input-sensitivity analysis was extensively conducted. It was shown that once the FRFs under a low level of input strength would blunt appearing the original structural mode becomes flatten with increasing the loading level to 0.5. Further increased loading to the originally-targeted loading enables the TMDs to facilitate in a active way until the targeted input strength.

4. As the input level further increases beyond the targeted input level, the equivalent damping ratios decreases compared to those for targeted one, causing undesired and frivolous motions of TMDs resulting in their FRFs to be more increased peaks and deep valleys, which might be unhelpful in controlling the main structure.

5. The approximate solution for FMTMD$_{\gamma\tau}$ was determined its optimal condition with just three design variables such as two bound frequency ratios γ_1 and β_γ, and a COF τ.

Chapter 5

Extreme Value Analysis for Frictional MTMDs

This study addresses the characteristics of stochastic responses of a system incorporated with optimal frictional tuned mass dampers (FTMDs). First, with the aim of finding the optimal parameters, a statistical linearization technique is employed, in which a nonlinear force term was replaced with linearized one that is equivalent in a statistical sense. In order to improve an accuracy for the estimation of the RMS value of FTMD based on the statistical linearization, this study exploits a statistical nonlinearization technique, which replaces nonlinear systems with a class of other well-solved nonlinear systems. A correction factor that is defined as the ratio of RMS displacement between nonlinear and linear system is proposed on the basis of the result of statistical nonlinearization technique. This study further derived an explicit formula for evaluating a peak factor for the frictional TMD. The correction factor and the peak factor are examined with numerical simulations.

5.1 Introduction

Tuned mass damper (TMD) is a passive control device that additionally attached to a vibrating structure so as to dampen the structural vibration. In principle, a TMD attracts vibration energy of the main structure into itself by resonance, and dissipates it through built-in energy dissipation devices. Since its invention of Frahm (1911), much effort was directed toward the design of a linear TMD that is connected to the main structure with a spring and a viscous damper in parallel (Den Hartog, 1956; Warburton, 1982; Asami et al., 2002; Bisegna and Caruso, 2012). Moreover incorporating such a linear dissipation device enables one to provide fruitful statistics of the response relevant to reliability such as level crossing rates (Lutes and Sarkani, 2004; Newland, 2012).

Although various forms of nonlinearity are ubiquitous in nature, and it is usually never welcomed in mechanical and structural engineering fields because of mathematical complexity involved. Particularly in implementing linear TMDs, the viscous element actually do display nonlinear behavior (Terenzi, 1999), which may lead to undesired side effects such as being out of optimal condition. In order for designers to accommodate such an undesired nonlinearity, several researchers investigated the behavior of nonlinear TMDs (Rüdinger, 2006, 2007; Love and Tait, 2015).

In some cases, such a nonlinear dissipation mechanism is incorporated in an intentional way in order to overcome some disadvantages of linear viscous elements, for example, the loss of its dissipation performance over time caused by liquid leakage. Inaudi and Kelly (1995) proposed a nonlinear TMD that uses friction mechanism as energy dissipation sources. Wang (2011) proposed a nonlinear TMD that incorporates the Coulomb-type frictional dissipating mechanism, and examined its feasibility through numerical simulations. Carpineto et al. (2014) examined the applicability of nonlinear TMDs consisted of steel wire ropes, whose hysteretic behaviors can be

described in terms of Bouc-Wen constitutive law.

Nonlinear differential equations that describe the above-mentioned problems are much more challenging to solve than their linear counterparts. One attractive method of solving the nonlinear differential equations is the statistical linearization which can replace a set of the nonlinear equations by a set of linear ones that is equivalent in a statistical sense. Some theoretical aspects of this technique including a variety of applications are well described in the literature (Roberts and Spanos, 2003; Socha, 2005a,b).

In spite of convenience in its applicability, the statistical linearization may be inaccurate in calculating the necessary responses. The inaccuracy can result from the discrepancy between the equivalent linear system whose responses are presumed to be Gaussian and the original one presumed to be non-Gaussian. Especially such a discrepancy may lead to inaccurate estimation of the RMS displacement and relevant peak values of the original nonlinear TMD, which may be of vital importance in designing its accommodating chamber.

In order to minimize the discrepancy, Love and Tait (2015) employed the concept of statistical nonlinearization to represent the nonlinear damping as amplitude-dependent viscous dapming and predicted the RMS response of the structure-TMD system. They obtained the probability density function for the TMD dispacement and estimated the peak response distribution. However, more detailed study is still necessary for the accuracy in estimation of RMS response and the peak response distribution.

This study addresses the RMS response and the extreme value distribution for the frictional tuned mass dampers (FTMDs). To predict more accurate peak distribution of TMDs, this study exploits the statistical nonlinearization technique, in which nonlinear systems are replaced with a class of other nonlinear systems whose exact solution have been already explicitly derived. A correction factor that is defined as the

ratio of RMS displacement between nonlinear and linear system is also derived based on the result of statistical nonlinearization technique. This study further derived an explicit formula for evaluating a peak factor for the frictional TMD. The correction factor and the peak factor are examined with numerical simulations.

5.2 FMTMD Optimization

5.2.1 Governing equations of motion

Consider a system comprised of a primary structure and N units of TMD, each of which is connected with a linear spring and a nonlinear element in parallel (see Figure 4.1). The structure-MTMD system can be represented as the following differential equations:

$$(m_s + m_T)\ddot{x}_s + \sum_{i=1}^{N} m_i\ddot{x}_i + c_s\dot{x} + k_s x = f_s \tag{5.1a}$$

$$m_i(\ddot{x}_s + \ddot{x}_i) + g_i + k_i x_i = 0 \qquad i = 1, \cdots, N \tag{5.1b}$$

where m_s, c_s and k_s are the mass, damping constant and spring constant of the primary structure; m_i and k_i are the mass and spring constant of the i-th unit of the TMDs; N is the number of TMDs; g_i is a dissipation force induced by relative motion of the i-th unit of the TMD; m_T is the total mass of the TMDs calculated by $\sum_{i=1}^{N} m_i$; x_s is the displacement of the primary structure, and x_i is the displacement of the i-th unit of the TMDs relative to that of the primary structure; A dot notation is used for indicating a derivative with respect to time t; The external force exerted on the primary structure and on the i-th unit of the TMDs are denoted as f_s, and f_i, respectively.

If the whole system is excited by a zero white-noise base acceleration, each of the force terms associated the i-th unit of MTMD is zero and that on the primary structure is $-(m_s+m_T)\ddot{u}_g$, where $\ddot{u}_g$ is the ground acceleration with a constant spectral intensity $S_{\ddot{u}_g}$, i.e.,

$$E[\ddot{u}_g(t)\ddot{u}_g(t+\Delta t)] = 2\pi S_{\ddot{u}_g}\delta(\Delta t), \tag{5.2}$$

where $E[\cdot]$ is an expectation operator and $\delta(\cdot)$ is the Dirac-delta function.

If the dissipative force is of power-law type then the force term g_i may be written parametrically as follows:

$$g_i = g_i(\dot{x}_i) = g_{io}|\dot{x}_i|^{\beta}\mathrm{sgn}(\dot{x}_i) \tag{5.3}$$

where g_{io} is a damping coefficient for the i-th TMD, sgn$[\cdot]$ is a signum function and β is a parameter that determines the type of dissipation force: values of zero and unity correspond to the Coulomb-type and viscous dissipation force, respectively.

Dividing Eqs. (5.1a) and (5.1b) by the mass of the primary structure m_s and that of the i-th TMD respectively yields the following equations:

$$(1+\mu_T)\ddot{x}_s + \sum_{i=1}^{N}\mu_i\ddot{x}_i + 2\zeta_s\omega_s\dot{x} + \omega_s^2 x = -(1+\mu_T)\ddot{u}_g \tag{5.4a}$$

$$\ddot{x}_s + \ddot{x}_i + g_i/m_i + \gamma_i^2\omega_s^2 x_i = 0 \qquad i = 1, \cdots, N \tag{5.4b}$$

where the normalized terms μ_i and γ_i are the ratio between the mass of the i-th TMD and that of the main structure, and the frequency ratio (i.e., the ratio between the

frequency of the TMD by itself and that of the main structure) given by

$$\mu_i = \frac{m_i}{m_s}, \tag{5.5a}$$

$$\gamma_i = \frac{\omega_i}{\omega_s} = \sqrt{\frac{k_i}{m_i}}\sqrt{\frac{m_s}{k_s}} = \sqrt{\frac{k_i}{k_s}}\mu_i^{-1/2} \tag{5.5b}$$

and μ_T is the ratio of the total mass given by $\sum_{i=1}^{N} \mu_i$.

A convenient reformulation of the equations of motion can be suitably made by replacing the associated terms with non-dimensional variables. First, x_s and x_i can be non-dimensionalized by normalizing them to the RMS displacement of the uncontrolled structure x_{ref}. With the help of the theoretical results for the stochastic response of a SDOF system excited by a white-noise stationary process (Lutes and Sarkani, 2004), the RMS displacement of the uncontrolled system can be calculated by

$$x_{\text{ref}} = \sqrt{\frac{\pi S_{\ddot{u}_g}}{2\zeta_s \omega_s^3}}. \tag{5.6}$$

Further, introducing non-dimensional displacements $y_s = x_s/x_{\text{ref}}$ and $y_i = x_i/x_{\text{ref}}$, and a time scale $t_o = \omega_s t$, the equations of motion can be non-dimensionalized as follows:

$$(1+\mu_T)y_s'' + \sum_{i=1}^{N} \mu_i y_i' + 2\zeta_s y_s' + y_s = -(1+\mu_T)w_g'' \tag{5.7a}$$

$$y_s'' + y_i'' + \psi_i + \gamma_i^2 y_i = 0 \qquad i = 1, \cdots, N \tag{5.7b}$$

where a prime notation denotes the derivation with respect to the non-dimensional time τ, and w_g'' is the non-dimensionalized ground acceleration exerted on the primary structure with its spectral intensity of

$$S_{w_g''} = \frac{S_{\ddot{u}_g}}{x_{\text{ref}}^2 \omega_s^3} = \frac{2\zeta_s}{\pi}. \tag{5.8}$$

And the non-dimensional dissipation force term ψ_i is written as follows:

$$\psi_i = \psi_i(y_i') = \frac{g_i(\dot{x}_i)}{m_i \omega_s^2 x_{\text{ref}}} = \eta_i |y_i'|^\beta \text{sgn}(y_i') \tag{5.9}$$

where

$$\eta_i = \frac{g_{io}/\mu_i}{m_s \omega_s^2 x_{\text{ref}}}. \tag{5.10}$$

Particularly for the Coulomb-type friction, the dissipate force is written in terms of a coefficient of friction (COF) of the i-th TMD. In this case, Eq. (5.10) becomes further expanded in terms of the COF as follows:

$$\eta_i = \frac{g_{io}/\mu_i}{m_s \omega_s^2 x_{\text{ref}}} = \frac{\tau_i m_i g/\mu_i}{m_s \omega_s^2 x_{\text{ref}}} = \frac{1}{\omega_s^2 x_{\text{ref}}/g} \tau_i. \tag{5.11}$$

The matrix equation of motion for the combined system with $N+1$ degree-of-freedoms can be consequently derived as follows:

$$My'' + Cy' + Ky + \psi = fw_g'' \tag{5.12}$$

where $y = [y_s, y_1, \cdots, y_N]^{\mathrm{T}}$, $\psi = [0, \psi_1, \cdots, \psi_N]^{\mathrm{T}}$, $f = [-(1+\mu_T), 0, \cdots, 0]^{\mathrm{T}}$ and

$$M = \begin{bmatrix} 1+\Sigma\mu_i & \mu_1 & \cdots & \mu_N \\ 1 & 1 & \cdots & 0 \\ \vdots & \vdots & \ddots & \vdots \\ 1 & 0 & \cdots & 1 \end{bmatrix}, \tag{5.13a}$$

$$C = \begin{bmatrix} 2\zeta_s & 0 & \cdots & 0 \\ 0 & 0 & \cdots & 0 \\ \vdots & \vdots & \ddots & \vdots \\ 0 & 0 & \cdots & 0 \end{bmatrix}, \tag{5.13b}$$

$$K = \begin{bmatrix} 1 & 0 & \cdots & 0 \\ 0 & \gamma_1^2 & \cdots & 0 \\ \vdots & \vdots & \ddots & \vdots \\ 0 & 0 & \cdots & \gamma_N^2 \end{bmatrix}. \tag{5.13c}$$

5.2.2 Statistical linearization

One attractive method of solving stochastic nonlinear differential equations is a statistical linearization which can replace a set of the nonlinear equations by a set of linear ones that is equivalent in a statistical sense. Some theoretical aspects and applications of this technique are described in the literature (Roberts and Spanos, 2003; Socha, 2005a,b). For the equations of motion for structure-FMTMD system described by Eq. (5.12), the statistical linearization technique enables the nonlinear force term ψ to be replaced with an equivalent term that minimizes the mean square of the error $E[\varepsilon^2]$ where the error ε is given by

$$\varepsilon = \psi - C^{\mathrm{eq}} y' \tag{5.14}$$

where C^{eq} is a parametric matrix to be determined that minimizes the described mean square of the error.

Under the assumption of stationary Gaussian excitation, the elements of the parametric matrix C^{eq} can be expressed by the following simple expression (details are supplemented with Appendix B).

$$c_{i+1}^{\text{eq}} = E[\partial_{y_i'}\psi_i] = E\left[\frac{\partial \psi_i}{\partial y_i'}\right] \quad i = 1, \cdots, N \tag{5.15}$$

where c_{i+1}^{eq} is the $(i+1)$-th element of the parametric matrix C^{eq} and $\partial_{y_i'}\psi_i$ denotes the partial derivative of the nonlinear force ψ_i with respect to the non-dimension velocity y_i'.

If the dissipative force is in a linear form (or when the parameter β is unity), it readily yields that $c_{i+1}^{\text{eq}} = \psi_i$. Note that $c_1^{\text{eq}} = 0$ as the first element of the nonlinear vector ψ is null [see its definition denoted in Eq. (B.23)].

If the force is of the Coulomb-type, however, it needs to be evaluated the right term of Eq. (5.15). The idealized Coulomb-type frictional force ψ_i and its derivative $\partial_{y_i'}\psi_i$ are depicted in Figure 4.3. Further, under the assumption that the responses of the equivalent stationary system are stationary zero-mean Gaussian processes, the relative non-dimensional velocity of the i-th TMD, y_i', also becomes Gaussian with corresponding variance, say $\sigma_{y_i'}$. Substituting the partial derivative of the friction force and using the sifting property of the Dirac delta function, the equivalent damping element c_{i+1}^{eq} can be consequently evaluated. Connected with the equivalency of the equivalent damping coefficient and its normalized form, Eq. (5.15) can be rearranged into the following form:

$$c_{i+1}^{\text{eq}} = 2\gamma_i \zeta_i^{\text{eq}} = \sqrt{\frac{2}{\pi}}\eta_i \frac{1}{\sigma_{y_i'}}. \tag{5.16}$$

where η_i is the frictional coefficient defined in Eq. (5.11). Further, rearranging Eq.

(5.32) in terms of the design variable, η_i gives:

$$\eta_i = \sqrt{2\pi}\gamma_i \zeta_i^{\mathrm{eq}} \sigma_{y_i'} \tag{5.17}$$

Hence we have derived a equivalent linear matrix C^{eq} comprised of the equivalent force term, so that the solution obtained from the linear MTMD part can be adapted, where the left hand term is the coefficient in the nonlinear system while the right hand terms are the coefficients in the equivalent linear system. And the expressions for the nonlinear term are explicit, since $\sigma_{y_i'}$ do not depend on the coefficients η_i. Hence, seeking the optimal nonlinear parameter η_i falls into finding the optimal parameters of linearized system. That can be accomplished by the procedure used in LMTMD optimization.

Further, the terms contained in the equivalent matrix can be converted into the normalized form as previously seen in the linear MTMD chapter as follows:

The matrix equation (5.12) can be rewritten by substituting the statistically linearized term into the nonlinear vector as follows:

$$My'' + (C + C^{\mathrm{eq}})y' + Ky = fw_g'' \tag{5.18}$$

where the matrices M, C and K are previously defined at Eqs. (5.10) and the equivalent damping matrix C^{eq} is defined as follows:

$$C^{\mathrm{eq}} = \begin{bmatrix} 0 & 0 & \cdots & 0 \\ 0 & c_1^{\mathrm{eq}} & \cdots & 0 \\ \vdots & \vdots & \ddots & \vdots \\ 0 & 0 & \cdots & c_N^{\mathrm{eq}} \end{bmatrix} \tag{5.19}$$

With introducing a non-dimensional state vector $z = [y^{\mathrm{T}}, y'^{\mathrm{T}}]^{\mathrm{T}}$, a first-order state-space model can be formulated as follows:

$$z' = Az + Bw_g'' \tag{5.20}$$

where the corresponding matrices A and B are given by

$$A = \begin{bmatrix} O & I \\ -M^{-1}K & -M^{-1}(C + C^{\mathrm{eq}}) \end{bmatrix}, \tag{5.21a}$$

$$B = \begin{bmatrix} O \\ -f \end{bmatrix}. \tag{5.21b}$$

Note that the equivalent damping matrix of the equivalent linear system consists of the non-dimensionalized relative velocities of TMDs [see Eq. (5.14)], and the relative velocities can be evaluated upon a determined system property [see Eq. (5.20)]. Hence, it is necessarily required to assume the initial system properties and to iterate the circumstances as the appropriate tolerance to be minimized.

If the external loading w_g'' is a steady-state stationary white noise with its spectral strength $S_{w_g''}$ as assumed previously, the covariance matrix $Q = E[zz^{\mathrm{T}}]$ can be obtained by solving the following Lyapunov equation (Lutes and Sarkani, 2004):

$$AQ + QA^{\mathrm{T}} + 2\pi S_{w_g''} BB^{\mathrm{T}} = O. \tag{5.22}$$

5.2.3 Optimization strategy

The response quantities of interest is the RMS displacement of the controlled main structure normalized to that of the uncontrolled one, σ_{y_s}. Attributed to its definition, the non-dimensional displacement of main structure σ_{y_s} would be in a range of zero to unity. Also it can be interpreted as a quantity for control efficiency such that σ_{y_s} is zero if the TMD completely suppress the vibration of main structure, and is unity when the TMD has no effect.

The mathematical description of the response of quantity can be established as follows:

$$\sigma_{y_s}^2 = E[y_s^2] = E[(s^{\mathrm{T}}z)^{\mathrm{T}}s^{\mathrm{T}}z] = \mathrm{tr}[SQ] \tag{5.23}$$

where $\mathrm{tr}[\cdot]$ is a trace operator, $s = [1, 0, \cdots, 0]^{\mathrm{T}}$ is the weighting vector corresponding to sifting the structural displacement, and S is the weighting matrix which can be calculated by $S = ss^{\mathrm{T}}$.

Then the optimization problem is formulated as:

$$\begin{aligned} &\underset{\gamma_d,\, \zeta_d}{\text{minimize}} && J = \sigma_{y_s} \\ &\text{subject to} && \gamma_d \in \Omega_\gamma,\ \zeta_d \in \Omega_\zeta \end{aligned} \tag{5.24}$$

where γ_d and ζ_d are the design variable vectors defined in the previous section that corresponds to appropriate constraints, and Ω_γ and Ω_ζ are the feasible regions for γ_d and ζ_d, respectively. Here, the feasible regions Ω_γ and Ω_ζ were set in a way that the frequency ratios γ_i, the damping ratios ζ_i, the bandwidth of frequency ratio β_γ and the fictitious damping ratio ζ_o are required to be non-negative.

The above Lyapunov equation can be efficiently solved by the well-established algorithms, for instance the algorithm proposed by Bartels and Stewart (1972), which is implemented in a commecial program such as MATLAB®. In the optimization procedure, this study adapted an iterative method for solving a sequence of Quadratic Programming Sub-problems subjected to a linearized constraint functions for its superior rate of convergence. At each iteration, to make an approximation of the Hessian matrix, Broyden-Fletcher-Goldfarb-Shanno algorithm was adopted for its effectiveness and good performance even for non-smooth optimization problems (Coleman et al., 1999).

The optimum of the frictional coefficient normalized to the static force for the displacement is x_{ref} is than arranged into the following form:

$$\eta_i^* = \sqrt{2\pi}\gamma_i^* \zeta_i^{\text{eq}*} \sigma_{y_i'}^* \tag{5.25}$$

where the optimal parameters γ_i^*, $\zeta_i^{\text{eq}*}$ and $\sigma_{y_i'}^*$ can be obtained by the procedure used in LMTMD optimization.

5.3 Improved Estimation of Peak Distribution

This section tries to improve the accuracy of the estimation of peak distribution of MTMDs by exploiting the statistical nonlinearization technique. The adjusting factor as an explicit expression is derived, which enables the RMS displacement of TMDs by statistical linearization to be corrected more precisely. Further, a formula for the peak factor of the response of the frictional TMD was also derived.

5.3.1 Statistical nonlinearization

Statistical nonlinearization is a technique in which nonlinear systems are replaced with a class of other nonlinear systems whose exact solution have been already explicitly derived (Caughey, 1986). The statistical nonlinearization departs from the statistical linearization in that it enables one to predict deviations from a Gaussian response approximation.

Consider the i-th oscillator attached with an energy dissipation element and a spring, whose values are optimized by employing the statistical linearization technique. The non-dimensionalized equation of motion for the i-th oscillator is as follows:

$$y_i'' + \eta_i^* |y_i'|^\beta \text{sgn}(y_i') + (\gamma_i^*)^2 y_i = -y_s'' \tag{5.26}$$

where y_i is the non-dimensionalized displacement of the i-th unit of TMD, y_s'' is the non-dimensionalized acceleration of the primary structure, γ_i^* and η_i^* are the optimal frequency ratio and damping coefficient for the i-th unit of TMD, respectively.

Now we wish to replace the equation of motion with another one of which analytic solution is already well-established. Consider the equation of motion described by

$$y_i'' + \eta_i^* H(E_i) y_i' + (\gamma_i^*)^2 y = -y_s'' \tag{5.27}$$

where $H(E_i)$ is a continuous function of the total energy for the i-th TMD described by the following energy expression:

$$E_i = \frac{1}{2} y_i'^2 + \frac{1}{2} (\gamma_i^*)^2 y_i^2. \tag{5.28}$$

Caughey and Ma (1982) have shown that when the response of the oscillator is governed by Eq. (5.27) under the white-noise excitation of its strength $S_{y_s''}$, the probability density of the envelope response $a_i(t)$ is given by

$$f_{A_i}(a_i) = C_0 a_i \exp\left(-\frac{\eta_i^*}{\pi S_{y_s''}} \int_0^{E_i} H(\iota) \mathrm{d}\iota \right) \tag{5.29}$$

where C_0 is a normalizing constant.

Note that the non-dimensional acceleration of the primary structure y_s'' does not actually belong to a white-noise process. However we presumably regard the process as similar to a white noise because, when the TMDs are designed appropriately, the response that once was a narrow band process becomes a wide band process, spreading its frequency contents to a wide range of frequency bandwidth.

In order for the original equations of motion Eq. (5.26) to be replaced as the form of Eq. (5.27) accurately as possible, the suitable function $H(E_i)$ should be constructed that minimizes the error between ψ_i^* and η_i^*. One can establish a function that ensures

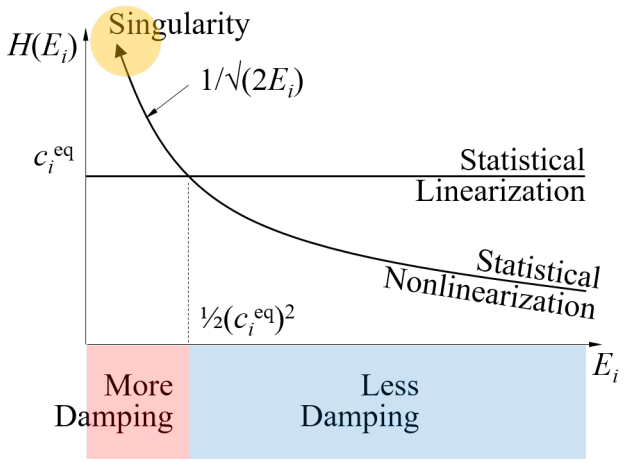

Figure 5.1: Energy functional adopted in this study

the same order as the original damping term η_i^*, for example, proposed by Roberts and Spanos (2003) as follows:

$$H(E_i) = 2^{(\beta+1)/2} \frac{\eta_i^*}{\sqrt{\pi}} \frac{\Gamma\left(\frac{\beta+2}{2}\right)}{\Gamma\left(\frac{\beta+3}{2}\right)} E_i^{(\beta-1)/2} \tag{5.30}$$

Energy functions $H(E_i)$ for $\beta = 0$ and $\beta = 1$ are depicted in Figure 5.1. If the energy function is constant irrespective of the mechanical energy E_i, the formulation falls into the statistical linearization, providing the equivalency of the original damping term η_i^* with an equivalent constant damping coefficient c_i^{eq}. The function $H(E_i) = 1/\sqrt{2E_i}$ for $\beta = 0$, on the other hand, provides amplitude-dependent damping coefficient. Such a response-dependent damping characteristic would provide a larger scatterness for low and high responses, which will be shown in the validation chapter. It should be also noted that the applied energy functional is singular and diverges if the response becomes lower. The singularity would provide infinite damping force, thus not allowing the oscillator to be in the zero-like response.

Once the energy functional and the dissipation force term is expressed in a relation

of Eq. (5.30), then the probability density function for the peak may be found from the exact solution of the problem. Substituting Eq. (5.30) into Eq. (5.29) and evaluating yields

$$f_{A_i}(a_i) = \frac{(\beta+1)\kappa_{\mathrm{o}}^{2/(\beta+1)}}{\Gamma\left(\frac{2}{\beta+1}\right)} a_i \exp(-\kappa_{\mathrm{o}} a_i^{\beta+1}) \tag{5.31}$$

where

$$\kappa_{\mathrm{o}} = \frac{2\eta_i^*}{\pi^{3/2} S_{y_s''}} \frac{\Gamma\left(\frac{\beta+2}{2}\right)}{\Gamma\left(\frac{\beta+3}{2}\right)} \frac{(\gamma_i^*)^{\beta+1}}{\beta+1} \tag{5.32}$$

The variance of a_i is determined by computing the second moment of $f_{A_i}(a_i)$, such that

$$\begin{aligned} \sigma_{a_i}^2 &= \frac{1}{2}\int_0^\infty a_i^2 f(a_i)\mathrm{d}a_i \\ &= \frac{\Gamma\left(\frac{4}{\beta+1}\right)}{2\Gamma\left(\frac{2}{\beta+1}\right)} \kappa_{\mathrm{o}}^{-2/(\beta+1)} \end{aligned} \tag{5.33}$$

where the associated parameters are given by

$$\kappa = \left[\frac{\Gamma\left(\frac{4}{\beta+1}\right)}{2\Gamma\left(\frac{2}{\beta+1}\right)}\right]^{(\beta+1)/2} \tag{5.34a}$$

$$\alpha_i = \frac{a_i}{\sigma_{a_i}} \tag{5.34b}$$

Consequently Eq. (5.31) can be normalized by σ_{a_i} to produce

$$f_{\mathrm{A}_i}(\alpha_i) = \frac{(\beta+1)\kappa^{2/(\beta+1)}}{\Gamma\left(\frac{2}{\beta+1}\right)} \alpha_i \exp(-\kappa \alpha_i^{\beta+1}) \tag{5.35}$$

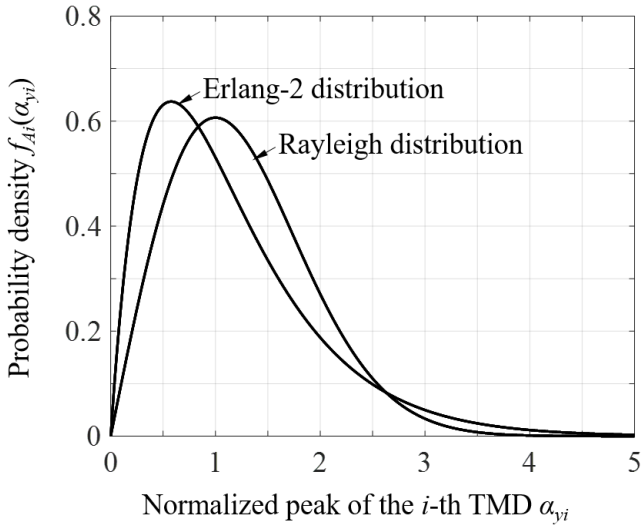

Figure 5.2: Probability density functions of peak for β =0 and 1

The derived probability density function is generic for any kind of power of β, and its characteristics are portrayed in Love and Tait (2015). This study, however, highlights the comparison between the linear one and the Coulomb-type friction. The associated parameter κ can be readily determined as $\sqrt{3}$, if β is zero, and becomes 1/2 if β is unity. In those cases, the corresponding variables follows to the Erlang-2 distribution and Rayleigh distribution with the following probability density functions:

$$f_{\mathrm{A}_i}(\alpha_i) = \begin{cases} 3\alpha_i \exp(-\sqrt{3}\alpha_i) & \text{if } \beta = 0 \\ \alpha_i \exp(-\dfrac{\alpha_i^2}{2}) & \text{if } \beta = 1 \end{cases} \tag{5.36}$$

Figure 5.2 depicts a comparison of the two probability density functions. This study goes further into two kind of forces, where $\beta = 0$ represents the Coulomb-type friction, and $\beta = 1$ for the viscously-linear damping.

5.3.2 Correction factor

In the preceding section, the RMS displacement of the TMD of the equivalent nonlinear system can be determined with Eq. (5.31). However, the determination of the input intensity induced by the motion of main structure $S_{y_s''}$ obstructs the way of evaluating the RMS response. Alternatively the RMS response can be determined by the procedure of statistical linearization technique, whose accuracy is assessed by various researchers. Love and Tait (2015) compared the RMS responses obtained by the statistical linearzation with those by a series of extensive simulation, and observed the predicted value overestimates in a level of approximately 13 percent under the case of TMD with 3 percent mass ratio. This section establishes a correction factor, which enables the RMS response by statistical linearization to be corrected with exploiting the solution of statistical nonlinearization technique.

Define $\eta_{i,\mathrm{L}}$ and $\kappa_{\mathrm{o,L}}$ as the force coefficient and κ_{o} for a linear case, and the $\eta_{i,\mathrm{F}}$ and $\kappa_{\mathrm{o,F}}$ as those for a Coulomb-type friction case. The elimination of the obstructive input strength $S_{y_s''}$ can be made by dividing $\kappa_{\mathrm{o,F}}$ into $\kappa_{\mathrm{o,L}}$ as follows:

$$\begin{aligned}\frac{\kappa_{\mathrm{o,F}}}{\kappa_{\mathrm{o,L}}} &= 2\frac{\eta_{i,\mathrm{F}}^*}{\eta_{i,\mathrm{L}}^*}\frac{\Gamma(1)}{\Gamma(3/2)}\frac{\Gamma(2)}{\Gamma(3/2)}\frac{(\gamma_i^*)}{(\gamma_i^*)^2} \\ &= \frac{8}{\pi}\frac{\eta_{i,\mathrm{F}}^*}{\eta_{i,\mathrm{L}}^*}(\gamma_i^*)^{-1}\end{aligned} \tag{5.37}$$

In the similar manner, the RMS displacement normalized to that of the linear one is given by

$$\begin{aligned}\left(\frac{\sigma_{a_i,\mathrm{F}}^*}{\sigma_{a_i,\mathrm{L}}^*}\right)^2 &= \frac{\Gamma(4)}{2\Gamma(2)}\frac{2\Gamma(1)}{\Gamma(2)}\frac{\kappa_{\mathrm{o,F}}^{-2}}{\kappa_{\mathrm{o,L}}^{-1}} \\ &= 6\left(\frac{\kappa_{\mathrm{o,F}}}{\kappa_{\mathrm{o,L}}}\right)^{-2}\kappa_{\mathrm{o,L}}^{-1}\end{aligned} \tag{5.38}$$

where the ratio $\kappa_{\mathrm{o,F}}/\kappa_{\mathrm{o,L}}$ can be evaluated from Eq. (5.37). Further, the parameter $\kappa_{\mathrm{o,L}}$ can be written in terms of the RMS displacement of the linear system by substituting $\beta = 1$ into Eq. (5.33) as follows:

$$\kappa_{\mathrm{o,L}} = \frac{1}{2(\sigma^*_{a_i,\mathrm{L}})^2} \tag{5.39}$$

The RMS displacement of the nonlinearized model can be adjusted from that of the linearized model. The ratio between the force constants can be calculated from Eq. (5.25) as

$$\frac{\eta^*_{i,\mathrm{F}}}{\eta^*_{i,\mathrm{L}}} = \frac{\eta^*_{i,F}}{2\gamma^*_i \zeta_i^{\mathrm{eq}*}} = \sqrt{\frac{\pi}{2}}\sigma^*_{y'_i,\mathrm{L}}. \tag{5.40}$$

By substituting Eq. (5.39) and (5.40) into Eq. (5.38), the ratio of RMS displacements can be evaluated by following expression:

$$\begin{aligned}\frac{\sigma^*_{a_i,\mathrm{F}}}{\sigma^*_{a_i,\mathrm{L}}} &= 6\left[\frac{8}{\pi}\sqrt{\frac{\pi}{2}}\sigma^*_{y'_i,\mathrm{L}}(\gamma^*_i)^{-1}\right]^{-2}\cdot(\sigma^*_{y'_i,\mathrm{L}})^2 \\ &= \sqrt{\frac{3\pi}{8}}\left(\frac{\sigma^*_{y_i,\mathrm{L}}}{\sigma^*_{y'_i,\mathrm{L}}}\right)^2\gamma_i^{*2}.\end{aligned} \tag{5.41}$$

Here we can exploit a well-known result of random vibration theory that for 'any' narrowband process, the characteristic frequency, which is exactly the same as the natural frequency for linear oscillator, may be approximated by the ratio of the RMS velocity to the RMS displacement (Lutes and Sarkani, 2004). With this idea, Eq. (5.41) is given by

$$\frac{\sigma^*_{a_i,\mathrm{F}}}{\sigma^*_{a_i,\mathrm{L}}} = \sqrt{\frac{3\pi}{8}} \approx 1.0854. \tag{5.42}$$

Equation (5.42) enables the RMS response by statistical linearization to be corrected with exploiting the solution of statistical nonlinearization technique. Some

features might be discussed. First, the constant term $\sqrt{3\pi/8} \approx 1.0854$ corrects the response to be increased about 8.5 percent; Second, the extent of correction does not relate to dynamic characteristics of oscillator such as dissipation force term, the equivalent damping ratio and the frequency ratio. Such dependency can be fruitful especially in designing of MTMDs. Although the optimal damping of the MTMD decreases with increasing the number of TMDs, the features fluctuate but the expression is not sensitive to the RMS displacement.

5.3.3 Peak factors

It is necessary to know the maximum response that is expected to occur during a certain period of time. This peak response provides the governing TMD displacement and can be used to determine the governing TMD loading. A peak response distribution can be derived from the response amplitude distribution provided by Eq. (5.36).

Linear oscillators

For a linear oscillator, the probability density function of its response is already well-established. The probability density of the maximum peak of envelope response from N cycles is given by

$$f_{\mathrm{A}_i}(\alpha_i) = N\alpha_i \exp\left[-N\exp\left(\frac{1}{2}\alpha_i^2\right) - \frac{1}{2}\alpha_i^2\right]. \tag{5.43}$$

Under the Poisson assumption, the peak factor for the linear oscillator PF_L is derived by (Davenport, 1964) as follows:

$$PF_L = \sqrt{2\ln N} + \frac{\gamma}{\sqrt{2\ln N}} \tag{5.44}$$

where γ is an Euler constant of 0.577.

Frictional oscillators

In the case of the friction TMD, following derivation is needed. By integrating Eq. (5.36), the cumulative probability distribution is defined as the integrated probability density as follows:

$$F_{\mathrm{A}_i}(\alpha_i) = 1 - q \tag{5.45}$$

where the function q is defined as

$$q = q(\alpha_i) = (1 + \sqrt{3}\alpha_i)e^{-\sqrt{3}\alpha_i}. \tag{5.46}$$

The probability that N successive peaks are all less than a_r is given by

$$P_{\mathrm{A}_i}(\alpha_i) = F_{\mathrm{A}_i}(\alpha_i)^N = (1 - q)^N \tag{5.47}$$

and the associated probability density function corresponds to

$$p_{\mathrm{A}_i}(\alpha_i) = \frac{\mathrm{d}P_{\mathrm{A}_i}(\alpha_i)}{\mathrm{d}\alpha_i} = N(1 - q)^{N-1}\frac{\mathrm{d}q}{\mathrm{d}\alpha_i} \tag{5.48}$$

Put $q(\alpha_i) = \xi/N$, where $0 \leq \xi \leq N$. For large values of N, we can write in the limit, the asymptotic form

$$\begin{aligned} p_{\mathrm{A}_i}(\alpha_i)\mathrm{d}\alpha_i &= \mathrm{d}[(1 - \xi/N)^N] \\ &= \mathrm{d}e^{-\xi} = -e^{-\xi}\mathrm{d}\xi \end{aligned} \tag{5.49}$$

With this form, the variable α_i can be written by connecting it with Eq. (5.46) as follows:

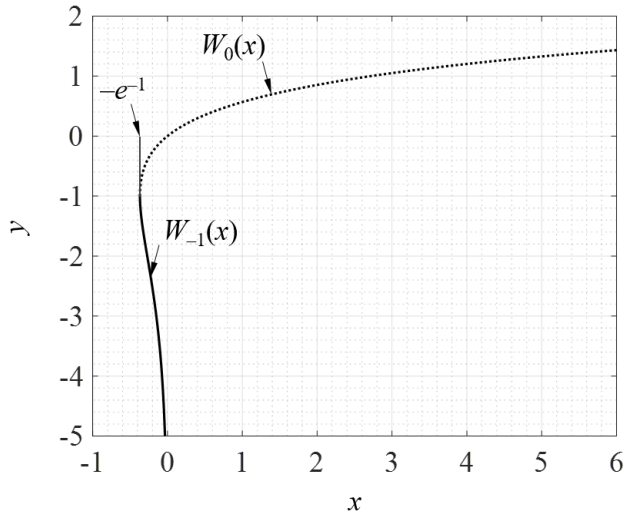

Figure 5.3: Lambert-W function

$$\xi = N(1+\sqrt{3}\alpha_i)e^{-\sqrt{3}\alpha_i}$$
$$\iff \alpha_i = -\frac{1}{\sqrt{3}}\left[1 + W_{-1}\left(-e^{-1}\frac{\xi}{N}\right)\right] \tag{5.50}$$

where $W_{-1}(\cdot)$ is a Lambert-W function (or a product log function), in which a single-valued branch of W_{-1} is defined by the additional constraints such that $\alpha_i = 0$, if $\xi = N$ and $\alpha_i \to \infty$, if $\xi = 0$. The Lambert-W function is depicted in Figure 5.3.

The peak factor for a oscillator with friction can be obtained by calculating the following integral:

$$PF_F = \int_0^\infty \alpha_i p_{\mathrm{A}_i}(\alpha_i)\mathrm{d}\alpha_i = -\frac{1}{\sqrt{3}}\int_0^N \left[1 + W_{-1}\left(-e^{-1}\frac{\xi}{N}\right)\right] e^{-\xi}\mathrm{d}\xi \tag{5.51}$$

In order to integrate the above equation, we adapt the bounded description of the $W-1$ given by (Chatzigeorgiou, 2013)

$$-1-\sqrt{2u}-u<W_{-1}(-e^{-u-1})<-1-\sqrt{2u}-\frac{2}{3}u. \tag{5.52}$$

Substituting Eq. (5.52) into Eq. (5.51) and rearranging it gives

$$PF_F=\frac{PF_L}{\sqrt{3}}+\frac{\gamma+\ln N}{\sqrt{3}} \tag{5.53}$$

where γ is an Euler constant of 0.577.

5.4 Model Evaluation

Nonlinear simulations are carried out to evaluate the validity of the model. A structure with a generalized mass of 1 ton, a natural frequency of 1 rad/sec, and an inherent damping of 1 percent is used. Two FMTMDs, 3 and 5 percent of mass ratios are considered. The optimal parameters are summarized in Table 5.1.

A first step for the simulation is to generate a time domain ground acceleration w_g''. '`wgn`' function in the MATLAB® is used for the signal generation. The white-noise generated by `wgn` is essentially the band-limited and max frequency is equal to half of the sampling frequency. The ideal white-noise has infinite variance but `wgn` requires to specify it as follows. $\sigma^2_{w_g''}$ is equated to the spectral strength of white noise required times half of the sampling frequency in rad/sec. In this study the sampling time is taken as 0.005 sec, which is suitable in calculating the nonlinear force, and in turn corresponding sampling frequency is followed as 200 Hz. The Runge-Kutta method is used to solve the equations of motion described as Eq. (5.18).

One of the sampled time histories for linear and frictional TMD of 3% mass ratio and their associated peak distributions are plotted in Figure 5.4, in which the envelopes of the response were obtained by constructing associated analytic signal via the Hilbert transform (Bendat and Piersol, 2011). Firstly, it was found that the linear TMD experiences in a way that the response and its peak follow Gaussian and

Rayleigh distribution as well-described by linear vibration theory. Compared to the linear TMD, on the other hand, the frictional TMD exhibits a drastic response, showing large displacement at the portion where a large response occurs and vice versa. Also it was shown that the Erlang-2 distribution can describe the peak distribution for the frictional TMD more precisely compared to the Rayleigh distribution.

The RMS response of the frictional TMD normalized to that of the linear one for the simulations are plotted in Figure 5.5, in which the ordinates are transformed into the standardized as normal distribution quantity in order to readily determine the extent of normality, and the vertical lines are the value predicted by statistical linearization (SL) and the value by Eq. (5.41), respectively. It was found from numerical simulations that the SL underestimates the RMS displacement of TMD significantly providing less than 3 percent quantile compared to the simulated results. However, Equation (5.41) predicts suitable values for the RMS displacement compared to the simulated results. As mentioned previously, the accuracy of the estimation does not depend on the mass ratio of the TMD. There was a slight difference in various mass ratio that the variance of the ratio tends to decrease when using heavier TMD. This trend is ascribed to the fact that heavier TMD provides a better performance that the main structure becomes wide-band process compared to the light TMD. Hence, the presumed condition of white-noise input becomes realistic when using heavier mass ratio. The latest result shows a 9 percent discrepancy in the value of a long-sought number called the Hubble constant, which describes how fast the universe is expanding.

5.5 Concluding Remarks

This study investigated the characteristics of the stochastic response of a system with frictional tuned mass dampers (FTMDs). In order to improve the accuracy for

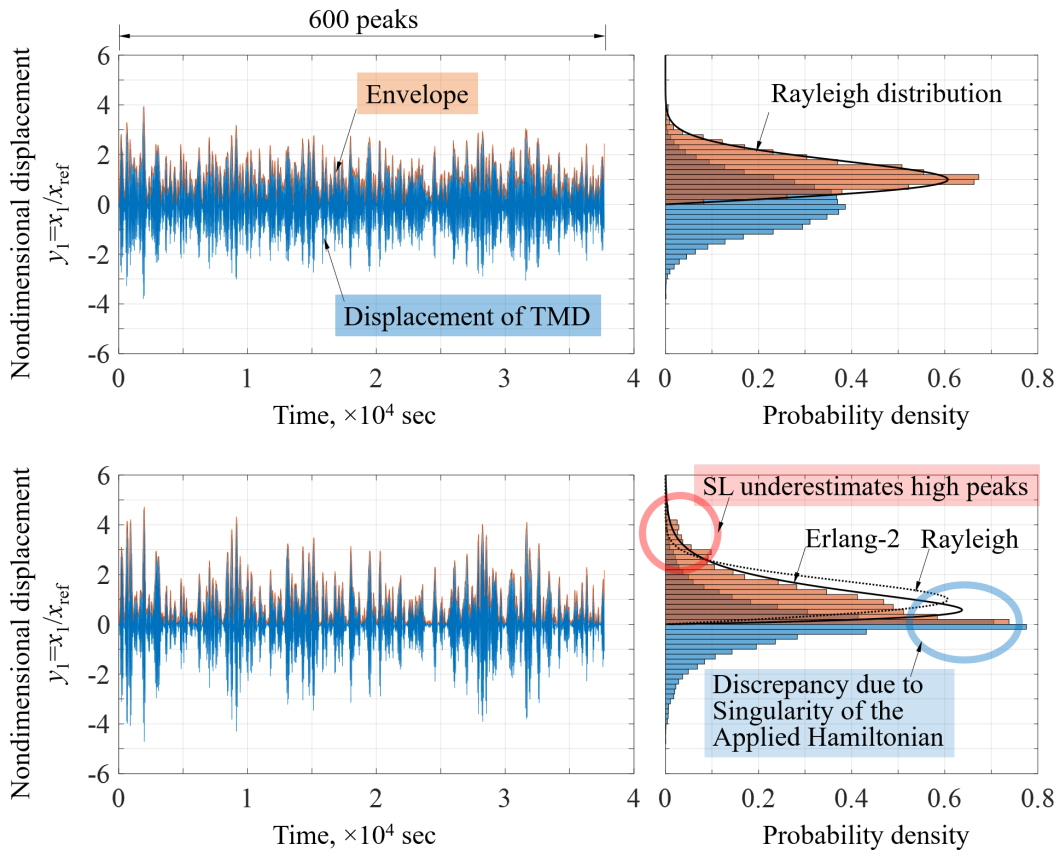

Figure 5.4: Simulated time histories and histograms for responses (μ_T=3%): Equivalent linear model (top) and original nonlinear model (bottom)

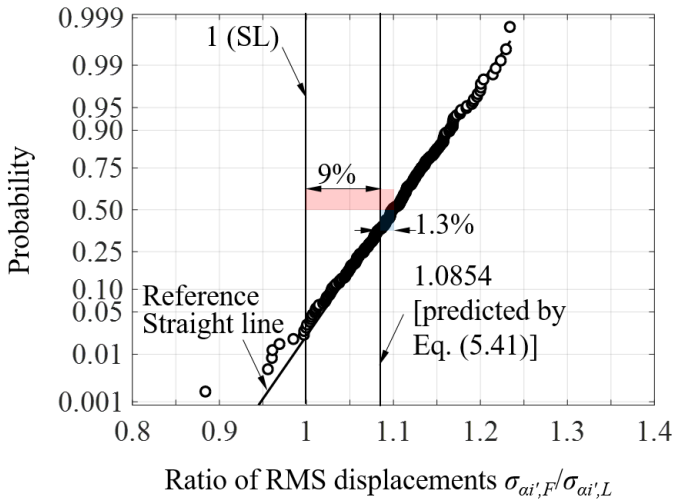
0.999
0.99
0.95
0.90
0.75
0.50
0.25
0.10
0.05
0.01
0.001
Probability
1 (SL)
9%
1.3%
1.0854
[predicted by
Eq. (5.41)]
Reference
Straight line
0.8
0.9
1
1.1
1.2
1.3
1.4
Ratio of RMS displacements $\sigma_{\alpha i',F}/\sigma_{\alpha i',L}$

(a) μ=1%

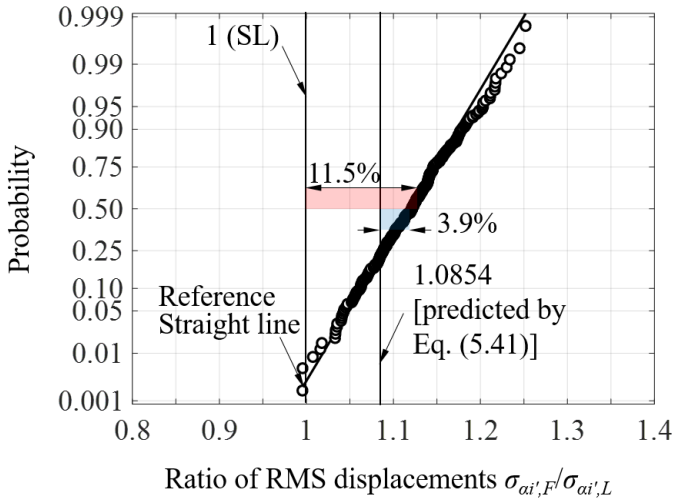
0.999
0.99
0.95
0.90
0.75
0.50
0.25
0.10
0.05
0.01
0.001
Probability
1 (SL)
11.5%
3.9%
1.0854
[predicted by
Eq. (5.41)]
Reference
Straight line
0.8
0.9
1
1.1
1.2
1.3
1.4
Ratio of RMS displacements $\sigma_{\alpha i',F}/\sigma_{\alpha i',L}$

(b) μ=3%

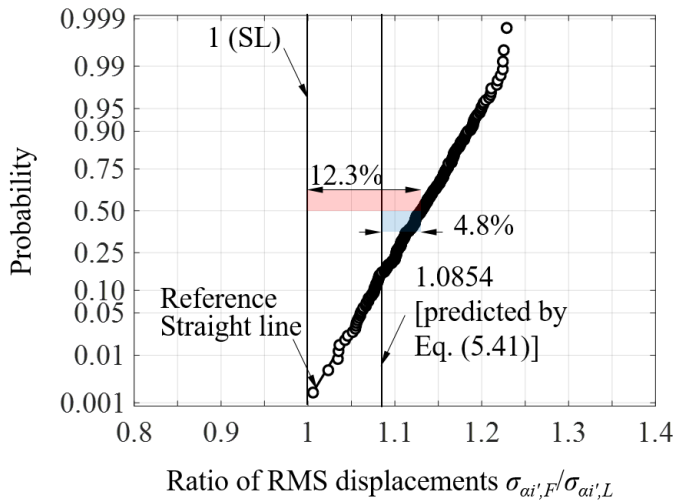

(c) μ=5%

Figure 5.5: Normal probability plot of simulated peak distribution ratio and predicted by simulations

the estimation of RMS displacement of the FTMDs, this study exploited a statistical nonlinearization technique, and derived a correction factor which accounts for the nonlinearity in evaluating the RMS response. Also, this study derived a closed-form expression for calculating peak factor. Based on the numerical simulations, the proposed correlation factor and the peak factor formula were validated extensively.

The key features can be drawn as follows:

1. Based on the statistical nonlinearization, this study derived the probability density function for the peak values of the FTMD unit. It was shown that, for the FTMD, the probability that any peak exceeds a certain value can be approximated as the Erlang-2 distribution, which is clearly distinguished from the solution of linear vibration theory that predicts that as Rayleigh distribution.

2. A correction factor that defines the ratio of RMS displacement between nonlinear and linear system was derived. Through the numerical simulations, it was found that the estimated value obtained by the statistical linearization underestimates the RMS displacement of TMD significantly providing less than 3 percent quantile compared to the simulated results. The model proposed by this study provides in a level of 10 % quantile showing less than 10% from the mean value of the simulated solution.

3. This study further derived an explicit formula for evaluating a peak factor for the frictional TMD. It was found from numerical simulations that the peak distribution is not dependent on the mass ratio of TMD, thereby the frequency ratio and damping ratio of TMD.

4. The predicted peak response showed some discrepancies with the simulated results; however, the maximum relative error was less than 13 percent. The results show a trend that as the DVA mass ratio decreases, the model tends to

overestimate the peak response of the TMD.

Table 5.1: Optimal parameters of FMTMDs of 10 units with 5% mass ratio

Mass ratio μ_T, %	Frequency ratio γ_i^*	Equivalent damping ratio $\zeta_i^{\mathrm{eq}*}$, %	Normalized friction force $\eta_i/(m_s\omega_s^2 x_{\mathrm{ref}})$, %	Normalized COF $\tau_i/(\omega_s^2 x_{\mathrm{ref}}/g)$, %
1	0.992	4.981	0.469	0.478
3	0.977	8.564	1.161	1.315
5	0.977	8.564	1.161	1.315

Chapter 6

Applications of MTMDs

This chapter presents several applications of multiple tuned mass dampers (MTMDs). The first section proposes a mechanism-based frictional pendulum tuned mass damper (FPTMD), which contributes to overcome some shortcomings of conventional translational TMDs with viscous damping. The nonlinear equations of motion of the proposed FPTMD are first derived and statistically linearized in order to obtain the optimal control parameters under earthquake excitation. The second section is a case study that provides a procedure for designing MTMDs, which covers modal analysis based on finite element method, optimal design of tuned mass dampers, and evaluating their control performance and robustness under the frequency-perturbed states. The final section presents a project in an attempt to mitigate an excessive vibration of a problematic structure. The overall process of the project includes the vibration performance evaluation, modal analysis based on finite element method and optimal design and manufacturing of tuned mass dampers.

6.1 Frictional Pendulum Tuned Mass Dampers

In this section, a mechanism-based frictional pendulum tuned mass damper (FPTMD) is proposed in order to overcome some shortcomings of conventional translational TMDs with viscous damping and extend the applicability of frictional TMDs. The nonlinear equations of motion of the proposed FPTMD are first derived and statistically linearized in order to obtain the optimal control parameters under earthquake excitation. The displacement time history of the primary structure predicted using the developed linearized model was shown to correlate well with that based on the exact nonlinear model. The gradient-based optimization was adopted in order to efficiently find the optimal parameters related to the pendulum length and the frictional force. Analyses of the optimal parameters obtained were also made to enhance the understanding of the FPTMD behavior which is unique and different from conventional translational TMDs.

6.1.1 Introduction

Tuned mass damper (TMD) is a mechanical device to dampen the dynamic response of structures through the resonant motion of the TMD. Because of its novelty for attenuating excessive vibrations of structures, various types of TMDs have been studied and applied in many ways.

One of the most widely used TMDs in practice is a translational–type linear TMD (TLTMD), which is composed of an auxiliary mass moving in a translational direction, a spring and a dashpot, since its invention by Frahm (1911). Many researchers including Den Hartog (1956) and Warburton (1982) provided the analytical solutions for the optimal parameters of TLTMDs, and their solutions are still popular in practical applications.

Although TLTMDs have sound theoretical basis and show satisfactory perfor-

mance in many applications, some shortcomings have been also encountered. One of the shortcomings is that TLTMDs require frictionless guides in order to facilitate the smooth movement of an auxiliary mass. In general, such a guide requires high cost for both fabrication and maintenance. The viscous damping elements mounted in TLTMDs can be degraded due to aging and they also have a risk of leakage.

Dry friction is an inherent mechanism of energy dissipation in nature. Several researchers studied dry friction devices as an alternative to viscous damping. Inaudi and Kelly (1995) investigated a translational-frictional type TMD (TFTMD) with damping provided by two friction devices acting at right angles to the motion of the secondary mass. Through response analysis based on the statistical linearization, they showed that TFTMDs can achieve the equivalent level of performance comparable to TLTMDs. Pointing out some advantages for taking account into the nonlinear behavior in TMDs, Ricciardelli and Vickery (1999) investigated a translational TMD with dry damping and indicated that the friction damper tends to be more effective for large amplitude, but less for low level of vibration. Gewei and Basu (2010) proposed a TMD with nonlinear dry friction at the interface between the primary structure and the TMD. Using an approximate analytical technique combined with statistical linearization method, they showed that frictional force can be as beneficial as proportional viscous damping force when using TMDs for suppression of vibration.

Meanwhile, a pendulum-type TMD (PTMD) can be another viable solution to circumvent technical difficulties involved in TLTMDs. In fact, a lot of PTMDs have been applied in many ways. For example, PTMDs were used to suppress wind-induced vibration of high-rise building structures (Irwin and B, 2001; Kwok and Samali, 1995). Gerges and Vickery (2005) conducted numerical studies to evaluate the optimal tuning parameters of PTMDs for the damped primary structures and demonstrated their efficiency under both wind and earthquake excitations. Setareh et al. (2006) conducted the analytical and experimental studies of a PTMD and indicated that a significant

reduction of the excessive floor vibrations can be efficiently achieved.

In order to introduce frictional mechanism into any PTMD applications, the use of frictional surface mimicking the trajectory of a moving pendulum appears ideal. However, it is very difficult to fabricate such a curved surface with a designed frictional coefficient corresponding to the exact trajectory of a moving pendulum. In this study, a mechanism-based frictional pendulum TMD (FPTMD) is first proposed which uses the frictional force between the third (or tertiary) mass and the surface of a primary structure. The nonlinear equations of motion which describe the behavior of the proposed FPTMD are then linearized in the statistical manner, in which the mean of squared errors between nonlinear and linearized responses is minimized. Further, the optimal parameters of FPTMD are obtained through the gradient-based optimization schemes. Finally, the optimization approach based on the statistical linearization in this study is validated by comparing with the numerical results obtained from directly solving the original nonlinear equations.

6.1.2 FPTMD proposed and equations of motion

Consider a primary structure having mass m_s, stiffness k_s and viscous constant c_s as shown in Figure 6.1. A pendulum of mass m_1 and length l_1 is attached to the primary structure by using a hinged joint and a massless rigid bar. It is possible to consider the inertial effect of the rigid bar, but its effect is neglected in this paper for the sake of simplicity. For a system with normal pendulum (Figure 6.1a), the massless rigid bar should be extended with additional length l_2. The end of this extended part should be pin-connected to the tertiary mass to form a three-hinge mechanism (Figure 6.1b).

As shown in Figure 6.1, let x_s be the displacement of the primary structure to the x-direction, x_1 and y_1 be the displacement of the secondary or pendulum mass to the x and y direction, and x_2 be the displacement of the tertiary mass, which dissipates the transferred energy through friction.

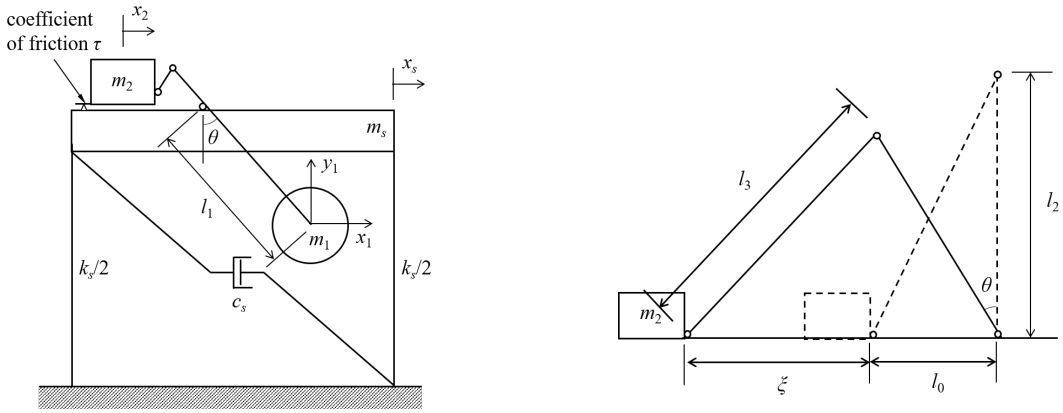

(a) System with normal pendulum

(b) Kinematic variables

Figure 6.1: Idealized structure-FPTMD system

The equations of motion can be derived using well-known Lagrange's method as follows. The Lagrangian function $\mathcal{L}$, defined as the difference between the total kinetic energy T and the potential energy V of the system, can be expressed as

$$\mathcal{L} = T - V = \frac{1}{2}m_s\dot{x}_s^2 + \frac{1}{2}m_1\left(\dot{x}_1^2 + \dot{y}_1^2\right) + \frac{1}{2}m_2\dot{x}_2^2 - \frac{1}{2}k_s x_s^2 - V_1 \tag{6.1}$$

Normalizing Eq. (1) with the mass of the primary structure M gives,

$$\mathcal{L}^* = \mathcal{L}/m_s = \frac{1}{2}\dot{x}_s^2 + \frac{1}{2}\mu\left(\dot{x}_1^2 + \dot{y}_1^2\right) + \frac{1}{2}\mu\nu\dot{x}_2^2 - \frac{1}{2}\omega_n x_s^2 - V_1^* \tag{6.2}$$

where $\mu = m_1/m_s$, $\nu = m_2/m_1$ and $\omega_s^2 = k_s/m_s$. In order to introduce the generalized

coordinates, we employ the geometric relations as follows,

$$x_1 = X + l_1 \sin\theta \tag{6.3a}$$

$$\dot{x}_1 = \dot{X} + l_1\dot{\theta}\cos\theta \tag{6.3b}$$

$$y_1 = l_1\left(1 - \cos\theta\right) \tag{6.3c}$$

$$\dot{y}_1 = l_1\dot{\theta}\sin\theta \tag{6.3d}$$

$$x_2 = X - \xi \tag{6.3e}$$

$$\dot{x}_2 = \dot{X} - \dot{\xi} \tag{6.3f}$$

where ξ is the displacement of the tertiary mass relative to the primary structure.

The next step is to express the displacement of the tertiary mass in terms of the angular displacement of the pendulum. By applying the law of the second cosine to the geometric configuration shown in Figure 6.1b, the kinematic relationship between θ and ξ can be obtained as follows,

$$l_3^2 = \left(l_0 + \xi\right)^2 + l_2^2 - 2\left(l_0 + \xi\right) l_2 \cos\left(\pi/2 - \theta\right) \tag{6.4}$$

It can be seen from Eq. (6.26) that the displacement of the tertiary mass can be expressed in terms of the angular displacement connected with the initial geometric parameters. Solving Eq. (6.26) for ξ and differentiating it gives the following relationships:

$$\xi = \xi\left(\theta\right) = l_2\left(\sin\theta - \eta_0 + \sqrt{\sin^2\theta + \eta_0^2}\right) \tag{6.5a}$$

$$\dot{\xi} = \dot{\xi}(\theta, \dot{\theta}) = \dot{\theta}\frac{d\xi}{d\theta} = l_1\eta_1\kappa\dot{\theta} \tag{6.5b}$$

where $\eta_0 = l_0/l_2$ and $\eta_1 = l_2/l_1$, and

$$\kappa = \kappa(\theta) = \cos\theta \left(1 + \frac{\sin\theta}{\sqrt{\sin^2\theta + \eta_0^2}} \right). \tag{6.6}$$

The Lagrangian equations of motion are as follows

$$\frac{d}{dt}\left(\frac{\partial L^*}{\partial \dot{X}}\right) - \frac{\partial L^*}{\partial X} = \Xi_X^* \tag{6.7a}$$

$$\frac{d}{dt}\left(\frac{\partial L^*}{\partial (l_1\dot{\theta})}\right) - \frac{\partial L^*}{\partial (l_1\theta)} = \Xi_{l_1\theta}^* \tag{6.7b}$$

where Ξ_X^* and $\Xi_{l_1\theta}^*$ are the non-conservative forces normalized to the mass of the primary structure acting on the corresponding degrees of freedom. Substituting Eqs. (6.3) into Eq. (6.8) and using elementary calculus, each term in Eq. (**??**) is given as

follows,

$$\frac{\partial L^*}{\partial \dot{X}} = \dot{X} + \mu(1+\nu)\dot{X} + \mu l_1[\cos\theta - \nu(\eta_1\kappa)]\dot{\theta} \tag{6.8a}$$

$$\frac{\partial L^*}{\partial X} = -\omega_s^2 X \tag{6.8b}$$

$$\frac{\partial L^*}{\partial (l_1\dot{\theta})} = \mu[\cos\theta - \nu(\eta_1\kappa)]\dot{X} + \mu l_1\left[1 + \nu(\eta_1\kappa)^2\right]\dot{\theta} \tag{6.8c}$$

$$\begin{aligned}\frac{\partial L^*}{\partial (l_1\theta)} = &-\mu\left[\sin\theta + \nu\left(\eta_1\frac{\mathrm{d}\kappa}{\mathrm{d}\theta}\right)\right]\dot{X}\dot{\theta} \\ &+ \mu l_1\nu(\eta_1\kappa)\left(\eta_1\frac{\mathrm{d}\kappa}{\mathrm{d}\theta}\right)\dot{\theta}^2 - \mu g\sin\theta\end{aligned} \tag{6.8d}$$

$$\begin{aligned}\Xi_X^* &= \frac{\Xi_X}{m_s} = \frac{F_X}{m_s} - \frac{c_s}{m_s}\dot{x}_s + \tau\frac{m_2}{m_s}g\,\mathrm{sgn}(\kappa\dot{\theta}) \\ &= F_X^* - 2\zeta_s\omega_s\dot{x}_s + \tau\mu\nu g\,\mathrm{sgn}(\kappa\dot{\theta})\end{aligned} \tag{6.8e}$$

$$\begin{aligned}\Xi_{l_1\theta}^* &= \frac{\Xi_{l_1\theta}}{m_s} = \frac{F_{l_1\theta}}{m_s} - \frac{m_2}{m_s}\tau g\,\mathrm{sgn}(\kappa\dot{\theta}) \\ &= F_{l_1\theta}^* - \tau\mu\nu g\,\mathrm{sgn}(\kappa\dot{\theta})\end{aligned} \tag{6.8f}$$

where η_1 is l_2/l_1; F_X and F_X^* are the external force exerted to the primary structure and its normalized form, $F_{l_1\theta}$ and $F_{l_1\theta}^*$ are an external force exerted to the secondary structure and its normalized form, respectively; ζ_s is the damping ratio of the primary structure, and τ is the friction coefficient. The earthquake ground motion is considered as the external force by expressing the external forces F_X^* and $F_{l_1\theta}^*$ as

$$F_X^* = -\left(1 + \mu + \mu\nu\right)\ddot{u}_g \tag{6.9a}$$

$$F_{l_1\theta}^* = 0 \tag{6.9b}$$

Substituting the expressions in Eq. (6.9) into Eq. (6.8) and rearranging yields the

governing nonlinear equations of motion of the FPTMD subjected to earthquake excitations.

$$\ddot{X} + 2\zeta_s\omega_s\dot{X} + \omega_s^2 X + \mu(1+\nu)\ddot{X} + \mu l_1[\cos\theta - \nu(\eta_1\kappa)]\ddot{\theta}$$
$$-\mu l_1\left[\sin\theta + \nu\left(\eta_1\frac{\mathrm{d}\kappa}{\mathrm{d}\theta}\right)\right]\dot{\theta}^2 - \tau\mu\nu g\,\mathrm{sgn}(\kappa\dot{\theta}) = -(1+\mu+\mu\nu)\ddot{u}_g \tag{6.10a}$$

$$[\cos\theta - \nu(\eta_1\kappa)]\,\ddot{X} + l_1[\nu(\eta_1\kappa)^2 + 1]\ddot{\theta} + l_1\nu(\eta_1\kappa)\left(\eta_1\frac{\mathrm{d}\kappa}{\mathrm{d}\theta}\right)\dot{\theta}^2$$
$$+g\sin\theta + \tau\nu g\,\mathrm{sgn}(\kappa\dot{\theta}) = 0 \tag{6.10b}$$

Eq. (6.10) describes the exact behavior of the FPTMD system proposed. Recalling that ν is the ratio of the tertiary mass to that of the pendulum, the terms associated with coefficient ν in Eqs. (6.10) effectively govern the motion of the tertiary mass. It is also noted that the terms for the tertiary mass are heavily dependent on the position of pendulum, θ, implying that the entire system would exhibit highly coupled nonlinear behavior.

The variation of κ is depicted in Figure 6.2 [also see Eq. (6.28)]. Several observations can be made from this figure. First, the parameter κ is always positive regardless of η_0 and θ, implying that the κ in the signum function of friction force term can be ignored [see Eq. (6.10b)]. Second, κ is asymmetric except for $\eta_0 \to \infty$, so the tertiary mass would provide a 'biased' friction force which may lead to the deterioration of energy dissipation. Considering that the asymmetric behavior of the system is not desirable, we simplify the equations of motion under the assumption of sufficiently short l_2. Under this assumption, the parameters η_0 and η_1 can be neglected. The

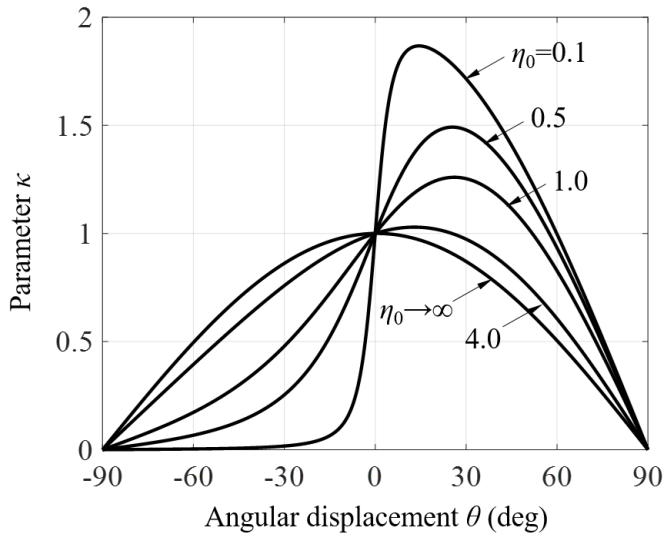

Figure 6.2: Parameter κ for various values of η_0

resulting simplified equations of motion are as follows:

$$\ddot{X} + 2\zeta_s\omega_s\dot{X} + \omega_s^2 X + \mu(1+\nu)\ddot{X} + \mu l_1(\cos\theta)\ddot{\theta}$$
$$-\mu l_1(\sin\theta)\dot{\theta}^2 - \tau\mu\nu g\,\mathrm{sgn}(\dot{\theta}) = -(1+\mu+\mu\nu)\ddot{u}_g \tag{6.11a}$$
$$(\cos\theta)\ddot{X} + l_1\ddot{\theta} + g\sin\theta + \tau\nu g\,\mathrm{sgn}(\dot{\theta}) = 0 \tag{6.11b}$$

Eqs. (25) and (26) can be recast into the following compact form

$$M\ddot{q} + C\dot{q} + Kq + \Phi = f\ddot{u}_g \tag{6.12}$$

where $q = [X, \theta]^{\mathrm{T}}$, $f = -[1 + \mu(1+\nu), 0]^{\mathrm{T}}$, and the M, C, K and Φ are the system

matrices and the nonlinear vector as follows.

$$M = \begin{bmatrix} 1 & 0 \\ 0 & 0 \end{bmatrix}, C = \begin{bmatrix} 2\zeta_s\omega_s & 0 \\ 0 & 0 \end{bmatrix}, K = \begin{bmatrix} \omega_s^2 & 0 \\ 0 & 0 \end{bmatrix}, \tag{6.13a}$$

$$\begin{aligned} \Phi = & \begin{bmatrix} \mu(1+\nu)\ddot{X} + \mu l_1(\cos\theta)\ddot{\theta} \\ (\cos\theta)\ddot{X} + l_1\ddot{\theta} \end{bmatrix} \\ & + \begin{bmatrix} -\mu l_1(\sin\theta)\dot{\theta}^2 - \tau\mu\nu g\,\mathrm{sgn}(\dot{\theta}) \\ \tau\nu g\,\mathrm{sgn}(\dot{\theta}) \end{bmatrix} + \begin{bmatrix} 0 \\ g\sin\theta \end{bmatrix}. \end{aligned} \tag{6.13b}$$

6.1.3 Statistical linearization

The objective of the statistical linearization is to substitute the nonlinear vector (Φ) with the linear vectors associated with equivalent mass, damping and stiffness matrices such that the error between the original and the equivalent system is minimized. Based on the derivation in the Appendix C, the matrices of the equivalent linear system are given as follows:

$$M^e = E\left[\frac{\partial\Phi}{\partial\ddot{q}}\right] = \begin{bmatrix} \mu\,(1+\nu) & \mu l_1 E\,[\cos\theta] \\ E\,[\cos\theta] & l_1 \end{bmatrix} \tag{6.14a}$$

$$C^e = E\left[\frac{\partial\Phi}{\partial\dot{q}}\right] = \begin{bmatrix} 0 & -2\mu l_1 E\left[(\sin\theta)\,\dot{\theta}\right] - E\left[\frac{\partial}{\partial\dot{\theta}}\left(\tau\mu\nu g\,\mathrm{sgn}\left(\dot{\theta}\right)\right)\right] \\ 0 & E\left[\frac{\partial}{\partial\dot{\theta}}\left(\tau\nu g\,\mathrm{sgn}\left(\dot{\theta}\right)\right)\right] \end{bmatrix} \tag{6.14b}$$

$$\begin{aligned} K^e = E\left[\frac{\partial\Phi}{\partial q}\right] = & \begin{bmatrix} 0 & -\mu l_1 E\left[(\sin\theta)\,\dot{\theta}\right] \\ 0 & -E\left[(\sin\theta)\,\ddot{X}\right] \end{bmatrix} \\ & + \begin{bmatrix} 0 & -\mu l_1 E\left[(\cos\theta)\,\dot{\theta}^2\right] \\ 0 & 0 \end{bmatrix} + \begin{bmatrix} 0 & 0 \\ 0 & gE\,[\cos\theta] \end{bmatrix} \end{aligned} \tag{6.14c}$$

The expectations of Eqs. (6.18) can be calculated explicitly when the response θ is assumed to be a zero-mean Gaussian process. First, the expected value of a cosine function can be explicitly obtained as follows.

$$E\left[\cos\theta\right] = \frac{1}{\sqrt{2\pi}\sigma_\theta}\int_{-\infty}^{\infty}\cos\theta\times\exp\left[-\dot{\theta}^2/2\sigma_\theta^2\right]\mathrm{d}\theta = \exp\left[-{\sigma_\theta}^2/2\right] \tag{6.15}$$

The averages of other terms can be calculated by assuming a property that two variables X and θ are uncorrelated, and each of these variables and its derivative are uncorrelated (Lutes and Sarkani, 2004).

$$E[(\sin\theta)\dot{\theta}] = E[\sin\theta]E[\dot{\theta}] = 0 \tag{6.16a}$$

$$E[(\sin\theta)\ddot{\theta}] = E[\sin\theta]E[\ddot{\theta}] = 0 \tag{6.16b}$$

$$E[(\sin\theta)\ddot{X}] = E[\sin\theta]E[\ddot{X}] = 0 \tag{6.16c}$$

$$E[(\cos\theta)\dot{\theta}^2] = E[\cos\theta]E[\dot{\theta}^2] = \sigma_{\dot{\theta}}^2\exp[-\sigma_\theta^2/2] \tag{6.16d}$$

In addition, under the Gaussian assumption, the expected value of the remained term in Eq. (6.14b) can be calculated as follows (Roberts and Spanos, 2003) DO NOT REFER:

$$E\left[\frac{\partial}{\partial\dot{\theta}}\left(\tau\nu g\,\mathrm{sgn}\left(\dot{\theta}\right)\right)\right] = \sqrt{\frac{2}{\pi}}\frac{\tau\nu g}{\sigma_{\dot{\theta}}} \tag{6.17}$$

Finally, we can obtain the linearized system parameters expressed in terms of

statistical moments and structural parameters:

$$\tilde{M} = M + M^e = \begin{bmatrix} 1+\mu(1+\nu) & \mu l_1 \exp\left[-{\sigma_\theta}^2/2\right] \\ \exp\left[-{\sigma_\theta}^2/2\right] & l_1 \end{bmatrix} \tag{6.18a}$$

$$\tilde{C} = C + C^e = \begin{bmatrix} 2\zeta_n\omega_n & -\sqrt{\frac{2}{\pi}}\frac{\tau\mu\nu g}{\sigma_{\dot{\theta}}} \\ 0 & \sqrt{\frac{2}{\pi}}\frac{\tau\nu g}{\sigma_{\dot{\theta}}} \end{bmatrix} \tag{6.18b}$$

$$\tilde{K} = K + K^e = \begin{bmatrix} \omega_n^2 & -\mu l_1 \sigma_{\dot{\theta}}^2 \exp\left[-{\sigma_\theta}^2/2\right] \\ 0 & g\exp\left[-{\sigma_\theta}^2/2\right] \end{bmatrix} \tag{6.18c}$$

The linearized structural properties are cast into the terms of statistical moments of the responses. It should be also noted that the statistical moments are also written in the terms of linearized matrices. Hence, the statistical linearization can be accomplished by iteratively solving those equations which are connected with the mechanical properties of linearized system and statistical moments up to an acceptable order of magnitude.

6.1.4 Gradient-based optimization

In this section, we seek to find the optimal parameters that would reduce the vibration of the primary structure. As we have constructed the explicit form for the linearized matrices, it is possible to use the gradient-based optimization which provides a fast searching direction in the feasible design region. The objective function and elements of its gradient are taken as follows,

$$J = \text{trace}\left[\hat{S}\hat{Q}\right] \tag{6.19a}$$

$$\frac{\partial J}{\partial d_i} = \text{trace}\left[\hat{S}\frac{\partial \hat{Q}}{\partial d_i}\right] \tag{6.19b}$$

where d_i is the i-th design variable (in this study, $d_1 = l_1$ and $d_2 = \tau\nu$), $\hat{S}$ is a weighting matrix, and $\hat{Q}$ is the state covariance matrix which is obtainable by solving the Lyapunov equation. One of the favorable choice of the weighing matrix is a null matrix except the first element is unity such that the performance measure J represents the RMS displacement of the primary structure. Note that the trace is a linear operator, hence it commutes with the partial derivative. Although the state covariance matrix $\hat{Q}$ is an implicit function of design variables, explicit expressions for Eq. (6.19a) can be obtained by differentiating the Lyapunov equation. Differentiating with respect to design variable gives us

$$\tilde{H}\frac{\partial \tilde{Q}}{\partial d_i} + \frac{\partial \tilde{Q}}{\partial d_i}\tilde{H}' + \left(\frac{\partial \tilde{H}}{\partial d_i}\tilde{Q} + \tilde{Q}\frac{\partial \tilde{H}'}{\partial d_i}\right) = O \tag{6.20}$$

Here we note that determining the gradient matrices in Eq. (6.20) needs solving the Lyapunov equation as well. The partial derivative of the system matrix with respect to the design variable d_i can be directly obtained as follows

$$\frac{\partial \tilde{H}}{\partial d_i} = \frac{\partial}{\partial d_i}\begin{bmatrix} H & D \\ O & \Lambda \end{bmatrix} = \begin{bmatrix} \frac{\partial H}{\partial d_i} & O \\ O & O \end{bmatrix} \tag{6.21}$$

And the first element of the matrix can be cast as follows

$$\frac{\partial H}{\partial d_i} = \frac{\partial}{\partial d_i}\begin{bmatrix} O & I \\ -\tilde{M}^{-1}\tilde{K} & -\tilde{M}^{-1}\tilde{C} \end{bmatrix} \tag{6.22}$$

Using chain rule and the basic identity of the derivative of the inverse matrix

(Jeffrey and Dai, 2008), the sub-matrices in Eq. (6.22) can be expressed as,

$$-\frac{\partial}{\partial d_i}\left(\tilde{M}^{-1}\tilde{K}\right) = -\tilde{M}^{-1}\frac{\partial \tilde{K}}{\partial d_i} - \frac{\partial \tilde{M}^{-1}}{\partial d_i}\tilde{K}$$
$$= -\tilde{M}^{-1}\frac{\partial \tilde{K}}{\partial d_i} + \tilde{M}^{-1}\frac{\partial \tilde{M}}{\partial d_i}\tilde{M}^{-1}\tilde{K} \tag{6.23a}$$
$$-\frac{\partial}{\partial d_i}\left(\tilde{M}^{-1}\tilde{C}\right) = -\tilde{M}^{-1}\frac{\partial \tilde{C}}{\partial d_i} - \frac{\partial \tilde{M}^{-1}}{\partial d_i}\tilde{C}$$
$$= -\tilde{M}^{-1}\frac{\partial \tilde{C}}{\partial d_i} + \tilde{M}^{-1}\frac{\partial \tilde{M}}{\partial d_i}\tilde{M}^{-1}\tilde{C} \tag{6.23b}$$

The derivatives of $\hat{M}$, $\hat{C}$ and $\hat{K}$ are obtained by differentiating Eqs. (6.18) with respect to the design variable di. The partial derivative of the matrices with respect to the design variables l_1 and τ are as follows:

$$\frac{\partial \tilde{M}}{\partial l_i} = \begin{bmatrix} 0 & \mu \exp\left[-{\sigma_\theta}^2/2\right] \\ 0 & 1 \end{bmatrix}, \qquad \frac{\partial \tilde{M}}{\partial \tau} = \begin{bmatrix} 0 & 0 \\ 0 & 0 \end{bmatrix} \tag{6.24a}$$
$$\frac{\partial \tilde{C}}{\partial l_1} = \begin{bmatrix} 0 & 0 \\ 0 & 0 \end{bmatrix}, \qquad \frac{\partial \tilde{C}}{\partial \tau} = \begin{bmatrix} 0 & -\sqrt{\frac{2}{\pi}}\frac{\mu\nu g}{\sigma_{\dot{\theta}}} \\ 0 & \sqrt{\frac{2}{\pi}}\frac{\nu g}{\sigma_{\dot{\theta}}} \end{bmatrix} \tag{6.24b}$$
$$\frac{\partial \tilde{K}}{\partial l_1} = \begin{bmatrix} 0 & -\mu\sigma_{\dot{\theta}}^2 \exp\left[-{\sigma_\theta}^2/2\right] \\ 0 & 0 \end{bmatrix}, \frac{\partial \tilde{K}}{\partial \tau} = \begin{bmatrix} 0 & 0 \\ 0 & 0 \end{bmatrix} \tag{6.24c}$$

In summary, it requires double loops to find the optimal parameters: inner loop for finding linearized matrices in statistical senses, and outer loop which seeks the optimized design parameters. The flowchart of iterative statistical linearization and optimum design process implemented is depicted in Figure 6.17. It should be noted that the double loops do not demand much numerical efforts since each loops tries to find the solution under the convex regions; the inner loop seeks to minimize the error

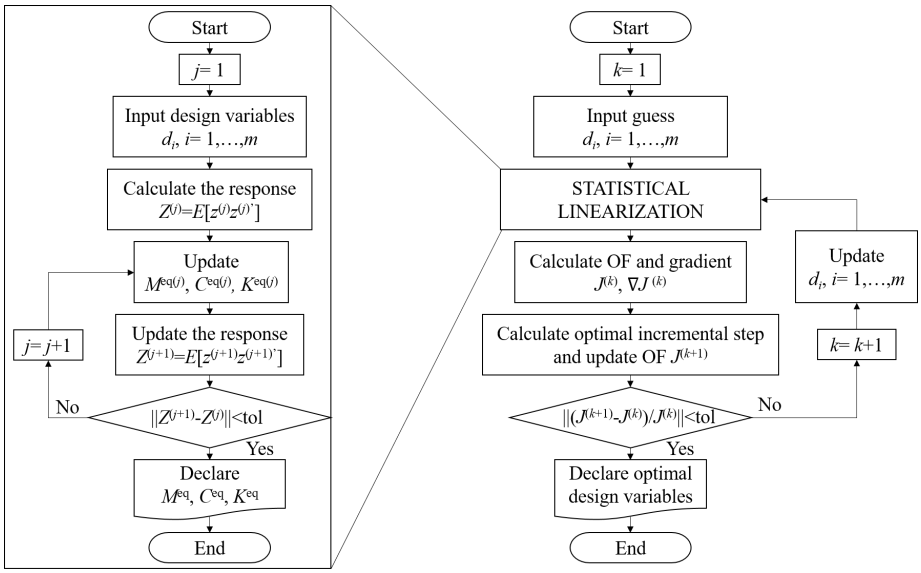

Figure 6.3: Flow chart of iterative statistical linearization and optimum design process implemented

terms written in the quadratic form, and the outer loop tries to minimize the convex objective function.

Once the objective function and its gradient have been established, various techniques are available to find the optimal parameters. Sequential Quadratic Programming method, or an iterative method for solving a sequence of Quadratic Programming Sub-problems subjected to a linearized constraint functions, was adapted in this study due to its superior rate of convergence. At each iteration Broyden-Fletcher-Goldfarb-Shanno algorithm was adopted for its effectiveness and good performance. MATLAB standard routine was used to find the optimum parameters (Coleman et al., 1999).

6.1.5 Numerical example

A single degree of freedom primary structure having a period of $T_s = 2$ sec (i.e. a natural frequency of $\omega_s = 3.14$ rad/sec) and a damping ratio 1% is considered as an example. In this study, the RMS displacement of the primary structure was selected as the objective function. The weighting matrix in Eqs. (6.19) is thus selected as follows,

$$\tilde{S} = \begin{bmatrix} 1 & 0 & \cdots & 0 \\ 0 & 0 & \cdots & 0 \\ \vdots & \vdots & \ddots & \vdots \\ 0 & 0 & \cdots & 0 \end{bmatrix} \tag{6.25}$$

The excitation is assumed to be filtered white noise process with its intensity S_0, which can be determined by the characteristic of the soil condition. In this case study, the primary structure is assumed to be excited by the ground motion with the peak ground acceleration (PGA) of 0.40g at the soil surface. The PGA level of 0.40g corresponds to the design PGA in seismically active region like southern California. The spectral intensity factor S_0 can be determined by using the following input-output relationship of the SDOF system under the white noise process (Crandall and Mark, 2014)

$$\sigma_{\ddot{u}_g}^2 = \frac{\pi}{2} \frac{S_0 \omega_g}{\zeta_g} (1 + 4\zeta_g^2) \tag{6.26}$$

where $\sigma_{\ddot{u}_g}$ is the RMS acceleration of the ground acceleration . The RMS acceleration level was then determined from the considered peak ground acceleration (PGA) and a peak factor of 3 as

$$\text{PGA} = 3\sigma_{\ddot{u}_g} \tag{6.27}$$

Table 6.1: Details of employed input motion

Variables		Value
PGA, g		0.40
Spectral intensity S_0, m^2/sec^3		0.0128
Stiff soil sites	Filter frequency ω_g, rad/sec	20.80
(Lin and Tyan, 1986)	Filter damping ratio ζ_g, %	40
Low-frequency filter	Filter frequency ω_2, rad/sec	0.40
(Clough and Penzien, 1993)	Filter damping ratio ζ_2, %	90

Thus, the spectral intensity can be determined by following relationship:

$$S_0 = \frac{2}{9\pi} \frac{\zeta_g (\mathrm{PGA})^2}{(1 + 4\zeta_g^2)\omega_g} \tag{6.28}$$

With assuming stiff soil condition (Lin and Tyan, 1986), the frequency and damping parameters for the soil filter were chosen as $\omega_g = 20.80$ rad/sec and $\zeta_g = 40\%$, respectively. The low-cut filter with the filter frequency ω_2 and filter damping ratio ζ_2 was also considered (Clough and Penzien, 1993). The details of the employed input motion are summarized in Table 6.1, and relevant technique to deal with the structural response under the filtered excitations, namely introducing a 'shaping filter' or 'pre-filter', is described in Appendix C.

Parametric studies

To check the validity of the linearized system, a comparison of the simulation results for the equivalent linear system is first examined by comparing the solution of the system [or the solution of Eqs. (6.10)] with that of the linearized system. Figure 6.4 shows a comparison between the exact and linearized solution with the FPTMD

properties of μ= 0.10, l_1= 99.5 cm, τ= 0.55 and ν= 0.30. From Figure 6.4a, it can be readily seen that the displacement history of the primary structure predicted using the linearized model correlates very well with that based on the exact nonlinear model.

To gain more insight into the characteristics of FPTMD, the angular velocities of the pendulum for the two models were compared in Figure 6.4b. The two models show comparable response during strong response phase, however, some discrepancy is also seen in the details of time history response. It is also worthwhile to recall that the dissipative force term contained in Eq. (6.18b) is inversely proportional to the RMS response of the angular velocity of the pendulum.

The discrepancy which arises from the Gaussian assumption can be also observed from the normalized dissipative hysteretic forces compared in Figure 6.5a. It can be seen from this comparison that the variance of the angular displacement of the exact model is a little bit larger compared to that of linearized model. Even though there exists some discrepancy in the variance of the angular displacement and hysteresis curve, the overall energy accumulation is similar in both models [see Figure 6.5b].

RMS response levels of the equivalent linearized system for various design parameters were also analyzed. Figure 5(a) depicts the RMS response level normalized to that of uncontrolled system for varying mass ratio ν and friction coefficient τ, with a pendulum length of $l_1 = 99.5$ cm. Here we can make several observations as follows. First, the maximum reduction in RMS response attainable is about 55% and 45% for 2% and 10% mass ratio, respectively. Second, the optimal parameters τ and ν for a fixed pendulum length are almost opposing each other. This is not surprising since the frictional force exerted by the motion of the tertiary mass is proportional to the friction coefficient τ and the mass ratio ν [see Eq. (82)].

Figure 6 shows the RMS responses of the equivalent system for various pendulum length l_1 and normalized friction force term $\tau\nu$. Here, the pendulum length was normalized to the reference pendulum defined as $l_{\text{ref}} = g/\omega_n^2$, where ω_n is the natu-

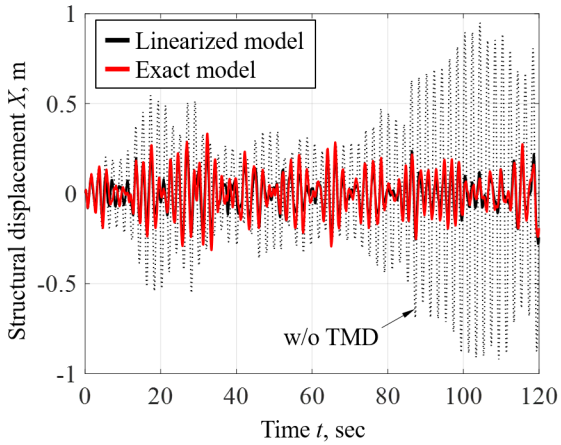

(a) Displacement of primary structures

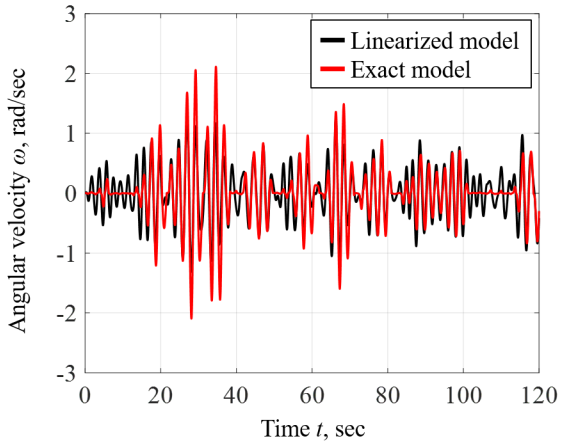

(b) Angular velocity of pendulums

Figure 6.4: Comparison of time histories between the exact and linearized solution

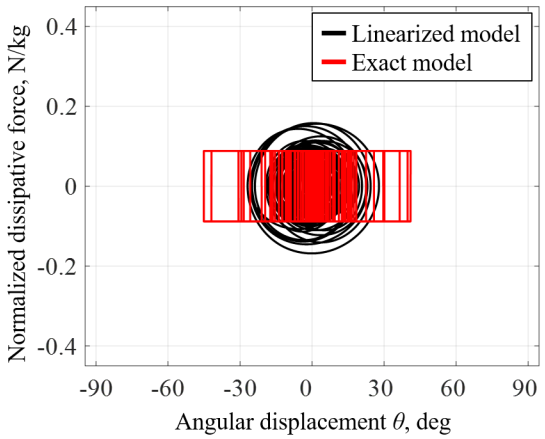

(a) Normalized dissipative force

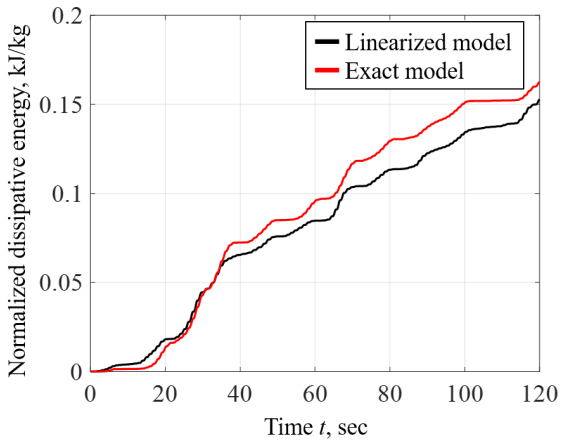

(b) Normalized dissipative energy

Figure 6.5: Comparison of indexes for energy dissipation between the exact and linearized solution

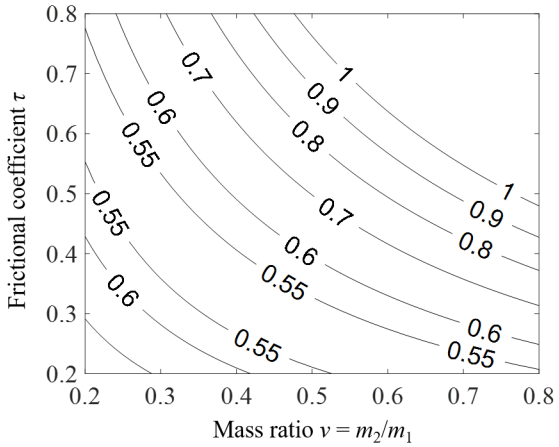

(a) μ=0.02

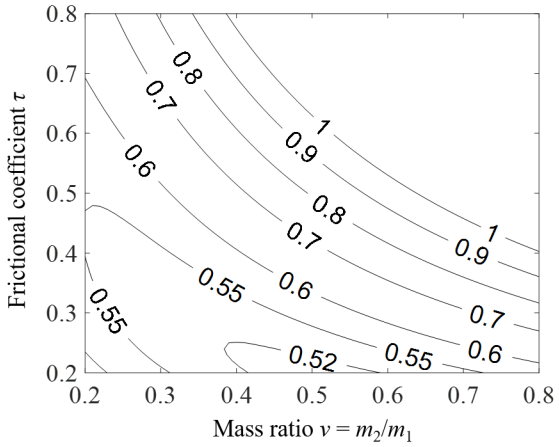

(b) μ=0.05

Figure 6.6: RMS response levels compared to uncontrolled case depending on mass ratio ν and friction coefficient τ (l_1=99.5 cm)

ral frequency of the primary structure. Again, the same trend is observed that the efficiency of FPTMD increases as the weight of the pendulum mass becomes larger. It should be emphasized that the optimal pendulum length for μ= 0.02 should be shorter than l_{ref} while that for μ= 0.10 should be longer than l_{ref}. This is in contradiction to the well-known fact in conventional translational TMD design that the optimal period of a TMD is close to a period slightly longer than that of a primary structure. Some explanation on this matter will be given in the next section.

Optimal parameters of FPTMD

The optimization procedure was programmed to find the optimal design parameters of FPTMD (refer to Figure 6.17). The two optimal parameters for the proposed FPTMD are presented in Figure 6.8 as a function of mass ratio and damping. From Figure 6.8a, it can be seen that the optimal pendulum length becomes longer with increasing mass ratio. The optimal parameter $\tau\nu$, corresponding to the frictional force, is plotted in Figure 6.8b. Unlike the optimal length, the parameter $\tau\nu$ does not vary widely, but is rather bounded in the range of 0.08 to 0.13.

Some explanations for the trends of the optimal parameters are given in the below. First, when the mass ratio is small, the optimal period shorter than that of the primary structure is demanded [see Figure 6.8a. This is again contradictory to the case of conventional TMDs for which the optimal period is slightly longer than that of the primary structure; as is well-known, the solution by Den Hartog (1956) suggests the optimal period as $(1+\mu)T_n$, where μ is the mass ratio of the TMD and T_n is the natural period of the primary structure. 6.9a shows the variation of the expectation of the cosine of the angular displacement, which is directly related to the potential force terms in Eqs. (6.14b) and (6.18b). The increase in the RMS response of the "light" pendulum decreases the potential force, thus shortening the "effective length" of the pendulum.

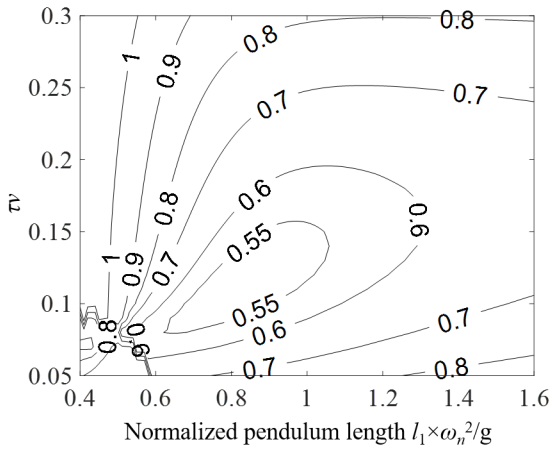

(a) μ=0.02

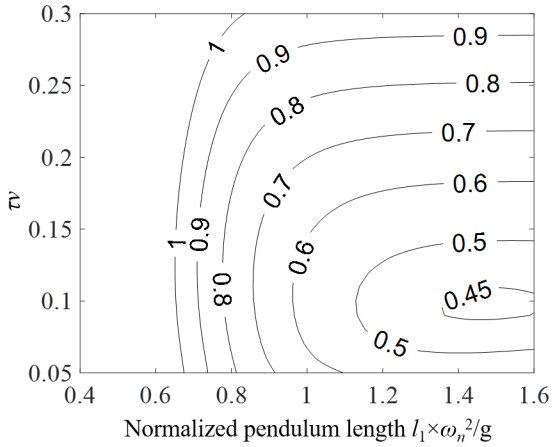

(b) μ=0.05

Figure 6.7: Contour of the normalized RMS response depending upon normalized frictional force and pendulum length (ν=0.7)

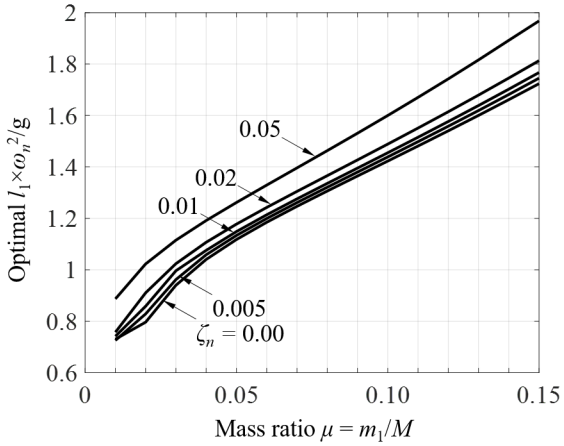

(a) Normalized pendulum length

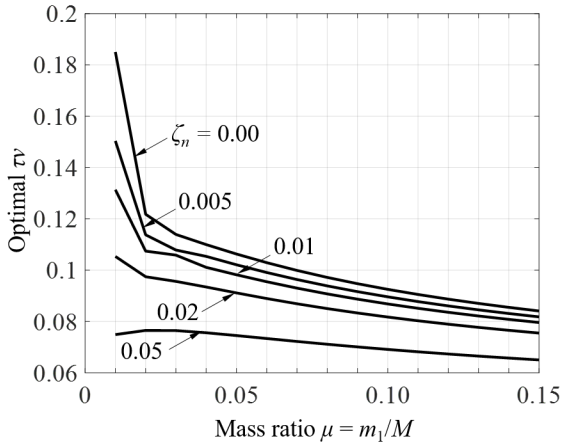

(b) Normalized frictional force

Figure 6.8: Optimal design parameters for various mass ratio μ

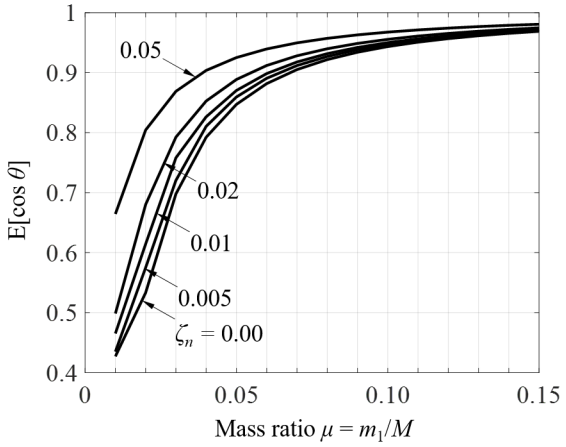

(a) Expectation of the cosine of the angular displacement

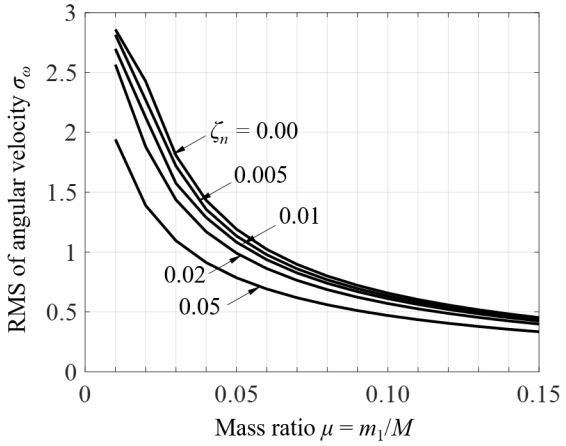

(b) RMS response of the angular velocity

Figure 6.9: Effect of mass ratio on angular displacement and velocity under optimal design condition

The trend of the optimal $\tau\nu$ depicted in Figure 6.8b may also seem contradictory to the case of conventional translational TMDs where larger optimal damping force is required as the mass ratio increases. However, this is also understandable with recalling that the dissipative force is proportional to the parameter $\tau\nu$, but is also inversely proportional to the RMS angular velocity of the pendulum. As can be observed from Figure 6.1b, the RMS angular velocity of the pendulum decays exponentially as the pendulum mass increases. Consequently, the required optimal frictional force expressed in terms of $\tau\nu$ should be more or less constant irrespective of the mass ratio.

6.1.6 Summary and conclusions

This study proposed a mechanism-based frictional pendulum TMD (FPTMD) in which the potential force is provided by a pendulum mass and the dissipative force is induced by the frictional force between a tertiary mass and the surface of a primary structure. The results of this study can be summarized as follows.

1. A mechanism-based friction-pendulum TMD utilizing a three-hinge mechanism was proposed which can overcome some shortcomings of traditional translational TMDs.

2. The exact and simplified nonlinear equations of motion for the proposed FPTMD were first derived. In order to circumvent the mathematical difficulties associated with highly nonlinear behavior of the FPTMD proposed, a statistical linearization technique was adopted to derive a set of equivalent linear equations.

3. A case study conducted based on the filtered white noise input showed that the displacement time history of the primary structure predicted using the developed linearized model correlates very well with that from the exact nonlinear

model. The angular velocity response of the pendulum predicted by the equivalent linear model was comparable to that based on the exact nonlinear model during strong response phase. However, some inevitable discrepancy was also observed in the details of the time history response.

4. In order to efficiently find the optimal parameters related to the pendulum length and the frictional force, the gradient-based optimization was adopted. To this end, a closed form for the gradient of the object function was derived. An iterative process which combines statistical linearization and optimization was implemented to obtain the optimal parameters under seismic excitation.

5. Analyses of the optimal parameters obtained were also made to enhance the understanding of the FPTMD behavior which is unique and different from conventional translational TMDs.

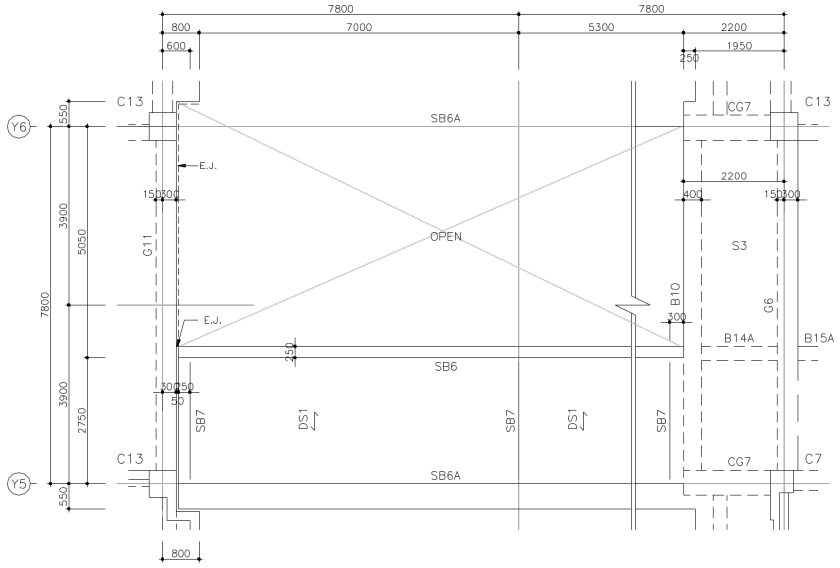

Figure 6.10: Drawing for examined floor

6.2 Vibration Attenuation of Hallway

This numerical study investigates the applicability of multiple tuned mass dampers (MTMDs) for suppressing human-induced floor vibration. A hallway at the 5th floor of Building 39 of Seoul National University was selected as an example structure. Field measurements were firstly conducted, and then the modal characteristics were calibrated with a finite element model. Linear and frictional MTMDs (LMTMDs and FMTMDs) with a total mass ratio of 5%, each of which systems consists of ten units of TMDs, are then designed according to the procedure described in Chapters 3 and 4. To investigate the effectiveness of designed TMDs, sensitivity analyses for the frequency perturbation of main structure and force amplitude variation were conducted. It was shown that FMTMDs are as effective as LMTMDs when subjected to near the targeted input level, and are more effective under the amplitude larger than the targeted one.

6.2.1 Description of the examined hallway

The hallway at the 5th floor of Building 39 of Seoul National University was selected as the examined floor, in which excessive vibration was often reported from walking faculties passing through. The floor structure is composed of a 150 mm-deep reinforced concrete slab supported by two types of 12.75 meter-long steel floor beams.

The dynamic properties including the natural frequency and corresponding modal mass were determined by experimental and numerical ways. First, the natural frequency of the hallway was found from the heel-drop test, and the modal mass was estimated by calibrating the test result with the result of modal analysis for a finite element model.

Modal characteristics

Free vibration tests were conducted by applying heel-drop impacts on the middle point of the hallway. Figure 6.11 depicts a time history and the associated Fourier transform for the hallway excited by a heel-drop impact. From the measurements, it was found that only the first mode with its natural frequency of 6.64 Hz dictates the dynamic response of the hallway. The damping ratio for the first mode was found from the half-power bandwidth method to be 1.13 percent.

Finite element analysis was conducted to analyze the dynamic behavior of the structure. A finite element model for the hallway was generated in ETABS® computer software and adjusted to match the free vibration tests. The structural members are set up based on the structural drawing shown in Figure 6.10. Some detailed techniques for modeling the floor are adopted according to the SCI-P354 (Smith et al., 2007). The dynamic modulus of elasticity of concrete was taken to be 38 MPa, which is about 1.35 times larger than an usual modulus for statics. The columns are modeled as uni-dimensional beam element, being pinned at their inflection point located at mid-

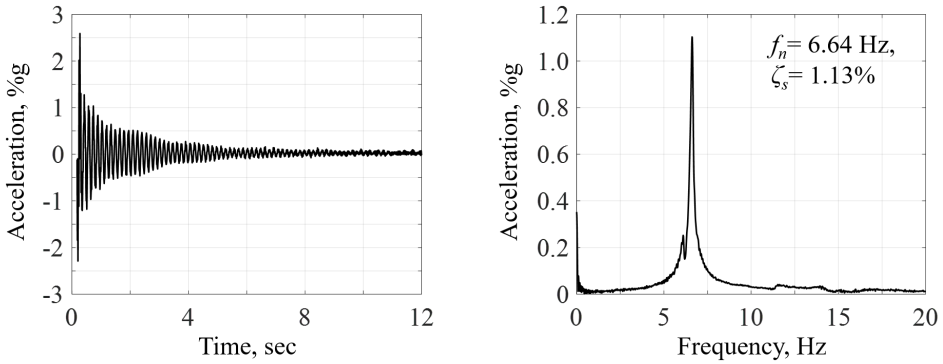

(a) Time history (b) Frequency response

Figure 6.11: Heel-drop test results

height between floors. The mass of the floor is set to be equivalent to the summation of self-weight and 30 percent of the prescribed design live loads. A value of 1.13 percent Rayleigh damping was applied, which corresponds to the measured value.

The mode shape of the first mode is presented in Figure 6.12, of which modal frequency and corresponding modal mass are calculated to be 6.75 Hz and 18.85 ton, respectively. The modal analysis result is in qualitative agreement with the field measurement, indicating a natural frequency for the first mode of 6.75 Hz that is only within 1 percent error with measured one.

Vibration performance evaluation

From additional field measurements, the maximum acceleration of approximately 2%g was observed, which is regarded as problematic for indoor footbridges according to the AISC Design Guide #11 (Murray et al., 1997).

For evaluation, the peak acceleration due to walking can be computed using the simplified design formula (Murray et al., 1997):

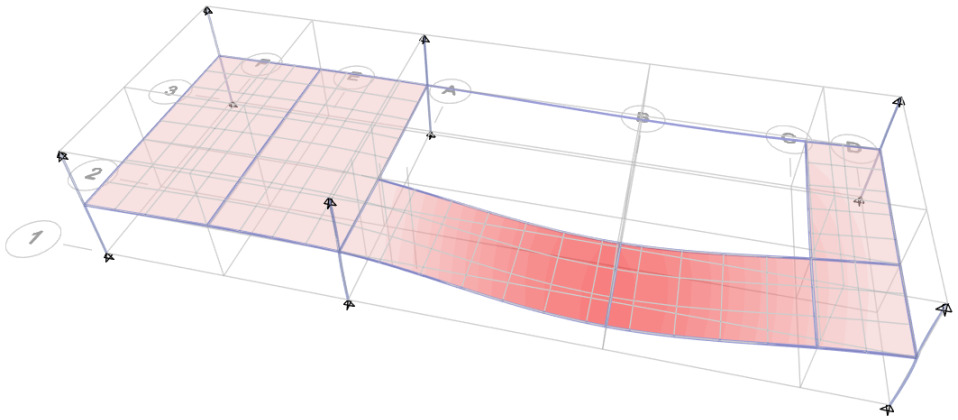

Figure 6.12: Calculated shapes of the first mode of the hallway (modal frequency and corresponding modal mass are calculated to be 6.75 Hz and 8.22 ton)

$$\frac{a_p}{g} = \frac{P_o \exp(-0.35 f_n)}{\beta W} \tag{6.29}$$

where a_p/g is the estimated peak acceleration in units of g, f_n is the natural frequency of the structure, and P_o is a constant force equal to 0.29 kN for floors and 0.41 kN for footbridges. The substitution of $f_n = 6.64$ Hz and $P_o = 0.29$ kN into Eq. (6.29) yields $a_p/g = 0.84\%$g.

A set of walking tests were also conducted, in which four occupied conditions were rather arbitrarily selected and tested; 10 and 15 people seated or standing. Three tests were repeated for each of the four occupied conditions. The forcing and measuring points were placed at the center of the floor to pick up the dynamic characteristics of the first mode. The peak acceleration measured from the walking tests was 0.73%g as an average spanning between 0.39%g and 1.31%g, which could exceed the threshold of 0.5%g for human comfort in an office environment recommended by (Murray et al., 1997). Note that the mean value of measured peak accelerations were rather lower than the estimated peak acceleration. Such a discrepancy is due to an assumption

on the simplified evaluation formula that the response would reach a fully resonance state, which is actually hard to built up. More realistic estimation can be made by appropriately applying relevant adjusting factor such as resonance amplification factor or modal shape factors (Smith et al., 2007).

6.2.2 Design of multiple tuned mass dampers

Two types of MTMDs, linear MTMD (LMTMD) and frictional MTMD (FMTMD), are designed according to the procedure described in Chapters 3 and 4. The total mass ratio μ_T is taken to be 5% (i.e. total mass of MTMDs is 942.5 kg) so that the TMD can produce an effective damping of 4-5% compared to the 1.13% original structural damping, which is determined from Figure 3.6. Both MTMDs are determined to consists of ten units of TMDs in order for each unit to weigh about 100 kg. All units of the MTMDs are designed to be located at the middle of the hallway where the modal shape value is the largest for their efficiency.

The optimal parameters for the MTMDs designed are presented in Table 6.2. The values of friction forces and COFs for the FMTMDs are normalized to their corresponding denominators. To convert those normalized values into actual physical values, the parameters such as the mass (m_s) and its RMS displacement under the uncontrolled condition ($\omega_s^2 x_{\text{ref}}$) should be identified. As described earlier, the mass of main structure appeared to be 18.85 ton and 6.64 Hz. The RMS acceleration is determined by applying $1/\sqrt{2}$ to the mean of peak acceleration.

6.2.3 Numerical investigation

Footfall loading model

The footfall force function is modeled as a Fourier series according to the SCI-P354 (Smith et al., 2007)

$$F(t) = q \sum_{i=1}^{H} \alpha_i \sin\left(2i\pi f_p t + \phi_i\right) \tag{6.30}$$

where q is the weight of an average person (normally taken as 746 N), H is the number of Fourier terms, α_i is the Fourier coefficient (or dynamic load factor) of the i-th term, f_p is the pace frequency, and ϕ_i is the phase lag of the i-th term. The dynamic load factors and the phase lags as proposed by Bachmann and Ammann (1987) are summarized in Table 6.3.

If the human exerts the footfall force on a concentrated location through moving in one direction with its velocity of v, the force can be simulated as a moving load which acts along the pathway. Considering the first mode governs with its shape of almost half-sine function, the equivalent dynamic force concentrated at the midpoint

Table 6.2: Optimal parameters of designed MTMDs

Frequency ratio γ_i^*	Damping ratio ζ_i^*, %	Normalized friction force $\eta_i/(m_s\omega_s^2 x_{\text{ref}})$, ‰	Normalized COF $\tau_i/(\omega_s^2 x_{\text{ref}})$, %
0.8356	2.513	8.811	12.518
0.8791	2.290	8.712	13.698
0.9174	2.152	8.503	14.559
0.9535	2.054	8.261	15.281
0.9890	1.982	8.001	15.922
1.0246	1.931	7.729	16.508
1.0612	1.898	7.442	17.049
1.0998	1.885	7.129	17.546
1.1423	1.903	6.771	17.977
1.1931	1.986	6.299	18.241

Table 6.3: Fourier coefficients for walking activities

Harmonic i	Dynamic load factor α_i	Phase angle ϕ_i
1	$0.436(if_p - 0.95)$	0
2	$0.006(if_p + 12.3)$	$-\pi/2$
3	$0.007(if_p + 5.20)$	π
4	$0.007(if_p + 2.00)$	$\pi/2$

of the floor $F^{\text{eq}}(t)$ can be expressed as follows (Chopra, 2007):

$$\begin{aligned} F_{\text{eq}}(t) &= \int_0^L F(t) \times \delta(x - vt) \times \sin\left(\frac{\pi x}{L}\right) \mathrm{d}x \\ &= q \sum_{i=1}^{H} \alpha_i \sin(2i\pi f_p t + \phi_i) \sin\left(\frac{\pi v}{L} t\right) \end{aligned} \tag{6.31}$$

where L is the beam span length, and $\delta(\cdot)$ is the Dirac delta function. The walking velocity v is approximated by the following equation (Bachmann and Ammann, 1987)

$$v = 1.67 f_p^2 - 4.83 f_p + 4.50 \tag{6.32}$$

where v is in m/s and the pace frequency f_p (Hz) is bounded between 1.7 Hz and 2.5 Hz.

In order to investigate the applicability of designed MTMDs, this study considered the most severe possible outcome that can be projected to occur in a given range of pace frequencies. Total 71 walking forces are simulated as the possible scenarios in deterministic ways, where the pace frequencies are determined to be spanned from 1.7 Hz to 2.5 Hz spacing 0.01 Hz, and their corresponding walking velocities.

MTMD performance evaluation

Figure 6.13 depicts simulated time response and associated peak acceleration spectrum. As for the uncontrolled structure, the maximum acceleration is about 1.2%g, which is considerable in excess of 0.5%g of maximum allowable peak acceleration according to the AISC DG #11. Not only in the vicinity of the pace frequency of 2.2 Hz, but also that of 1.7 Hz might be problematic by resonant by the third force component. It can be seen that both designed MTMDs are effective in attenuating the excessive vibration, enabling the hallway to be within the acceptable threshold for offices according to the AISC DG #11.

Sensitivity analysis

Natural frequency perturbation A natural frequency of a floor structure might be uncertain or change according to various situations such as modeling error in identifying the structural properties, or random deterioration of material or structural properties over time. This study presumably considered that the natural frequency of the examined floor would be uncertain with its variance of 10%, which is also consistent with the previous researches such as Ellingwood (1996) that used 10% COV for dead load.

Figure 6.14 depicts the peak acceleration spectrum of the structure where the natural frequency is perturbed to the lower or higher value of 10%. The pace frequency producing maximum acceleration for each case were different because each floor was excited by the harmonic components matching the divisor of the natural frequency of the structure. That is, the uncontrolled structure with frequency-perturbed to the lower value of 10% is mainly excited by the third component (6.64/3= 2.21 Hz or 5.98/3 = 1.99 Hz), while that with 10%-higher frequency perturbation is excited by the two components, the third (7.30/3= 2.43 Hz) and the fourth (7.30/4 = 1.83 Hz).

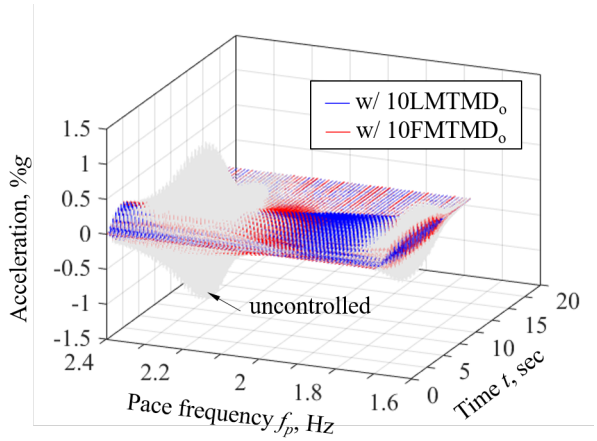

(a) Time responses

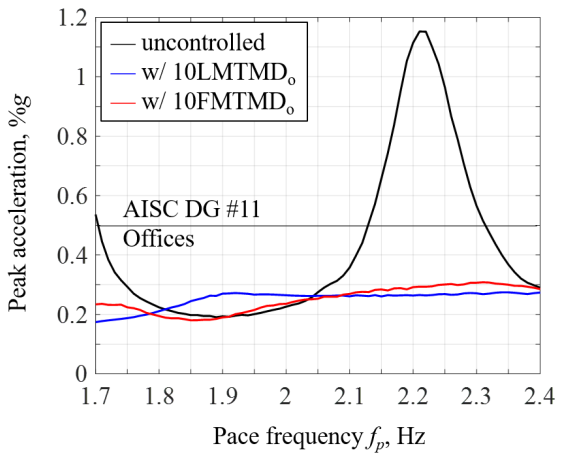

(b) Peak acceleration spectrum

Figure 6.13: Simulated time response and associated peak acceleration spectrum of examined structure with nominal natural frequency

It is observed that significant reduction can be achieved with both MTMDs, successfully attenuating the excessive vibration. The maximum acceleration of the dampened structures are around 0.4 %g, which is significantly reduced compared to the uncontrolled structure and is much below the allowable peak acceleration of 1.1%g. Interestingly, the $FMTMD_o$ is found to be more effective than $LMTMD_o$ under the condition that the main structure is near but not resonant. The undesired large response outside the resonant bandwidth may ascribed to the characteristic of the frequency response function of the system-MTMD system, in which some regions outside the resonant bandwidth become larger compared to the uncontrolled case [see Figure 3.10]. The FMTMDs, fortunately, have smoothed frequency responses due to the large values of equivalent damping of MTMDs under the condition that the uncontrolled response is smaller than specified in designing procedures. Such a sensitivity of the equivalent damping of the frictional mechanism on the input intensity may contribute to the beneficial effect on the reduction of the response outside the resonant bandwidth.

Input-intensity sensitivity Figures 6.15 depict the peak acceleration spectrum when the input-intensity is of 50% and of 150% compared to the design-specified intensity. When the forcing function is 50% lower than the design-specified loading, the $FMTMD_o$ showed its ineffectiveness compared to $LMTMD_o$, though appropriately controlling the excessive vibration under the resonant condition. The relative inefficiency of the FMTMD may be due to the large values of equivalent damping of MTMDs under the condition that the uncontrolled response is smaller than specified in designing procedures. As the input level further increases beyond the targeted input level up to 150%, the $FMTMD_o$ become more effective in a whole range of pace frequencies.

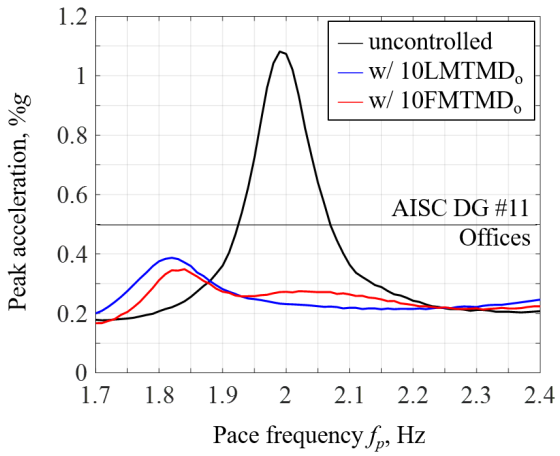

(a) 10% lower than nominal

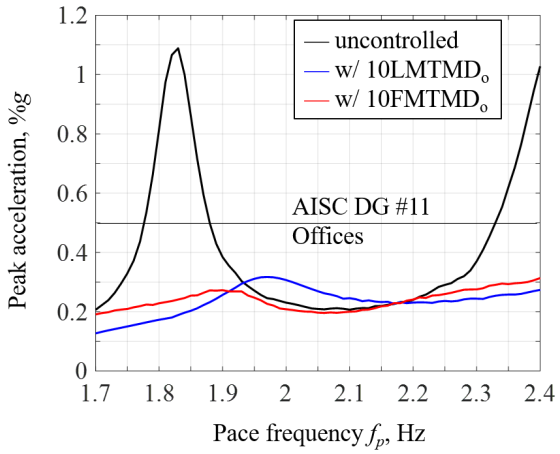

(b) 10% higher than nominal

Figure 6.14: Peak acceleration spectrum under perturbed natural frequencies

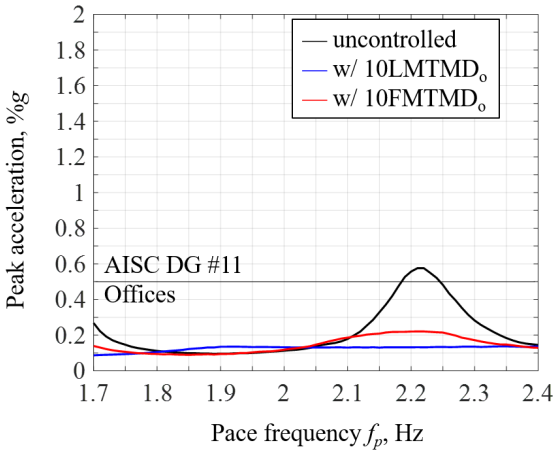

(a) 50% lower than design-specified intensity

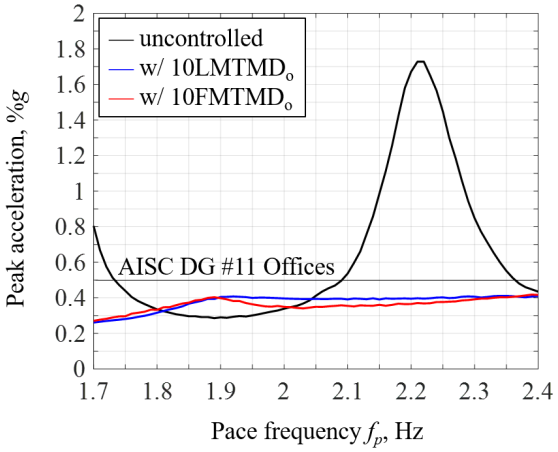

(b) 50% higher than design-specified intensity

Figure 6.15: Peak acceleration spectrum under various input intensity

6.2.4 Results and discussion

The applicability of MTMDs for the attenuation of floor vibration was investigated based on numerical analyses. This study provided the optimal parameters of the MTMDs. Based on the numerical simulations, it was shown that MTMDs designed according to the proposed procedure exhibits performance under the realizable range of walking frequencies.

6.3 Project: Vibration Mitigation of Floating Café

This section presents a project in an attempt to mitigate an excessive vibration of a problematic structure, which was conducted by the authors collaborated with Bosung ENG Group who provided safety design and with DRB Holding Co.,Ltd. who supported in manufacturing process. The overall process of the project includes the vibration performance evaluation, modal analysis based on finite element method and optimal design and manufacturing of tuned mass dampers. From a comparison between before and after installation of designed TMD, it was shown that the problematic vibration can be significantly reduced to the performance level required by the clients.

6.3.1 Introduction

On 5th March of 2015 at a newly constructing department store, very uncomfortable vibration was experienced by the workers. The problematic spot locates at a part of the third floor, at which a floating café was planned to become occupied. In order to check safety and eliminate such an intolerable vibration, the client decided to request Bosung ENG Group who was in charge of the structural design of the department building. Three days later, a team for solving the problem was constituted, which composed of Steel Structures and Seismic Laboratory of the Seoul National University, Bosung ENG Group who provided safety design and with DRB Holding Co., Ltd. who supported in manufacturing process. Starting with a preliminary measurement conducted on 8th of that month, the overall process of the project was carried out, which includes the vibration performance evaluation, modal analysis based on finite element method and optimal design and manufacturing of tuned mass dampers. The structural members are set up based on the structural drawing shown in Figure 6.16.

6.3.2 Description of floating café

The floating café is composed of a 150 mm-deep reinforced concrete slab supported by two steel beams of its length 12 m with its depth of 700 mm. The dynamic properties including the natural frequency and corresponding modal mass were determined by experimental and numerical ways.

Preliminary vibration tests were conducted by applying heel-drop impacts on the tip of the cantilever arms. Figure 6.17 depicts a time history and the associated Fourier transform for the hallway excited by a heel-drop impact. From the measurements, it was found that the first two modes with its natural frequency of 6 Hz and 20 Hz dictate the dynamic response of the structure. The damping ratios were found from the half-power bandwidth method to be 1% and 3%, respectively. It was concluded from the preliminary test that the floating café can be probably excited by the third component (6/3= 2 Hz), which resulted in an excessive vibration that was intolerable for workers during the construction.

A finite element model was constructed to analyze the dynamic behavior of the

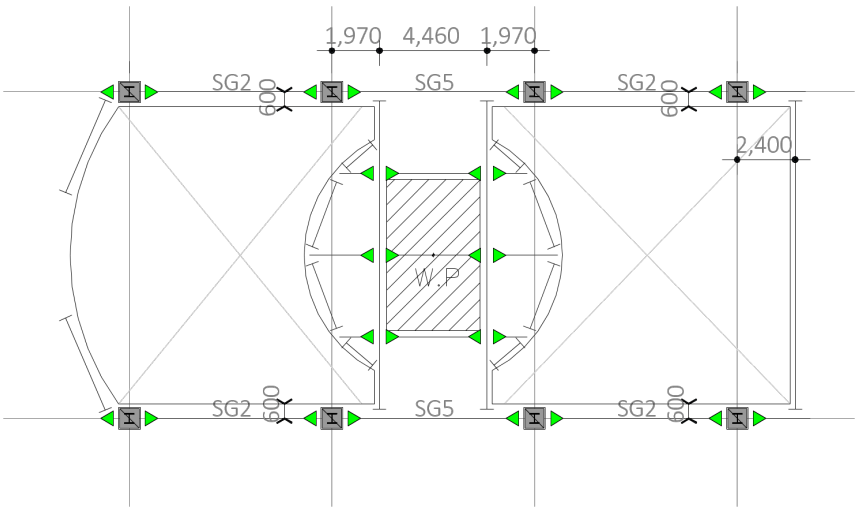

Figure 6.16: Drawing for floating café

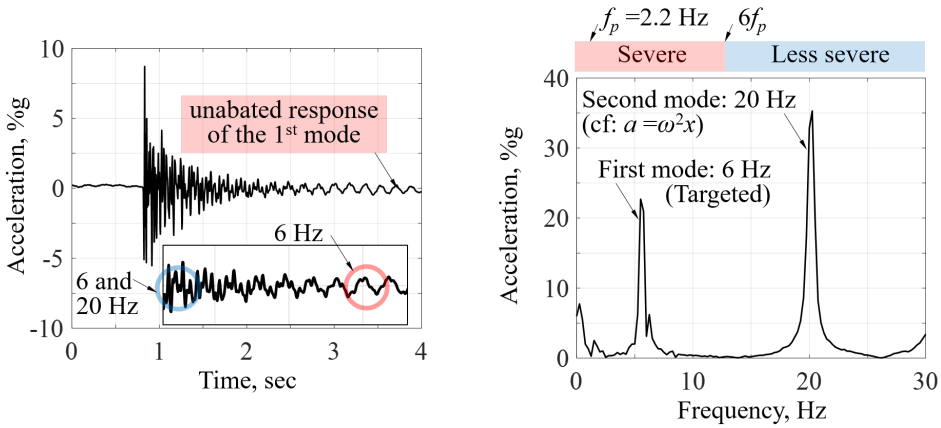

(a) Time history

(b) Frequency response

Figure 6.17: Preliminary test results

structure. The structural members are set up based on the structural drawing shown in Figure 6.16. Some detailed techniques for modeling the floor are adopted according to the SCI-P354 (Smith et al., 2007). The dynamic modulus of elasticity of concrete was taken to be 38 MPa, which is about 1.35 times larger than an usual modulus for statics. The columns are modeled as uni-dimensional beam element, being pinned at their inflection point located at mid-height between floors. The mass of the floor is set to be equivalent to the summation of self-weight and 30 percent of the prescribed design live loads. A value of 1 percent Rayleigh damping was applied, which corresponds to the measured value for the first mode of the structure.

The mode shape of the governing first mode is presented in Figure 6.18. The modal analysis result is in qualitative agreement with the field measurement, indicating a natural frequency for the first mode of 6.057 Hz that is only within 1 percent error with measured one.

Table 6.4: Modal properties of floating café

		Values	
		1st mode	2nd mode
Under construction (Tested)	Frequency, Hz	6.057	19.060
	Mass, ton	3.319	0.125
Finished (Predicted)	Frequency, Hz	6.1348	19.174
	Mass, ton	7.283	0.203

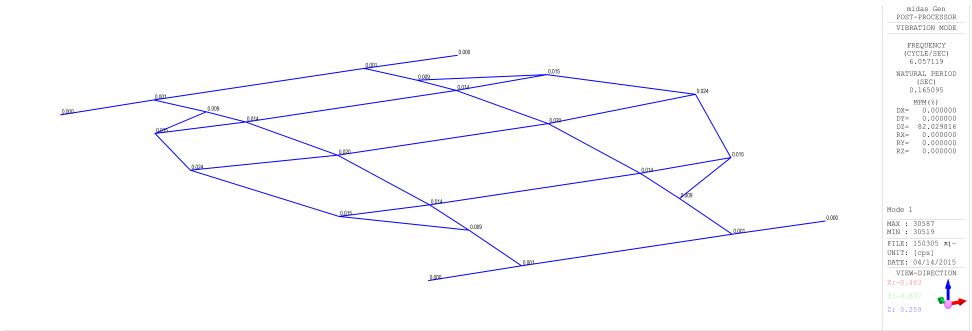

Figure 6.18: Mode shape of the first mode

6.3.3 Design of multiple tuned mass dampers

Two sets of $FMTMD_o$, each set of which consists of three units are designed and implemented in this study. The FMTMDs were designed by Steel Structures and Seismic Design Laboratory in Seoul National University, and manufactured by Dongil DRB Holding Co., Ltd.. The design procedure for the TMDs are regulated according to those proposed by this study (see Design procedures covered in Chapter 4). The RMS acceleration in %g is usually taken as lower than the peak acceleration, but it is taken as same as the peak value as a conservative manner. In order to attain

Table 6.5: Optimal parameters of designed MTMDs

Type	Frequency ratio γ_i^*	Equivalent damping ratio $\zeta_i^{\mathrm{eq}*}$, %	Normalized friction force $\eta_i/(m_s\omega_s^2 x_{\mathrm{ref}})$, %	Normalized COF $\tau_i/(\omega_s^2 x_{\mathrm{ref}}/g)$, %
$\mathrm{FMTMD_o}$	0.911	4.220	24.31	21.07
	0.994	3.960	27.70	29.40
	1.081	3.873	29.40	35.88

the suppression level of increasing the damping ratio of 5%, the mass ratios for both TMDs are taken as 5%, and the number of TMDs is taken to be five units (see Figure 3.6).

Designed MTMDs are manufactured. Figure 6.17 shows the overview and detailed view of the TMDs. After all, the TMDs are installed. Figure 6.19 shows the installed locations and in-field tuning process.

6.3.4 Vibration serviceability assessment

Figure 6.20 compares the measured accelerations of the main structure before and after activating the MTMDs, in which the left, centered and right panels are those measured at the tip, at the center of the café, and the top of one of the TMD. It is clear that the acceleration levels are significantly lower when the TMDs are activated. While the time history of the tucked TMD is almost identical to the main structure, the activated TMD shows a large response of acceleration, participating in the vibration dissipation.

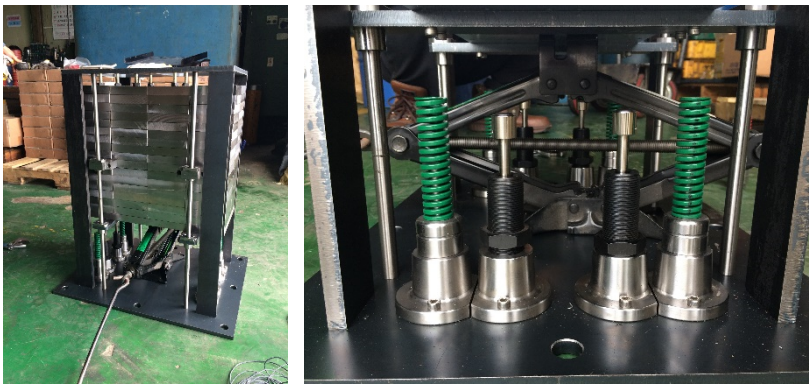

(a) Overview (b) Details

(c) Installed locations (d) In-field tuning

Figure 6.19: Manufactured TMD unit

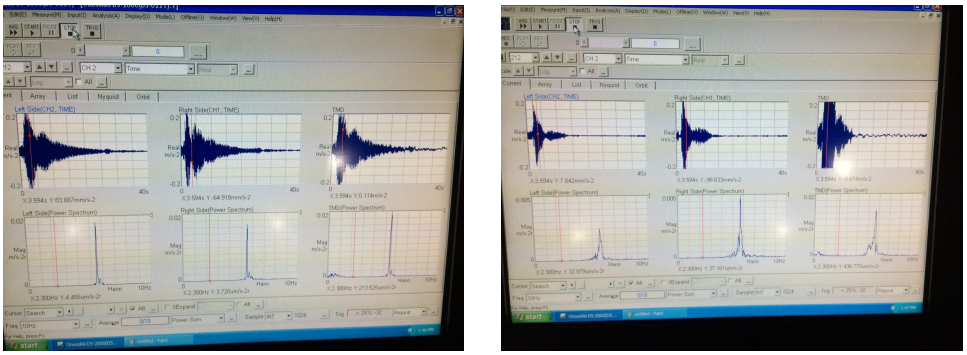

(a) Uncontrolled (b) Activated

Figure 6.20: Measured accelerations of the main structure

6.3.5 Results and discussion

The applicability of MTMDs for the attenuation of floor vibration was investigated based on numerical analyses. This study provided the optimal parameters of the MTMDs. Based on the numerical simulations, it was shown that MTMDs designed according to the proposed procedure exhibits performance under the realizable range of walking frequencies.

Chapter 7

Summary and Conclusions

This study presented a framework for the design of multiple tuned mass dampers (MTMDs), widely covering all the design aspects such as control efficiency, optimal design parameters, their robustness, and stroke limitation issues. Optimal design of linear MTMDs (LMTMDs) were firstly discussed. It was confirmed that optimal damping ratios decrease as the number of TMD increases. Such a relationship between optimal damping and the number of TMD induces an idea that, with a large number of TMDs, frictional mechanism inherent in TMD operation would be sufficient to satisfy the required small damping ratio. Based on the remark, the design of frictional MTMDs (FMTMDs), which dissipate the transferred energy through inherent friction mechanism.

Chapter 3 provided a framework for design of LMTMDs. The optimal parameters of various LMTMD configurations are investigated, of which constraints are such as the frequency ratios, damping ratios, mass distributions and combinations thereof. Second, two different optimization schemes are employed: Nominal performance optimization (NPO) and Robust performance optimization (RPO). In order to allow

the designer to consider the performance evaluation and the stroke limitations simultaneously, this study provides contour maps for the RMS displacement of the main structure and the largest RMS displacement of the LMTMDs that can be useful in the design process. The main findings can be summarized as follows:

1. Among the considered MTMD configurations, LMTMD_o is found to be most efficient in terms of suppressing the structural vibration, but some configurations like LMTMD_γ, LMTMD_ζ and $\text{LMTMD}_{\gamma\zeta}$ can also exhibit their control performance similar to LMTMDo. Two other configurations LMTMD_μ and $\text{LMTMD}_{\mu\zeta}$, however, not only deteriorate their control efficiency but also require large amount of damping coefficient compared to the other MTMDs, especially the number of TMDs becomes larger.

2. The optimal parameters like frequency ratios and damping ratios of MTMD are found under the condition that the main structure is excited by a ground motion of stationary zero-mean white-noise. From NPO solution, it was found that the optimal parameters of MTMDs extend that of the single TMD.

3. From the backbone curve predicted by the classical solution of Warburton (1982), the optimal frequency range tends to span further as the number of TMDs increases, and the damping ratio per an unit TMD becomes smaller. The rate of increasing the span and decreasing the damping ratio is drastic when the total mass ratio is larger, showing insignificant difference with a larger number of TMDs.

4. The RPO solution, which helps take into account the perturbation of the natural frequency of main structure, was found with the Point estimation method. Compared to the NPO solution, the RPO solution provides more wider frequency spans and decreased damping ratio. Based on the comparative analysis

in the frequency domain, the RPO based solution provides more robust solution.

5. Considering the analyzed results that the $\text{LMTMD}_{\gamma\zeta}$ exhibits the performance to the optimal solution LMTMD_{o} with much reduced design variables, this study proposed an approximate solution for $\text{LMTMD}_{\gamma\zeta}$.

6. To allow the designer to consider the performance evaluation and the stroke limitations simultaneously, this study provides contour maps for the RMS displacement of the main structure and the largest RMS displacement of the LMTMDs that can be useful in the design process.

Chapter 4 provided a framework for design of FMTMDs. The optimal parameters of various FMTMD configurations were investigated, of which constraints are such as the frequency ratios, damping ratios, mass distributions and combinations thereof. Four of the feasible FMTMD configurations are formulated and comparably analyzed, each of which is constrained in a way of linearly distributed frequency ratios, uniformly distributed coefficients of friction (COFs), and/or combinations thereof. An approximate design formula is developed for $\text{FMTMD}_{\gamma\tau}$ configuration utilized under the constraint of frequency ratios and COFs. In order to cope with the difficulties inherent in nonlinearity of the system, this study adopted a statistical linearization technique, which enables the complicated nonlinear force terms to be linearized in a statistical sense. The key features of this chapter includes:

1. The optimal parameters like frequency ratios and equivalent damping ratios of MTMD, which are obtained from a statistical linearization technique, are found under the condition that the main structure is excited by a ground motion of stationary zero-mean white-noise.

2. From the backbone curve predicted by the classical solution, the optimal frequency range tends to span further as the number of TMDs increases, and the

damping ratio per an unit TMD becomes smaller. The rate of increasing the span and decreasing the damping ratio is drastic when the total mass ratio is larger, showing insignificant difference with a larger number of TMDs.

3. An input-sensitivity analysis was extensively carried out. It was shown that once the FRFs under a low level of input strength would blunt appearing the original structural mode becomes flatten with increasing the loading level to 0.5. Further increased loading to the originally-targeted loading enables the TMDs to facilitate in a active way until the targeted input strength. As the input level further increases beyond the targeted input level, the equivalent damping ratios decreases compared to those for targeted one, causing undesired and frivolous motions of TMDs resulting in their FRFs to be more increased peaks and deep valleys, which might be unhelpful in controlling the main structure.

4. The approximate solution for FMTMD$_{\gamma\tau}$ was determined its optimal condition with just three design variables such as two bound frequency ratios γ_1 and β_γ, and a COF τ.

Chapter 5 addressed RMS responses and extreme value distributions for the frictional multiple tuned mass dampers (FMTMDs). In designing of optimal FMTMD, the nonlinear system arising from the frictional elements were replaced into an equivalent linear system by means of statistical linearization. In order to improve an accuracy for the estimation of peak distribution of MTMDs, this study exploited a statistical nonlinearization technique, which replaces nonlinear systems with a class of other nonlinear systems of which exact solution has been explicitly derived. A correction factor that defines the ratio of RMS displacement between nonlinear and linear system was derived, based on the result of statistical nonlinearization technique. This study further derived an explicit formula for evaluating a peak factor for the frictional TMD. Those correction factor and formula for the peak factor were examined with

Monte Carlo Simulation. The main findings are summarized below:

1. Based on the statistical nonlinearization, this study derived the probability density function for the peak values of the FTMD unit. It was shown that, for the FTMD, the probability that any peak exceeds a certain value can be approximated as the Erlang-2 distribution, which is clearly distinguished from the solution of linear vibration theory that predicts that as Rayleigh distribution.

2. A correction factor that defines the ratio of RMS displacement between nonlinear and linear system was derived. Through the numerical simulations, it was found that the estimated value obtained by the statistical linearization underestimates the RMS displacement of TMD significantly providing less than 3 percent quantile compared to the simulated results. The model proposed by this study provides in a level of 10 % quantile showing less than 10% from the mean value of the simulated solution.

3. This study further derived an explicit formula for evaluating a peak factor for the frictional TMD. It was found from numerical simulations that the peak distribution is not dependent on the mass ratio of TMD, thereby the frequency ratio and damping ratio of TMD.

4. The predicted peak response showed some discrepancies with the simulated results; however, the maximum relative error was less than 13 percent. The results show a trend that as the DVA mass ratio decreases, the model tends to overestimate the peak response of the TMD.

Chapter 6 dealt with several applications of multiple tuned mass dampers (MTMDs). In the first section, a mechanism-based frictional pendulum tuned mass damper (FPTMD) was proposed, which contributes to overcome some shortcomings of conventional translational TMDs with viscous damping. In the second section, a numerical

study was carried out to provide a design procedure of MTMDs, which covered modal analysis based on finite element method, optimal design of tuned mass dampers, and evaluating their control performance and robustness under the frequency-perturbed states. The final section presented a project in an attempt to mitigate an excessive vibration of a problematic structure. The overall process of the project includes the vibration performance evaluation, modal analysis based on finite element method and optimal design and manufacturing of tuned mass dampers. The main findings are summarized below:

1. A mechanism-based friction-pendulum TMD utilizing a three-hinge mechanism was proposed which can overcome some shortcomings of traditional translational TMDs. The exact and simplified nonlinear equations of motion for the proposed FPTMD were first derived. In order to circumvent the mathematical difficulties associated with highly nonlinear behavior of the FPTMD proposed, a statistical linearization technique was adopted to derive a set of equivalent linear equations.

2. The applicability of MTMDs for the attenuation of floor vibration was investigated based on numerical and experimental ways. First, the hallway at the 5th floor of Building 39 of Seoul National University was selected as the example structure. The overall process of the project includes the vibration performance evaluation, modal analysis based on finite element method and optimal design and manufacturing of tuned mass dampers.

Appendices

Appendix A

Point Estimation Method

Point estimation method (PEM) is a class of numerical methods for evaluating the statistical moments of a given function that consists of random input variables. A typical work out of the method involves (1) determining specific points of input variables and associated weighting factors, followed by (2) evaluating the statistical moments of the given function at the discrete points, and (3) combining all of evaluated statistical moments with associated weighting factors for the final calculation. The numerical answer can be treated as an approximate value of the statistical moments of the given function.

The PEM is effective and powerful compared to several relevant techniques such as direct integration method, Monte Carlo Simulation and Response Surface Method, especially when the associated random variables are in a large number. Some details on the determination of 'points' varies depending on the number of the specific points per an input variable.This study dealt with $2N + 1$ scheme which requires $2N + 1$ specific points per an input variable. More details on its theoretical aspects can be found in the literature Rosenblueth (1975) and Hong (1998), and those on its

applications can also be found in Morales and Perez-Ruiz (2007) and Caramia et al. (2010).

Consider a function $Y = Y(X_1, \cdots, X_N)$ where the individual variables X_j, $j = 1, \cdots, N$ are random. The procedure for computing the moments of the output variables can be summarized by the following step:

1. Set the vector consists of l-th moment of the output variable to be zero, and set the variable index j as one.

2. Determine the two standard locations for the individual variable X_j:

$$\chi_{j,1} = \frac{\lambda_{j,3}}{2} + \sqrt{\lambda_{j,4} - \frac{3}{4}\lambda_{j,3}^2} \tag{A.1a}$$

$$\chi_{j,2} = \frac{\lambda_{j,3}}{2} - \sqrt{\lambda_{j,4} - \frac{3}{4}\lambda_{j,3}^2} \tag{A.1b}$$

where $\lambda_{j,3}$ and $\lambda_{j,4}$ denote the third and fourth standard central moments of the input random variable X_j with probability density function $f_{X_j}(x_j)$, that is:

$$\lambda_{j,3} = \frac{M_3(X_j)}{\sigma_{X_j}^3}, \tag{A.2a}$$

$$\lambda_{j,4} = \frac{M_4(X_j)}{\sigma_{X_j}^4}, \tag{A.2b}$$

$$M_3(X_j) = \int_{-\infty}^{\infty} (x_j - \mu_{X_j})^3 \mathrm{d}x_j, \tag{A.2c}$$

$$M_3(X_j) = \int_{-\infty}^{\infty} (x_j - \mu_{X_j})^4 \mathrm{d}x_j \tag{A.2d}$$

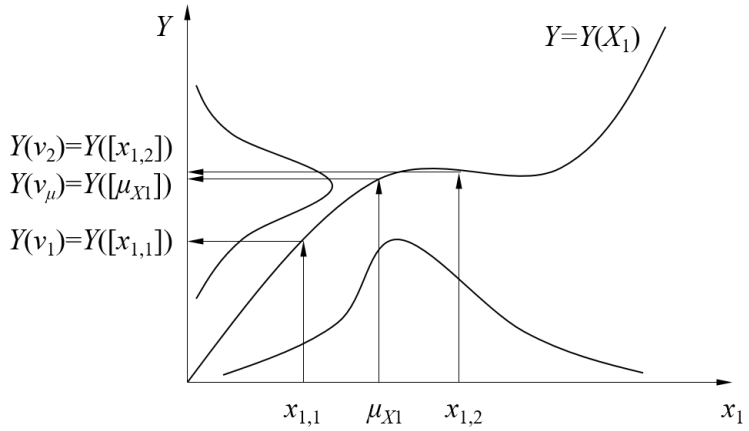

Figure A.1: Two deterministic points and evaluated values for these points

where μ_{X_j} and σ_{X_j} in the relationship are the mean and the standard deviation of X_j, respectively. Note that $\lambda j, 1$ equals zero, $\lambda j, 2$ is unity, and $\lambda_{j,3}$ and $\lambda_{j,4}$ are the skewness and kurtosis of the random variable x_t, respectively. Particularly, the third central moment $\lambda_{j,3}$ yields zero when the variable X_j is symmetric.

3. Determine the two points $x_{j,1}$ and $x_{j,2}$ [see Figure A.1]:

$$x_{j,1} = \mu_{X_j} + \chi_{j,1}\sigma_{X_j} \tag{A.3a}$$

$$x_{j,2} = \mu_{X_j} + \chi_{j,2}\sigma_{X_j} \tag{A.3b}$$

As can be deduced from Eq. (A.2), these determined points depend on the first three moments of f_{X_t}.

4. Evaluate the given function Y for both locations $x_{j,k}$ using the two input vari-

able vectors:

$$\nu_1 = [\mu_{X_1}, \mu_{X_2}, \cdots, x_{j,1}, \cdots, \mu_{X_N}] \tag{A.4a}$$

$$\nu_2 = [\mu_{X_1}, \mu_{X_2}, \cdots, x_{j,2}, \cdots, \mu_{X_N}] \tag{A.4b}$$

5. Determine the associated weight factors:

$$w_{j,1} = \frac{1}{\chi_{j,1}(\chi_{j,1} - \chi_{j,2})} \tag{A.5a}$$

$$w_{j,2} = -\frac{1}{\chi_{j,1}(\chi_{j,1} - \chi_{j,2})} \tag{A.5b}$$

6. Update $E(Y^l)$:

$$E(Y^l) = E(Y^l) + \sum_{k=1}^{2} w_{j,k}[Y(\nu_k)]^l \tag{A.6}$$

7. Repeat the above steps for $j = j + 1$ until the list of random input variables is exhausted.

8. Evaluate the function Y at the input vector consists of mean points:

$$\nu_\mu = [\mu_{X_1}, \mu_{X_2}, \cdots, \mu_{X_j}, \cdots, \mu_{X_N}] \tag{A.7}$$

9. Determine the weight factor for the input vector ν_μ:

$$w_\mu = 1 - \sum_{j=1}^{N} \frac{1}{\lambda_{j,4} - \lambda j, 3^2} \tag{A.8}$$

10. Update $E(Y^l)$:

$$\begin{aligned} E(Y^l) &= E(Y^l) + w_\mu [Y(\nu_\mu)]^l \\ &= \sum_{j=1}^{N} \sum_{k=1}^{2} w_{j,k} [Y(\nu_k)]^l + w_\mu [Y(\nu_\mu)]^l \end{aligned} \tag{A.9}$$

The procedure previously described is valid in the case that the input random variables are uncorrelated each other. If the input random variables are correlated to some extent, an additional treatment should be preceded in a way that transforms the set of correlated input variables into an uncorrelated set of variables. The details about the procedure are described in the literature (Hong, 1998).

Appendix B

Statistical Linearization

One attractive method for solving nonlinear stochastic differential equations is a statistical linearization which can replace a set of nonlinear differential equations by a set of equivalent linear equations in a statistical sense. This appendix is dedicated to briefly present a coverage on the statistical linearization, particularly for the case when the input is a zero-mean stationary white-noise excitation, and the response processes of concern are also stationary. A comprehensive example is followed by the presented coverage. Additional issues on the technique involving an extension to non-stationary process problem and its accuracy are detailed in Roberts and Spanos (2003), and recent research on advanced theoretical issues and its applications of this technique are well reviewed in the literature (Socha, 2005a,b).

B.1 Formulation

Consider a system that includes nonlinear force term ψ in the form

$$My'' + Cy' + Ky + \psi(y, y', y'') = fu \tag{B.1}$$

where M, C and K denote the mass, viscous damping and stiffness matrices, respectively, y is a generalized coordinate vector, a prime notation denotes the derivative, ψ is a nonlinear vector whose entries are function of the coordinate vector y and its derivatives, u is a scalar random process and f is an influence vector for the process u.

The first step of the statistical linearization is to formulate a set of equivalent linear equations by replacing the nonlinear vector ψ with the linear vectors associated with equivalent mass, damping and stiffness matrices such that the error between the original and the equivalent system is to be minimized.

The equivalent linear system is defined by

$$My'' + Cy' + Ky + M^{\mathrm{eq}}y'' + C^{\mathrm{eq}}y' + K^{\mathrm{eq}}y = fu \tag{B.2}$$

where M^{eq}, C^{eq} and K^{eq} are the equivalent matrices to be suitably determined.

The difference ε between the original and the equivalent linear system, or the error can be defined by

$$\varepsilon = \psi - M^{\mathrm{eq}}y'' - C^{\mathrm{eq}}y' - K^{\mathrm{eq}}y \tag{B.3}$$

A variety of error measures can be considered(Socha, 2005a), but the mean square of the error is one of the commonly used measures owing to its simplicity and clarity of conceptual aspect. The mean-squared error to be minimized is then defined as

$$\begin{aligned} E[\varepsilon^{\mathrm{T}}\varepsilon] = {} & E[\psi^{\mathrm{T}}\psi] - 2E[\psi^{\mathrm{T}}(M^{\mathrm{eq}}y'' + C^{\mathrm{eq}}y' + K^{\mathrm{eq}}y)] \\ & + E[(M^{\mathrm{eq}}y'' + C^{\mathrm{eq}}y' + K^{\mathrm{eq}}y)^{\mathrm{T}}(M^{\mathrm{eq}}y'' + C^{\mathrm{eq}}y' + K^{\mathrm{eq}}y)]. \end{aligned} \tag{B.4}$$

B.2 Solution Procedure

B.2.1 Error minimization

From Eq. (B.4) it is seen that the error measure $E[\varepsilon^{\mathrm{T}}\varepsilon]$ is simply a quadratic form with respect to the parametric matrices M^{eq}, C^{eq} and K^{eq}. The next step is to determine the parametric matrices of equivalent system that minimize the error measure.

One can minimize the quadratic measure by applying the first order necessary conditions such as:

$$\frac{\partial}{\partial K^{\mathrm{eq}}} E[\varepsilon^{\mathrm{T}}\varepsilon] = 0 \tag{B.5a}$$

$$\frac{\partial}{\partial C^{\mathrm{eq}}} E[\varepsilon^{\mathrm{T}}\varepsilon] = 0 \tag{B.5b}$$

$$\frac{\partial}{\partial M^{\mathrm{eq}}} E[\varepsilon^{\mathrm{T}}\varepsilon] = 0 \tag{B.5c}$$

As a representative case, we only present some core operations for stiffness term [Eq. (B.5a)]. Applying the necessary condition to the third term contained in the second expectation in Eq. (B.4) gives us

$$\frac{\partial}{\partial K^{\mathrm{eq}}} E[\psi^{\mathrm{T}} K^{\mathrm{eq}} y] = E[\psi y^{\mathrm{T}}] \tag{B.6}$$

Next, applying the necessary condition to the last term contained in the third expectation in Eq. (B.4) gives us

$$\frac{\partial}{\partial K^{\mathrm{eq}}} E[y^{\mathrm{T}} K^{\mathrm{eq}T} K^{\mathrm{eq}} y] = 2K^{\mathrm{eq}} E[y y^{\mathrm{T}}] \tag{B.7}$$

The expectation of the elastic and damping forces of the equivalent system can be reduced to

$$\frac{\partial}{\partial K^{\mathrm{eq}}} E[y^{\mathrm{T}} K^{\mathrm{eq}\mathrm{T}} C^{\mathrm{eq}} y'] = C^{\mathrm{eq}} E[y' y^{\mathrm{T}}] \tag{B.8}$$

Repeating similar operations for damping and mass and applying the linear property of the expectation operator $E[\cdot]$, Eqs. (B.5) can be rewritten into the following form:

$$\begin{aligned}\frac{\partial}{\partial K^{\mathrm{eq}}}E[\varepsilon^{\mathrm{T}}\varepsilon] &= -2E[\psi y^{\mathrm{T}}] + 2M^{\mathrm{eq}}E[y''y^{\mathrm{T}}] + 2C^{\mathrm{eq}}E[y'y^{\mathrm{T}}] + 2K^{\mathrm{eq}}E[yy^{\mathrm{T}}] \\ &= 0 \end{aligned} \tag{B.9a}$$

$$\begin{aligned}\frac{\partial}{\partial C^{\mathrm{eq}}}E[\varepsilon^{\mathrm{T}}\varepsilon] &= -2E[\psi y'^{\mathrm{T}}] + 2M^{\mathrm{eq}}E[y''y'^{\mathrm{T}}] + 2C^{\mathrm{eq}}E[y'y'^{\mathrm{T}}] + 2K^{\mathrm{eq}}E[yy'^{\mathrm{T}}] \\ &= 0 \end{aligned} \tag{B.9b}$$

$$\begin{aligned}\frac{\partial}{\partial M^{\mathrm{eq}}}E[\varepsilon^{\mathrm{T}}\varepsilon] &= -2E[\psi y''^{\mathrm{T}}] + 2M^{\mathrm{eq}}E[y''y''^{\mathrm{T}}] + 2C^{\mathrm{eq}}E[y'y''^{\mathrm{T}}] + 2K^{\mathrm{eq}}E[yy''^{\mathrm{T}}] \\ &= 0 \end{aligned} \tag{B.9c}$$

Assuming that the output vector y and its derivatives y' and y'' in Eqs. (B.9) are Gaussian process, the following formula can be used (Lutes and Sarkani, 2004)

$$E[h(x)x^{\mathrm{T}}] = E\left[\frac{\partial h}{\partial x}\right]E[xx^{\mathrm{T}}] \tag{B.10}$$

where $h(\cdot)$ is a scalar function and x is a Gaussian vector. Using the formula, Eqs. (B.9) can be written as follows.

$$E[\psi y^{\mathrm{T}}] = E\left[\frac{\partial \psi}{\partial y}\right]E[yy^{\mathrm{T}}] \tag{B.11a}$$

$$E[\psi y'^{\mathrm{T}}] = E\left[\frac{\partial \psi}{\partial y'}\right]E[yy'^{\mathrm{T}}] \tag{B.11b}$$

$$E[\psi y''^{\mathrm{T}}] = E\left[\frac{\partial \psi}{\partial y''}\right]E[yy''^{\mathrm{T}}] \tag{B.11c}$$

With introducing a combining vector $\hat{y} = [y^{\mathrm{T}}, y'^{\mathrm{T}}, y''^{\mathrm{T}}]^{\mathrm{T}}$, we can rewrite the equations into the following form:

$$E\left[\frac{\partial \psi}{\partial \hat{y}}\right] E[\hat{y}\hat{y}^{\mathrm{T}}] = [K^{\mathrm{eq}}\, C^{\mathrm{eq}}\, M^{\mathrm{eq}}] E[\hat{y}\hat{y}^{\mathrm{T}}] \tag{B.12}$$

Noting that the matrix $E[\hat{y}\hat{y}^{\mathrm{T}}]$ is non-singular, the equation that determines the parameters of the statistically linearized system are obtained as follows.

$$E\left[\frac{\partial \psi}{\partial \hat{y}}\right] = [K^{\mathrm{eq}}\, C^{\mathrm{eq}}\, M^{\mathrm{eq}}] \tag{B.13}$$

Consequently, if the nonlinear vector ψ is explicitly written in terms of the associated coordinate y and its derivatives and is differentiable to those terms, the equivalent matrices can be determined as Eq. (B.13) by applying the expectation to those partial derivatives.

B.2.2 Response evaluation

Once the elements of the equivalent linear system were established, the response of the system can be suitably obtained by means of the standard linear theory. Among various approaches, this coverage adopted the state variable approach. The equations of motion for the equivalent linear system can be rewritten into the state variable form as follows.

$$z' = Az + Bu \tag{B.14}$$

where $z = [y^{\mathrm{T}}, y'^{\mathrm{T}}]^{\mathrm{T}}$ and the matrices A and B are as follows:

$$A = \begin{bmatrix} O & I \\ -(M + M^{\mathrm{eq}})^{-1}(K + K^{\mathrm{eq}}) & -(M + M^{\mathrm{eq}})^{-1}(C + C^{\mathrm{eq}}) \end{bmatrix}, \tag{B.15a}$$

$$B = \begin{bmatrix} O \\ (M + M^{\mathrm{eq}})^{-1} f \end{bmatrix}. \tag{B.15b}$$

If the external loading u is a zero-mean stationary white-noise excitation with its spectral strength S_u, the covariance matrix $Q = E[zz^{\mathrm{T}}]$ can be obtained by solving the following Lyapunov equation (Lutes and Sarkani, 2004):

$$AQ + QA^{\mathrm{T}} + 2\pi S_u BB^{\mathrm{T}} = O \tag{B.16}$$

In those cases where the external loading u is not a white-noise excitation, it is available to augment the order of the overall system by applying the concept of a 'pre-filter', which is briefly covered in Appendix C. If needed, please refer to Roberts and Spanos (2003).

One can find from the preceding procedure that a cyclic relationship between the equivalent elements and the responses of the equivalent linear system, or between Eq. (B.13) and Eq. (B.16). To find the response and corresponding equivalent elements, hence, an iterative scheme followed by an appropriate initial estimate should be employed. It should be emphasized that the existence and uniqueness of the procedure are guaranteed in a rigorous way (Roberts and Spanos, 2003), so that the search procedure within the cyclic relationship, hence, is of valuable in finding the solution.

B.3 Examples of Systems with Power-Law Damping

This section presents a comprehensive example of a structure-FMTMD system, in which the main structure is controlled by the frictional multiple tuned mass damper in a passive way. Consider a structure-MTMD system by Eq. (4.8), in which the dissipative force of the i-th TMD ψ_i is as follows:

$$\psi_i = \psi_i(y_i') = \eta_i |y_i'|^{\beta} \mathrm{sgn}(y_i') \tag{5.9}$$

where η_i is the constant, and sgn[$\cdot$] is a signum function.

The statistical linearization technique enables the nonlinear force term $\psi = [0, \psi_i, \cdots, \psi_N]^{\mathrm{T}}$ to be replaced with an equivalent term that minimizes the mean square of the error $E[\varepsilon^2]$ where the error ε is given by

$$\varepsilon = \psi - C^{\mathrm{eq}} y' \tag{B.17}$$

where C^{eq} is a parametric matrix to be determined that minimizes the described mean square of the error.

Under the assumption of stationary Gaussian excitation, the elements of the parametric matrix C^{eq} can be obtained by Eq. (B.13), of which partial differentiation is done in an element-wise way, as follows:

$$c_{i+1}^{\mathrm{eq}} = E[\partial_{y_i'} \psi_i] = E\left[\frac{\partial \psi_i}{\partial y_i'}\right] \quad i = 1, \cdots, N \tag{B.18}$$

where ψ_i is the nonlinear force induced by the response of the i-th element, and $\partial_{y_i'} \psi_i$ denotes the partial derivative of the nonlinear force ψ_i with respect to the non-dimension velocity y_i'. The idealized Coulomb-type frictional force $hat\psi_i$ and its derivative $\partial_{y_i'} \hat{\psi}_i$ are depicted in Figure. Also it should be noted that $c_1^{\mathrm{eq}} = 0$ as the first element of the nonlinear vector ψ is null [see its definition denoted in Eq. (B.23)].

Further, under the assumption that the responses of the equivalent stationary system are stationary zero-mean Gaussian processes, the relative non-dimensional velocity of the i-th TMD, y_i', also becomes Gaussian with corresponding variance, say $\sigma_{y_i'}$. Then the expectation value in the Eq. (B.18) is evaluated by following expression:

$$E\left[\frac{\partial \psi_i}{\partial y_i'}\right] = \frac{1}{\sqrt{2\pi}\sigma_{y_i'}} \int_{-\infty}^{\infty} \frac{\partial \psi_i}{\partial y_i'} \exp[-y_i'^2 / 2\sigma_{y_i'}] \, \mathrm{d}y_i' \tag{B.19}$$

And the partial derivative of Eq. (B.19) is given by

$$\frac{\partial \psi_i}{\partial y_i'} = \begin{cases} 2\eta_i\, \delta(y_i') & \text{if } \beta = 0 \\ \eta_i \beta |y_i'|^{\beta-1} & \text{if } \beta > 0 \end{cases} \tag{B.20}$$

where $\delta(\cdot)$ is the Dirac delta function.

Substituting the partial derivative of the friction force and using the sifting property of the Dirac delta function, the equivalent damping element c_{i+1}^{eq} can be consequently evaluated. Connected with the equivalency of the equivalent damping coefficient and its normalized form, Eq. (B.18) can be rearranged into the following form:

$$c_{i+1}^{\text{eq}} = 2\gamma_i \zeta_i^{\text{eq}} = \begin{cases} \sqrt{\dfrac{2}{\pi}}\, \eta_i \dfrac{1}{\sigma_{y_i'}} & \text{if } \beta = 0 \\ \dfrac{\eta_i \beta \Gamma(\beta/2)(\sqrt{2}\sigma_{y_i'})^{\beta-1}}{\sqrt{\pi}} & \text{if } \beta > 0 \end{cases} \tag{B.21}$$

Rearranging Eq. (B.18) in terms of the design variable, η_i gives:

$$\eta_i = \begin{cases} \sqrt{2\pi}\gamma_i \zeta_i^{\text{eq}} \sigma_{y_i'} & \text{if } \beta = 0 \\ \dfrac{2\sqrt{\pi}(\sqrt{2}\sigma_{y_i'})^{1-\beta}}{\beta \Gamma(\beta/2)} \mu_i \gamma_i \zeta_i^{\text{eq}} & \text{if } \beta > 0 \end{cases} \tag{B.22}$$

Hence we have a equivalent linear matrix C^{eq} comprised of the equivalent force term, so that the solution obtained from the linear MTMD part can be adapted. Further, the terms contained in the equivalent matrix can be converted into the normalized form as previously seen in the linear MTMD chapter as follows:

The matrix equation (4.7) can be rewritten by substituting the statistically linearized term into the nonlinear vector as follows:

$$My'' + (C + C^{\text{eq}})y' + Ky = fw_g'' \tag{B.23}$$

where the matrices M, C and K are previously defined at Eqs. (4.9) and the equivalent damping matrix C^{eq} is defined in Eq. (4.21). With introducing a non-dimensional state vector $z = [y^{\mathrm{T}}, y'^{\mathrm{T}}]^{\mathrm{T}}$, a first-order state-space model can be formulated as Eq. (4.25), where the corresponding matrices A and B are given by

$$A = \begin{bmatrix} O & I \\ -M^{-1}K & -M^{-1}(C + C^{\mathrm{eq}}) \end{bmatrix}, \tag{B.24a}$$

$$B = \begin{bmatrix} O \\ -f \end{bmatrix}. \tag{B.24b}$$

Note that the equivalent damping matrix of the equivalent linear system consists of the non-dimensionalized relative velocities of TMDs [see Eq. (4.13)], and the relative velocities can be evaluated upon a determined system property [see Eq. (B.24)]. Hence, it is necessarily required to assume the initial system properties and to iterate the circumstances as the appropriate tolerance to be minimized.

As assumed that the external loading w_g'' is a zero-mean stationary white-noise excitation with its spectral strength $S_{w_g''}$, the covariance matrix $Q = E[zz^{\mathrm{T}}]$ can be obtained by solving the following Lyapunov equation

$$AQ + QA^{\mathrm{T}} + 2\pi S_{w_g''} BB^{\mathrm{T}} = O \tag{B.25}$$

One can find from the preceding procedure that a cyclic relationship between the equivalent elements and the responses of the equivalent linear system, or between Eq. (B.21) and Eq. (B.25). To find the response and corresponding equivalent elements, hence, an iterative scheme followed by an appropriate initial estimate should be employed. It should be emphasized that the existence and uniqueness of the procedure are guaranteed in a rigorous way (Roberts and Spanos, 2003), so that the search procedure within the cyclic relationship, hence, is of valuable in finding the solution.

Appendix C

Applying Pre-Filters

This appendix is dedicated to describe the techniques which is useful to deal with the structural response under non-white excitations by introducing a 'shaping filter' or 'pre-filter'. More detailed description on this issue can be referred to various textbooks or relevant documents, and this appendix part is excerpted from Chapter 7.4.2 from Roberts and Spanos (2003).

Suppose that a system is written in the form of state-space description. The pre-filter determines the transfer function between the input which is white noise and the output is of non-white excitation process. Under the circumstance, the original system is able to be described as an augmented, which consists of the original system and the pre-filter components in series. The schematic flow is depicted in Figure C.1. When the switch is closed after the pre-filtered output has reached stationary, it is clear that the non-stationary response of the original system will not be influenced by the transient response of the pre-filter.

The consequence of employing a switch into the augmented system can be realized by taking adequate initial conditions for the covariance matrix of the overall state

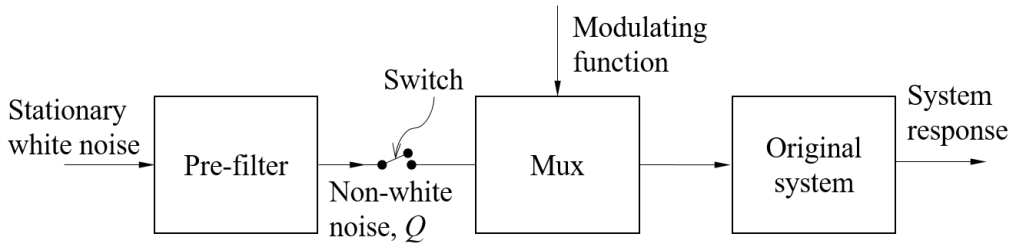

Figure C.1: Block diagram representation of the use of pre-filters to determine system response in the non-stationary case

variable vector, z. Thus, let $z = [x^{\mathrm{T}}, \chi^{\mathrm{T}}]^{\mathrm{T}}$, where x is the augmented state vector, and χ is the state vector associated with the pre-filter output.
First, suppose that the equation of motion was written as a first-order state-space equation as follows:

$$x' = Ax + Bu_g'' \tag{C.1}$$

where u_g'' is a ground acceleration and

$$A = \begin{bmatrix} O & I \\ -M^{-1}K & -M^{-1}C \end{bmatrix}, \tag{C.2a}$$

$$B = \begin{bmatrix} O \\ -f \end{bmatrix}. \tag{C.2b}$$

In the limited case where the input vector is of single degree of freedom, the process Q_s is governed by pre-fileter equations of the following general form

$$\nu_{m-1}\chi^{(m-1)} + \nu_{m-2}\chi^{(m-2)} + \cdots + \nu_0\chi^{(0)} = Q_s, \tag{C.3a}$$

$$\chi^{(m)} + \lambda_{m-1}\chi^{(m-1)} + \cdots + \lambda_0\chi^{(0)} = n, \tag{C.3b}$$

where $\lambda_0, \lambda_1, \cdots, \lambda_{m-1}$ and $\nu_0, \nu_1, \cdots, \nu_{m-1}$ are filter constants and n is a stationary white noise process, with unit strength. The superscript (n) denotes the n-th derivative. The vector χ may be defined by $\chi = [\chi^{(0)}, \chi^{(1)}, \cdots, \chi^{(m-1)}]^{\mathrm{T}}$. With this definition, Equation (C.3) may be written in the standard state variable form i.e.

$$\chi' = E\chi + F \tag{C.4}$$

where

$$E = \begin{bmatrix} 0 & 1 & \cdots & 0 \\ 0 & 0 & \cdots & 0 \\ \vdots & \vdots & \ddots & \vdots \\ -\lambda_0 & -\lambda_1 & \cdots & -\lambda_{m-1} \end{bmatrix}, \tag{C.5a}$$

$$F = \begin{bmatrix} 0 & 0 & \cdots & 0 \end{bmatrix}. \tag{C.5b}$$

In those cases where the random ground acceleration is filtered white-noise, it is possible to augment the overall system by introducing a 'shaping filter'. The augmented system is then governed by the usual state variable equation of the form

$$x' = Gx + W \tag{C.6}$$

where

$$G = \begin{bmatrix} E & D \\ O & F \end{bmatrix}, \tag{C.7a}$$

$$W = [0^{\mathrm{T}}, F^{\mathrm{T}}]^{\mathrm{T}}. \tag{C.7b}$$

D is defined by

$$D = a(t) \begin{bmatrix} O \\ M^{-1}v \end{bmatrix} \nu^{\mathrm{T}} \tag{C.8}$$

where

$$\nu = \begin{bmatrix} \nu_1 & \nu_2 & \cdots & \nu_{m-1} \end{bmatrix}^{\mathrm{T}}. \tag{C.9}$$

As indicated, the augmented system matrix G is time dependent through the introduction of the modulating function $a(t)$ that appears in D.

The covariance martrix V for x is governed by the usual differential matrix equation for a system drive by white noise. In the present notation this equation may be written as

$$V' = GV + VG^{\mathrm{T}} + P \tag{C.10}$$

where

$$P = \begin{bmatrix} 0 & 0 & \cdots & 0 \\ 0 & 0 & \cdots & 0 \\ \vdots & \vdots & \ddots & \vdots \\ 0 & 0 & \cdots & 1 \end{bmatrix}. \tag{C.11}$$

In solving Eq. (C.11) it is essential to start the integration procedure at the instant the switch is closed. At this time (t=0, say), some elements in V, which relate directly to χ will be non-zero. To demonstrate this, it is convenient to partition V, according to (C.1). Thus

$$V = \begin{bmatrix} V_{zz} & V_{z\chi} \\ V_{z\chi}^{\mathrm{T}} & V_{\chi\chi} \end{bmatrix} \tag{C.12}$$

Bibliography

[1] Abé, M. "Tuned Mass Dampers for Structures with Bilinear Hysteresis". *Journal of Engineering Mechanics* 122.8 (1996), pp. 797–800.

[2] Abé, M and Fujino, Y. "Dynamic characterization of multiple tuned mass dampers and some design formulas". *Earthquake engineering & structural dynamics* 23.8 (1994), pp. 813–835.

[3] Abé, M and Igusa, T. "Tuned mass dampers for structures with closely spaced natural frequencies". *Earthquake engineering & structural dynamics* 24.2 (1995), pp. 247–261.

[4] Alexander, NA and Schilder, F. "Exploring the performance of a nonlinear tuned mass damper". *Journal of Sound and Vibration* 319.1 (2009), pp. 445–462.

[5] Asami, T, Nishihara, O, and Baz, AM. "Analytical Solutions to H_∞ and H_2 Optimization of Dynamic Vibration Absorbers Attached to Damped Linear Systems". *Journal of Vibration and Acoustics* 124.2 (2002), pp. 284–295.

[6] Bachmann, H and Ammann, W. *Vibrations in structures: induced by man and machines*. Vol. 3. Iabse, 1987.

[7] Bartels, RH. and Stewart, GW. "Solution of the matrix equation AX+ XB= C". *Communications of the ACM* 15.9 (1972), pp. 820–826.

[8] Bendat, JS and Piersol, AG. *Random data: analysis and measurement procedures*. Vol. 729. John Wiley & Sons, 2011.

[9] Bisegna, Paolo and Caruso, Giovanni. "Closed-form formulas for the optimal pole-based design of tuned mass dampers". *Journal of sound and vibration* 331.10 (2012), pp. 2291–2314.

[10] Caramia, P, Carpinelli, G, and Varilone, P. "Point estimate schemes for probabilistic three-phase load flow". *Electric Power Systems Research* 80.2 (2010), pp. 168–175.

[11] Carpineto, N, Lacarbonara, W, and Vestroni, F. "Hysteretic tuned mass dampers for structural vibration mitigation". *Journal of Sound and Vibration* 333.5 (2014), pp. 1302–1318.

[12] Casado, CM, Sebastián, J de, Díaz, IM, and Poncela, A. "Vibration serviceability assessment and passive vibration control of a lively footbridge". *Proceedings of Fifth World Conference on Structural Control and Monitoring*. 2010.

[13] Caughey, TK. "On the response of non-linear oscillators to stochastic excitation". *Probabilistic Engineering Mechanics* 1.1 (1986), pp. 2–4.

[14] Caughey, TK and Ma, F. "The exact steady-state solution of a class of non-linear stochastic systems". *International Journal of Non-Linear Mechanics* 17.3 (1982), pp. 137–142.

[15] Chakraborty, S and Roy, BK. "Reliability based optimum design of Tuned Mass Damper in seismic vibration control of structures with bounded uncertain parameters". *Probabilistic Engineering Mechanics* 26.2 (2011), pp. 215–221.

[16] Chang, CC. "Mass dampers and their optimal designs for building vibration control". *Engineering Structures* 21.5 (1999), pp. 454–463.

[17] Chatzigeorgiou, I. "Bounds on the Lambert function and their application to the outage analysis of user cooperation". *IEEE Communications Letters* 17.8 (2013), pp. 1505–1508.

[18] Chen, Genda and Wu, Jingning. "Optimal placement of multiple tune mass dampers for seismic structures". *Journal of Structural Engineering* 127.9 (2001), pp. 1054–1062.

[19] Chopra, AK. *Dynamics of structures: theory and applications to earthquake engineering. 2007*. Prentice-Hall, 2007.

[20] Clark, AJ. "Multiple passive tuned mass damper for reducing earthquake induced building motion". *Proc.* Vol. 9. 1988, pp. 779–784.

[21] Clough, RW and Penzien, J. "Dynamics of structures. 1993". *Copyright of Applied Mechanics & Materials* (1993).

[22] Coleman, TF, Branch, MA, and Grace, A. *Optimization toolbox for Use with MATLAB: User's guide*. Mathworks Incorporated, 1999.

[23] Crandall, SH and Mark, WD. *Random vibration in mechanical systems*. Academic Press, 1963.

[24] Crandall, SH and Mark, WD. *Random vibration in mechanical systems*. Academic Press, 2014.

[25] Davenport, AG. "Note on he distribution of the largest value of a random function with application to gust loading". *Proceedings, Institution of Civil Engineering*. Vol. 28. 1964, pp. 187–196.

[26] De, S, Wojtkiewicz, SF, and Johnson, EA. "Efficient optimal design and design-under-uncertainty of passive control devices with application to a cable-stayed bridge". *Structural Control and Health Monitoring* 24.2 (2017).

[27] Dehghan-Niri, E, Zahrai, SM, and Mohtat, A. "Effectiveness-robustness objectives in MTMD system design: An evolutionary optimal design methodology". *Structural control & health monitoring* 17.2 (2010), pp. 218–236.

[28] Den Hartog, JP. *Mechanical Vibrations*. 1956.

[29] Ellingwood, Bruce R. "Reliability-based condition assessment and LRFD for existing structures". *Structural Safety* 18.2-3 (1996), pp. 67–80.

[30] Frahm, H. *Device for damping vibrations of bodies*. US Patent 989958. 1911.

[31] Fu, TS and Johnson, EA. "Distributed mass damper system for integrating structural and environmental controls in buildings". *Journal of Engineering Mechanics* 137.3 (2010), pp. 205–213.

[32] Fujino, Yozo and Abe, Masato. "Design formulas for tuned mass dampers based on a perturbation technique". *Earthquake engineering & structural dynamics* 22.10 (1993), pp. 833–854.

[33] Gerges, RR and Vickery, BJ. "Optimum design of pendulum-type tuned mass dampers". *The Structural Design of Tall and Special Buildings* 14.4 (2005), pp. 353–368.

[34] Gewei, Z and Basu, B. "A study on friction-tuned mass damper: harmonic solution and statistical linearization". *Journal of Vibration and Control* (2010), p. 1077546309354967.

[35] Ghorbani-Tanha, AK, Noorzad, A, and Rahimian, M. "Mitigation of wind-induced motion of Milad Tower by tuned mass damper". *The structural design of tall and special buildings* 18.4 (2009), pp. 371–385.

[36] Gupta, YP and Chandrasekaran, AR. "Absorber system for earthquake excitation". *Proceedings of the Fourth World Conference on Earthquake Engineering*. 1969, pp. 139–48.

[37] Halsted III, DM and Taylor, DL. "Optimum vibration absorbers for linear damped systems". *Journal of Mechanical Design* 103 (1981), p. 909.

[38] Hoang, N, Fujino, Y, and Warnitchai, P. "Optimal tuned mass damper for seismic applications and practical design formulas". *Engineering Structures* 30.3 (2008), pp. 707–715.

[39] Hoang, N and Warnitchai, P. "Design of multiple tuned mass dampers by using a numerical optimizer". *Earthquake engineering & structural dynamics* 34.2 (2005), pp. 125–144.

[40] Hong, HP. "An efficient point estimate method for probabilistic analysis". *Reliability Engineering & System Safety* 59.3 (1998), pp. 261–267.

[41] Igusa, T and Xu, K. "Vibration control using multiple tuned mass dampers". *Journal of sound and vibration* 175.4 (1994), pp. 491–503.

[42] Inaudi, J and Kelly, J. "Mass Damper Using Friction-Dissipating Devices". *Journal of Engineering Mechanics* 121.1 (1995), pp. 142–149.

[43] Irwin, PA and B, Brian. "Recent applications of damping systems for wind response". *Proceeings of the 6th World Congress of the Council on Tall Buildings and Urban Habitat*. 2001.

[44] Jangid, RS. "Optimum Multiple Tuned Mass Dampers for base-excited undamped system". *Earthquake engineering & structural dynamics* 28.9 (1999), pp. 1041–1049.

[45] Jangid, RS and Datta, TK. "Performance of multiple tuned mass dampers for torsionally coupled system". *Earthquake engineering & structural dynamics* 26.3 (1997), pp. 307–317.

[46] Jeffrey, A and Dai, HH. *Handbook of mathematical formulas and integrals*. Academic Press, 2008.

[47] Joshi, AS and Jangid, RS. "Optimum parameters of multiple tuned mass dampers for base-excited damped systems". *Journal of sound and vibration* 202.5 (1997), pp. 657–667.

[48] Kareem, A, Kijewski, T, and Tamura, Y. "Mitigation of motions of tall buildings with specific examples of recent applications". *Wind and Structures* 2.3 (1999), pp. 201–251.

[49] Kareem, A and Kline, S. "Performance of multiple mass dampers under random loading". *Journal of structural engineering* 121.2 (1995), pp. 348–361.

[50] Kashani, R, Pearce, A, and Markham, B. "Tuned Damping of Balcony Vibration". *Journal of Performance of Constructed Facilities* 28.3 (2012), pp. 450–457.

[51] Kawaguchi, A, Teramura, A, and Omote, Y. "Time history response of a tall building with a tuned mass damper under wind force". *Journal of wind engineering and industrial aerodynamics* 43.1 (1992), pp. 1949–1960.

[52] Krenk, Steen. "Frequency analysis of the tuned mass damper". *Journal of applied mechanics* 72.6 (2005), pp. 936–942.

[53] Kwok, KCS and Macdonald, PA. "Full-scale measurements of wind-induced acceleration response of Sydney Tower". *Engineering Structures* 12.3 (1990), pp. 153–162.

[54] Kwok, KCS and Samali, B. “Performance of tuned mass dampers under wind loads”. *Engineering Structures* 17.9 (1995), pp. 655–667.

[55] Leung, AYT, Zhang, H, Cheng, CC, and Lee, YY. “Particle swarm optimization of TMD by non-stationary base excitation during earthquake”. *Earthquake Engineering & Structural Dynamics* 37.9 (2008), pp. 1223–1246.

[56] Li, C. “Optimum multiple tuned mass dampers for structures under the ground acceleration based on DDMF and ADMF”. *Earthquake engineering & structural dynamics* 31.4 (2002), pp. 897–919.

[57] Li, C and Liu, Y. “Further characteristics for multiple tuned mass dampers”. *Journal of Structural Engineering* 128.10 (2002), pp. 1362–1365.

[58] Li, C and Qu, W. “Optimum properties of multiple tuned mass dampers for reduction of translational and torsional response of structures subject to ground acceleration”. *Engineering Structures* 28.4 (2006), pp. 472–494.

[59] Li, C and Zhu, B. “Estimating double tuned mass dampers for structures under ground acceleration using a novel optimum criterion”. *Journal of sound and vibration* 298.1 (2006), pp. 280–297.

[60] Li, HN and Ni, XL. “Optimization of non-uniformly distributed multiple tuned mass damper”. *Journal of Sound and Vibration* 308.1 (2007), pp. 80–97.

[61] Li, Q, Fan, J, Nie, J, Li, Q, and Chen, Y. “Crowd-induced random vibration of footbridge and vibration control using multiple tuned mass dampers”. *Journal of Sound and Vibration* 329.19 (2010), pp. 4068–4092.

[62] Lievens, K, Lombaert, G, De Roeck, G, and Van den Broeck, P. “Robust design of a TMD for the vibration serviceability of a footbridge”. *Engineering Structures* 123 (2016), pp. 408–418.

[63] Lin, CC, Ueng, JM, and Huang, TC. "Seismic response reduction of irregular buildings using passive tuned mass dampers". *Engineering Structures* 22.5 (2000), pp. 513–524.

[64] Lin, CC, Wang, JF, and Chen, BL. "Train-induced vibration control of high-speed railway bridges equipped with multiple tuned mass dampers". *Journal of Bridge Engineering* 10.4 (2005), pp. 398–414.

[65] Lin, CC, Wang, JF, Lien, CH, Chiang, HW, and Lin, CS. "Optimum design and experimental study of multiple tuned mass dampers with limited stroke". *Earthquake Engineering & Structural Dynamics* 39.14 (2010), pp. 1631–1651.

[66] Lin, JS and Tyan, JY. "Equivalent stationary motion and average response spectra". *Earthquake engineering & structural dynamics* 14.2 (1986), pp. 267–279.

[67] Liu, MY, Chiang, WL, Hwang, JH, and Chu, CR. "Wind-induced vibration of high-rise building with tuned mass damper including soil–structure interaction". *Journal of Wind Engineering and Industrial Aerodynamics* 96.6 (2008), pp. 1092–1102.

[68] Love, JS and Tait, MJ. "The peak response distributions of structure–DVA systems with nonlinear damping". *Journal of Sound and Vibration* 348 (2015), pp. 329–343.

[69] Lucchini, A, Greco, R, Marano, GC, and Monti, G. "Robust design of tuned mass damper systems for seismic protection of multistory buildings". *Journal of Structural Engineering* 140.8 (2013), A4014009.

[70] Luft, RW. "Optimal tuned mass dampers for buildings". *Journal of the Structural Division* 105.12 (1979), pp. 2766–2772.

[71] Lutes, LD and Sarkani, S. *Random vibrations: analysis of structural and mechanical systems*. Butterworth-Heinemann, 2004.

[72] Marano, GC, Greco, R, and Sgobba, S. "A comparison between different robust optimum design approaches: application to tuned mass dampers". *Probabilistic Engineering Mechanics* 25.1 (2010), pp. 108–118.

[73] McNamara, RJ. "Tuned mass dampers for buildings". *Journal of the Structural Division* 103.9 (1977), pp. 1785–1798.

[74] Morales, Juan M and Perez-Ruiz, Juan. "Point estimate schemes to solve the probabilistic power flow". *IEEE Transactions on Power Systems* 22.4 (2007), pp. 1594–1601.

[75] Mrabet, E, Guedri, M, Ichchou, MN, and Ghanmi, S. "Stochastic structural and reliability based optimization of tuned mass damper". *Mechanical Systems and Signal Processing* 60–61.0 (2015), pp. 437–451.

[76] Murray, TM, Allen, DE, and Ungar, EE. "Floor vibrations due to human activity" (1997).

[77] Newland, DE. *An introduction to random vibrations, spectral & wavelet analysis*. Courier Corporation, 2012.

[78] Nguyen, TH, Saidi, I, Gad, EF, Wilson, JL, and Haritos, N. "Performance of distributed multiple viscoelastic tuned mass dampers for floor vibration applications". *Advances in Structural Engineering* 15.3 (2012), pp. 547–562.

[79] Nishihara, O and Asami, T. "Closed-form solutions to the exact optimizations of dynamic vibration absorbers (minimizations of the maximum amplitude magnification factors)". *Journal of vibration and acoustics* 124.4 (2002), pp. 576–582.

[80] Pinkaew, T, Lukkunaprasit, P, and Chatupote, P. "Seismic effectiveness of tuned mass dampers for damage reduction of structures". *Engineering Structures* 25.1 (2003), pp. 39–46.

[81] Poovarodom, N, Kanchanosot, S, and Warnitchai, P. "Application of nonlinear multiple tuned mass dampers to suppress man-induced vibrations of a pedestrian bridge". *Earthquake engineering & structural dynamics* 32.7 (2003), pp. 1117–1131.

[82] Rathi, AK and Chakraborty, A. "Reliability-based performance optimization of TMD for vibration control of structures with uncertainty in parameters and excitation". *Structural Control and Health Monitoring* (2016).

[83] Ricciardelli, F and Vickery, BJ. "Tuned vibration absorbers with dry friction damping". *Earthquake Engineering & Structural Dynamics* 28.7 (1999), pp. 707–723.

[84] Roberts, JB and Spanos, PD. *Random vibration and statistical linearization.* Courier Corporation, 2003.

[85] Rosenblueth, Emilio. "Point estimates for probability moments". *Proceedings of the National Academy of Sciences* 72.10 (1975), pp. 3812–3814.

[86] Rüdinger, F. "Optimal vibration absorber with nonlinear viscous power law damping and white noise excitation". *Journal of Engineering Mechanics* 132.1 (2006), pp. 46–53.

[87] Rüdinger, F. "Tuned mass damper with nonlinear viscous damping". *Journal of Sound and Vibration* 300.3–5 (2007), pp. 932–948.

[88] Sadek, F, Mohraz, B, Taylor, AW, and Chung, RM. "A method of estimating the parameters of tuned mass dampers for seismic applications". *Earthquake Engineering & Structural Dynamics* 26.6 (1997), pp. 617–636.

[89] Saidi, I, Gad, EF, Wilson, JL, and Haritos, N. "Development of passive viscoelastic damper to attenuate excessive floor vibrations". *Engineering structures* 33.12 (2011), pp. 3317–3328.

[90] Setareh, M and Hanson, R. "Tuned Mass Dampers for Balcony Vibration Control". *Journal of Structural Engineering* 118.3 (1992), pp. 723–740.

[91] Setareh, M, Ritchey, JK, Baxter, AJ, and Murray, TM. "Pendulum tuned mass dampers for floor vibration control". *Journal of performance of constructed facilities* 20.1 (2006), pp. 64–73.

[92] Sgobba, S and Marano, GC. "Optimum design of linear tuned mass dampers for structures with nonlinear behaviour". *Mechanical Systems and Signal Processing* 24.6 (2010), pp. 1739–1755.

[93] Skogestad, S and Postlethwaite, I. *Multivariable feedback control: analysis and design*. Vol. 2. Wiley New York, 2007.

[94] Sladek, JR and Klingner, RE. "Using tuned mass dampers to reduce seismic response". *Proceedings of the World Conference on Earthquake Engineering*. Vol. 7. publisher not identified. 1980, p. 265.

[95] Smith, AL, Hicks, SJ, and Devine, PJ. *Design of floors for vibration: A new approach*. Steel Construction Institute Ascot, Berkshire, UK, 2007.

[96] Socha, L. "Linearization in analysis of nonlinear stochastic systems: recent results—part I: theory". *Applied Mechanics Reviews* 58.3 (2005), pp. 178–205.

[97] Socha, L. "Linearization in analysis of nonlinear stochastic systems, recent results—part II: applications". *Applied Mechanics Reviews* 58.5 (2005), pp. 303–315.

[98] Soom, AA and Lee, M. “Optimal design of linear and nonlinear vibration absorbers for damped systems”. *Journal of Vibration, Acoustics, Stress, and Reliability in Design* 105.1 (1983), pp. 112–119.

[99] Soto-Brito, R and Ruiz, SE. “Influence of ground motion intensity on the effectiveness of tuned mass dampers”. *Earthquake engineering & structural dynamics* 28.11 (1999), pp. 1255–1271.

[100] Tanaka, H and Mak, CY. “Effect of tuned mass dampers on wind induced response of tall buildings”. *Journal of Wind Engineering and Industrial Aerodynamics* 14.1 (1983), pp. 357–368.

[101] Terenzi, G. “Dynamics of SDOF systems with nonlinear viscous damping”. *Journal of Engineering Mechanics* 125.8 (1999), pp. 956–963.

[102] Thompson, AG. “Optimum tuning and damping of a dynamic vibration absorber applied to a force excited and damped primary system”. *Journal of Sound and Vibration* 77.3 (1981), pp. 403–415.

[103] Tsai, HC. “The effect of tuned-mass dampers on the seismic response of base-isolated structures”. *International Journal of Solids and Structures* 32.8–9 (1995), pp. 1195–1210.

[104] Tsai, HC and Lin, GC. “Optimum tuned mass dampers for minimizing steady-state response of support-excited and damped systems”. *Earthquake Engineering & Structural Dynamics* 22.11 (1993), pp. 957–973.

[105] Van Nimmen, K, Verbeke, P, Lombaert, G, De Roeck, G, and Van den Broeck, P. “Numerical and experimental evaluation of the dynamic performance of a footbridge with tuned mass dampers”. *Journal of Bridge Engineering* (2016), p. C4016001.

[106] Varela, WD and Battista, RC. “Control of vibrations induced by people walking on large span composite floor decks”. *Engineering Structures* 33.9 (2011), pp. 2485–2494.

[107] Villaverde, R. “Reduction seismic response with heavily-damped vibration absorbers”. *Earthquake Engineering & Structural Dynamics* 13.1 (1985), pp. 33–42.

[108] Wang, JF, Lin, CC, and Chen, BL. “Vibration suppression for high-speed railway bridges using tuned mass dampers”. *International Journal of Solids and Structures* 40.2 (2003), pp. 465–491.

[109] Wang, JF, Lin, CC, and Lian, CH. “Two-stage optimum design of tuned mass dampers with consideration of stroke”. *Structural Control and Health Monitoring* 16.1 (2009), pp. 55–72.

[110] Wang, M. “Feasibility study of nonlinear tuned mass damper for machining chatter suppression”. *Journal of Sound and Vibration* 330.9 (2011), pp. 1917–1930.

[111] Warburton, GB. “Optimum absorber parameters for various combinations of response and excitation parameters”. *Earthquake Engineering & Structural Dynamics* 10.3 (1982), pp. 381–401.

[112] Webster, AC and Vaicaitis, R. “Application of tuned mass dampers to control vibrations of composite floor systems”. *Engineering Journal of the American Institute of Steel Construction* 29.3 (1992), pp. 116–124.

[113] Wirsching, PH and Campbell, GW. “Minimal structural response under random excitation using the vibration absorber”. *Earthquake Engineering & Structural Dynamics* 2.4 (1973), pp. 303–312.

[114] Wirsching, PH and Yao, JTP. "Safety design concepts for seismic structures". *Computers & Structures* 3.4 (1973), pp. 809–826.

[115] Wong, KKF. "Seismic Energy Dissipation of Inelastic Structures with Tuned Mass Dampers". *Journal of Engineering Mechanics* 134.2 (2008), pp. 163–172.

[116] Wong, KKF and Chee, YL. "Energy dissipation of tuned mass dampers during earthquake excitations". *The Structural Design of Tall and Special Buildings* 13.2 (2004), pp. 105–121.

[117] Wong, KKF and Harris, JL. "Seismic damage and fragility analysis of structures with tuned mass dampers based on plastic energy". *The Structural Design of Tall and Special Buildings* 21.4 (2012), pp. 296–310.

[118] Wong, KKF and Johnson, J. "Seismic Energy Dissipation of Inelastic Structures with Multiple Tuned Mass Dampers". *Journal of Engineering Mechanics* 135.4 (2009), pp. 265–275.

[119] Xu, K and Igusa, T. "Dynamic characteristics of multiple substructures with closely spaced frequencies". *Earthquake engineering & structural dynamics* 21.12 (1992), pp. 1059–1070.

[120] Yamaguchi, H and Harnpornchai, N. "Fundamental characteristics of multiple tuned mass dampers for suppressing harmonically forced oscillations". *Earthquake engineering & structural dynamics* 22.1 (1993), pp. 51–62.

[121] Yang, F, Sedaghati, R, and Esmailzadeh, E. "Optimal design of distributed tuned mass dampers for passive vibration control of structures". *Structural Control and Health Monitoring* 22.2 (2015), pp. 221–236.

[122] Yang, Y, Dai, W, and Liu, Q. "Design and implementation of two-degree-of-freedom tuned mass damper in milling vibration mitigation". *Journal of Sound and Vibration* 335 (2015), pp. 78–88.

[123] Yu, H, Gillot, F, and Ichchou, M. “Reliability based robust design optimization for tuned mass damper in passive vibration control of deterministic/uncertain structures”. *Journal of Sound and Vibration* 332.9 (2013), pp. 2222–2238.

[124] Zhang, Z and Balendra, T. “Passive control of bilinear hysteretic structures by tuned mass damper for narrow band seismic motions”. *Engineering Structures* 54 (2013), pp. 103–111.

[125] Zuo, L. “Effective and robust vibration control using series multiple tuned-mass dampers”. *Journal of Vibration and Acoustics* 131.3 (2009), p. 031003.

[126] Zuo, L and Nayfeh, SA. “Minimax optimization of multi-degree-of-freedom tuned-mass dampers”. *Journal of Sound and Vibration* 272.3-5 (2004), pp. 893–908.

[127] Zuo, L and Nayfeh, SA. “Optimization of the Individual Stiffness and Damping Parameters in Multiple-Tuned-Mass-Damper Systems”. *Journal of Vibration and Acoustics* 127.1 (2005), pp. 77–83.

Abstract (in Korean)

최근 건축재료기술 및 이에 상응하는 설계기술의 발전은 건축물의 경량화 및 고층화를 가능케 하였으며, 이에 따라 건물의 진동 성능은 설계 시점이나 시공 전후에 필수적으로 고려해야 할 요소 중 하나가 되었다. 진동제어기술은 이러한 경량/고층 건물의 수요증가와 맞물려 그 수요 역시 점증하고 있다. 이 중 동조질량감쇠기(Tuned mass damper, TMD)는 원구조물과 동조하는 부가질량, 공진을 유도하기 위한 복원기구 및 유입된 진동에너지를 소산하기 위한 감쇠기구로 구성되며, 우수한 성능과 간편한 원리에 따른 구현의 용이성으로 인해 가장 널리 쓰이는 진동제어 장치이다.

다중동조질량감쇠기(Multiple TMD, MTMD)는 여러 개의 적절히 설계된 TMD들을 배치하여 원구조물의 진동을 저감하는 하나의 시스템을 일컫는다. MTMD를 구현하고자 할 경우, 단일TMD와는 달리 단일 고유진동수가 아니라 넓은 진동수대역에 걸쳐 각 단위TMD들이 공진하여 진동에너지를 흡수할 수 있도록 시스템을 구성해야 한다. MTMD의 최적 설계를 위해서는 기존 단일TMD와는 달리 각 단위TMD들의 최적 동특성을 찾기 위한 최적화를 수행해야 하며, 또한 MTMD의 적용으로 인해 유발될 것으로 예상되는 부작용들을 충분히 고려해야 한다.

본 논문은 MTMD의 최적 설계안을 도출하며, 본 논문의 주제는 1) 선형 속도의 존감쇠를 통해 에너지를 소산하는 이른바 선형 다중동조질량감쇠기(Linear MTMD, LMTMD)의 최적설계, 2) Coulomb타입의 마찰력을 통해 에너지를 소산하는 마찰 다중동조질량감쇠기(Frictional MTMD, FMTMD)의 최적설계 및 3) FMTMD의 정확한 RMS변위 추정을 위한 보정계수, 극값분포 확률밀도함수와 그에 따른 피크팩터 추정식 개발 등을 포괄한다.

본 연구는 실용적으로 여겨지는 여섯 가지 LMTMD 구성에 대한 최적해를 도출하였으며, 이 중 최적해에 버금가는 성능을 보유하되 세 개의 매개변수로 TMD의 동특성을 기술할 수 있는 LMTMD구성에 대한 설계식을 제안하였다. 또한 본 연구에서 도출한

최적해 분포로부터 동일한 총부가질량비를 가질 경우에는 그 진동성능에는 유의미한 차이가 나타나지 않으나, 단위 갯수가 늘어남에 따라 최적성능 발현에 요구되는 총점성감쇠기구의 용량이 감소함을 보였다. 다만 이러한 요구감쇠의 감소는 결과적으로 각 단위TMD의 요구변위 증가로 이어져 기구를 보다 더 정밀하게 만들어야 할 조건을 추가로 부여한다.

본 연구에서는 또한 네 개의 FMTMD구성에 대한 최적해를 도출하였으며, 이 중 적은 매개변수를 가지면서도 높은 성능을 발현하는 구성에 대한 설계식을 제안하였다. 본 연구는 비선형 거동을 보이는 마찰력을 통계적으로 등가를 갖는 선형 속도의존 하중으로 대체한 후, 이 때의 오차를 최소화하는 선형 속도의존하중 및 그에 대응되는 마찰력을 제시하였다. 또한 마찰력 도입에 따라 하중의 크기가 TMD성능에 미치는 영향을 다각적으로 분석하였다.

본 연구는 또한 통계적 선형화를 통해 예측된 RMS 변위값이 실제 값을 8% 가량 과소평가하는 것을 보였으며, 통계적 비선형화기법을 통해 상기 예측된 RMS변위값을 보정하는 식을 제시하였다. 또한 FMTMD의 과도한 응답을 미리 예측하게 하기 위해 피크팩터 산정을 위한 식을 유도하고 이를 제시하였다.

본 연구에서는 마찰-진자형 TMD를 개발하여 이 성능을 수치적 방식을 통해 확인하였으며, 또한 바닥진동 제어 시 요구되는 TMD설계 전반의 과정을 체계적으로 정리하여 응용부분에 추가하였다. 마지막으로 MTMD를 적용한 실제 프로젝트를 제시함으로써 이론적 고찰뿐만 아니라 실제적 부분을 충실하게 다루었다. 본 연구의 결과는 제작, 설치 및 제어가 훨씬 용이한 Modular TMD 혹은 Portable TMD의 개발에 활용될 수 있다.

주요어: 동조질량감쇠기, 다중동조질량감쇠기, 마찰기구, 진동제어, 통계적선형화, 바닥진동

학번: 2011-30173